Physicochemical and numerical modeling of electrokinetics in inhomogenous matrices

Paz Garcia, Juan Manuel; Riberio, Alexandra; Rodriguez-Maroto, José Miguel ; Johannesson, Björn ; Ottosen, Lisbeth M.

Publication date:
2012

Document Version
Publisher's PDF, also known as Version of record

Physicochemical and numerical modeling of electrokinetics in inhomogeneous matrices

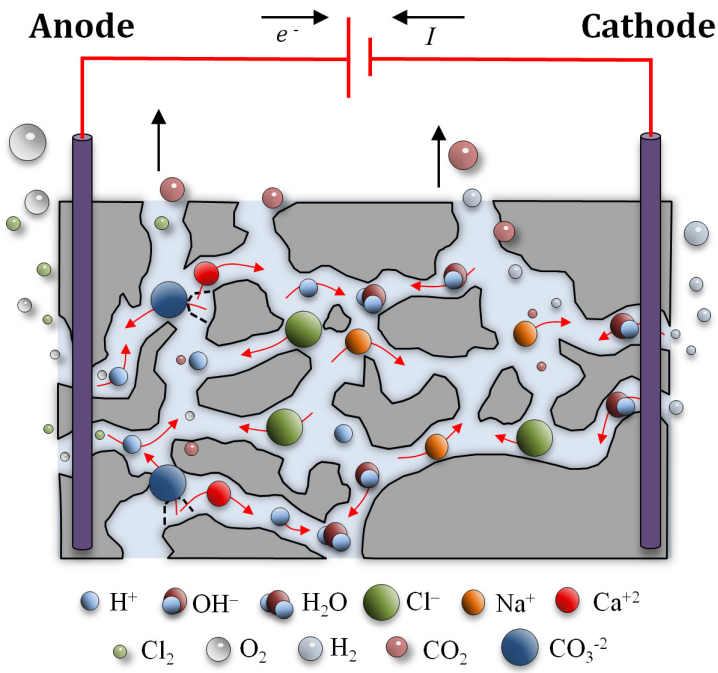

Juan Manuel Paz Garcia

PhD Thesis

Department of Civil Engineering

2012

DTU Civil Engineering Report R-276 (UK)
November 2012

DTU Civil Engineering
Department of Civil Engineering

Physicochemical and Numerical Modeling of Electrokinetics in Inhomogeneous Matrices

Juan Manuel Paz García

Supervisors:

Associate Prof. Lisbeth M. Ottosen[1]
Associate Prof. Björn Johannesson[1]
Associate Prof. Alexandra B. Ribeiro[2]
Prof. José Miguel Rodríguez-Maroto[3]

Assessment committee:

Associate Prof. John Mortensen[4]
Associate Prof. Claudio Cameselle[5]
Prof. Ivars Neretnieks[6]

[1]Dept. of Civil Engineering, Technical University of Denmark, Denmark
[2]Dept. of Environmental Sciences and Engineering, New University of Lisbon, Portugal
[3]Dept. of Chemical Engineering, University of Malaga, Spain
[4]Dept. of Science, Systems and Models, Roskilde University, Denmark
[5]Dept. of Chemical Engineering, University of Vigo, Spain
[6]School of Chemical Science and Engineering, KTH Royal Institute of Technology, Sweden

Preface

This thesis is submitted by Juan Manuel Paz García, as a partial fulfillment of the requirements for the Danish PhD degree at the Technical University of Denmark.

The present thesis is based on the scientific papers submitted and the conference contributions presented during the PhD project "*Physicochemical and numerical modeling of electrokinetics in inhomogeneous matrices*". The report is divided in 3 parts.

Part I PhD dissertation The knowledge collected in the appended publications is compiled in this of the thesis, which is a dissertation aiming to organize the information and explain the methodology used. Part I is divided in three chapters.

Chapter 1 contains the description of the PhD project, the statement of the research objectives and a summary of the main results achieved and published during the research period. It aims to organize the content and link between the published papers.

Chapter 2 explain the fundamentals of the generalized physicochemical model that has been proposed for the mathematical description of the electrokinetic reactive-transport phenomena through porous media.

Chapter 3 aims to increase the reproducibility of the research by means of a detailed explanation of the numerical procedures followed for the computer-aid solution of the proposed physicochemical model. Accordingly, the knowledge gained during the PhD project can be disseminated not only from a theoretical approach, but also by means of a practical point of view.

In the Part I of the PhD thesis especial attention is paid on those details not described in the published papers. Nevertheless, some repetition of the content already included in the appended papers is unavoidable.

Part II Appendices They consist of chosen simulations for the illustration of specific examples and some directions related to the numerical implementation of the computational model.

Part III Appended publications This part collects the relevant peer-reviewed scientific publications submitted during the PhD project, including journal papers and conference contributions. These publications are the result of the progressive development of a generalized model for electrokinetics.

Most of the research work developed during the PhD project has been carried out at the Department of Civil Engineering of the Technical University of Denmark (BYG·DTU) under the supervision of Associate Professor Lisbeth M. Ottosen and the co-supervision of Associate Professor Björn Johannesson. The group of co-supervisors included the international researchers Associate Professor Alexandra B. Ribeiro (New University of Lisbon, Portugal) and Professor José Miguel Rodríguez-Maroto (University of Málaga, Spain).

Part of the PhD studies has been carried out in the University of Malaga, by short research stays for a direct collaboration with the external supervisor. Additionally, during the PhD scholarship, Juan Manuel had three stays abroad, hosted by international prestigious universities:

- February 2011. Department of Solid Mechanics, Lund University, Lund, Sweden. Hosted by Prof. Matti Ristinmaa.
- March – July 2011. Department of Civil and Environmental Engineering. Northeastern University, Boston, Massachusetts, USA. Hosted by Prof. Akram N. Alshawabkeh.
- June – August 2012. Department of Chemical and Environmental Engineering. Universidad Técnica Federico Santa María, Valparaíso, Chile. Hosted by Prof. Henrik K. Hansen, in the framework of the EU project ELECTROACROSS (FP7-PEOPLE-2010-IRSES-269289).

The present research is part of a more general project entitled "Fundamentals of Electrokinetics in Inhomogeneous Matrices", sponsored by The Danish Agency of Science Technology and Innovation, which aims to extend and strengthen the understanding of the different physicochemical processes governing an electrokinetic system.

Lyngby, 31th August 2012
J.M. Paz-García

Acknowledgments

I, Juan Manuel Paz García, gratefully acknowledge the support from the Danish Council for Independent Research | Technology and Production Sciences, under the Danish Agency of Science Technology and Innovation, for the financial support in the project "Fundamentals of Electrokinetics in Inhomogeneous Matrices".

I acknowledge the financial support from the EU project ELECTROACROSS (FP7-PEOPLE-2010-IRSES-269289), which sponsored my research stay at the Universidad Técnica Federico Santa María, in Valparaíso (Chile). I acknowledge the economic contribution from Otto Mønsted funds, which partially sponsored the conference participation expenses.

I am truly grateful to my supervisor, Lisbeth M. Ottosen, for her trust on me and her unconditional support during the project research. I also thank my team of co-supervisors: Björn Johannesson, Alexandra Ribeiro and José Miguel Rodríguez-Maroto. Only through the support of this team of experts, the results achieved during this multidisciplinary project were possible. The entire team of supervisors provided invaluable technical guidance in a constant attitude of sincere dedication, commitment and friendship, acting as a continuous inspiration source.

I sincerely thank my colleagues at the Section for Construction Materials at the Department of Civil Engineering of the Technical University of Denmark and the Group of Environmental Management and Engineering at the Department of Chemical Engineering of the University of Málaga (Spain), for their selfless help, useful guidance, respect and cooperative effort.

I really appreciate the kindly welcome I received during my external stays by Matti Ristinmaa and Neils Ottosen and their research group, at the University of Lund (Sweden); by Akram N. Alshawabkeh and his research group, at Northeastern University (US); and by Henrik K. Hansen and his research group at the Universidad Técnica Federico Santa María (Chile).

Finally, I warmly thank to my family and friends. Because you make me fell at home whatever I am, and because you helped me to become who I am and to get what I have got. You are all part of this work and I will always be grateful to you.

Abstract

An electric field externally applied to a porous material, results in mobilization of chemical species through the electrolyte and transport of the pore solution itself. Based on this, several techniques have been developed aiming at removing of selected contaminants or injecting specific compounds into porous solid matrices of different kinds. These techniques are typically denoted as electrokinetic treatments.

In these kind of electrochemically-induced transport processes, the driving force is related the concentration gradients and the unbalanced in ionic charge produced by the electrochemical reactions taking place at the electrodes as a consequence of the applied electric field. Additionally, non-electroneutral electric double-layers at the interfaces between electrolyte and solid surfaces are affected by the induced electric potential, resulting in electrokinetic transport.

In addition to the electrochemical reactions, these kinds of transport processes are strongly influenced by the chemical interactions between the species present in the heterogeneous system, either dissolved in the electrolyte, precipitated or adsorbed at the solid surface.

Physicochemical models form a necessary basis for the understanding of the involved processes and the development of a theoretical framework able to take into account the complex interactions taking place in any electrokinetic or electrochemically-induced process. The mathematical solution, normally by means of computer-aid numerical methods, allows the corroboration of the assumptions and, eventually, the development of prediction tools for optimizing the different treatments.

In accordance to this, the primary objectives proposed for the present project "Physicochemical and numerical modeling of electrokinetics in inhomogeneous matrices" are:

1. to formulate a fundamental theory that mathematically explain the physicochemical processes taking place during electrokinetic treatments

2. to build a reliable and accurate numerical model which enables the prediction of the desired effects and the side effects effects in and on the materials from the treatments

A physicochemical model has been proposed based on the Nernst-Planck-Poisson system. The model includes the transport of water through the porous media, the

monitoring of the degree of saturation, the pH value and the porosity throughout the domain; and a comprehensive set of chemical and electrochemical reactions involving solid, gaseous and aqueous species and water in both the electrolyte and the solid structure. This coupled reactive-transport model, covering such a number of physical and chemical aspects in the process, is assumed an innovative contribution to the state of the art of modeling of electrokinetics processes. Furthermore, the physicochemical model is described in a generalized manner, so it can be used to simulate a wide range of electrokinetic treatments for different inhomogeneous matrices.

A numerical model has been built for the mathematical solution of the proposed physicochemical model. The numerical model is mainly based on a finite elements method for the integration of the transient system of partial differential equations coupled with a Newton-Raphson method for computing chemical equilibrium.

During the development of the proposed physicochemical and numerical model, different electrokinetic systems have been studied. Some worth mentioning investigations and the results drawn from the simulations are summarized below.

1. The electro-desalination treatment of bricks and other construction materials using a buffer substance enhancement was studied. Simulation-based analysis showed good prediction of the removal efficiencies and rates for chlorides nitrates and sulfates. Simulation thrown light on some aspects not easily observed experimentally, such as the chemical species distribution throughout the process or the possibility of precipitation of salts within the porous structure. It was found, for example, that formation of gypsum is a limiting factor in the desalination of sulfate-contaminated bricks or stones, and that there is a connection between the presence of magnesium and the capacity of buffering the alkaline front produced in the cathodic reaction.

2. Using the chemical equilibrium model or the reactive-transport combined model, some feasibility studies for the mobilization of specific contaminants were carried out. For example, speciation analysis of Pb in soil was studied for the selection of different extracting agents in order to design a combined acid enhanced with selective chelators EK treatment. Different extracting agents were tested using the speciation numerical model, such as EDTA, acetic acid, citric acid and nitric acid. Results showed that citric acid and EDTA are the extracting agent which increase more the solubility of Pb in soil, and that the efficiency of the process is strongly limited by the buffering capacity of the soil itself, not only because it determines the pH value, but also because there is a tendency of forming calcium citrate insoluble lead carbonate.

3. The proposed model was used for the simulation-based analysis of the transient formation of the diffuse layer of the electric double layer in the vicinities

of a reactive surface. In this case, the model was adapted to simulate a microscale system. Concentration profiles of the ionic species in the diffuse layer were obtained, satisfying not only the electrical balance between the electrolyte and the surface charge, but also the chemical equilibrium condition between the chemical species in the electrolyte. Apart from this new approach for the distribution of species under chemical equilibrium conditions, some conclusions were drawn from the simulations. For example, concentration profiles for the non-ionic species are formed at the vicinities of the charged surface as a result of the chemical interaction with the ionic species in the system. Results also show that the transient formation of electric double layers may be controlled by the kinetics of the surface reactions, and not by the electro-diffusion transport process.

The results summarized here are just a sample of the many possibilities offered by the simulation-based analysis that can be obtained using the proposed physicochemical and numerical model.

Resumé

Påtrykkes et elektrisk felt over et porøst materiale, vil kemiske forbindelser transporteres gennem elektrolytten, og der kan yderligere være transport af selve elektrolytten. Med baggrund i dette, er en række teknikker blevet udviklet med det formål at fjerne udvalgte forureningskomponenter eller injicere specifikke forbindelser i det porøse, faste materiale af varierende type.

Sådanne teknikker kaldes typisk for elektrokinetisk behandling. For de elektrokinetisk inducerede transportprocesser er den drivende kraft relateret til de koncentrationsgradienter og den ubalance i ionladning som dannes pga. de elektrokemiske reaktioner, som foregår ved elektroderne under påtrykning af det elektriske felt. I tillæg påvirkes de ikke-elektroneutrale elektriske dobbeltlag mellem elektrolyt og fast overflade af det inducerede elektriske potentiale, hvilket resulterer i transport. Transportprocesserne er i høj grad påvirkede af interaktioner mellem kemiske forbindelser i det heterogene system, enten opløste i elektrolytten, udfældede på de faste overflader eller adsorberede.

Fysisk-kemsike modeller danner den nødvendig baggrund for forståelse af de involverede processer, og udviklingen af en teoretisk ramme muliggør at inddrage de komplekse interaktioner, som foregår i enhver elektrokinetisk eller elektrokemisk induceret proces. Den matematiske løsning, ofte ved hjælp af computerunderstøttede numeriske metoder, tillader validering af antagelser og eventuelt udvikling af værktøjer til optimering af de forskellige behandlinger.

I baggrund i dette, er de væsentligste formål med dette projekt "Physicochemical and numerical modeling of electrokinetics in inhomogeneous matrices":

1. At formulere en fundamental teori som matematisk forklarer de fysiskkemiske processer som foregår under elektrokinetisk behandling

2. At bygge en pålidelig og præcis numerisk model, som muliggør forudsigelse af ønskede effekter og sideeffekter i og på materialerne som resultat af behandlingen

En fysisk-kemisk model baseret på Nernst-Planck-Poisson systemet er blevet udviklet. Inkluderet i modellen er transport af vand gennem det porøse medium, sammen med et antal kemiske og elektrokemiske reaktioner involverende faste, gasformige og opløste forbindelser i både vandfase og den faste fase. Kombinationen af elektrokinetisk transport model med kemiske reaktioner på denne måde er ikke set tidligere. Den

fysisk-kemiske model er beskrevet på en generel måde, så den kan bruges til simulering af elektrokinetisk behandling af inhomogene materialer i bred forstand.

En numerisk løsning er blevet udviklet, og den er hovedsagelig baseret på en finite elements metode til integration af det transiente system af partielle differentialligninger, i kobling med en Newton-Raphson metode til inddragelse af kemisk ligevægt.

Forskellige elektrokinetiske systemer er blevet studeret under udviklingen af den foreslåede fysisk-kemiske og numeriske model. De væsentligste af disse undersøgelser og de fundne resultater fra simuleringerne er sammenfattet nedenfor.

1. Elektro-afsaltning af mursten og andre porøse bygningsmaterialer blev studeret. I dette system anvendes et buffermateriale ved elektroderne. Simuleringsbaserede analyser viste en god forudsigelse af effektiviteten af saltfjernelse og hastighed for chlorider, nitrater og sulfater. Simuleringen belyste nogle aspekter, som ikke er nemme at observere eksperimentelt, så som fordelingen af kemiske forbindelser under hele processen og muligheden for udfældning af salte i den porøse struktur. F.eks. blev det fundet, at dannelsen af gips kan være en begrænsende faktor for afsaltning af sulfat-forurenede mursten eller natursten, og der er en sammenhæng mellem tilstedeværelsen af magnesium og bufferkapaciteten overfor den basiske front, som produceres ved katoden.

2. Ved at anvende den kemiske ligevægtsmodel eller den kombinerede reaktions- og transport model blev der udført nogle feasibility-studier for mobiliseringen af specifikke forureningskomponenter. En specieringsanalyse for bly i jord blev f.eks. udført med det formål at vælge forskellige ekstraktionskemikalier for at kunne designe en kombineret syreekstraktion og anvendelse af kompleksbindere under elektokinetisk behandling. Forskellige ekstraktionsmidler blev testet ved anvendelse af den numeriske model til speciereing, så som EDTA, eddikesyre, citronsyre og salpetersyre. Resultaterne viste, at citronsyre og EDTA var de ekstraktionsmidler, som i størst grad øgede opløseligheden af bly i jord. Yderligere blev det fundet, at effektiviteten af processen begrænses stærkt af selve jordens bufferkapacitet; ikke kun fordi den bestemmer jordens pH værdi men også fordi der er en tendens til dannelse af uopløselige blycarbonater.

3. Den foreslåede model blev anvendt til simuleringsbaseret analyse af den kortvarige dannelse af dannelse af det diffuse dobbeltlag i umiddelbar nærhed af en reaktiv overflade. I dette tilfælde blev modellen adapteret til at simulere et mikroskalasystem. Koncentrationsprofiler af ioner i det diffuse lag som opfyldte ikke alene den elektriske balance mellem elektrolyt og overflade ladning men også de kemiske ligevægtsforhold mellem kemiske forbindelser i elektrolytten blev opnået. I tillæg til denne nye tilgang til fordeling af ioner under kemiske ligevægtsforhold, blev der draget konklusioner på baggrund af simuleringer. F.eks.

bliver koncentrationsgradienter for ikke-ionformige specier dannet ved den ladede overflade som resultat af de kemiske interaktioner mellem ioner i systemet. Et andet resultat er at den hurtige dannelse af elektriske dobbeltlag kan blive kontrolleret af overfaldereaktionernes kinetik og ikke af elektro-diffusion transport processer.

De resultater som er opsummeret ovenfor er eksempler på de mange muligheder, som kan undersøges ved simuleringsbaserede analyser, når det udviklede fysisk-kemiske og numeriske model anvendes.

Contents

Table of Symbols

Symbol	Units	Description
$\mathbf{B}$	–	The gradient of the shape function
c_i	$\mathrm{mol\,m^{-3}}$	Chemical concentration referred to the volume of solvent
$\mathbf{C}_e$	m	Mass matrix (local)
$\mathbf{C}_\pi$	m	Mass matrix (for the property π in the entire domain)
$\mathbf{C}$	m	Mass matrix (for the global system)
D_i	$\mathrm{m^2\,s^{-1}}$	Diffusion coefficient
D_θ	$\mathrm{m^2\,s^{-1}}$	Water diffusivity coefficient
$D_{\theta,0}$	$\mathrm{m^2\,s^{-1}}$	Material characteristic parameter for water diffusivity
e	–	Index for the finite elements, $e = 1, 2, ..., N^e$
E	V	Redox potential
E^0	V	Standard redox potential
$\mathbf{E}$	–	Free charge density
$f_r(\mathbf{x})$	–	Chemical equilibrium function for the reaction r
F	$\mathrm{C\,mol^{-1}}$	Faraday constant
$\mathbf{f}_e$	$[\pi]\ \mathrm{m\,s^{-1}}$	Load/boundary vector (local)
$\mathbf{f}_\pi$	$[\pi]\ \mathrm{m\,s^{-1}}$	Load/boundary vector (for the property π in the entire domain)
$\mathbf{f}$	$[\pi]\ \mathrm{m\,s^{-1}}$	Load/boundary vector (for the global system)
$\mathbf{f}^\star$	$[\pi]\ \mathrm{m\,s^{-1}}$	Load/boundary vector (simplified matrix notation)
g_i	$\mathrm{mol}\,s^{-1}$	Rate of production of i
G_i	$\mathrm{mol\,m^{-3}\,s^{-1}}$	Rate of production of i per unit of volume
G_θ	$\mathrm{s^{-1}}$	Rate of production of water, Degree of saturation per second
i	–	Index for chemical species, $i = 1, 2, ..., N$
I	A	Electric current
$\mathbf{J}_i$	$\mathrm{mol\,m^{-2}\,s^{-1}}$	Flux term for the species i in the continuity equation
$\mathbf{J}_\theta$	$\mathrm{m\,s^{-1}}$	Flux term for the degree of saturation in the continuity equation

Symbol	Units	Description
k_e	$[k_e]$	Element characteristic parameter
K	$\mathrm{m^2\,s}$ or $\mathrm{m^2\,V^{-1}\,s}$	Transport coefficient
K^*	$\mathrm{m^2\,s}$ or $\mathrm{m^2\,V^{-1}\,s}$	Effective transport coefficient
$K_{eq,r}$	–	Equilibrium constant for the reaction r
$K_{\mathrm{e.o.}}$	$\mathrm{m^2\,V^{-1}\,s}$	Electroosmotic permeability
$\mathbf{K}_e$	$[k_e]\ \mathrm{m^{-1}}$	Conductivity matrix (local)
$\mathbf{K}_\pi$	$[k_e]\ \mathrm{m^{-1}}$	Conductivity matrix (for the property π in the entire domain)
$\mathbf{K}$	$[k_e]\ \mathrm{m^{-1}}$	Conductivity matrix (for the global system)
$\mathbf{K}^\star$	$[k_e]\ \mathrm{m^{-1}}$	Conductivity matrix (simplified matrix notation)
n_i	mol	Total amount of i in moles
N	–	Total number of chemical species
N^e	–	Total number of finite elements
$\mathbf{N}$	–	Shape function
M	–	Total number of chemical equilibrium reactions
p	–	Porosity
Q	–	Reaction quotient
r	–	Index for the chemical reactions ($r = 1, 2, ..., M$)
R	$\mathrm{J\,K^{-1}\,mol^{-1}}$	is the universal gas constant
U_i	$\mathrm{m^2\,V^{-1}\,s^{-1}}$	Ionic mobility
$\mathbf{u}$	$\mathrm{m\,s^{-1}}$	Fluid velocity
w	–	Weight function in the space domain
$\mathbf{x}$	–	Reaction extents vector
z_i	–	ionic charge
α	–	Integration constant (Newmark approach)
β	–	Integration constant (Newmark approach)
ε	$\mathrm{C\,V^{-1}\,m^{-1}}$)	water permittivity
ζ	V	Zeta potential
θ	$\mathrm{m^3\,m^{-3}}$	Degree of saturation
Θ	–	Integration constant (one time-step approach)
ϑ	–	Material characteristic parameter for water apparent diffusivity
μ	$\mathrm{N\,s\,m^{-2}}$	Viscosity of water
$\nu_{i,r}$	–	Stoichiometric coefficient of the species i in the reaction r
ξ_r	–	Extent of the reaction
π	$[\pi]$	Arbitrary property
ρ	$\mathrm{C\,m^{-3}}$	Charge density
τ	–	Normalized time
τ_c	–	Tortuosity-constrictivity factor
ϕ	V	Electric potential
ψ_i	V	Overpotential factors for the reduction reaction of i
$\omega(\tau)$	–	Weight function in the time domain

Part I

Dissertation

Chapter 1

Introduction and summary of the research

1.1 Objectives

When applying an electric field to a fine-porous moist material, transport of ionic species and water occurs. This means that transport of matter is possible in such dense materials where a pressure gradient may be inefficient.

Electrokinetics have been suggested for various purposes in civil, chemical, biochemical and environmental engineering. Nevertheless, the implementation of the methods has been slow even though very good results have been obtained in laboratory and pilot scale as, for example, the chloride removal from concrete to avoid reinforcement corrosion or the removal of heavy metals from contaminated soils. One major reason for the slow implementation is that the fundamentals of the physicochemical processes are not yet well understood, meaning that success or failure cannot be sufficiently foreseen prior to an action.

The PhD project "*Physicochemical and Numerical Modeling of Electrokinetics in Inhomogeneous Matrices*" is part of the research project "*Fundamentals of Electrokinetics in Inhomogeneous Matrices*", sponsored by the Danish Research for Technology and Production Science.

The primary aim of the overall project "*Fundamentals of Electrokinetics in Inhomogeneous Matrices*" is to identify the key processes in any electrokinetic (EK) treatment of fine-porous materials and to formulate a fundamental theory which enables precise prediction of the desired effects and side effects from the treatment.

The specific objectives achieved through the PhD project "*Physicochemical and Numerical Modeling of Electrokinetics in Inhomogeneous Matrices*" are summarized in the followings:

1. The mathematical representation of a generalized physicochemical model has been formulated for the description of the reactive-transport phenomena through porous media taking place in electrokinetics/electrochemically-induced treatments. The model takes into account:

    - Different ionic transport contributors, i.e. diffusion, ionic migration and advection.
    - Simultaneous transport of water, ions and non-ionic aqueous species in unsaturated moist porous media.
    - The effects of competitive electrochemical reactions at the electrodes.
    - Homogeneous and heterogeneous chemical reactions between the dissolved species in the electrolyte and the solid structure.
    - Changes in composition and porosity of the solid porous structure during the EK treatment.

The physicochemical model has been formulated in a generalized manner. As a result, the model can be used to describe both electrochemically-induced and free-diffusion transport processes thought porous media in several applications for civil, chemical, biochemical and environmental engineering fields, among others. In this context, the model proposed here is suitable for:

- Micro- and macroscale heterogeneous systems, composed as a combination of different sections of inhomogeneous solid matrices with their own composition and properties.
- Different electrical working conditions, i.e. constant electric current, constant current density, constant voltage, pulse discontinuous current or free-diffusion simulations.

2. A numerical model, i.e. a tailor-made computer program, has been built for the computer-aided solution of the abstract mathematical formulation. Some characteristics of the numerical model presented are:

   - It faithfully reproduces the described physicochemical model, i.e. the number of simplifications done to the physiochemical laws during the numerical implementation process is minimal.
   - The numerical implementation has been optimized to allow simulations with reasonable low computational time.
   - The numerical model is easily adaptable for simulating different systems with their own physicochemical properties, dimensions and components.

3. From the simulations run on specific electrokinetic treatments using the implemented numerical model, it is possible to:

   - Increase the understanding of the physicochemical laws that govern the electrokinetic phenomena.
   - Explore the simulated systems to gain new insights into the technology.
   - Optimize the existing experimental electrokinetic techniques.
   - Develop an engineering tool able to predict results, estimate the performance and optimize the working conditions for any electrokinetic treatment.

1.2 Introduction

Electrokinetics consists of the application of an external electric field for the mobilization of chemicals species through the pore electrolyte in a porous media.

Some authors distinguish between the general concept "electrochemically-induced transport", referring to the main physicochemical transport phenomena taking place under external electric fields, and the term "Electrokinetics" referring only to the transport phenomena which underlying source is related to the electric double layer between the electrolyte and the solids surfaces [Delgado et al. 2007]. Nevertheless, "electrokinetic transport" is still the most widely used term to denote this engineering field and it is, in many cases, accepted as a synonym of the electrochemically-induced transport in porous media.

EK applications have been used since beginnings of the 19^{th} century. The technology was set down in the field of soil remediation after the works presented by [Acar and Alshawabkeh 1993] and [Yeung and Mitchell 1993]. Since this branch of knowledge was originally engineered for the recuperation of contaminated soil, "Electrokinetic soil remediation" or just "Electrokinetic Remediation", abbreviated as EKR, are the most common terms referring to the EK applications.

Nowadays, the EKR technology is continuously developed. Recently, an increasing number of EK applications in the fields of civil, chemical, biochemical and environmental engineering have been proposed, out of the field of soil remediation. Some examples are the electrokinetic desalination (EKD) of construction materials, see e.g. [Ottosen and Rörig-Dalgaard 2007, 2009, Ottosen et al. 2010, Rörig-Dalgaard et al. 2012, Kamran et al. 2012]; or the electro-dialytic processes on ashes, chromate-copper-arsenate treated wood waste, sediments and sludge as e.g. [Jensen et al. 2007, Ottosen et al. 2007, Ribeiro et al. 2007, Kirkelund et al. 2009, Lima et al. 2010].

Furthermore, it was found a connection between the principles in EK phenomena and some other available techniques involving the transport of chemicals through porous media. There are techniques or processes involving reactive-transport through porous media, in which the driving-force is only a gradient of concentration (free-diffusion), as e.g. chloride diffusion through cement-based materials exposed to marine environments [Nielsen and Geiker 2003]. Standard desalination techniques, such as the use of poulticing or the submersion in low salted water, are also examples of this process.

In some other cases, an external electric field is applied for a specific purpose, producing EK transport as a side effect. For example, cathodic protection techniques on reinforced concrete consist of the application of a low level direct current to the reinforcement in order to bring about an alkaline environment and prevent the corrosion [Harris et al. 1997, Li and Page 1998, Jennings and Mansharamani 1999, Li and Page 2000, Castellote et al. 2000, Popov et al. 2008, Voinitchi et al. 2008, Bertolini

et al. 2009, Koster et al. 2010, Kamran et al. 2012]. This low level current will irremediably produce the migration of ions in the porous media, including chloride which is repulsed by the reinforcement, which acts as a cathodic electrode.

The status of the technique and the main physicochemical aspects of electrokinetics can be found in the book [Reddy and Cameselle 2009]. Additionally, in [Ottosen et al. 2008] and extensive revision of the techniques and its applications in different civil and environmental engineering fields is discussed.

Most of the published studies about the EK technology have been carried out following an experimental approach. Several feasibility studies have been published showing the performance of the technique depending on different parameters, such as the solid matrix characteristics (e.g. calcareous versus non calcareous soil or natural contaminated versus laboratory contaminated matrices), the electrical conditions (e.g. constant current, constant voltage or pulse current), and the target contaminant (e.g. heavy metals, organic contaminant or an specific anion).

Nowadays, most of the experimental works are focused on the development of the so-called enhanced EK techniques, which aim to improve the selective removal of a target contaminant, reducing the energy consumption and minimizing the side effects on the treated porous body. A review of different enhanced electrokinetics techniques can be found in [Yeung and Gu 2011].

A common conclusion from these specific feasibility studies is that the efficiency of the EK treatments frequently depends more on the chemical properties of the treated material and the target contaminants than on the applied electric conditions. As a result, the proposed models for EK transport should focus not only on the purely physical ionic transport process but also on the different chemical interactions.

Some physicochemical models have been published discussing the fundamentals of electrokinetics, as e.g. [Acar et al. 1995, Choi and Lui 1995, Yeung and Datla 1995, Alshawabkeh and Acar 1996, Jacobs and Probstein 1996, Alshawabkeh et al. 1999, Herruzo et al. 2000, Yeung 2006, Delgado et al. 2007]. Nevertheless, compared to the experimental-based investigations, the number of publications about numerical modeling of electrokinetics has been moderately small. Due to the large amount of coupled physicochemical phenomena taking place, simultaneously, during a EK process; and due also to the uncertainties in the parameters defining the constitutive equations, modeling of EK techniques is not straightforward.

Physicochemical models are a necessary basis for the understanding of the involved processes and the development of a theoretical framework able to take into account the complex interactions taking place in any EK process. The model solution, by means of computer-aid numerical methods, allows the corroboration of the assumptions and, eventually, the development of prediction tools for optimizing the different EK techniques.

For the present investigation, an important number of proposed physicochemical and numerical models have been reviewed and used as a reference. These models have been published by several authors who followed different approaches. Some of the most relevant are:

1. Models for the integration of the Nernst-Planck-Poisson system of equations or the Nernst-Planck equations coupled with the electroneutrality condition, see e.g. [Rubinstein and Segel 1979, Alshawabkeh and Acar 1996, Samson and Marchand 1999, Mahamet et al. 2007, Lu et al. 2010, Johannesson 2003, Sokalski et al. 2003, Johannesson 2009, Johannesson et al. 2009].

2. Models for reactive-transport including chemical reactions by assuming chemical equilibrium conditions, solving kinetic equations or a combination of both, as e.g. [Rubin 1983, Lichtner 1985, Wilson et al. 1995, Jacobs and Probstein 1996, Samson et al. 2000, Vereda-Alonso et al. 2004, Ribeiro et al. 2005, Javadi and Al-Najjar 2007, Vereda-Alonso et al. 2007, Al-Hamdan and Reddy 2008, Johannesson 2009, Rodriguez-Maroto and Vereda-Alonso 2009, Li et al. 2010].

Finally, in the appended papers and conference contributions collected in Part III, extensive literature reviews are included about the specific researches in which the publications are focused. In this context, different issues discussed, as: fundamentals of electrokinetics in [Paz-Garcia et al. 2011d, Paz-García et al. 2012], electric double layers models in [Paz-Garcia et al. Submitted 2012b], fundamentals of chemical equilibrium in [Paz-Garcia et al. Submitted 2012a], chemical equilibrium calculations and models in [Paz-Garcia et al. Submitted 2012a], finite elements modeling in [Paz-Garcia et al. 2011d, Paz-García et al. 2012 In press], surface complexation models in [Paz-Garcia et al. Submitted 2012b], EK desalination and coupling between moisture and ionic transport in [Paz-García et al. 2012 In press, Paz-Garcia et al. Submitted 2012c].

1.3 Summary of the research

Despite the generally accepted physicochemical model describing the transport of matter though porous media is somewhat simple and the transport contributors which described it have been accepted by different authors, the mathematical solution of the nonlinear system of differential equations is not easy, even by using sophisticated numerical methods. When chemical aspects are included for modeling the reactive-transport process, the solution becomes even more complicated.

Most of the numerical models published about EK transport or ionic diffusion through porous medium, normally simplify the continuity equations considering only the most important transport contributors. For example, the ionic migration term

is ignored in some free-diffusion problems. In some other cases, diffusion flow is sometimes ignored in electrochemically-induced transport, where the ionic migration becomes predominant. These simplified models provide approximate results that may be useful for the estimation of the behavior of the process and its efficiency in a general manner.

Since the concentration, the pH value, the degree of saturation and the porosity, among other parameters, vary during the process and along the domain, it is not straightforward to identify which terms are predominant in the long-term. This is the case, for example, when the acidic and alkaline fronts produced in the electrode processes meet each other. In this very narrow region, there is a extremely sharp pH profile where the concentrations gradients of protons and hydroxides may be several orders of magnitude higher than along the rest of the electrolyte. Therefore, in this narrow region neither diffusion nor ionic migration, may be considered as a predominant transport process.

The physicochemical model described in this project aims at being a generalized tool which allows the prediction of results and increases the understanding of the governing processes in electrokinetics. The computational model is congruent with the mathematical representation of the physicochemical model described. Thus, no simplifications of the model are done during the numerical implementation.

The model includes the main transport terms identified in electrokinetic and electrochemically-induced transport processes through partially-saturated porous media, that are diffusion, ionic migration and advection due to electroosmosis and to gradients of degree of saturation. In addition to this, the physicochemical model includes different chemical and electrochemical reactions, which may be easily adapted depending on the chemical species included in the studied system.

The model described in this PhD dissertation is the result of a continuous evolution of the same physicochemical model, progressively extended with new features after achieving an accurate numerical implementation. The verification of the model was done by comparison between simulation and experimental results.

Since one of the objectives of the project is the development of an accurate and reliable numerical model, an important effort has been paid on the optimization of the codes and routines. Simulations have been compared with already published experimental data instead of with new laboratory results, which would have required and important research time.

Next, the methodology and results of the PhD research are summarized. This research abstract is chronologically organized, and based on the published scientific papers, for a better monitoring of the results and the difficulties experienced and solved during the project.

1.3.1 Modeling of electrokinetic processes by finite elements integration of the Nernst-Planck-Poisson system of equations

In a first stage of the research, a physicochemical model for the electrochemically-induced transport of ions through porous media was proposed, based on the time-transient strongly coupled Nernst-Planck-Poisson (NPP) system (see Section 2.1). The proposed model and the procedures followed for the numerical implementation was published in the scientific paper [Paz-Garcia et al. 2011d].

A finite elements (FE) method was implemented and used for the numerical integration of the NPP model, following the ideas introduced in the theoretical and numerical models for ionic transport reported in [Johannesson 1999, 2003, Johannesson and Ottosen 2008, Johannesson 2009]. The novel scientific contribution in the model presented in [Paz-Garcia et al. 2011d] with respect to the aforementioned published literature, is that it includes different chemical aspects related to electrokinetic transport, as e.g. the electrochemical processes at the electrodes.

Electrochemical reactions at the electrodes, where the electric current is converted into an ionic current or vice-versa, are necessary to establish the driving-force in any electrochemically-induced ionic transport process (See Section 2.2.1). The numerical model is built in such a manner that the electrode processes can be adapted depending on the external electric conditions, as discussed in [Paz-Garcia et al., 2010] where simulations under constant voltage and constant DC current were compared. The model can also be used for free-diffusion simulations, i.e. with no external electric field (See Section A.1).

In this first phase of the project, the transport of ions due to advective electroosmotic flow was included, which is assumed essential in many EK treatments. The chemical equilibrium concept was introduced, as a first approach to the chemical reactivity of the system, with the water auto-ionization equilibrium reaction. Assuring water equilibrium makes possible monitoring the pH changes during the process, which is one of most important parameters in any EK treatment.

This physicochemical and numerical model presented in this article can be seen as the cornerstone for the PhD project. Most of the physicochemical laws were discussed, and the numerical approaches were enhanced and optimized in the subsequent investigations.

1.3.2 Feasibility study of the use of different extractant agents in the remediation of a mercury contaminated soil from Almadén

The efficiency of the EK treatments depends not only on the physical properties of the porous structure but also on the chemical properties of the solid matrix and the target contaminants. Experimental and theoretical feasibility studies are necessary to determine which contaminants are mobilized and which enhanced techniques must be used in any case.

The scientific paper [Subires-Munoz et al. 2011], was the result of a collaboration with the Department of Chemical Engineering of the University of Málaga (Spain). In [Subires-Munoz et al. 2011] experimental and modeling work was carried out for the comparison of iodide (I^-), nitric acid (HNO_3), Ethylenediaminetetraacetic acid (EDTA) and thiosulfate $\left(S_2O_3^{-2}\right)$ for the selective removal of mercury from soil using extracting agent enhanced EKR techniques.

The extracted agent enhanced EKR technique consists of the use of some specific chelator for the selective removal of contaminants. The chelator has the ability to create an soluble aqueous complex with the target contaminant. According to this, contaminants that tends to form precipitated species can be selectively removed from the solid matrix.

In this paper, the risk assessment of the contamination and the feasibility study of the remediation were based on a standard sequential extraction procedure (SEP) together with lixiviation tests. Results obtained allow the prediction of the mercury removal reached in bench scale tests of the flushing technique.

In addition to this, the weak acid soluble fraction in the soil after each treatment was observed to be much higher than before the treatment, which may be easier to be treated by a subsequent remediation technique, such as acid-enhanced EKR treatment, in order to increase the removal efficiency.

From the point of view of the development of a generalized reactive-transport model, the participation in this collaborative work led to a better understanding of the influence of the chemical aspects on the efficiency of any electrokinetic treatment. For example, the speciation of the contaminants strongly depends on the pH of the electrolyte, which in turn may affect the porous structure and vice-versa. The study of the reactivity of the chemical system should take into account not only the contaminants, but also the other species in the electrolyte and the porous solid structure.

1.3.3 A generalized model for transport of contaminants in soil by electric fields

The scientific paper [Paz-García et al. 2012], was published as the result of the research stay in the Department of Civil and Environmental Engineering at Northeastern University, Boston, Massachusetts, USA.

In this investigation, a physicochemical model is proposed for the electrokinetic removal of contaminants in soil by an acid enhanced EKR technique. The enhanced model is used to simulate electrokinetic cleanup of lead and copper contaminants at an army firing range. Acid enhancement is achieved by the use of adipic acid to neutralize the basic front produced for the cathodic electrochemical reaction.

The physicochemical model proposed in this investigation is based on the integration of a set of continuity equations for the chemical species in the system. In this case, the electroneutrality condition is used, instead of the Poisson's equation, for coupling between the electric potential in the electrolyte and the ionic concentrations.

In contrast to the models presented in [Paz-Garcia et al. 2011d, Paz-García et al. 2012 In press, Paz-Garcia et al. Submitted 2012c], the physicochemical model presented in this investigation is based on a saturated soil, in terms of water content. Therefore, advective flow due to hydraulic gradients is included in the physicochemical model instead of the flow due to gradients of degree of saturation used in the other cases.

The participation in this collaborative work brought new and useful insights with respect to the chemical aspects of the process and the strategies for coupling chemical reaction with ionic transport in a reactive-transport model.

1.3.4 Computing chemical equilibrium systems with an algorithm based on the extent of the reactions

Based on the experience gained in the aforementioned collaborations, a mathematical and numerical model for computing multi-species chemical equilibrium systems was developed.

Modeling of chemical reaction systems and, in particular, its numerical implementation, are not straightforward tasks. Furthermore, in order to satisfactory couple reaction and transport processes, the computer-aided numerical solution must be simultaneously precise and computationally fast. In the transport process finite elements numerical model, the concentrations in any transient are calculated simultaneously for the entire discretized domain by means of algebra of matrices. In contrast, the chemical equilibrium calculations have to be computed node-by-node. Consequently, in a reactive-transport numerical model, the computational time may increase several orders of magnitude with respect to a model without chemical equi-

librium. If the chemical equilibrium module is not fast enough, the numerical solution may get unfeasible even for the most powerful computers available today.

According to this, an huge effort was carried out for the optimization of the chemical equilibrium module, which was submitted for publication in [Paz-Garcia et al. Submitted 2012a]. This scientific paper describes with detail the mathematical and numerical model for chemical equilibrium computing. The model can be used as a tool for batch equilibrium reactions, but is is specifically designed to be coupled with the transport process model for the reactive-transport modeling of electrokinetics. Heterogeneous precipitation/dissolution reactions and the formation and release of gas bubbles are some of the phenomena foreseen in the model. The latter aspect is not normally included in standard chemical equilibrium models not specifically designed for reaction in porous media.

An important number of chemical equilibrium software is available. Nevertheless, the model presented here contains advantages compared to this available software with respect to the overall reactive-transport model, since:

1. It is completely compatible with the Nernst-Planck-Poisson system or equations, as it does not modify the ionic charge balance during the calculations.

2. It is completely compatible with the finite element method used for the numerical solution of the transport process. It is also applicable to simulations on two- and three-dimensional domains without any modification.

3. As built in the same programing language, Matlab ®, the reactive-transport model is completely coupled.

Furthermore, the model is based on the reaction extents as state variables, which means that it is possible to be further developed to include chemical kinetics aspects as explored in [Paz-Garcia et al. Submitted 2012b].

1.3.5 Modeling of electrokinetic desalination of bricks

In this stage of the research, the model was extended in two directions: First, the chemical equilibrium module and the transport module were coupled in a single reactive-transport model. Second, it was accomplished the coupling between the simultaneous transport of moisture and aqueous species through unsaturated porous media.

The numerical implementation of the transport of moisture and its effect in the advective transport of aqueous species using a finite elements method was described in [Paz-Garcia et al. 2011a].

Different physicochemical phenomena affects to the water content in porous media during an EK process. For instance, water dissociates at the electrodes due to

the electrolysis reactions. In the region where the acidic and the alkaline front collide, water is formed by chemical reaction. Due to the continuous release of gaseous H_2 and O_2 in the electrode processes, the water content in the porous media would always be in moisture unsaturated conditions, unless a source of water is incorporated to the experimental setup.

The transport of water in the media is modeled as a combination of different physical phenomena, were capillary forces are the more important. In addition to this, electroosmotic flow has also been included, since it is crucial in any electrokinetic treatment.

In [Paz-García et al. 2012 In press], the coupled reactive-transport model with moisture transport were used to simulate an EKD treatment for chloride removal from contaminated bricks. In order to validate the numerical model, results from simulations were compared to experimental results. The comparison showed that the model is able to satisfactory predict results from EKD treatments. In this work, some enhancements are propose to optimize the technique consisting of using a carbonated clay buffer substance at the electrodes.

This research is, therefore, a consolidation of the physicochemical model and its numerical implementation. Results from simulations were consistent with those obtained experimentally. Simulation-based analysis increase the understanding of the procedures and allow the optimization of existing techniques.

1.3.6 Modeling of the formation of electric double layers including chemical reaction effects

As mentioned before, the term "electrokinetic transport" is sometimes reserved to the transport phenomena which underlying source is the interaction between the electrolyte and the charged surface of the porous structure or the suspended particles, i.e. electroosmosis and electrophoresis. This kind of EK transport is related to the existence of the so-called electric double layer, which is a microscale physical phenomenon that produces a macroscale transport effect.

Transport of matter due to electroosmotic flow is one of the most important aspects in electrokinetic phenomena. Electroosmosis is essential, for example, in the transport of non-ionic species such as organic contaminants in soil or other porous media. It is also predominant in any transport phenomena of low concentrated electrolytes.

In [Paz-Garcia et al. Submitted 2012b], a microscopic study of the formation of an electric double layer is done using the physicochemical and numerical model developed in the project. The electric double layer model incorporates different chemical aspects, such as the chemical equilibrium between ions in the electrolyte and a surface

complexation reaction determining the surface charge and electric potential. Chemical aspects are not included in standard models for electric double layers.

Some important aspects can be highlighted from this research. First, the versatility of the model is demonstrated, as it is shown its validity not only for macro- but also for microscale problems. Second, the conclusions from the microscale study are applicable to macroscale models, as done in [Paz-Garcia et al. Submitted 2012c], where the electroosmotic transport is modeled with a variable electroosmotic permeability based on the results from [Paz-Garcia et al. Submitted 2012b]. Finally, in this research the chemical reaction is modeled as a combination of fast reversible reaction, under the assumption of chemical equilibrium, and slow reversible reaction, determined by their kinetic equations.

In microscopic models, the transport and the kinetic rates are in such an order of magnitude that chemical heterogeneous equilibrium may not be a valid assumption. Consequently, the surface reactivity is modeled using a kinetic equation based on published data, while only aqueous species are assumed under chemical equilibrium.

Results show that the formation of an electric double layer may be dominated by the kinetic of the surface reaction more than the transport rates of the ions in the electrolyte. This conclusion may have important impact on those treatments based on electroosmotic transport, as well as when using AC current or pulse DC current.

1.3.7 Simulation-based analysis of the differences in the removal rate of chlorides, nitrates and sulfates by electrokinetic desalination

The research line about modeling of electrokinetic desalination treatments, presented in [Paz-García et al. 2012 In press], was continued in the paper [Paz-Garcia et al. Submitted 2012c] and the conference contribution [Paz-Garcia et al. 2011b].

In this investigations, the buffer substance enhanced electrokinetic desalination technique was theoretically studied for an optimization of the existing treatment. In this context, a variation of the experimental setup is proposed consisting of using electrodes compartments open to the atmosphere to avoid the accumulation of gases that may produce hydraulic gradients flows and overpotential polarization effects.

Chlorides, nitrates and sulfates are considered the main responsible for salt-induced decay on building materials and sculptures. The study carried out in [Paz-Garcia et al. Submitted 2012c] aims at explaining the lower removal efficiency of sulfate with respect to the other two anions. Simulation results are congruent with those obtained experimentally. Simulations suggest that the differences in the removal rate and efficiency are mainly due to the chemical reactivity of the target ions. In particular, it is observed that sulfates tend to precipitate in the form of gypsum when calcium is present in the system. In the buffered substance enhanced system, a calcium

front, that travels from anode to cathode, is formed as the result of the dissolution of calcium carbonate in the buffering process. In addition to this, it was observed a relation between the presence of magnesium in the chemical system and the buffering capacity with respect to the alkaline front produced in the cathodic reaction.

In this model, an innovative and more realistic approach for modeling the simultaneous oxidation of water and chloride in the anodic reaction is described. Overpotential factors are included, to favor the production of chlorine with respect to the oxygen. Chlorine gas formation is experimentally observed in most of the electrodesalination treatments involving chlorides.

In this simulation-based theoretical study, the proposed physicochemical and numerical model was eventually used as a tool for predicting results and for optimizing the existing experimental techniques. Results from this investigation encourage the authors to further simulation-based analysis on existing techniques.

1.3.8 Future work

Two-dimensional model

As the transport process takes place mainly along the straight line between the two electrodes used to produce the ionic current, one-dimensional models for electrokinetic treatments normally gives sufficiently good results. Therefore, in the appended papers, the system has been simplified to a one-dimensional domain.

In some situations, the study of two-dimensional systems may be of interest. In [Paz-Garcia et al. 2011c], for example, the two-dimensional numerical model was introduced for the study of the asymmetrical process taking place in the electrodesalination of a brick wall in which the electrodes are placed in the same facade of the wall.

The proposed physicochemical reactive-transport model, explained in Chapter 2, is described in such a manner that it is suitable for one-, two- and three-dimensional problems. It is possible to adapt the FE numerical model for the solution of two- and three-dimensional models. However, two-dimensional finite elements methods are considerable slower in terms of computational speed. Numerical procedures for the one-dimensional model, explained in Chapter 3, have been optimized to reduce the computational time required.

The implementation of a computationally optimized two-dimensional finite elements method is proposed as an interesting enhancement of the generalized model presented here. Therefore, in Appendix A.4, an introduction of two-dimensional finite elements implementation for the ENPP reactive-transport model is included. With two-dimensional models, the range of EK treatments that can be simulated increases significantly.

Chemical kinetic rate dominated systems

Reactive-transport models presented in [Paz-Garcia et al. 2011b,d,c, Paz-García et al. 2012 In press, Paz-Garcia et al. Submitted 2012b,S] are based on the chemical equilibrium assumption as explained in [Paz-Garcia et al. Submitted 2012a]. That is, the transport rates are assumed slow with respect to the chemical reaction rates and, therefore, reversible reactions are assumed in constant chemical equilibrium state during the process.

Despite it is mathematically possible, including the kinetic equations in the govern equations results in a very complicated system to be solved due to the nonlinearity of the rate equations. This is specially true when the orders of magnitude of the kinetic rates differ between each other and between the transport rates. Moreover, rate laws for specific chemical systems are not easily found in literature and they have to be studied experimentally, which is not a straightforward task in any multi-species system.

In [Johannesson 2009], a model for the numerical integration of the Nernst-Planck equation including chemical kinetic equations in the generation term was described. In [Paz-Garcia et al. Submitted 2012b], where a microscopic model for the formation of electric double layers was discussed, chemical kinetics was included for the heterogeneous surface reaction, while the condition of chemical equilibrium was accepted for the species at the electrolyte. In microscopic systems, the representative length and the time-steps used for the transient integration are considered too small to accept the chemical equilibrium assumption for heterogeneous reactions. The combination of the chemical equilibrium assumption for sufficiently fast reversible reactions with the chemical kinetic equation for slow reactions resulted in a practical solution in terms of allowing a sophisticated numerical solution leading to accurate simulation results.

A generalized numerical implementation of the chemical equilibrium reactive-transport model including kinetic rate equations for selected slow reactions is proposed as a future enhancement of the model presented in this dissertation. This enhancement would increase the realism of the results and the range of potentially studied systems, as e.g. EKR treatments of organic contaminated soil.

Chapter 2

The physicochemical model and its mathematical representation

2.1 Transport phenomena

The conservation of mass equation in differential form, referred to a microscopic control volume and for a solute chemical species (as e.g. an ion) is expressed as:

$$\frac{\partial c_i}{\partial t} = -\nabla \mathbf{J}_i + G_i \tag{2.1}$$

where $i = 1, 2, ..., N$ is an index for the chemical species, N is the total number of chemical species, c_i ($\mathrm{mol\,m^{-3}}$) is the concentration referred to the volume of solvent (water), $\mathbf{J}_i$ ($\mathrm{mol\,m^{-2}\,s^{-1}}$) is the flux term and G_i ($\mathrm{mol\,m^{-3}\,s^{-1}}$) is the rate of production of i per unit of volume.

In electrochemically-induced transport of chemicals through porous media, the flux term $\mathbf{J}_i$ is, indeed, a combination of different transport contributors including diffusion, ionic migration and several advective terms such as electroosmosis. In the following sections, these transport contributors are explained.

2.1.1 Electro-diffusion transport

Fick's law of diffusion postulates that the flux of matter goes from regions of higher concentration to regions of lower concentration with a magnitude that is proportional to the concentration gradient. The flux due to diffusion is described by the empirical constitutive equation:

$$\mathbf{J}_{i,\,\mathrm{diff.}} = -D_i \nabla c_i \tag{2.2}$$

where D_i ($\mathrm{m^2\,s^{-1}}$) is the diffusion coefficient or diffusivity and the minus sign indicates that the flux goes from higher to lower concentrations.

Fick's law of diffusion is valid for the transport of non-charged species such as gases or non-ionic aqueous complexes. When considering the transport of charged species, as e. g. ions, the effects of the electrostatic forces between them have to be taken into consideration. Different ions have different transport rates. Therefore, during a free-diffusion process, where the only driving-force is a gradient of concentration, electric unbalances arise leading to an electric potential in the electrolyte. This electric potential is typically denoted as diffusion potential and the transport process accounting for the electrostatic interaction of ions is denoted as electro-diffusion phenomena [Mitchell and Soga 1976, Yeung and Mitchell 1993].

Electromigration, or ionic migration, refers to the transport of ions and charged small particles due to the electrostatic forces without an underlying source related to the existence of an electric double layer. Electromigration is accepted to be proportional to the ionic concentration, the gradient of electric potential in the electrolyte and a transport coefficient denoted as ionic mobility U_i ($\mathrm{m^2\,V^{-1}\,s^{-1}}$) as:

$$\mathbf{J}_{i,\,\mathrm{e.m.}} = -U_i\, c_i \nabla\phi \tag{2.3}$$

In dilute solution, the ionic mobility and the diffusion coefficient are related by the Nernst-Einstein equation [Yeung 2006, Tankovsky and Syrakov 2009], as:

$$U_i = \frac{z_i\, F}{R\, T}\, D_i \tag{2.4}$$

where z_i (dimensionless) is the ionic charge (in mol of electrons per mol of compound), F ($\approx 96\,485\,\mathrm{C\,mol^{-1}}$) is the Faraday constant, T (K) is the absolute temperature and R ($\approx 8.314\,\mathrm{J\,K^{-1}\,mol^{-1}}$) is the universal gas constant.

The ionic mobility coefficient may have positive or negative sign as it depends on the ionic charge. In free-diffusion processes, ionic migration transport takes place counteracting the diffusion, in order to reduce the electric potential (diffusion potential) in the system and to keep the electroneutrality condition. The constitutive equation that describes the transport of ionic species is, therefore, a combination of diffusion and electromigration fluxes, and the overall process is denoted as electro-diffusion transport.

$$\mathbf{J}_i = -D_i \nabla c_i - U_i\, c_i \nabla\phi \tag{2.5}$$

2.1.2 Nernst-Planck equation

When the conservation of mass, Eq. (2.1), is described using the electro-diffusion flux term, Eq. (2.5), is denoted as Nernst-Planck equation (NP) :

$$\frac{\partial c_i}{\partial t} = -\nabla\left(\mathbf{u}\, c_i - D_i \nabla c_i - U_i\, c_i \nabla\phi\right) + G_i \tag{2.6}$$

where $\mathbf{u}$ ($\mathrm{m\,s^{-1}}$) is the fluid velocity which induces advective transport on the aqueous species.

EK treatments are specially useful for the transport of matter in porous systems in which the hydraulic flow due to pressure gradients is inefficient. Consequently, the transport due to pressure gradient is not included in this model. The flow of moisture through the unsaturated media is modeled as a combination of transport due to saturation degree gradients and electroosmosis, as explained in Sections 2.1.5 and 2.1.6.

Inhomogeneous matrices are solid porous structures not uniform in their physicochemical properties. A porous solid matrix is inhomogeneous, for example, if the composition, the porosity and the water content depend on the position. In addition to this, a solid matrix is inhomogeneous if the cross-sectional area (in one-dimensional problems) or the thickness (in two-dimensional problems) changes in the position, or if it is composed by a set of homogeneous sub-matrices. Frequently, due to the asym-

metry of the system, a matrix initially homogeneous becomes inhomogeneous during the process.

In order to properly model the transport of matter through porous inhomogeneous matrices in a generalized manner, all addends in the Nernst-Planck equation are referred to the assumed-constant volume of heterogeneous matrix, i.e. the volume of solid plus the volume of available pore, denoted as matrix volume.

Let p (dimensionless) be the porosity (pore volume to total volume ratio) and θ (dimensionless) be the volumetric water content (water volume to pore volume ratio). Let us consider that pore solution is dilute enough to consider the density of the electrolyte equal to the density of water. The Nernst-Planck equation is redefined as:

$$\frac{\partial\left(p\theta c_i\right)}{\partial t} = -\nabla\left(p\theta\mathbf{u}c_i - p\theta D_i\nabla c_i + p\theta U_i\, c_i\nabla\phi\right) + p\theta G_i \tag{2.7}$$

2.1.3 Poisson's equation

In any control volume of an electrolyte, the electrostatic forces between ions keep the electrolyte in electrically neutral conditions or with a very low electric unbalance. This tendency is known as electroneutrality [Rubinstein, 1990]. In this context, the electric balance in such a control volume of electrolyte is, indeed, an ionic charge balance and it is denoted as charge density, ρ ($\mathrm{C\,m^{-3}}$), calculated as:

$$\rho = F\sum c_i\, z_i \tag{2.8}$$

From the standard definition of the differential form of the Gauss' law in the absence of changing magnetic field, a relation between the electric potential and the free charge density in the electrolyte is obtained, denoted as the Poisson's equation in electrostatics [Johannesson 2010a, Pamukcu 2009].

$$\varepsilon\nabla^2\phi = -\rho \tag{2.9}$$

where ε ($\mathrm{C\,V^{-1}\,m^{-1}}$) is the permittivity in water, defined as a measure of the resistance that is encountered when forming an electric field in a medium.

The Nernst-Planck-Poisson model consists of N Nernst-Planck equations, Eq. (2.7), coupled with the Poisson's equation, Eq. (2.9). This transient system of nonlinear partial equations is strongly coupled between the electric potential and the aqueous concentration and it is the most accepted model or the transport of matter through porous media [Pamukcu 2009, Johannesson 2010b, Lu et al. 2010].

2.1.4 Effective transport coefficients

The NP equation, Eq. (2.6), is defined for the transport through an ideal cylindrical capillary-tube. In real porous media, the effects of non-ideal pores have to be taken into account.

Transport coefficients listed in standard databases, such as in [Vanysek 2007], are defined for dilute electrolytes. In not-ideal systems, transport processes are hindered by the physical properties of the porous media. These transport coefficients, are denoted as apparent or effective transport coefficients.

There is not consensus about how to calculate effective transport coefficients from the coefficients in ideal conditions. As a general rule, it is accepted that the parameters that affect to the transport of matter through porous media are the porosity, p, the saturation degree, θ, the tortuosity and the constrictivity.

Tortuosity (dimensionless) is a measure of the actual distance covered through the porous structure and the straight line distance, as a consequence of the curvature of the capillary tube. The constrictivity (dimensionless) is a measure of the flow velocity hindering due to the the formation of bottlenecks as a consequence of cross-sectional area variations in the capillary tubes. See the examples in Fig. 2.1.

It is difficult to quantify these physical parameters. As a result, a combined tortuosity-constrictivity factor τ_c (dimensionless) is defined, grouping the simultaneous effects of the tortuosity and the constrictivity of the porous structure.

The tortuosity-constrictivity factor affects to all those constitutive empirical equations referred to a control volume. It is typically assumed as a constant and included in the effective transport coefficient. According to this, a generalized description of the effective transport coefficients is suggested in this model consisting of:

$$K^* = \frac{p\,\theta}{\tau_c} K \tag{2.10}$$

where K is a transport coefficient.

2.1.5 Advection due to gradients of the degree of saturation

Moisture transport in unsaturated porous media is due to a combination of different phenomena where capillary forces are accepted as the main driving-force [Janz 1997, Pachepsky et al. 2003, Roels et al. 2003, Nguyen et al. 2008, Johannesson et al. 2009, Johannesson and Janz 2009]. Accordingly, the transport of the electrolyte solution through unsaturated porous medium is modeled by means of the Richard's equation [Richards 1931]. Richard's suggested that the Darcy's law originally devised for saturated flow in porous media is also applicable to unsaturated flow in porous media [Pachepsky et al. 2003].

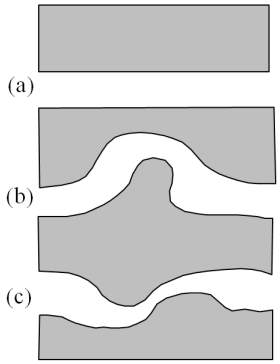

Figure 2.1: a) Ideal capillary-tube b) Tortuous capillary-tube c) High constrictivity capillary-tube

The fluid velocity related to the transport of water by gradients of saturation degree, based on an adapted Richard's equation, is:

$$\mathbf{u}_{\text{Richards}} = -D_\theta \nabla \theta \tag{2.11}$$

$D_\theta \left(\text{m}^2\,\text{s}^{-1}\right)$ is the water diffusivity coefficient, which is a characteristic material parameter.

2.1.6 Advection due to electroosmotic flow

Electroosmotic flow is the motion of liquid induced by an applied electric potential across a porous material. Electroosmotic advection is essential, for example, for the migration of non-ionic species through porous media, such as the removal of organic contaminants from soil.

The origin of electroosmotic transport is related to the existence of the electric double layer in the interface of the porous surface and the electrolyte [Dongqing 2004, Lyklema 2005]. According to this, electroosmosis and electroosmotic advection are strictly speaking EK processes [Delgado et al. 2007].

Most of the porous solid matrices have some surface charge. Consequently, ions with the opposite charge of the surface are attracted forming a narrow region where the electrolyte is not electrically neutral, denoted as diffuse layer.

In an electrochemically-induced treatment, ions in the diffuse layer move as a bulk towards the electrode of opposite charge due to ionic migration forces. This phenomenon produces friction forces on the electrolyte, which moves in the same direction by electroosmosis and produces electroosmotic advection on the dissolved species.

In macroscopic systems, electroosmotic velocity of the fluid is assumed to be proportional to the gradient of electric potential and a transport coefficient, $K_{\text{e.o.}}$ ($\text{m}^2\,\text{V}^{-1}\,\text{s}$), denoted as electroosmotic permeability.

$$\mathbf{u}_{e.o.} = -K_{\text{e.o.}}\nabla\phi \tag{2.12}$$

The electroosmotic permeability coefficient depends on the magnitude of the zeta or electrokinetic potential ζ (V), which is the electric potential in the region close to the solid surface where the migration diffuse layer occurs [Lyklema 2005].

The Helmholtz-Smoluchowski (HS) model is the most accepted relation between the zeta potential and the electroosmotic permeability [Acar and Alshawabkeh 1993, Yeung and Datla 1995].

$$K_{\text{e.o.}} = -\frac{\varepsilon}{\mu}\zeta \tag{2.13}$$

where μ ($\text{N}\,\text{s}\,\text{m}^{-2}$) is the viscosity of water. The minus sign indicates that negative surface potential produces direct electroosmotic flow, i.e. from anode to cathode.

The zeta potential is not constant as it depends on the concentration and composition of the electrolyte and the chemical properties of the solid surface. Most of the models accounting for electroosmotic flow consider a constant electroosmotic permeability coefficient equal to the optimal experimentally observed value, which is in a short range of 10^{-8} to 10^{-9} ($\text{m}^2\,\text{s}^{-1}\,\text{V}^{-1}$).

2.1.7 Extended Nernst-Planck-Poisson model

According to the previous definitions, the flow of moisture through the unsaturated media is modeled as a combination of transport due to gradients of degree of saturation and electroosmosis as:

$$\mathbf{u} = -D_\theta\nabla\theta - K_{\text{e.o.}}\nabla\phi \tag{2.14}$$

The Nernst-Planck equation for the transport the aqueous species accounting for the advective term is redefined as:

$$\frac{\partial\left(p\theta c_i\right)}{\partial t} = -\nabla\left(-\frac{p\theta}{\tau_c}c_i D_\theta\nabla\theta - \frac{p\theta}{\tau_c}D_i\nabla c_i - \frac{p\theta}{\tau_c}\left(U_i + K_{\text{e.o.}}\right)c_i\nabla\phi\right) + p\theta G_i \tag{2.15}$$

where the tortuosity-constrictivity hindering factor has been included in the constitutive empirical equations, as the gradient of the property is defined for a tortuous control volume, instead of a ideal capillary-tube.

Using the definition of the effective transport coefficient described in Section 2.1.4, the Nernst-Planck equation for macroscale non-ideal porous systems is:

$$\frac{\partial\left(p\theta c_i\right)}{\partial t} = -\nabla\left(-c_i D_\theta^* \nabla\theta - D_i^* \nabla\left(c_i\right) - \left(U_i^* + K_{\text{e.o.}}^*\right) c_i \nabla\phi\right) + p\theta G_i \tag{2.16}$$

where now D_i^*, U_i^* and $K_{\text{e.o.}}^*$ are respectively the diffusion, ionic migration and electroosmotic permeability effective coefficients, defined as explained in Eq. (2.10). In turn, it has been experimentally demonstrated that the moisture diffusivity has a strongly nonlinear dependence on the degree of saturation. Accordingly, the effective moisture diffusivity is modeled as:

$$D_\theta^* = \frac{p\theta^\vartheta}{\tau_c} D_{\theta,0} \tag{2.17}$$

where ϑ (dimensionless) and $D_{\theta,0}$ are material characteristic.

It is possible to calculate the advective flux of aqueous species without including the water transport in the system of equations. Nevertheless, water transport has many important implications in most of the EK treatments. For example, electroosmotic transport of fine porous media may produce a dry region, normally at the vicinities of one of the electrodes, producing the open-circuit of the ionic/electric current system. According to this, and taking into account that one of the goals of the project is the proposal of a generalized model able to predict most of the EK treatments, the NPP system has been extended to include in the chemical system the water transport and its chemical reactivity.

Let us consider that the first chemical species in the set of N chemical species, $i = 1$ is assigned to the water i.e. $c_1 = c_{\text{H}_2\text{O}}$. As the concentrations c_i are referred to the volume of water, the water concentration, $c_{\text{H}_2\text{O}}$ is a constant depending only on the temperature. According to this, the diffusion term for water is null and the constant $c_{\text{H}_2\text{O}}$, which is common in the other transport terms, may be canceled from the continuity equation. In addition to this, the electromigration term for water is zero, as the ionic charge of water is zero. As a result, a transport equation for the chemical species water is, indeed, a continuity equation for the saturation degree, referred to the total matrix volume as:

$$\frac{\partial\left(p\theta\right)}{\partial t} = -\nabla\mathbf{J}_\theta + p\theta G_\theta \tag{2.18}$$

where the generation term on the water content G_θ (s^{-1}) is defined as the rate of production of water G_{H_2O} ($\text{mol}\,\text{m}^{-3}\,\text{s}^{-1}$) divided by the constant value $c_{\text{H}_2\text{O}}$ ($\text{mol}\,\text{m}^{-3}$). The flux term, $\mathbf{J}_\theta$ ($\text{m}\,\text{s}^{-1}$), is defined as:

$$\mathbf{J}_\theta = -D_\theta^* \nabla\theta - K_{\text{e.o.}}^* \nabla\phi \tag{2.19}$$

The extended Nernst-Planck-Poisson (ENPP) model for a chemical aqueous system with N chemical species, consists of a water continuity equation, Eq. (2.18),

$(N-1)$ Nernst-Planck equations for the $(N-1)$ aqueous species , Eq. (2.16), and the Poisson equation in electrostatics, Eq. (2.9).

2.2 Chemical reaction

The ENPP model includes a generation term, G_i, which is the rate of production of i per unit of volume and it is, therefore, related to the formation/consumption due chemical reactions. Nevertheless, the solution of the ENPP system of equations accounting for the chemical kinetics equations is extremely difficult, particularly from the point of view of the numerical implementation.

Chemical kinetic equations are strongly nonlinear which makes the solution of the system of equations very complicated. In addition to this, the transformations due to chemical reaction have very different kinetic rates, changing from several order of magnitude with respect to each other, and compared to the transport rates than govern the purely-physical transport process. According to this, different approaches have been taken in this thesis depending on the nature of the chemical reaction, that can be summarized as follows:

1. Electrochemical reactions are implicitly included into the ENPP model of equations as incoming or out-coming fluxes of ions at the electrodes. As the electric current is converted into an ionic current in the electrode processes, the kinetic rate of the electrochemical reactions is determined by the external electric conditions and the conservation of energy principle.

2. Those reversible chemical reactions that are fast enough, in both direct and reverse directions, to assume that they can reach the chemical equilibrium condition in any time-step of the numerical integration of the transient system, are modeled using a coupled module for computing chemical equilibrium.

3. Irreversible reactions and reversible reactions that are too slow to satisfy the assumption of chemical equilibrium, are modeling using their chemical kinetic equation.

4. Gas/liquid equilibria is modeled based in the Henry's law. Kinetic rates for the equilibrium of the gases and the volatile aqueous species are very slow compared to the transport rates. Nevertheless, the release of bubbles from the system to the surrounding atmosphere is considered in both the electrochemical reaction and the aqueous equilibrium reactions. In any case, the concentration of volatile aqueous species is limited to a maximum value that predicts the production of bubbles with a partial pressure equal to the surrounding atmosphere, whereon the bubbles are irreversibly released.

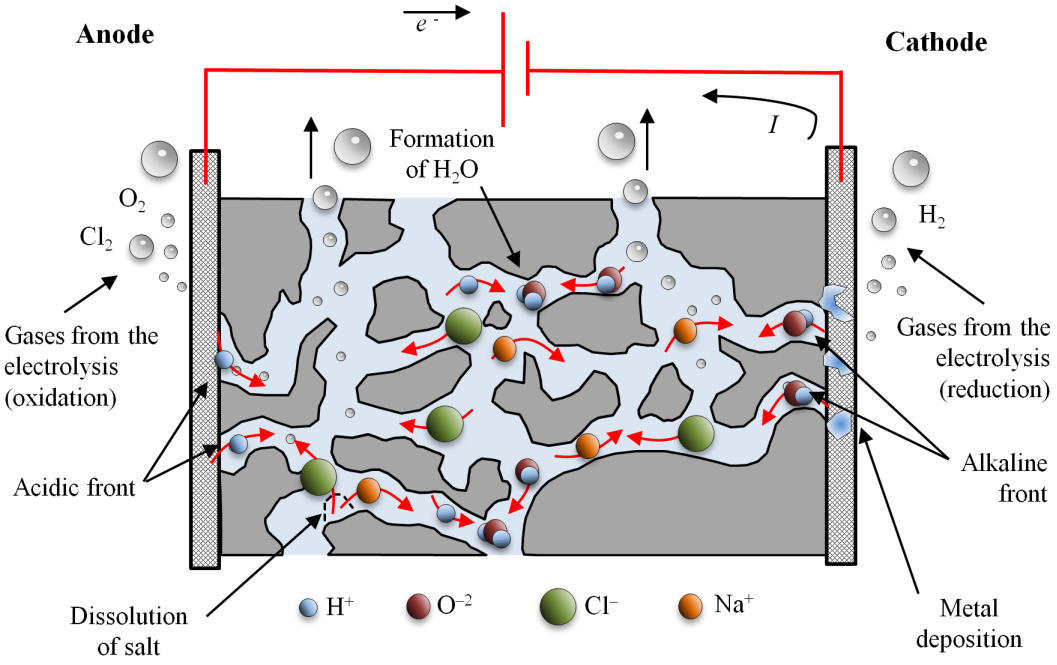

Figure 2.2: Scheme for an electrochemically-induced transport process

The chemical equilibrium model and the gas/liquid equilibrium assumptions, items 2 and 4, are detailed described in [Paz-Garcia et al., Submitted 2012a]. Consequently, only a brief summary is included here.

Fig. 2.2, shows a scheme for an electro-desalination treatment of a porous body contaminated with NaCl, as a representative example of an electrokinetic process. This scheme attends to illustrate some of the different physicochemical phenomena taking place in any electrokinetic treatment, such as:

- The electrochemically-induced transport of aqueous species through porous media
- The formation of an acidic front at the anode and an alkaline front at the cathode as a result of the water electrolysis reactions at the electrodes
- The neutralization of the aforementioned acidic and alkaline fronts leading to the formation of water somewhere inside the porous structure
- The release of gas bubbles due formed by chemical reaction
- The competitive redox reactions at the electrodes, depending on the chemical species and the conditions at the vicinities of the electrodes
- The heterogeneous precipitation/dissolution processes, leading to changes of the porous structure

Enhancing the transport model with the chemical reaction features allows the development of a generalized and realistic reactive-transport model, which is suitable for the simulation of a wide range of EK processes.

2.2.1 Electrochemically-induced transport

When an external electric field is applied to a total- or partially-saturated porous material an electric potential develops, as explained in Section 2.1.3. As a result of this potential, a number of transport phenomena are produced affecting to ionic and non-ionic chemical species, suspended particles and the electrolyte itself. Electrochemically-induced transport is, therefore, a general term that includes both electro-diffusion processes and electrokinetic transport (such as electroosmosis or electrophoresis) taking place in porous media under electric fields.

These kind of processes are denoted as electrochemically-induced transport because they always involve electrochemical reactions at the electrodes. An electrochemical (or redox) reaction is a chemical reaction in which electrons are exchanged leading to changes in the oxidation state between reactants and products. In an electrochemical reaction, electric energy is transformed into chemical energy or vice versa.

An electrochemical system that spontaneously produces a voltage is a galvanic cell or battery. On the other hand, an electrochemical reaction forced towards the non-spontaneous direction by an externally applied electric current is called electrolytic reaction.

To establish an external electric field into an electrolyte solution, an electric potential drop is enforced between a couple of electrodes. Oxidation electrolytic reactions (releasing electrons) are forced at the anode, and reduction electrolytic reactions (gaining electrons) at the cathode. The power supply forces the flux of electrons through the conductors from anode to cathode. Consequently, the anode becomes positively charged and attracts the anions, and the cathode becomes negative and attracts the cations.

Taken into account the electrochemical reactions, electrochemically-induced ionic transport can be modeled as a positive or negative flux of ions at the electrode interfaces. These ions are the products or the reactants of the electrolytic reactions forced by the external electric field. The flow of ionic current injected to the system (either for the injection of positive ions or the removal of negative ions) is equivalent to the electric current established between electrodes. For details about the competitive electrochemical reactions see Section 2.2.2.

The incoming and outgoing flux of ions is represented by the chemical reaction term, G_i in the continuity Nernst-Planck equation, Eq. (2.1). The extensive property g_i ($\mathrm{mol}\, s^{-1}$) is used instead of the intensive property G_i ($\mathrm{mol\, m^{-3}\, s^{-1}}$) since the

flux of ions is injected into a dimensionless control volume, which represents the electrode/electrolyte interface.

In an ideal system, the electric current through the conductors have the same magnitude than the ionic current through the electrolyte. The relation between the electric and ionic current, and so the magnitude of the injected ionic charge flux into the porous system at the electrode processes, is obtained from the Faraday's law of electrolysis as:

$$I = F \sum_{i=1}^{N} g_i \, z_i \tag{2.20}$$

where I (A) is the electric current.

The flux of ions produces sharp gradients of concentration and electric unbalances, leading to the development of an electric potential, due to the strongly coupled electro-diffusion interaction of ions. The electric potential developed affects to all the ions and charged species in the electrolyte system, and not only those participating in the electrochemical reactions. And so, electrochemical reactions promote the ionic migration of all charged species in the system.

2.2.2 Electrochemical reactions

Depending on the nature of the porous structure and the electrolyte, different competitive electrochemical reactions can occur. In aqueous media, water electrolysis are always likely to happen. Some common competitive reactions are the formation of chlorine gas at the anode and the deposition of non-amphoteric metals at the cathode surface.

If the concentrations at the vicinities of the electrodes are known, the Nernst equation can be used to calculate the electrochemical potential for each electrochemical half reaction, as:

$$E = E^0 - \frac{R\,T}{\nu\,F} \ln Q \tag{2.21}$$

where Q (dimensionless) is the reaction quotient, defined as the product of the activities of the chemical species to the power of their stoichiometric coefficients, for non-equilibrium conditions. In the special case that the reaction is at equilibrium, the reaction quotient is equal to the equilibrium constant. ν is its valence i.e. the equivalent number of electrons exchanged in the electrochemical reaction, E (V) is the redox potential in the reduction sense and E^0 (V) is the standard redox potential measured under standard conditions i.e. 25°C, 1 mol L for each ion participating in the reaction, partial pressures of 1 atm for the gases and metals in their pure state. The standard reduction potential is defined relative to a standard hydrogen reference

electrode (SHE), which is arbitrarily given a potential of 0 V [Chang and Overby 2011].

Based on the redox potential, the effects of the competitive electrode reactions can be quantified. For example, at the cathode the main electrode reaction is the water reduction, given as:

$$2H_2O + 2e^- \rightarrow 2OH^- + H_2\,(g) \quad ; \quad E^0 = -0.83 \tag{2.22}$$

In desalination treatments, alkaline and alkali-earth metals are normally the only cations in the system. The electrochemical potential for the reduction of this metals is always to low to be competitive with respect to the water electrolytic reaction.

$$Na^+ + e^- \rightleftarrows Na^0 \quad ; \quad E^0 = -2.71 \tag{2.23}$$
$$K^+ + e^- \rightleftarrows K^0 \quad ; \quad E^0 = -2.93 \tag{2.24}$$
$$Ca^{+2} + 2e^- \rightleftarrows Ca^0 \quad ; \quad E^0 = -2.87 \tag{2.25}$$
$$Mg^{+2} + 2e^- \rightleftarrows Mg^0 \quad ; \quad E^0 = -2.37 \tag{2.26}$$

In EKR treatments of heavy metal contaminated soil, competitive reactions at the cathode are likely to happen, as e.g.:

$$Cu^{+2} + 2e^- \rightleftarrows Cu^0 \quad ; \quad E^0 = 0.3419 \tag{2.27}$$
$$Pb^{+2} + 2e^- \rightleftarrows Pb^0 \quad ; \quad E^0 = –0.1262 \tag{2.28}$$
$$Ni^{+2} + 2e^- \rightleftarrows Ni^0 \quad ; \quad E^0 = –0.257 \tag{2.29}$$

If metal deposition occurs as a consequence of competitive electrode reactions, some overpotential polarization effects will arise, increasing the voltage drop associated with the electrochemical reaction and increasing the energy consumption of the process.

On the other hand, as water electrolytic reactions always involve the release of gases in both the reduction and the oxidation, competitive redox reactions involving release of gaseous species require special attention.

At the anode, the most common competitive reaction to the water electrolysis is the chloride oxidation to give gaseous chlorine, as:

$$4H^+ + 4e^- + O_2\,(g) \leftarrow 2H_2O \quad ; \quad E^0 = 1.23 \tag{2.30}$$

$$2e^- + Cl_2\,(g) \leftarrow 2Cl^- \quad ; \quad E^0 = 1.36 \tag{2.31}$$

Reactions expressed in Eqs. (2.30) and (2.31) are written in the reduction sense, despite they are forced towards oxidation.

In [Paz-Garcia et al. Submitted 2012c] a model for the quantification of the competitive electrode reactions at the anode is proposed. In that work, the simultaneous production of chlorine and oxygen at the anode is modeled based on the partial pressures of the released bubbles and taking into account concentration polarization effects at the electrode surface.

Assuming room temperature, the redox potential of the oxygen and chorine oxidation is:

$$E_{\mathrm{O_2}} = \left(E^0_{O_2} + \psi_{O_2}\right) - 0.059\,\mathrm{pH} + \frac{0.059}{4}\,\log\left(\mathrm{P_{O_2}}\right) \tag{2.32}$$

$$E_{\mathrm{Cl_2}} = \left(E^0_{Cl_2} + \psi_{\mathrm{Cl_2}}\right) - 0.059\log\left[\mathrm{Cl^-}\right] + +\frac{0.059}{2}\,\log\left(\mathrm{P_{Cl_2}}\right) \tag{2.33}$$

where $\psi_{\mathrm{O_2}}$ and $\psi_{\mathrm{Cl_2}}$ (V) represents the polarization or overpotential factors, accounting for the variations in the theoretical and experimentally observed redox potential. In this case, the polarization effects are assumed to be due to the combination of bubble release and concentration overpotential, and so they arise from the difficulty of the transfer between the initial and final components of a reaction occurring at the electrode [Marcus 2011]. It is related, for example, to the easiness for the produced bubbles of O_2 or Cl_2 to be desorbed and released from the surface of the electrode.

The partial pressures of the gases can have very small values. The lower the partial pressure, the more favored the half reaction is. Therefore, the redox potential may be assumed equal for all the electrochemical reactions involving gaseous species in any electrode, being the partial pressure of the gases the fitting parameter. Let us assumed that the bubbles of gas formed at the electrode surface and released from the system are multi-component gas bubbles with a total pressure equal to the pressure of the surrounding atmosphere, normally 1 atm. For the case of the two competitive reactions in studied at the anode, it leads to:

$$P_{\mathrm{O_2}} + P_{\mathrm{Cl_2}} = 1 \tag{2.34}$$

From the previous assumptions, the efficiency of the competitive electrolytic reactions can be related to the partial pressures, which are, in turn, a function of the ionic concentration in the vicinities of the electrodes. For a further discussion, see [Paz-Garcia et al. Submitted 2012c].

2.2.3 Chemical equilibrium

A set of nonlinear algebraic equations is developed from the mass balance and the mass action equations describing the chemical equilibrium [Rawlings and Ekerdt 2002, Bethke 2008]. The mathematical and numerical method for chemical equilibrium calculations used here is detailed described in [Paz-Garcia et al. Submitted 2012a].

Let i and r be respectively the indexes for the chemical species and the chemical reactions describing the secondary species, with $i = 1, 2, ..., N$ and $r = 1, 2, ..., M$; where N is the total number of species, $(N - M)$ is the number of master species and M is the number of chemical equilibrium reactions used to defined the secondary species as function of the master species.

For a set of N chemical species, the M stoichiometric equations are defined as:

$$\nu_r n_r \rightleftarrows \sum_{i=1}^{N} \nu_{i,r} n_i \tag{2.35}$$

where the extensive variable n_i (mol) denotes the total amount of the i^{th} species in the system and $\nu_{i,r}$ is the stoichiometric coefficient for the i^{th} species in the r^{th} reaction. In this model, stoichiometric equations have to be written in the form of dissociation or dissolution reactions with only one reactant. By definition, each r^{th} secondary species participates only in the r^{th} stoichiometric equation that describes it and its stoichiometric coefficient is normalized to the value $\nu_r = 1$.

When N chemical species in non-equilibrium react with each other to reach the chemical equilibrium state, a mass conservation equation can be written as a function of the extent of the reaction ξ_r. The reaction extent is the extensive quantity describing the progress of a chemical reaction equal to the number of chemical transformations [McNaught and Wilkinson 1997]. In order to reach the chemical equilibrium state, any reversible reaction can proceed towards the products or towards the reactants, so ξ_r can be either a positive or a negative value.

According to the previous definition, the total amount of each species at equilibrium is given by the mass balance equation along the chemical reaction path, in the form of:

$$n_{i,\text{eq.}} = n_{i,\text{init.}} + \sum_{r=1}^{M} \xi_r \nu_{i,r} \tag{2.36}$$

Let $\mathbf{x} = \left[\; \xi_1, \, \xi_2, \, \cdots \, , \, \xi_M \; \right]$ be the vector containing the reaction extents for the M reactions. The function $f_r(\mathbf{x})$ is defined as a measure of the Gibbs energy of the chemical system according to the thermodynamic description of the chemical potential [Bethke 2008] and it tends to zero when the systems approaches to the equilibrium. Thus, the function $f_r(\mathbf{x})$ represents the distance to the equilibrium state for the r^{th} reversible reaction.

Using logarithms, $f_r(\mathbf{x})$ can be expressed as:

$$f_r(\mathbf{x}) = \sum_{r=1}^{M} (\nu_{i,r} \ln a_i) - \ln K_{eq,r} \tag{2.37}$$

where $K_{eq,r}$ is the equilibrium constant for the r^{th} reaction and a_i (dimensionless) is the chemical activity.

As the chemical equilibrium model described in [Paz-Garcia et al. Submitted 2012a] can be used in microscopic reactive transport processes and batch reaction simulations, chemical activity theories are included. Davies and Setschenow equations are used for the calculation of the activity factors for ionic and non-ionic aqueous species respectively.

In the case of macroscale reactive-transport systems, the ionic strength of the media uses to be too high for the theories for accurately estimating the chemical activity. Furthermore, the uncertainly induced by the empirical transport coefficients, used to describe the constitutive equations is much higher than the losses of assuming ideal conditions for the chemical activities. Consequently, in macroscale models the activity is defined equal to the molal concentration ($\text{mol}\,\text{kg}^{-1}$) for aqueous species and, in the case of the solvent and the solid species, activities are set to a fixed value of 1.

Heterogeneous precipitation/dissolution reactions are included in the model. This means that the equilibrium reaction for the solid species is only included in the set of chemical reactions when the saturation index predicts the existence of the precipitated phase. For kinetics considerations, the model does not assume equilibrium between the electrolyte and the surrounding atmosphere. Nevertheless, free release of pure bubbles with 1 atm pressure is assumed when concentration of volatile aqueous species reach a saturation level determined by its Henry's constant.

The M equilibrium equations are coupled in a matrix system of equations and solved by means of a Newton-Raphson method, enhanced with a line-search approach which assures the convergence and deals with the non-negative concentration constraints of all the chemical species [Press et al. 1992].

Chapter 3

Numerical Model

3.1 Transport phenomena

A finite elements method (FEM) is implemented and used for the integration of the strongly coupled Nernst-Planck-Poisson system of partial differential equations [Zienkiewicz and Taylor 2005, Ottosen and Petersson 1992, Ottosen and Ristinmaa 2005].

In [Paz-Garcia et al. 2011d], the FEM for the integration of the transient NPP system was explained. In the subsequent publications [Paz-García et al. 2012 In press, Paz-Garcia et al. Submitted 2012b,S], the numerical implementation has been adapted according to the modifications proposed in the physicochemical model. Nevertheless, the description of the numerical method in the published papers is short in order to match the journal requirements. Therefore, a detailed description is included here in order to increase the reproducibility of the methods described.

3.1.1 Finite elements method in fluid dynamics

The FEM is a numerical method for finding approximate solutions to systems of partial differential equations (PDE). The FEM is widely used in the field of solid and structural mechanics, as e.g. [Zienkiewicz and Taylor 2005]. There is also some literature about fluid mechanics and convection dominated problems [Zienkiewicz 1991]. Nevertheless, up to now, the use of the FEM for the ionic transport of porous media is rare.

The numerical procedure consists of dividing the domain into a number of finite elements, limited by discrete nodal points. As a result, the system of differential equations is converted to a matrix system of algebraic equations, easily solvable by matrix algebra. Using the FEM it is also possible to discretize the system in the time domain to solve transient problems, as the case of the multi-species ENPP system.

Let π be a state variable property and let us consider a partial differential equation to be integrated by finite elements in the form:

$$\underbrace{\frac{\partial \pi}{\partial t}}_{Accumulation} = \underbrace{-\frac{\partial \mathbf{J}_\pi}{\partial x}}_{Flux} + \underbrace{G_\pi}_{Generation} \tag{3.1}$$

and

$$\mathbf{J}_\pi = -k_e \frac{d\pi}{dx} \tag{3.2}$$

which is equivalent to a mass conservation equation for the property π in a microscopic control volume. In this example, a one-dimensional problem is considered. See Section A.4 for a discussion about two-dimensional finite elements modeling. In addition to this, in this section only the discretization in the space in discussed. See Section 3.1.4 for the discretization in the time domain.

The property k_e is a parameter containing some physical characteristic value for the e^{th} finite element, such as a transport coefficient, $e = 1, 2, ..., N^e$ is an index for the elements and N^e the total number of finite elements. k_e may also include some information about the macroscopic parameters (the cross sectional area or the porosity) and the mean value of a state variable assumed constant to linearize nonlinear system of equations. For details see Section 3.1.6.

The goal of the numerical method is to calculate an approximate solution for the continuous property π in the domain of integration. To do that, the continuous differential equation is discretized and solved to calculate the value of π at the nodal points. The approximate continuous function is obtained by interpolation between nodes.

Interpolation between nodes is done by means of the so-called shape functions. Additionally, the FEM requires the use of the so-called weight function, $w(x)$, which is an arbitrary function that multiplies the entire partial differential equation for the discretization process. A Galerkin method for weighting the residuals is proposed, which consists of using a weight function similar to the shape functions that interpolates the state variable between nodes [Ottosen and Petersson 1992]. Furthermore, linear piecewise shape and weight functions are used, which are sufficiently accurate with a proper number of finite elements.

Fig. 3.1 shows an scheme for the discretization of a single finite element e. Let $\mathbf{N} = [1 - {}^{x}/_{L_e},\ {}^{x}/_{L_e}]$ be the linear piecewise shape function used to interpolate between nodal points that limits a single finite element. L_e is the length of any one-dimensional finite element, which may be different from element to element, and x is the distance between nodes. The gradient of the shape function is given by $\mathbf{B} = [{}^{-1}/_{L_e},\ {}^{1}/_{L_e}]$. Let $\mathbf{a}_\pi$ be a vector containing the discretized function for the property π, i.e. the value of the property π at the discrete nodes.

According to the previous definitions, the approximate solution of the continuous property π, the weight function w and their gradients are obtained by the product between the shape functions and the values at the discrete nodes, as:

$$\begin{aligned} \pi = \mathbf{N}\mathbf{a}_\pi \quad &, \quad w = \mathbf{w}^{\mathrm{T}}\mathbf{N}^{\mathrm{T}} \\ \nabla\pi = \mathbf{B}\mathbf{a}_\pi \quad &, \quad \nabla w = \mathbf{w}^{\mathrm{T}}\mathbf{B}^{\mathrm{T}} \end{aligned} \tag{3.3}$$

where, for convenience, the weight function has been defined using its transpose, indicated with the superscript T.

To proceed with the discretization in the space domain, the "strong formula" i.e. the partial differential equation expressed in Eq. (3.1), is multiplied by the weight function and integrated over the length of the finite element, as:

$$\underbrace{\int_0^{L_e} w\frac{d\pi}{dt}dx}_{Accumulation} = \underbrace{\int_0^{L_e} w\, k_e \frac{d}{dx}\left(\frac{d\pi}{dx}\right)dx}_{flux} + \underbrace{\int_0^{L_e} w\, G_\pi dx}_{Generation} \tag{3.4}$$

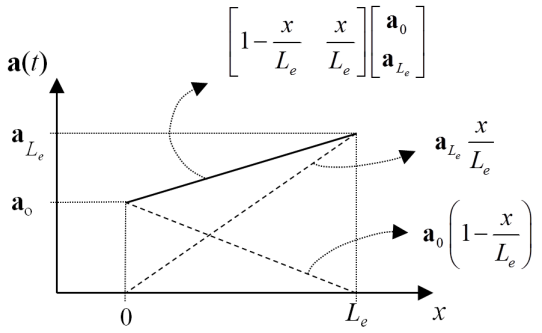

Figure 3.1: Linear piecewise shape functions for an single finite element in a one-dimensional domain

The method of integration by parts is used in the flux term, reducing the order of the derivative and obtaining two different addends:

$$\int_0^{L_e} w\, k_e \frac{d}{dx}\left(\frac{d\pi}{dx}\right) dx = \left[w k_e \frac{d\pi}{dx}\right]_0^{L_e} - \int_0^{L_e} \frac{dw}{dx} k_e \frac{d\pi}{dx} dx \tag{3.5}$$

where:

$$\left[w k_e \frac{d\pi}{dx}\right]_0^{L_e} = -\left[w \mathbf{J}_\pi\right]_0^{L_e} \tag{3.6}$$

Substituting Eq. (3.5) into Eq. (3.4) and reorganizing the terms, one gets:

$$\int_0^{L_e} w \frac{d\pi}{dt} dx + \int_0^{L_e} \frac{dw}{dx} k_e \frac{d\pi}{dx} dx + \left[w \mathbf{J}_\pi\right]_0^{L_e} - \int_0^{L_e} w\, G_\pi dx = 0 \tag{3.7}$$

Using the notation described in Eq. (3.3) for the approximate functions, the previous equation gives:

$$\mathbf{w}^{\mathrm{T}} \left(\int_0^{L_e} \mathbf{N}^{\mathrm{T}} \mathbf{N} \frac{d\mathbf{a}_\pi}{dt} dx + \int_0^{L_e} \mathbf{B}^{\mathrm{T}} k_e \mathbf{B} \mathbf{a}_\pi dx + \left[\mathbf{N}^{\mathrm{T}} \mathbf{J}_\pi\right]_0^{L_e} - \int_0^{L_e} \mathbf{N}^{\mathrm{T}} G_\pi dx \right) = 0 \tag{3.8}$$

The term $\mathbf{w}^{\mathrm{T}}$, common in all addends, is cancelled. As $\mathbf{a}_\pi$ is a discrete variable and the parameter k_e is an assumed-constant value for the finite element, only the vectors $\mathbf{N}$ and $\mathbf{B}$ and their products are integrated. The following definitions are done for the studied one-dimensional case:

- $\mathbf{C}_e$ is the local mass matrix for the element e:

$$\mathbf{C}_e = \int_0^{L_e} \mathbf{N}^{\mathrm{T}} \mathbf{N} dx = \frac{L_e}{6} \begin{bmatrix} 1 & 2 \\ 2 & 1 \end{bmatrix} \tag{3.9}$$

- $\mathbf{K}_e$ is the local conductivity matrix for the element e:

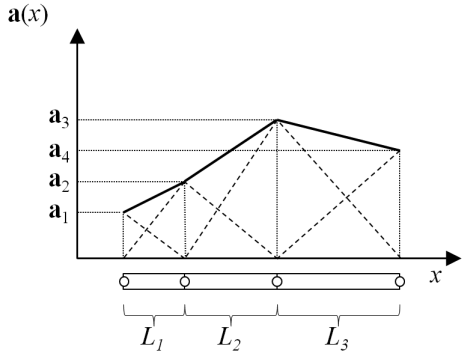

Figure 3.2: Linear piecewise shape function interpolating a one-dimensional domain with three finite elements

$$\mathbf{K}_e = k_e \int_0^{L_e} \mathbf{B}^{\mathrm{T}}\mathbf{B} dx = \frac{k_e}{L_e}\begin{bmatrix} 1 & -1 \\ -1 & 1 \end{bmatrix} \tag{3.10}$$

- $\mathbf{f}_b$ is a boundary vector associated to the flow of property π at the boundaries of the domain:

$$\mathbf{f}_{b,\,e} = \left[\mathbf{N^T}\,\mathbf{J}_\pi\right]_0^{L_e} = \left[\mathbf{J}_\pi\right]_0^{L_e}\begin{bmatrix} -1 \\ 1 \end{bmatrix} \tag{3.11}$$

- $\mathbf{f}_l$ is denoted as load vector and it is associated to the generation term:

$$\mathbf{f}_{l,\,e} = \int_0^{L_e} \mathbf{N}^{\mathrm{T}} G\, dx = -G_\pi \frac{L_e}{2}\begin{bmatrix} 1 \\ 1 \end{bmatrix} \tag{3.12}$$

According to the previous definitions, Eq. (3.1) is converter to the discrete equation:

$$\mathbf{C}_e \frac{d\mathbf{a}_\pi\,(t)}{dt} + \mathbf{K}_e\,\mathbf{a}_\pi\,(t) + \underbrace{\mathbf{f}_{b,\,e} + \mathbf{f}_{l,\,e}}_{\mathbf{f}_e(t)} = 0 \tag{3.13}$$

defined between the limits of a single element, i.e. the nodal points which define it. $\mathbf{f}_e\,(t)$ includes both the boundary and load vectors, and it has been considered time dependent as the generation term function is undefined.

Each finite element e is characterized with its own local matrices $\mathbf{C}_e$ and $\mathbf{K}_e$ and the local vector $\mathbf{f}_e$.

3.1.2 Assembly process

Eq. (3.13) is defined only for an individual finite element. As shown in Fig. 3.2, every two consecutive finite elements in a one-dimensional system share a common node. The piecewise shape functions interconnect consecutive elements in order to keep the continuity condition.

A global equation is built covering all the elements in the domain. This process is done by assembling the local discrete equations for all elements in the system. As an example of the assembly process, let consider the conductivity matrix defined in Eq. (3.10). The global conductivity matrix for the property π, denoted as $\mathbf{K}_\pi$ and defined for all the elements in the entire domain, is given by:

$$\mathbf{K}_\pi = \begin{bmatrix} k_1 & -k_1 & 0 & \cdots & 0 \\ -k_1 & (k_1+k_2) & -k_2 & \ddots & \vdots \\ 0 & -k_2 & \ddots & \ddots & 0 \\ \vdots & \ddots & \ddots & (k_{N^e-1}+k_{N^e}) & -k_{N^e} \\ 0 & \cdots & 0 & -k_{N^e} & k_{N^e} \end{bmatrix} \tag{3.14}$$

As an example, let us consider the 3 elements system described in Fig. 3.2. In this case, the global assembled matrix, $\mathbf{K}_\pi$, would be:

$$\mathbf{K}_\pi = \begin{bmatrix} k_1 & -k_1 & 0 & 0 \\ -k_1 & (k_1+k_2) & -k_2 & 0 \\ 0 & -k_2 & (k_2+k_3) & -k_3 \\ 0 & 0 & -k_3 & k_3 \end{bmatrix} \tag{3.15}$$

It can be seen that the assembly process is not straightforward because there are some overlapping between the local matrices of any consecutive elements. When numerically implementing the assemblage procedure the most intuitive way to do it is by means of an iterative loop as shown in Alg. (3.1). This procedure typically requires high computational times and it may be, in many cases, the bottleneck (in terms of calculation speed) for any finite element implementation. In the case of a one-dimensional problem, this function can be efficiently optimized to a vectorized version, i.e. calculated without using any iterative procedure. In a one-dimensional problem, the assembled matrix for the entire system results in a tridiagonal matrix, i.e. a matrix where only the main diagonal and the diagonal just below and above it are nonzero.

Algorithm 3.1 Standard "For loop" for the assembly process

For $e = 1$ until $e = N^e$
  $\mathbf{K}_\pi(e,e) = \mathbf{K}_\pi(e,e) + k_e\,\mathbf{K}_e(e,e)$
  $\mathbf{K}_\pi(e,e+1) = \mathbf{K}_\pi(e,e+1) + k_e\,\mathbf{K}_e(e,e+1)$
  $\mathbf{K}_\pi(e+1,\,e) = \mathbf{K}_\pi(e+1,\,e) + k_e\,\mathbf{K}_e(e+1,\,e)$
  $\mathbf{K}_\pi(e+1,\,e+1) = \mathbf{K}_\pi(e+1,\,e+1) + k_e\,\mathbf{K}_e(e+1,\,e+1)$
end

Instead of the loop, the Matlab® function "spdiags" is suggested, which generates a sparse matrix from the aforementioned three diagonals. A sparse matrix is a matrix in which most of the elements are nonzero. The proposed function builds

the assembled matrix already in a sparse form, saving significant amount of physical memory. It works in a vectorized way, thus the computational time is between 1 and 4 orders of magnitude lower than the "for loop" version.

3.1.3 Finite element integration of the Nernst-Planck-Poisson system

Following the same procedure as described in Section 3.1.1, the Nernst-Planck-Poisson system of partial differential equations is converted to a matrix system of algebraic equations.

Let $\mathbf{a}_\theta$, $\mathbf{a}_i$ and $\mathbf{a}_\phi$ be, respectively, the discrete form of the state variables at the nodal points for the degree of saturation, the molal concentration and the electrical potential. Let w be the arbitrary weight function. Similarly to Eq. (3.3), the following standard FEM vectorial notations are defined for the approximate solution.

$$\begin{array}{cccc} \theta = \mathbf{N}\,\mathbf{a}_\theta & , & c_i = \mathbf{N}\,\mathbf{a}_i & , & \phi = \mathbf{N}\,\mathbf{a}_\phi & , & w = \mathbf{w}^{\mathrm{T}}\mathbf{N}^{\mathrm{T}} \\ \nabla\theta = \mathbf{B}\,\mathbf{a}_\theta & , & \nabla c_i = \mathbf{B}\,\mathbf{a}_i & , & \nabla\phi = \mathbf{B}\,\mathbf{a}_\phi & , & \nabla w = \mathbf{w}^{\mathrm{T}}\mathbf{B}^{\mathrm{T}} \end{array} \tag{3.16}$$

According to this, the assembled global NPP system of equations in the finite element notation consists of:

- One discretized equation for the water transport:

$$\mathbf{C}_\theta \frac{\partial \mathbf{a}_\theta\,(t)}{\partial t} + \mathbf{K}_\theta^{\mathrm{mt}}\mathbf{a}_\theta\,(t) + \mathbf{K}_\theta^{\mathrm{eo}}\mathbf{a}_\phi\,(t) + \mathbf{f}_\theta = 0 \tag{3.17}$$

- One discretized Nernst-Planck equations for the transport of each of the aqueous species:

$$\mathbf{C}_i \frac{\partial \mathbf{a}(t)}{\partial t} + \mathbf{K}_i^{\mathrm{mta}}\mathbf{a}_\theta(t) + \mathbf{K}_i^{\mathrm{diff}}\mathbf{a}_i(t) + \mathbf{K}_i^{\mathrm{emo}}\mathbf{a}_\phi(t) + \mathbf{f}_i(t) = 0 \tag{3.18}$$

- The discretized Poisson's equation in electrostatics,

$$\sum_{i=1}^{N} \mathbf{E}_i\,\mathbf{a}_i(t) + \mathbf{K}^\phi\mathbf{a}_\phi(t) + \mathbf{f}_\phi(t) = 0 \tag{3.19}$$

Table 3.1 lists the matrices and vectors used in the discretized equations and their definition. The ionic migration and the electroosmotic advection transport terms have been grouped in a single term. Additionally, the characteristic value k_e used in the construction of the matrices is also included in the table. The characteristic value includes the effective transport coefficients and the mean value for some variables that are assumed constant during the transient integration as an strategy for solving the nonlinear system of equations, as explained see Section 3.1.6.

The k_e characteristic element value may include additional terms, not shown in Table 3.1, related to the empirical expressions used to define the effective transport

Table 3.1: Terminology for the discrete NPP system

Matrix	Related term	k_e value
$\mathbf{C}_\theta$	Accumulation for θ	$A\,p\,L_e/6$
$\mathbf{C_i}$	Accumulation for i	$A\,p\,\theta\,L_e/6$
$\mathbf{K}^{\mathrm{mt}}$	Moisture transport	$A\,p\,\theta^{\vartheta}\tau^{-1}D_\theta L_e^{-1}$
$\mathbf{K}^{\mathrm{eo}}$	Electroosmosis	$A\,p\,\theta\tau^{-1}K_{e.o.}L_e^{-1}$
$\mathbf{K}_i^{\mathrm{mta}}$	Moisture transport advection	$A\,p\,\theta^{\vartheta}\tau^{-1}D_\theta c_i L_e^{-1}$
$\mathbf{K}_i^{\mathrm{diff}}$	Diffusion	$A\,p\,\theta\tau^{-1}D_i L_e^{-1}$
$\mathbf{K}_i^{\mathrm{emo}}$	Electromigration and electroosmotic advection	$A\,p\,\theta\tau^{-1}\left(U_i + K_{e.o.}\right)c_i L_e^{-1}$
$\mathbf{E}_i$	Free charge density	$A\,\theta F\,z_i\,L_e/6$
$\mathbf{K}^{\phi}$	Electric potential	$\varepsilon\,L_e^{-1}$
$\mathbf{f}_\theta$	load/boundary vector for water	-
$\mathbf{f}_i$	load/boundary vector fro the species i	-
$\mathbf{f}_\phi$	load/boundary vector for ionic charge	-

coefficients for macroscopic problems, as well as additional terms used to define a macroscopic domain, such as the porosity or the cross-sectional area.

For a system with N chemical species (including water), the $N+1$ discrete equations are coupled to form a global matrix system as:

$$\underbrace{\begin{bmatrix} \mathbf{C}_\theta & 0 & \cdots & \cdots & 0 \\ 0 & C_2 & \ddots & \ddots & \vdots \\ \vdots & \ddots & \ddots & \ddots & \vdots \\ \vdots & \ddots & \ddots & \mathbf{C}_N & 0 \\ 0 & \cdots & \cdots & 0 & 0 \end{bmatrix}}_{\mathbf{C}} \underbrace{\frac{\partial}{\partial t}\begin{bmatrix} \mathbf{a}_\theta \\ \mathbf{a}_2 \\ \vdots \\ \mathbf{a}_N \\ \mathbf{a}_\phi \end{bmatrix}}_{\frac{\partial \mathbf{a}(t)}{\partial t}} + \underbrace{\begin{bmatrix} \mathbf{K}_\theta^{\mathrm{mt}} & 0 & \cdots & \cdots & \mathbf{K}_\theta^{\mathrm{eo}} \\ \mathbf{K}_2^{\mathrm{mta}} & K_2^{\mathrm{diff}} & \ddots & \ddots & \mathbf{K}_2^{\mathrm{emo}} \\ \vdots & \ddots & \ddots & \ddots & \vdots \\ \mathbf{K}_N^{\mathrm{mta}} & \ddots & \ddots & \mathbf{K}_N^{\mathrm{diff}} & \mathbf{K}_N^{\mathrm{emo}} \\ 0 & \mathbf{E}_2 & \cdots & \mathbf{E}_N & \mathbf{K}^{\phi} \end{bmatrix}}_{\mathbf{K}} \underbrace{\begin{bmatrix} \mathbf{a}_\theta \\ \mathbf{a}_2 \\ \vdots \\ \mathbf{a}_N \\ \mathbf{a}_\phi \end{bmatrix}}_{\mathbf{a}(t)} + \underbrace{\begin{bmatrix} \mathbf{f}_\theta \\ \mathbf{f}_2 \\ \vdots \\ \mathbf{f}_N \\ \mathbf{f}_\phi \end{bmatrix}}_{\mathbf{f}(t)} \tag{3.20}$$

which can be expressed in a simplified notation as:

$$\mathbf{C}\frac{\partial \mathbf{a}(t)}{\partial t} + \mathbf{K}\,\mathbf{a}(t) + \mathbf{f}(t) = 0 \tag{3.21}$$

In the previous global system, instead of the Nernst-Planck equation for water, the continuity equation referred to the degree of saturation is sued. Therefore, instead of the index $i = 1$, the subscript θ is used for define it. The indexes $i = 2, ..., N$ are

used for the aqueous species excluding water. On the other hand, the absence of subscripts in Eq. (3.21) means that the matrices and vectors are globally defined for the entire domain and the whole coupled system.

3.1.4 Discrete approximation in time

After the assembly process, the matrix system describing the ENPP system in the spatial domain is described by the Eq. (3.21). Now a linear finite element in the time domain is defined in a similar manner as done for the space domain. The time element length (or duration) between the present time t_0 and the next profile in the transient integration, denoted as $t_0 + \Delta t$, is normalized as:

$$\tau = \frac{t}{\Delta t} \tag{3.22}$$

According to this, the time $\mathbf{a}_0 = \mathbf{a}(\tau = 0)$ correspond to the already known transient profile $\mathbf{a}_0 = \mathbf{a}(t_0)$ and the profile $\mathbf{a}_1 = \mathbf{a}(\tau = 1)$ corresponds to the next transient profile, $\mathbf{a}_1 = \mathbf{a}(t_0 + \Delta t)$, to be numerically calculated in the method. The shape function for the normalized one-dimensional linear element is:

$$\mathbf{N} = \left[1 - \frac{\tau_t}{\Delta t},\ \frac{\tau_t}{\Delta t}\right] \tag{3.23}$$

The gradient of the shape function is obtained as:

$$\mathbf{B} = \frac{1}{\Delta t}\,[-1,\ 1] \tag{3.24}$$

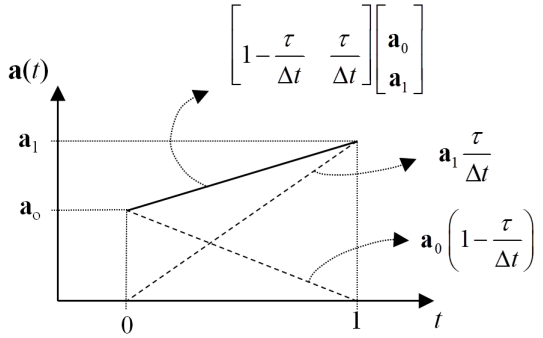

Figure 3.3: Linear piecewise finite element in the time domain

The finite element in the time domain and the shape functions used for its calculation are shown in Fig. 3.3. The procedure to calculate the discretized weak formula in the time is similar to that followed in the discretization in the space. The equation is multiplied by a time-dependent weight function, denoted as $\omega(\tau)$, and integrated between the limits of the normalized time element.

$$\int_0^1 \omega(\tau)\left(\mathbf{C}\frac{\partial \mathbf{a}(\tau)}{\partial t} + \mathbf{K}\,\mathbf{a}(\tau) + \mathbf{f}(\tau)\right) d\tau = 0 \tag{3.25}$$

The linear function interpolating between time steps is:

$$\mathbf{a}(\tau) = \begin{bmatrix} 1-\frac{\tau}{\Delta t} & \frac{\tau}{\Delta t} \end{bmatrix} \begin{bmatrix} \mathbf{a}_0 \\ \mathbf{a}_1 \end{bmatrix} = \left(1-\frac{\tau}{\Delta t}\right)\mathbf{a}_0 + \frac{\tau}{\Delta t}\mathbf{a}_1 \tag{3.26}$$

and

$$\frac{\partial \mathbf{a}(\tau)}{\partial t} = \frac{1}{\Delta t}\begin{bmatrix} -1 & 1 \end{bmatrix} \begin{bmatrix} \mathbf{a}_0 \\ \mathbf{a}_1 \end{bmatrix} = \frac{1}{\Delta t}(\mathbf{a}_1 - \mathbf{a}_0) \tag{3.27}$$

The vector $\mathbf{f}(t)$, which may be time dependent if the boundary flow or the generation term is defined as a function of the time such as, e.g. a kinetic chemical reaction, is approximated in a similar manner:

$$\mathbf{f}(\tau) = \left(1 - \frac{\tau}{\Delta t}\right)\mathbf{f}_0 + \frac{\tau}{\Delta t}\mathbf{f}_1 \tag{3.28}$$

According to the previous definitions, Eq. (3.25) is expressed as:

$$\int_0^1 \omega(\tau)\left(\frac{\mathbf{C}}{\Delta t}(\mathbf{a}_1 - \mathbf{a}_0) + \mathbf{K}\left(\left(1 - \frac{\tau}{\Delta t}\right)\mathbf{a}_0 + \frac{\tau}{\Delta t}\mathbf{a}_1\right) + \left(1 - \frac{\tau}{\Delta t}\right)\mathbf{f}_0 + \frac{\tau}{\Delta t}\mathbf{f}_1\right) d\tau = 0 \tag{3.29}$$

Eq. (3.29) is divided by the term:

$$\Delta t \int_0^1 \omega(\tau)\, d\tau \tag{3.30}$$

giving:

$$\frac{\mathbf{C}}{\Delta t}(\mathbf{a}_1 - \mathbf{a}_0) + \mathbf{K}(\mathbf{a}_0 + \Theta(\mathbf{a}_1 - \mathbf{a}_0)) + \mathbf{f}_0 + \Theta(\mathbf{f}_1 - \mathbf{f}_0) = 0 \tag{3.31}$$

where the property Θ is defined as:

$$\Theta = \frac{\int_0^1 \omega(\tau)\ (\tau/\Delta t)\ d\tau}{\int_0^1 \omega(\tau)\, d\tau} \quad ; \quad 0 \leq \Theta \leq 1 \tag{3.32}$$

Eq. (3.25) can be rearranged to give the global matrix system of equations:

$$\mathbf{K}^\star\,\mathbf{a}_1 = \mathbf{f}^\star \tag{3.33}$$

where

Table 3.2: Single time-step algorithms

Scheme	Θ	Stability condition
Truly explicit	0.0	conditional
Crank-Nicolson	0.5	unconditional
Galerkin	0.666	unconditional
Liniger	0.878	unconditional
Truly implicit	1.0	unconditional

$$\mathbf{K}^{\star} = \frac{\mathbf{C}}{\Delta t} + \mathbf{K}\,\Theta \tag{3.34}$$

and

$$\mathbf{f}^{\star} = \frac{\mathbf{C}}{\Delta t} + \mathbf{K}\,(\Theta - 1) + (\Theta - 1)\,\mathbf{f}_0 - \Theta \mathbf{f}_1 \tag{3.35}$$

The integration constant Θ, which has an arbitrary value between 0 and 1, is a stability factor which determines the influence of the present and future profiles on the conductivity matrices during any time step of the numerical integration. The time integration constant Θ is evaluated by inserting weight functions $\omega(\tau)$ in Eq. (3.32). Classical weight functions are presented in Table 3.2.

3.1.5 Solution of the matrix system with boundary conditions

The matrix system of linear equations in the form:

$$\mathbf{K}^{\star}\,\mathbf{a} = \mathbf{f}^{\star} \tag{3.36}$$

is solved simply by:

$$\mathbf{a} = (\mathbf{K}^{\star})^{-1}\,\mathbf{f}^{\star} \tag{3.37}$$

Most programing languages includes vectorized versions of this matrix operation. In Matlab®, the solution of a matrix system of equations is typically done by a "left division operation" invoked by the "backslash operator" in the form:

$$\mathbf{a} = \mathbf{K}^{\star} \backslash \mathbf{f}^{\star} \tag{3.38}$$

The solution of the matrix system of equations constricted to boundary conditions is done by means of a special procedure. The term "boundary conditions" refers to some values of the vector with the state variables, $\mathbf{a}$, that are forced to a predefined result.

For example, let us consider a matrix system with 4 equations in the form:

$$\begin{pmatrix} k_{11} & k_{12} & k_{13} & k_{14} \\ k_{21} & k_{22} & k_{23} & k_{24} \\ k_{31} & k_{32} & k_{33} & k_{34} \\ k_{41} & k_{42} & k_{43} & k_{44} \end{pmatrix} \begin{pmatrix} a_1 \\ a_2 \\ a_3 \\ a_4 \end{pmatrix} = \begin{pmatrix} f_1 \\ f_2 \\ f_3 \\ f_4 \end{pmatrix} \tag{3.39}$$

Let us consider that the value a_3 is forced to a predefined result. Consequently, it has not to be computed in the solution of the matrix system of equation which is, therefore, simplified to:

$$\begin{pmatrix} k_{11} & k_{12} & k_{14} \\ k_{21} & k_{22} & k_{24} \\ k_{41} & k_{42} & k_{44} \end{pmatrix} \begin{pmatrix} a_1 \\ a_2 \\ a_4 \end{pmatrix} = \begin{pmatrix} f_1 \\ f_2 \\ f_4 \end{pmatrix} + a_3 \begin{pmatrix} k_{31} \\ k_{32} \\ k_{34} \end{pmatrix} \tag{3.40}$$

where only the non-predefined values of $\mathbf{a}$ are unknowns.

In order to keep the forced value and, at the same time, satisfy the continuity condition, it is necessary to complete the matrix system of equations with a vector, $\mathbf{f}_r$, denoted as reactive boundary vector, as:

$$\mathbf{K}^\star \, \mathbf{a} = \mathbf{f}^\star + \mathbf{f_r} \tag{3.41}$$

In the finite elements method it has the information of the flux necessary to keep the corresponding forced value in any specific node with a boundary condition. Consequently, $\mathbf{f}_r$ will be zero in all elements except of those with a predefined forced value. In the example, it would be:

$$\begin{pmatrix} k_{11} & k_{12} & k_{13} & k_{14} \\ k_{21} & k_{22} & k_{23} & k_{24} \\ k_{31} & k_{32} & k_{33} & k_{34} \\ k_{41} & k_{42} & k_{34} & k_{44} \end{pmatrix} \begin{pmatrix} a_1 \\ a_2 \\ a_3 \\ a_4 \end{pmatrix} = \begin{pmatrix} f_1 \\ f_2 \\ f_3 \\ f_4 \end{pmatrix} + \begin{pmatrix} 0 \\ 0 \\ f_{r,3} \\ 0 \end{pmatrix} \tag{3.42}$$

where $\mathbf{f}_r$ is been calculated by:

$$\mathbf{f}_r = \mathbf{K}^\star \, \mathbf{a} - \mathbf{f}^\star \tag{3.43}$$

The procedure can be easily extended if more than one predefined value (boundary conditions) are used.

In the case of the ENPP model, boundary conditions are used when simulating an EK treatment under constant voltage difference between electrodes. In these cases, the electric potential is fixed to a value of zero at the cathode, used as a reference, and the corresponding potential drop value at the anode.

3.1.6 Iterative solution of the nonlinear matrix system

Most of the terms in the Nernst-Planck-Poisson system of equations are nonlinear, i.e. every addends depends on more than one state variable or their first or second derivative. For instance, the electromigration term is assumed proportional to the aqueous concentration and the gradient of electric potential. At the macroscale, the transport terms are also multiplied by some parameters such as the porosity or the cross-sectional area and the water content.

Some authors have proposed Newton-Raphson schemes for the solution of the nonlinear system of equations [Ottosen and Ristinmaa 2005]. Nevertheless, the ENPP system presented here is so strongly nonlinear and the number of variables is so high that the Newton-Raphson was concluded to be too costly, in terms of computational time. Instead, the solution of the nonlinear system is done by means of a generalized iterative method.

In this context, the nonlinear system is linearized by assuming that, in any of the transport terms in the discretized equations, only one of the variables is a state variable while all the other variables have comparable small variations in the time-step that it is possible to accept a constant value for them. For example, the electromigration transport term is solved assuming that the electric potential ϕ is a state variable, while the concentration c_i is a characteristic value of the element. The chosen state variables and the linearized variables included in the characteristic element parameter are summarized in Table 3.1.

In the case of the electromigration term, it means that the conductivity matrix calculated in Eq. (3.10), multiplies only the vector with the discrete values of the electric potential and the mean ionic concentration of the species i is used as a characteristic value, together with the element length and the transport coefficient as:

$$\mathbf{K}_e^{\text{emo}}\mathbf{a}_\phi = \frac{U_{i,e}\, c_{i,e}}{L_e}\begin{bmatrix} 1 & -1 \\ -1 & 1 \end{bmatrix}\begin{bmatrix} a_{\phi,0} \\ a_{\phi,Le} \end{bmatrix} \tag{3.44}$$

In order to increase the accuracy of the calculated results, the mean value of the element in the time domain between the two consecutive transient profiles is used to estimate the linearized parameters. Consequently, the characteristic value is calculated as:

$$\overline{\mathbf{a}} = \frac{\mathbf{a}\,(t_0 + \Delta t) + \mathbf{a}\,(t_0)}{2} \tag{3.45}$$

Obviously, the mean value of the element is not possible to be immediately calculated as the transient profile $\mathbf{a}\,(t_0 + \Delta t)$ is unknown. An iterative procedure is necessary, as explained in Alg. (3.2).

In Alg. (3.2), $\mathbf{a}_{\text{new}}$ and $\mathbf{a}_{\text{old}}$ are used to define the intermediate profiles in the numerical iteration. First, the known transient profile $\mathbf{a}\,(t_0)$ is used to estimate the

Algorithm 3.2 Iterative procedure for the solution of the nonlinear system of equations

While $\|\mathbf{a}_{\text{new}} - \mathbf{a}_{\text{old}}\| >$ accepted value
  $\mathbf{a}_{\text{old}} = \mathbf{a}_{\text{new}}$
  Update matrices and vectors: $\mathbf{K}(\overline{\mathbf{a}})$ and $\mathbf{f}(\overline{\mathbf{a}})$
  $\mathbf{a}_{\text{new}} = \mathbf{K}(\overline{\mathbf{a}}) \backslash \mathbf{f}(\overline{\mathbf{a}})$
  $\overline{\mathbf{a}} = (\mathbf{a}_{\text{new}} - \mathbf{a}_{t_0})/2$
end

value of the characteristic parameter k_e and calculate the matrices in the global matrix system of equations. A intermediate profile $\mathbf{a}_{\text{new}}$ is obtained, which is not accepted. This intermediate profile is used to calculate the mean value $\overline{\mathbf{a}}$. Then, matrices are recalculated and the matrix system is solved again. The procedure is repeated a number of times until two consecutive solutions are the same of very similar.

The error is calculated as the scalar product of two consecutive profiles. The acceptance criteria used in the simulations included in the appended published papers and those presented in this dissertation was 10^{-19}, which resulted in a moderate low number of iterations per time-step (between 5 and 25).

3.2 Chemical modeling

As mentioned before, the numerical implementation of the chemical equilibrium modeled is detailed described in [Paz-Garcia et al. Submitted 2012a]. Here only the aspects related to the numerical implementation of the electrochemical reactions are discussed.

3.2.1 Electrode processes

As explained in Section 3.1.5, simulations on EK treatments by FE methods, require the use of some boundary conditions associated to the electrode reactions.

The electric current is transformed to an ionic current by means of the electrochemical reaction at the electrodes. As a result, a flux of ionic charge is injected in the system at the electrode surfaces. In one-dimensional domains, the electrode/electrolyte interface is normally represented by only one nodal point.

The $\mathbf{f}$ vector, defined as a load/boundary vector, includes the effects of external flow at the boundaries of any control volume and the generation (chemical reaction) term. The $\mathbf{f}$ value at the corresponding anode and cathode nodal points, is calculated from the corresponding ionic charge flux, g_i, related to the electrode processes.

Different approaches are taken depending on the working conditions of the electrokinetic process. These working conditions are normally constant DC current or constant potential different between electrodes. Both cases are discussed below.

Constant DC current case:

Let us consider a EKD treatment in which two competitive electrochemical reactions are taken place at the anode: water oxidation, Eq. (2.30), and chloride oxidation, Eq. (2.31). Only water reduction, Eq. (2.22), is taking placed at the cathode.

The ionic current at the anode is a combination of incoming protons, and outgoing chloride ions as:

$$\frac{I}{F} = z_{\mathrm{H^+}} g_{\mathrm{H^+,\,Anode}} + z_{\mathrm{Cl^-}} g_{\mathrm{Cl^-,\,Anode}} \tag{3.46}$$

While, at the cathode, all the electric current is transformed to hydroxide ions flux.

$$\frac{I}{F} = z_{\mathrm{OH^-}} g_{\mathrm{OH^-,\,Cathode}} \tag{3.47}$$

The fraction of ionic current resulting from the reaction at the Eqs. (2.30) and (2.31) may be related to the partial pressure of the reactant gases, as quantified in:

$$g_{\mathrm{Cl^-}} = \frac{I}{F\, z_{Cl^-}} \left(\frac{1}{2} \frac{P_{\mathrm{Cl_2}}}{(1 - P_{\mathrm{Cl_2}})} \right) \tag{3.48}$$

$$g_{\mathrm{H^+}} = \frac{I}{F\, z_{H^+}} \left(1 - \frac{1}{2} \frac{P_{\mathrm{Cl_2}}}{(1 - P_{\mathrm{Cl_2}})} \right) \tag{3.49}$$

where the factor 1/2 comes from the stoichiometric proportion of Eqs. (2.30) and (2.31), since one mole of reduced Cl_2 generates half moles of electrons than the case of O_2.

The partial pressure of chlorine gas $P_{\mathrm{Cl_2}}$ is computed by substituting Eq. (2.34) into the equation resulting from $E_{\mathrm{Cl_2}} = E_{\mathrm{O_2}}$ using Eqs. (2.32) and (2.33). In this model, $P_{\mathrm{Cl_2}}$ is therefore a function of the pH, the concentration of chloride ions in the vicinities of the anode and the overpotential factors. See [Paz-Garcia et al. Submitted 2012c] for two-dimensional plots showing the $P_{\mathrm{Cl_2}}$ value for different conditions.

In addition to the flux of ions, in order to keep the mass balance, the corresponding amount of water dissociated during the electrolysis reaction has to be included, which is proportional to the above calculated flux of protons and hydroxides by the stoichiometric relations given in Eq. (2.30) and Eq. (2.22).

$$\mathbf{f}_{\mathrm{H_2O,\,anode}} = -\frac{1}{2} \mathbf{f}_{\mathrm{H^+,\,anode}} \tag{3.50}$$

$$\mathbf{f}_{\mathrm{H_2O,\,cathode}} = -\mathbf{f}_{\mathrm{OH^-,\,cathode}} \tag{3.51}$$

It should be noted that the consumption of water by electrolysis is higher at the cathode than at the anode, which would produce gradients of saturation degree with the corresponding water transport and advective flow.

Constant voltage drop case:

The constant voltage case is modeled similarly to the constant current case, but it requires specific treatment.

First, a potential difference is set between the electrodes. For example, 0 V on the cathode (used as reference) and 5 V at the anode. The matrix system of equations is solved using these boundary conditions. According to what is explained in Section 3.1.5, the system calculates some values for $\mathbf{f}_r$ "reaction vector" related to the boundary conditions used. In this case, these vectors represent the amount of ionic charge that must be injected in system to give the intended potential difference.

The $\mathbf{f}_{r,\phi}$ obtained by the procedure for soling matrix systems of equations with forced boundary conditions, is a theoretical flux of ionic charge without physical meaning. The only realistic way to introduce ionic charge into the system is through the ions produced at the electrode reactions. Therefore, the flow of ionic charge in the $\mathbf{f}_{r,\phi,\,\mathrm{anode}}$, is converted into a flow of protons $\mathbf{f}_{\mathrm{H^+},\,\mathrm{anode}}$, and chlorides $\mathbf{f}_{\mathrm{Cl^-},\,\mathrm{anode}}$, while the cathode $f_{\phi,\,\mathrm{cathode}}$ becomes results in an hydroxides flow $\mathbf{f}_{\mathrm{OH^-},\,\mathrm{cathode}}$.

This conversion is done as part of the iterative procedure for solving the system of nonlinear equations. In any iteration of the numerical loop, the boundary/load vector is also updated and the system is solved using this new boundary/load vector value.

In the subsequent iterations, the boundary conditions are also applied, but the reactive vector is progressively decreased. The reactive vector value obtained in any iteration is added to the boundary/load vector from the iteration before, and the solution of the matrix system is repeated as many times as necessary until the reactive vector is minimized to zero or nearly zero value.

Therefore, the resolution loop nonlinear system, explained in Alg. (3.2), will have two acceptance conditions: one for comparing two consecutive profiles and another one for checking the minimization of the the reaction vector $\mathbf{f}_r$.

By this procedure, the one can find the flow of ions, resulting from the electrochemical reactions, that produced the intended potential difference, which is a very realistic manner to model electrochemically-induced ionic transport under constant voltage difference.

Part II

Appendices

A.1 Simulations on diffusion and electro-diffusion

The physicochemical and numerical proposed model is not restricted to simulate transport processes electrochemically-induced. In the absence of external electric fields and the corresponding electrochemical reactions, the model can be used for the simulation of free-diffusion processes, where the only driving-force is a gradient of concentration or a gradient of water content.

For example, free-diffusion simulations can be proposed in order to predict the chloride penetration rate into a concrete structure exposed to marine environment, which is crucial for the durability of reinforced concrete. Other examples are the standard desalination processes consisting of submerging samples into deionized water, as done in the treatments used for the desalination of historic finds and wood from sunk ships.

Many physicochemical models have been proposed for the prediction of ionic diffusion problems, focusing only on the Fick's law of diffusion, i.e. ignoring the effects of the diffusion potential and the ionic migration. The approximate results obtained in these diffusion models are assumed less accurate than those from enhanced models taking into account the electro-diffusion coupled transport. The bigger the difference between the diffusivities and the ionic charge of the diffusing ions, the larger the error in this kind of simplified models.

For example, the diffusion coefficients at infinite dilution for chloride and sodium ions are $D_{\mathrm{Cl}} = 2.03 \times 10^{-9}\ \mathrm{m^2\,s^{-1}}$ and $D_{\mathrm{Na}} = 1.33 \times 10^{-9}\ \mathrm{m^2\,s^{-1}}$ (from [Parkhurst and Appelo, 1999]). In an equimolar solution of NaCl undergoing a diffusion transport process from a region of higher to lower concentration, chloride ions would tend to diffuse faster than sodium ions. However, it is experimentally observed that both ions diffuse in a very similar rate, which is approximately the mean value of the diffusion rates. The reason why the salt diffuses almost as a bulk is the aforementioned electrostatic interactions between ions. The diffusion potential, originated due to the different diffusion rates, affects the ions so that it slows down the faster ions and speed up the slowest ions in order to keep the electric balance in the system according to the electroneutrality condition [Mitchell and Soga 1976, Rubinstein 1990].

To illustrate this phenomena, simulations of electro-diffusion and Fick's diffusion processes are compared. Fig. A.4 shows transient profiles for the one-dimensional penetration of NaCl into a porous structure. A chemically inert porous material with a porosity of 0.01 and with its pore structure completely saturated with pure water is placed into contact at one of its surface with an electrolyte solution of NaCl $0.05\,\mathrm{mol\,kg^{-1}}$ (as e.g. seawater). The amount of solution in contact with the exposed surface, outside the porous body, is assumed large enough to maintain constant concentration. Accordingly, the assumed-constant concentrations at the external surface is used as a boundary condition. The thickness of the porous material is 10 mm.

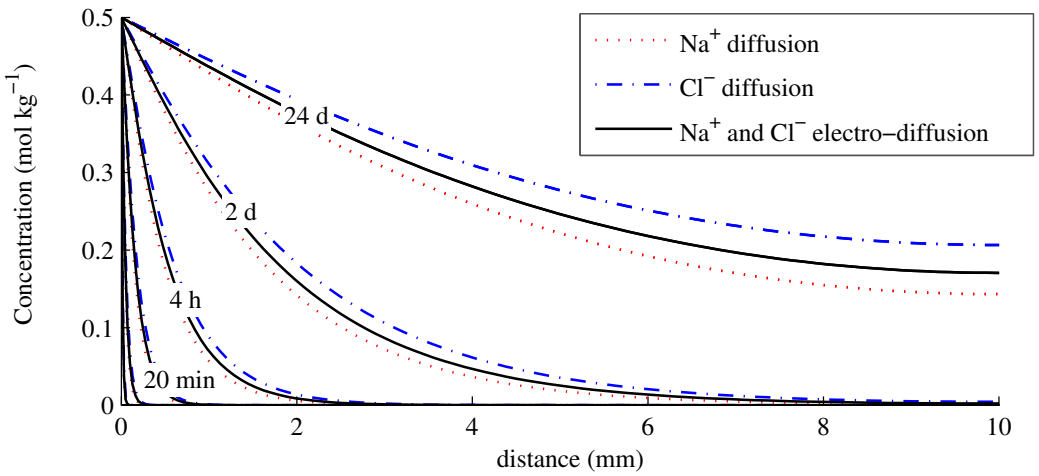

Figure A.4: Simulations for the electro-diffusion penetration of NaCl into a chemically inert porous media. Fick's diffusion, i.e. without the effects of the diffusion potential, is shown for comparison.

Results for Fick's diffusion are compared to the electro-diffusion case. As expected, in the hypothetical free-diffusion case without electrostatic forces, chloride migrates faster than sodium. In a more realistic case, including the effects of the electrostatics forces, the electro-diffusion process predicts the migration of both ions at a similar rate. Chloride is slowed down while sodium is accelerated, and both ions migrate, apparently, at the same rate.

A.2 Sparse matrices

Chemical systems, even the most simple ones, normally include a significant number of chemical species. For example, as shown in [Paz-Garcia et al. [Submitted 2012a]], a simple system consisting of solid $CaCO_3$ which dissolves in pure water involves at least 12 aqueous and solids species as: H_2O , H^+ , OH^- , Ca^{+2} , CO_3^{-2} , HCO_3^-, H_2CO_3, $CaOH^+$, $CaCO_3\,(aq)$, $Ca\,(OH)_2\,(s)$, $CaCO_3$, and $CaCO_3\,(s)$. If the ion Cl^{-1} is included in the same system, the number of species would be at least 17. The total number of chemical species in typical solid matrices under EK treatments, such a soil or masonry bricks, may be much higher. For example, in [Paz-Garcia et al. Submitted 2012c], 48 chemical species where included in simulations on electrokinetic desalination of bricks.

As the accuracy of the numerical method increases with the number of nodes, the number of finite elements would be high, so that the number of nodes, N_{nodes}. The global matrix system of equations obtained in the ENPP model, expressed in Eq. (3.21) will be formed by squared matrices and vectors of size equal to $(N+2) \times N_{\text{nodes}}$, in the order of a few thousands of rows and columns.

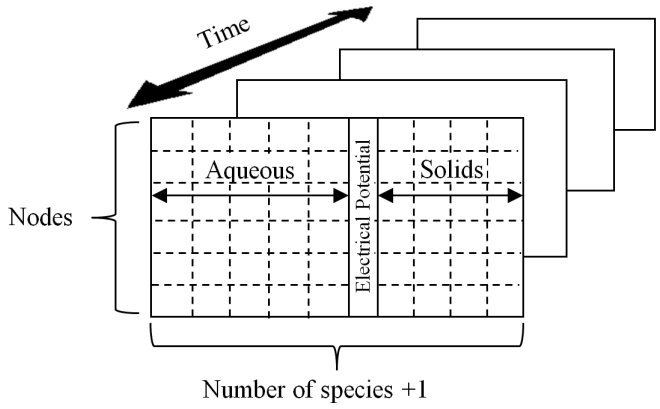

Figure A.5: Three-dimensional matrix for the storage of the transient profiles

As mentioned before, only a small fractions of the elements in the matrices are nonzero, i.e. the matrix system of equations in a finite elements model is sparse. Matlab®, as many other programming languages, includes specific built-in functions which efficiently deal with sparse matrices [Lindfield and Penny 1997, Gilbert et al. 1991, Moler 2004].

Sparse matrices models properly implemented with their sparse matrices functions do a better management of the physical memory of the computer, which results in an increase of the computational speed. Simulations are one or more order of magnitude faster than those not implemented with specific functions for sparse matrices and may even overload the physical memory making impossible the simulation.

Matlab® does not automatically treat a matrix as sparse and the sparsity features are not introduced until invoked. Consequently, the programmer has to use those specific functions for sparse matrices when implementing the numerical model. An example of this kind of functions is the function "spdiags", mentioned in Section 3.1.2.

A.3 Hyper-matrices

The organization and storage of the transient profiles obtained in the numerical procedure has been organized by means of tridimensional matrices, denoted as hyper-matrices in Matlab®.

Vectors $\mathbf{a}(t)$ obtained for each transient profile are rearranged in matrix form. A row for any node and a column for any species and for the electric potential. Every matrix associated to a transient profile, is part of a three-dimensional hyper-matrix as shown in Fig. A.5.

This procedure for memory storing of the transient profiles result in a very intuitive setup for the subsequent management of the data, such as the plotting routines or importing/exporting data functions. Additionally, it is possible to store only a

fraction of the computed transient profiles. Therefore, an important amount of physical memory is released, which is available for the system in the calculations, which results also in faster computations.

The hyper-matrices storage procedure proposed here is fully compatible with two- and three-dimensional domains, since the information is stored in the nodes of the matrices and not in the finite element itself.

A.4 Two-dimensional model

As mentioned before, it is possible to implement two- and three-dimensional finite elements numerical models for the solution of reactive-transport processes.

There is no differences on the physicochemical when it is applied to one- or two-dimensional models. Nevertheless, the numerical solution requires specific implementation. Two-dimensional finite elements modeling is a common tool for the study of solid mechanics. In the case of strongly nonlinear coupled reactive-transport systems, as the extended NPP system, the two-dimensional implementation is also possible. Further discussion on two-dimensional FE modeling can be found in specific bibliography [Ottosen and Petersson 1992, Ottosen and Ristinmaa 2005, Zienkiewicz and Taylor 2005] .

The implementation of two-dimensional finite elements models affects only to the transport process model, as the chemical equilibrium module described in [Paz-Garcia et al. Submitted 2012a] is completely compatible irrespectively of the dimensions of the model, since the chemical equilibrium computation is done node-by-node of the spatial domain.

In the current appendices, a brief introduction of two-dimensional finite elements modeling is described, as a proposal for a future generalized implementation. The most simple linear triangular finite element is used here.

Two-dimensional triangular element

In a two-dimensional finite elements model, the two-dimensional domain is also divided in nodes, which are defined by their coordinates in the plane.

Here, a triangular element defined in a square net is used, assumed as the most simple and popular two-dimensional element. Let us consider a triangular finite element, limited by the nodes i, j, and k, as shown in Fig. A.6. The nodes are defined by their coordinates in the plane.

In this case, the shape function N is a vector function defined as:

$$\mathbf{N}^e = \left[\begin{array}{ccc} N_i^e & N_j^e & N_k^e \end{array} \right] \tag{A.52}$$

where

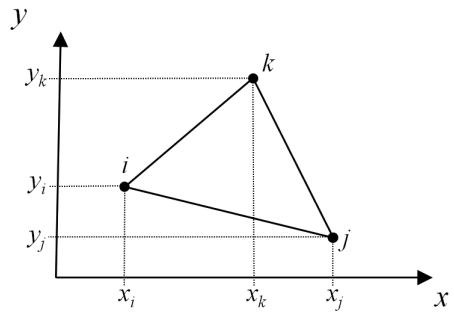

Figure A.6: Triangular two-dimensional finite element

$$N_i^e = \frac{1}{2A}\left((x_j y_k - x_k y_j) + (y_j - y_k)\, x + (x_k - x_j)\, y\right) \tag{A.53}$$

$$N_j^e = \frac{1}{2A}\left((x_k y_i - x_i y_k) + (y_k - y_i)\, x + (x_i - x_k)\, y\right) \tag{A.54}$$

$$N_k^e = \frac{1}{2A}\left((x_i y_j - x_j y_i) + (y_i - y_j)\, x + (x_j - x_i)\, y\right) \tag{A.55}$$

and

$$2A = (x_j y_k - x_k y_j) - (x_i y_k - x_k y_i) - (x_i y_j - x_j y_i) \tag{A.56}$$

The vector function B, defined as the gradient of the shape function N, is a matrix defined as:

$$\mathbf{B}^e = \nabla \mathbf{N}^e = \begin{bmatrix} \frac{\partial N^e}{\partial x} \\ \frac{\partial N^e}{\partial y} \end{bmatrix} = \begin{bmatrix} \frac{\partial N_i^e}{\partial x} & \frac{\partial N_j^e}{\partial x} & \frac{\partial N_k^e}{\partial x} \\ \frac{\partial N_i^e}{\partial y} & \frac{\partial N_j^e}{\partial y} & \frac{\partial N_k^e}{\partial y} \end{bmatrix} \tag{A.57}$$

equivalent to:

$$\mathbf{B}^e = \frac{1}{2A}\begin{bmatrix} y_i - y_k & y_k - y_i & y_i - y_j \\ x_k - x_j & x_i - x_k & x_j - x_i \end{bmatrix} \tag{A.58}$$

In any case, the products $\mathbf{B}^{\mathrm{T}}\mathbf{B}$ and $\mathbf{N}^{\mathrm{T}}\mathbf{N}$ give 3 by 3 matrices.

Two-dimensional topology matrix

Let us consider a two-dimensional domain defined by a square net done in Fig. A.7, where nodes have been numbered column by column and the triangular elements have also been numbered using small triangles.

A topology matrix collects the information about which nodes belongs and determine any triangular element. The topology matrix for the domain defined in Fig. A.7 is:

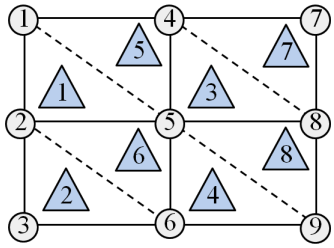

Figure A.7: Two-dimensional domain divided in triangular finite elements

$$\begin{bmatrix} 1 & 2 & 5 \\ 2 & 3 & 6 \\ 4 & 5 & 8 \\ 5 & 6 & 9 \\ \vdots & \vdots & \vdots \\ 5 & 9 & 8 \end{bmatrix} \tag{A.59}$$

where any e^{th} row has the indexes of the nodes that belongs to the e^{th} element.

Two-dimensional assembly

The main difference with respect to the one-dimensional domain is that it is not straightforward to determine which nodes are describing any finite element. Nodes that surround a finite element are not necessarily consecutive in the vector **a** with the value of the state variables at the discrete nodes. Therefore, the assembly process get complicated and vectorized sparse functions for the one-dimensional implementation unfit, leading to slow two-dimensional simulations (in terms of computational time).

Alg. (A.3) shows a pseudo-code for the procedure followed for the two-dimensional assembly process. Item 5 in the Alg. (A.3) requires special attention. As an example, let us consider the first and second elements in the domain defined in Fig. A.7. Nodes 1^{st} , 2^{nd} and 5^{th} nodes limit the first element while the 2^{nd}, 3^{rd} and 6^{th} nodes limit the second element.

Let us consider the matrix equation for the first and second elements before the assembly process as:

$$\begin{bmatrix} k_{1,(1,1)} & k_{1,(1,2)} & k_{1,(1,3)} \\ k_{1,(2,1)} & k_{1,(2,2)} & k_{1,(2,3)} \\ k_{1,(3,1)} & k_{1,(3,2)} & k_{1,(3,3)} \end{bmatrix} \begin{bmatrix} a_{1,1} \\ a_{1,2} \\ a_{1,3} \end{bmatrix} = \begin{bmatrix} f_{1,1} \\ f_{1,2} \\ f_{1,3} \end{bmatrix} \tag{A.60}$$

and

Algorithm A.3 Two-dimensional assembly pseudo-code

For $e = 1$ until $e =$ total number of nodes

1. The 3 nodes that limits the triangular element are obtained from the topology matrix
2. The characteristic element mean value k_e is calculated form the mean value at the 3 limiting nodes.
3. The coordinates of the elements $\begin{pmatrix} x_i & y_i \end{pmatrix}$, $\begin{pmatrix} x_j & y_j \end{pmatrix}$ and $\begin{pmatrix} x_k & y_k \end{pmatrix}$ are obtained depending on their position in the two-dimensional grid.
4. The mass matrix $\left(\mathbf{C}_e = \int_{S_e} \mathbf{N}^{\mathrm{T}} k_e \mathbf{N}\, dS_e\right)$ or the conductivity matrix $\left(\mathbf{K}_e = \int_{S_e} \mathbf{B}^{\mathrm{T}} k_e \mathbf{B}\, dS_e\right)$ is computed, being S_e the surface of the element.
5. The local matrices are added to the global matrix in their corresponding position

end

$$\begin{bmatrix} k_{2,(1,1)} & k_{2,(1,2)} & k_{2,(1,3)} \\ k_{2,(2,1)} & k_{2,(2,2)} & k_{2,(2,3)} \\ k_{2,(3,1)} & k_{2,(3,2)} & k_{2,(3,3)} \end{bmatrix} \begin{bmatrix} a_{2,1} \\ a_{2,2} \\ a_{2,3} \end{bmatrix} = \begin{bmatrix} f_{2,1} \\ f_{2,2} \\ f_{2,3} \end{bmatrix} \tag{A.61}$$

The first subscripts is the index for the element and the subsequent subscripts are for the position in the matrix or vector. According to the topology matrix, it is observed that:

$$\begin{aligned} a_1 &= a_{1,1} \\ a_2 &= a_{1,2} = a_{2,1} \\ a_3 &= a_{2,2} \\ a_5 &= a_{1,3} \\ a_6 &= a_{2,3} \end{aligned}$$

In the first iteration of the Alg. (A.3), the values for the first element are placed in their proper position of an empty global matrix as:

$$\mathbf{K} = \begin{bmatrix} k_{1,(1,2)} & k_{1,(1,2)} & 0 & 0 & k_{1,(1,3)} & 0 & \cdots \\ k_{1,(2,1)} & k_{1,(2,2)} & 0 & 0 & k_{1,(2,3)} & 0 & \cdots \\ 0 & 0 & 0 & 0 & 0 & 0 & \cdots \\ 0 & 0 & 0 & 0 & 0 & 0 & \cdots \\ k_{1,(3,1)} & k_{1,(3,2)} & 0 & 0 & k_{1,(3,3)} & 0 & \cdots \\ 0 & 0 & 0 & 0 & 0 & 0 & \cdots \\ \vdots & \vdots & \vdots & \vdots & \vdots & \vdots & \ddots \end{bmatrix} \tag{A.62}$$

and

$$\mathbf{f} = \begin{bmatrix} f_{1,1} \\ f_{1,2} \\ 0 \\ 0 \\ f_{1,3} \\ \vdots \end{bmatrix} \tag{A.63}$$

In the second iteration, the values for the second element and added to the previous matrix, in their proper location as:

$$\mathbf{K} = \begin{bmatrix} k_{1,(1,2)} & k_{1,(1,2)} & 0 & 0 & k_{1,(1,3)} & 0 & \cdots \\ k_{1,(2,1)} & \left(k_{1,(2,2)} + k_{2,(1,1)}\right) & k_{2,(1,3)} & 0 & k_{1,(2,3)} & k_{2,(1,3)} & \cdots \\ 0 & k_{2,(2,1)} & k_{2,(2,2)} & 0 & 0 & k_{2,(2,3)} & \cdots \\ 0 & 0 & 0 & 0 & 0 & 0 & \cdots \\ k_{1,(3,1)} & k_{1,(3,2)} & 0 & 0 & k_{1,(3,3)} & 0 & \cdots \\ 0 & k_{2,(3,1)} & k_{2,(3,2)} & 0 & 0 & k_{2,(3,3)} & \cdots \\ \vdots & \vdots & \vdots & \vdots & \vdots & \vdots & \ddots \end{bmatrix} \tag{A.64}$$

and

$$\mathbf{f} = \begin{bmatrix} f_{1,1} \\ f_{1,2} + f_{2,1} \\ f_{2,2} \\ 0 \\ f_{1,3} \\ f_{2,3} \\ \vdots \end{bmatrix} \tag{A.65}$$

This assembly process, dependent on the topology matrix, is undoubtedly more complicated and computationally costly than the one-dimensional case. As mentioned

in Section 1.3.8, the two-dimensional model is proposed as a future enhancement of the present model.

A.5 Discrete approximation in time with quadratic elements

In transient systems with drastic changing boundary conditions and sharp gradients of the state variables, the finite elements time integration of a nonlinear partial differential equations system may produce erroneous results [Zienkiewicz 1991, Ottosen and Petersson 1992, Zienkiewicz and Taylor 2005, Ottosen and Ristinmaa 2005]. In order to improve the stability of the transient integration, a quadratic element for the time domain integration, known as Newmark time integration scheme, can be used.

In the quadratic element, in contrast to the linear element, the next time-step of the numerical integration $\mathbf{a}(t_0 + \Delta t)$ is computed, not only from the information in the current time-step $\mathbf{a}(t_0)$, but also from the information of a time-step before the current one, i.e. $\mathbf{a}(t_0 - \Delta t)$. This numerical procedure significantly reduces numerical errors related to oscillatory results, isolated peaks and destabilization of the numerical process.

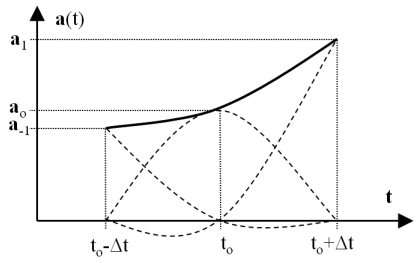

Figure A.8: Quadratic element for time discretization approach

The shape function, in the Newmark time discretization approach, is a quadratic polynomial function in the form:

$$\mathbf{N} = \frac{1}{\Delta t^2}\left[(t-\Delta t)\frac{t}{2},\ -(t-\Delta t)(t+\Delta t),\ (t+\Delta t)\frac{t}{2}\right] \tag{A.66}$$

As done in the linear element case, a change of variable is used to normalized the finite element. In this context, using $\tau\Delta t = t - t_0$, the approximate quadratic function interpolating between nodes is obtained as:

$$\mathbf{Na}(\tau) = \left[(\tau-1)\frac{\tau}{2},\ -(\tau-1)(\tau+1),\ (\tau+1)\frac{\tau}{2}\right]\begin{bmatrix} a_{-1} \\ a_0 \\ a_1 \end{bmatrix} \tag{A.67}$$

The matrix function, discretized in the spatial domain, shown in Eq. (3.21) is multiplied by an arbitrary time-dependent weight function and integrated through the domain of the element:

$$\int_{-\Delta t}^{\Delta t} \omega(t)\left(\mathbf{C}\frac{d\mathbf{a}(t)}{dt} + \mathbf{K}\mathbf{a}(t) + \mathbf{f}(t)\right)dt = \int_{-1}^{1} \omega(\tau)\left(\mathbf{C}\frac{d\mathbf{a}(\tau)}{dt} + \mathbf{K}\mathbf{a}(\tau) + \mathbf{f}(\tau)\right)d\tau = 0 \tag{A.68}$$

The following scalar parameters are defined which values depend on the chosen weight function:

$$\alpha = \frac{\int_{-1}^{1}\omega\left(\tau+\frac{1}{2}\right)d\tau}{\int_{-\mathbf{1}}^{\mathbf{1}}\omega d\tau} \quad ; \quad \beta = \frac{\int_{-1}^{1}\omega(\tau+1)\frac{\tau}{2}d\tau}{\int_{-1}^{1}\omega d\tau} \tag{A.69}$$

By substituting Eq. (A.67) into Eq. (A.68), and using the scalar parameters β and δ the following function is obtained:

$$\begin{aligned}\frac{\mathbf{C}}{\Delta t}\left((\alpha-1)\mathbf{a}_{-1} + (1-2\alpha)\mathbf{a}_0 + \alpha\mathbf{a}_1\right) + \\ + \mathbf{K}\left((1/2+\beta-\alpha)\mathbf{a}_{-1} + (1/2+\alpha-2\beta)\mathbf{a}_0 + \beta\mathbf{a}_1\right) + \\ + (1/2+\beta-\alpha)\mathbf{f}_{-1} + (1/2+\alpha-2\beta)\mathbf{f}_0 + \beta\mathbf{f}_1 = 0\end{aligned} \tag{A.70}$$

where the following linear combinations of α and β have been used:

$$\begin{aligned} -2\tau &= 1-2\alpha \\ -(\tau-1)(\tau+1) &= 1/2 - 2\beta + \alpha \\ \tau - 1/2 &= \alpha - 1 \\ \tau/2(\tau-1) &= 1/2 + \beta - \alpha \end{aligned}$$

Table A.3: α and β values for different evaluated shape functions.

Scheme	Weight function $\omega(\tau)$	α	β
Forward quadratic	$-(1-\tau)\tau/2$	$-1/2$	$-1/5$
Middle quadratic	$(1-\tau)(1+\tau)$	$1/2$	$1/10$
Backward quadratic	$(1+\tau)\tau/2$	$3/2$	$4/5$
Linear	$(1+\tau)/2$	$5/6$	$1/3$

Eq. (A.70) can be reorganized to obtain a simplified matrix system of equations in the form of:

$$\mathbf{K}^{\star}\mathbf{a}_1 + \mathbf{f}^{\star} = 0 \tag{A.71}$$

where

$$\mathbf{K}^{\star} = \frac{\mathbf{C}}{\Delta t}\alpha + \mathbf{K}\beta \tag{A.72}$$

and

$$\begin{aligned}\mathbf{f}^{\star} = \left(\frac{\mathbf{C}}{\mathbf{\Delta t}}(1-2\alpha) + \mathbf{K}(1/2+\alpha-2\beta)\right)a_0 + \\ + \left(\frac{\mathbf{C}}{\Delta t}(\alpha-1) + \mathbf{K}(1/2+\beta-\alpha)\right)a_{-1} + \\ + (1/2+\beta-\alpha)\mathbf{f}_{-1} + (1/2+\alpha-2\beta)\mathbf{f}_0 + \beta\mathbf{f}_1\end{aligned} \tag{A.73}$$

The time integration constants α and β depends on the chosen weight for the discretization process. Different evaluated shape functions and the corresponding α and β values are shown in Table A.3.

List of Figures

List of Tables

List of Algorithms

Bibliography

Y.B. Acar and A.N. Alshawabkeh. Principles of electrokinetic remediation. *Environ. Sci. Technol.*, 27(13):2638–2647, 1993.

Y.B. Acar, R.J. Gale, A.N. Alshawabkeh, R.E. Marks, S. Puppala, M. Bricka, and R. Parker. Electrokinetic remediation: Basics and technology status. *J. Hazard. Mater.*, 40(2):117–137, 1995.

A.Z. Al-Hamdan and K.R. Reddy. Electrokinetic remediation modeling incorporating geochemical effects. *J. Geotech. Geoenviron.*, 134:91–105, 2008.

A.N. Alshawabkeh and Y.B. Acar. Electrokinetic remediation II: Theoretical model. *J. Geotech. Eng-ASCE*, 122(3):186–196, 1996.

A.N. Alshawabkeh, A.T. Yeung, and M.R. Bricka. Practical aspects of in-situ electrokinetic extraction. *J. Environ. Eng.*, 125(1):27–35, 1999.

L. Bertolini, L. Coppola, M. Gastaldi, and E. Redaelli. Electroosmotic transport in porous construction materials and dehumidification of masonry. *Constr. Build. Mater.*, 23(1):254–263, 2009.

C.M. Bethke. *Geochemical and biogeochemical reaction modeling.* Cambridge University Press, 2 edition, 2008.

M. Castellote, C. Andrade, and C. Alonso. Electrochemical removal of chlorides: Modelling of the extraction, resulting profiles and determination of the efficient time of treatment. *Cem. Concr. Res.*, 30(4):615–621, 2000.

R. Chang and J.S. Overby. *General chemistry - The essential concepts.* McGraw-Hill, New York, 2011.

Y.S. Choi and R. Lui. A mathematical model for the electrokinetic remediation of contaminated soil. *J. Hazard. Mater.*, 44(1):61–75, 1995.

A.V. Delgado, F. Gonzalez-Caballero, R.J. Hunter, L.K. Koopal, and J. Lyklema. Measurement and interpretation of electrokinetic phenomena. *J. Colloid Interf. Sci.*, 309(2):194–224, 2007.

L. Dongqing. Basics of electrical double layer. In *Electrokinetics in microfluidics*, chapter 2. Academic Press, 2004.

J.R. Gilbert, C. Moler, and R. Schreiber. Sparse matrices in MATLAB: design and implementation. *SIAM J. Matrix Anal. Appl.*, 1:1–47, 1991.

M.T. Harris, D.W. DePaoli, and M.R. Ally. Modeling the electrokinetic decontamination of concrete. *Sep. Sci. Technol.*, 32:827–848, 1997.

F.G. Herruzo, J.M.R. Maroto, R.A.G. Delgado, C.G. Lahoz, and C.V. Alonso. Limpieza de suelos por electrodescontaminacion (I). *Ing. Quim.*, 32(369):215–222, 2000.

R.A. Jacobs and R.F. Probstein. Two-dimensional modeling of electroremediation. *AIChE J.*, 42(6):1685–1696, 1996.

M. Janz. *Methods of measuring the moisture diffusivity at high moisture levels*. PhD thesis, University of Lund, 1997.

A. Javadi and M. Al-Najjar. Finite element modeling of contaminant transport in soils including the effect of chemical reactions. *J. Hazard. Mater.*, 143(3):690–701, 2007.

A.A. Jennings and P. Mansharamani. Modeling electrokinetically-enhanced aggregate remediation. *Environm. Modell. Softw.*, 14(6):625–634, 1999.

P.E. Jensen, B.K. Ahring, and L.M. Ottosen. Organic acid enhanced electrodialytic extraction of lead from contaminated soil fines in suspension. *J. Chem. Technol. Biot.*, 82(10):920–928, 2007.

B. Johannesson. A theoretical model describing diffusion of a mixture of different types of ions in pore solution of concrete coupled to moisture transport. *Cem. Concr. Res.*, 33(4):481–488, 2003.

B. Johannesson. Ionic diffusion and kinetic homogeneous chemical reactions in the pore solution of porous materials with moisture transport. *Comput. Geotech.*, 36 (4):577–588, 2009.

B. Johannesson. Comparison between the Gauss' law method and the zero current method to calculate multi-species ionic diffusion in saturated uncharged porous materials. *Computers and Geotechnics*, 37(5):667–677, 2010a.

B. Johannesson. Development of a generalized version of the Poisson-Nernst-Planck equations using the hybrid mixture theory: Presentation of 2D numerical examples. *Transport porous med.*, 85(2):565–592, 2010b.

B. Johannesson and M. Janz. A two-phase moisture transport model accounting for sorption hysteresis in layered porous building constructions. *Build. Environ.*, 44(6): 1285–1294, 2009.

B. Johannesson and L.M. Ottosen. Modeling of electromigration salt removal methods in building materials. In *Proceedings from Salt Weathering on Building and Stone Sculptures*, pages 351–360, 2008.

B. Johannesson, Y. Hosokawa, and K. Yamada. Numerical calculations of the effect of moisture content and moisture flow on ionic multi-species diffusion in the pore solution of porous materials. *Comput. Struct.*, 87(1-2):39–46, 2009.

B.F. Johannesson. Diffusion of a mixture of cations and anions dissolved in water. *Cem. Concr. Res.*, 29(8):1261–1270, 1999.

K. Kamran, L. Pel, A. Sawdy, H. Huinink, and K. Kopinga. Desalination of porous building materials by electrokinetics: an NMR study. *Mater. Struct.*, 45:297–308, 2012.

G.M. Kirkelund, L.M. Ottosen, and A. Villumsen. Electrodialytic remediation of harbour sediment in suspension - Evaluation of effects induced by changes in stirring velocity and current density on heavy metal removal and pH. *J. Hazard. Mater.*, 169:685–690, 2009.

T. Koster, W. Peelen, J. Larbi, M. de Rooij, and R. Polder. Numerical model of Ca(OH)2 transport in concrete due to electrical currents. *Mater. Corros.*, 61(6): 518–523, 2010.

B. Li, B. Lu, Z. Wang, and J.A. McCammon. Solutions to a reduced Poisson-Nernst-Planck system and determination of reaction rates. *Physica A*, 389(7):1329–1345, 2010.

L.Y. Li and C.L. Page. Modelling of electrochemical chloride extraction from concrete: influence of ionic activity coefficients. *Comput. Mater. Sci.*, 9(3):303–308, 1998.

L.Y. Li and C.L. Page. Finite element modelling of chloride removal from concrete by an electrochemical method. *Corros. Sci.*, 42(12):2145–2165, 2000.

P.C. Lichtner. Continuum model for simultaneous chemical reactions and mass transport in hydrothermal systems. *Geochim. Cosmochim. Acta*, 49(3):779–800, 1985.

A.T. Lima, A.B. Ribeiro, J.M. Rodríguez-Maroto, E.P. Mateus, A.M. Castro, and L.M. Ottosen. Experimental and modeling of the electrodialytic and dialytic treatment of a fly ash containing Cd, Cu and Pb. *J. Appl. Electrochem.*, 40(9):1689–1697, 2010.

G.R. Lindfield and J.E.T. Penny. Using matlab for sparse matrices. *Int. J. Math. Edu. Sci. Technol.*, 28(3):427–436, 1997.

B. Lu, M.J. Holst, J. Andrew McCammon, and YC Zhou. Poisson-Nernst-Planck equations for simulating biomolecular diffusion-reaction processes I: Finite element solutions. *J. Comput. Phys.*, 229(19):6979–6994, 2010.

J. Lyklema. *Fundamentals of interface and colloid science*, volume 5. Academic Press, 2005.

A. Mahamet, K. Urtenov, E.V. Kirillova, N.M. Seidova, and V.V. Nikonenko. Decoupling of the Nernst-Planck and Poisson equations. application to a membrane system at overlimiting currents. *J. Phys. Chem. B*, 111(51):14208–14222, 2007.

P. Marcus. *Corrosion mechanisms in theory and practice*. CRC Press, Taylor & Francis Group, Boca Raton, 3 edition, 2011.

A.D. McNaught and A. Wilkinson. *Compendium of Chemical Terminology: Iupac Recommendations*. Blackwell Science, 2 edition, 1997.

J.K. Mitchell and K. Soga. *Fundamentals of soil behavior*. Wiley New York, 1976.

C.B. Moler. *Numerical computing with MATLAB*. Society for Industrial Mathematics, 2004.

T.Q. Nguyen, J. Petkovic, P. Dangla, and V. Baroghel-Bouny. Modelling of coupled ion and moisture transport in porous building materials. *Constr. Build. Mater.*, 22 (11):2185–2195, 2008.

E.P. Nielsen and M.R. Geiker. Chloride diffusion in partially saturated cementitious material. *Cem. Concr. Res.*, 33(1):133–138, 2003.

L.M. Ottosen and I. Rörig-Dalgaard. Electrokinetic removal of Ca(NO3)2 from bricks to avoid salt-induced decay. *Electrochim. Acta*, 52(10):3454–3463, 2007.

L.M. Ottosen and I. Rörig-Dalgaard. Desalination of a brick by application of an electric dc field. *Mater. Struct.*, 42(7):961–971, 2009.

L.M. Ottosen, G.M. Nystrom, P.E. Jensen, and A. Villumsen. Electrodialytic extraction of Cd and Cu from sediment from sisimiut harbour, greenland. *J. Hazard. Mater.*, 140(1-2):271–279, 2007.

L.M. Ottosen, I.V. Christensen, I. Rorig-Dalgaard, P.E. Jensen, and H.K. Hansen. Utilization of electromigration in civil and environmental engineering - Processes, transport rates and matrix changes. *J. Environ. Sci. Health, Part A*, 43(8):795–809, 2008.

L.M. Ottosen, C.M.D. Ferreira, and I.V. Christensen. Electrokinetic desalination of glazed ceramic tiles. *J. Appl. Electrochem.*, 40(6):1161–1171, 2010.

N.S. Ottosen and H. Petersson. *Introduction to the finite element method*. Prentice-Hall, 1992.

N.S. Ottosen and M. Ristinmaa. *The mechanics of constitutive modeling*. Elsevier Science, 2005.

Y. Pachepsky, D. Timlin, and W. Rawls. Generalized Richards' equation to simulate water transport in unsaturated soils. *J. Hydrol.*, 272:3–13, 2003.

S. Pamukcu. Electrochemical transport and transformations. In Krishna R. Reddy and Claudio Cameselle, editors, *Electrochemical Remediation Technologies for Polluted Soils, Sediments and Groundwater*, pages 29–64. Wiley Online Library, 2009.

D.L. Parkhurst and C.A.J. Appelo. *User's guide to PHREEQC (version 2) - A computer program for speciation, batch-reaction, one-dimensional transport, and inverse geochemical calculations*. U.S. Department of the Interior, Water-Resources Investigations Reports (99-4259), 1999.

J.M. Paz-Garcia, B. Johannesson, and L.M. Ottosen. Numerical simulations of electrokinetic processes comparing the use of a constant voltage difference or a constant current as driving force. Poster in Annual meeting of the Danish Electrochemical Society - Conference on Electrochemical Science and Technology, 2010.

J.M. Paz-Garcia, B. Johannesson, L.M. Ottosen, A.N. Alshawabkeh, A.B. Ribeiro, and J.M. Rodriguez-Maroto. Coupling the transport of water and aqueous species in finite element modeling of electrokinetics. In *Proceedings from The 12th Mediterranean Congress of Chemical Engineering*, Barcelona, Spain., November 15-18 2011a.

J.M. Paz-Garcia, B. Johannesson, L.M. Ottosen, A.B. Ribeiro, and J.M. Rodriguez-Maroto. Influence of the chemical interactions on the removal rate of different salts in electrokinetic desalination processes. In *SWBSS 2011, Salt Weathering on Buildings and Stone Sculptures. Limassol, Cyprus, 19–22 October, 2011.*, 2011b.

J.M. Paz-Garcia, B. Johannesson, L.M. Ottosen, A.B. Ribeiro, and J.M. Rodriguez-Maroto. Two-dimensional modeling of the electrokinetic desalination treatment of a brick wall. In *10th Symposium on Electrokinetic Remediation - Developments in Electrokinetic Remediation of Soils, Sediments and Construction Materials*, 2011c.

J.M. Paz-Garcia, B. Johannesson, L.M. Ottosen, A.B. Ribeiro, and J.M. Rodriguez-Maroto. Modeling of electrokinetic processes by finite element integration of the

Nernst-Planck-Poisson system of equations. *Sep. Purif. Technol.*, 79(2):183–192, 2011d.

J.M. Paz-García, K. Baek, I.D. Alshawabkeh, and A.N. Alshawabkeh. A generalized model for transport of contaminants in soil by electric fields. *J. Environ. Sci. Health, Part A*, 47(2):308–318, 2012.

J.M. Paz-García, B. Johannesson, L.M. Ottosen, A.N. Alshawabkeh, A.B. Ribeiro, and J.M. Rodríguez-Maroto. Modeling of electrokinetic desalination of bricks. *Electrochim. Acta*, 2012 In press.

J.M. Paz-Garcia, B. Johannesson, L.M. Ottosen, A.B. Ribeiro, and J.M. Rodriguez-Maroto. Computing chemical equilibrium systems with an algorithm based on the reaction extents. *Comput. Chem. Eng.*, Submitted 2012a.

J.M. Paz-Garcia, B. Johannesson, L.M. Ottosen, A.B. Ribeiro, and J.M. Rodriguez-Maroto. Modeling of the formation of electric double layers including chemical reaction effects. *AIChE J.*, Submitted 2012b.

J.M. Paz-Garcia, B. Johannesson, L.M. Ottosen, A.B. Ribeiro, and J.M. Rodriguez-Maroto. Simulation-based analysis of the differences in the removal rate of chlorides, nitrates and sulfates by electrokinetic desalination treatments. *Electrochim. Acta*, Submitted 2012c.

K. Popov, I. Glazkova, V. Yachmenev, and A. Nikolayev. Electrokinetic remediation of concrete: Effect of chelating agents. *Environm. Pollut.*, 153(1):22–28, 2008.

W.H. Press, S.A. Teukolsky, W.T. Vetterling, and B.P. Flannery. Root finding and nonlinear sets of equations. In *Numerical recipes in C: The art of Scientific Computing*, chapter 9. Cambridge University Press, 1992.

J.B. Rawlings and J.G. Ekerdt. *Chemical reactor analysis and design fundamentals*, volume 67. Nob Hill Publishing, 2002.

K.R. Reddy and C. Cameselle. *Electrochemical remediation technologies for polluted soils, sediments and groundwater*. John Wiley And Sons Inc, 2009.

A.B. Ribeiro, J.M. Rodriguez-Maroto, E.P. Mateus, and H. Gomes. Removal of organic contaminants from soils by an electrokinetic process: the case of atrazine. Experimental and modeling. *Chemosphere*, 59(9):1229–1239, 2005.

AB Ribeiro, JM Rodríguez-Maroto, EP Mateus, E. Velizarova, and L.M. Ottosen. Modeling of electrodialytic and dialytic removal of Cr, Cu and As from CCA-treated wood chips. *Chemosphere*, 66(9):1716–1726, 2007.

L. A. Richards. Capillary conduction of liquids in porous mediums. *Physics*, 1(5): 318–333, 1931.

J.M. Rodriguez-Maroto and C. Vereda-Alonso. Electrokinetic modeling of heavy metals. In K.R. Reddy and C. Camesselle, editors, *Electrochemical Remediation Technologies for Polluted Soils, Sediments and Groundwater*, chapter 25, pages 537–562. Wiley Online Library, 2009.

S. Roels, J. Carmeliet, and H. Hens. Modelling unsaturated moisture transport in heterogeneous limestone. *Transport porous med.*, 52(3):333–350, 2003.

I. Rörig-Dalgaard, L.M. Ottosen, and H.K. Hansen. Diffusion and electromigration in clay bricks influenced by differences in the pore system resulting from firing. *Constr. Build. Mater.*, 27(1):390–397, 2012.

J. Rubin. Transport of reacting solutes in porous media: Relation between mathematical nature of problem formulation and chemical nature of reactions. *Water Resour. Res*, 19(5):1231–1252, 1983.

I. Rubinstein. *Electro-diffusion of ions*. Society for Industrial Mathematics, 1990.

I. Rubinstein and L.A. Segel. Breakdown of a stationary solution to the Nernst-Planck-Poisson equations. *J. Chem. Soc., Faraday Trans. 2*, 75:936–940, 1979.

E. Samson and J. Marchand. Numerical solution of the extended Nernst-Planck model. *J. Colloid Interf. Sci.*, 215(1):1–8, 1999.

E. Samson, J. Marchand, and J.J. Beaudoin. Modeling the influence of chemical reactions on the mechanisms of ionic transport in porous materials: An overview. *Cem. Concr. Res.*, 30(12):1895–1902, 2000.

T. Sokalski, P. Lingenfelter, and A. Lewenstam. Numerical solution of the coupled Nernst-Planck and Poisson equations for liquid junction and ion selective membrane potentials. *J. Phys. Chem. B*, 107(11):2443–2452, 2003.

J.D. Subires-Munoz, A. Garcia-Rubio, C. Vereda-Alonso, C. Gomez-Lahoz, J.M. Rodriguez-Maroto, F. Garcia-Herruzo, and J.M. Paz-Garcia. Feasibility study of the use of different extractant agents in the remediation of a mercury contaminated soil from almaden. *Sep. Purif. Technol.*, 79:151–156, 2011.

N. Tankovsky and E. Syrakov. A modified Einstein-Nernst relation between mobility and diffusion of charges to evaluate the non-equilibrium, transient processes of ions in electrolytes. *Ionics*, 15(5):589–595, 2009.

P. Vanysek. Ionic conductivity and diffusion at infinite dilution. In *CRC Handbook of Chemistry and Physics*, volume 83. CRC Press, 2007.

C. Vereda-Alonso, J. Miguel Rodriguez-Maroto, R.A. Garcia-Delgado, C. Gómez-Lahoz, and F. Garcia-Herruzo. Two-dimensional model for soil electrokinetic remediation of heavy metals: Application to a copper spiked kaolin. *Chemosphere*, 54 (7):895–903, 2004.

C. Vereda-Alonso, C. Heras-Lois, C. Gomez-Lahoz, F. Garcia-Herruzo, and J.M. Rodriguez-Maroto. Ammonia enhanced two-dimensional electrokinetic remediation of copper spiked kaolin. *Electrochim. Acta*, 52(10):3366–3371, 2007.

D. Voinitchi, S. Julien, and S. Lorente. The relation between electrokinetics and chloride transport through cement-based materials. *Cement Concrete Comp.*, 30 (3):157–166, 2008.

D.J. Wilson, J.M. Rodríguez-Maroto, and C. Gómez-Lahoz. Electrokinetic remediation II. Amphoteric metals and enhancement with a weak acid. *Sep. Sci. Technol.*, 30(16):3111–3128, 1995.

A.T. Yeung. Contaminant extractability by electrokinetics. *Environ. Eng. Sci.*, 23 (1):202–224, 2006.

A.T. Yeung and S. Datla. Fundamental formulation of electrokinetic extraction of contaminants from soil. *Can. Geotech. J.*, 32(4):569–583, 1995.

A.T. Yeung and Y.Y. Gu. A review on techniques to enhance electrochemical remediation of contaminated soils. *J. Hazard. Mater.*, 2011.

A.T. Yeung and J.K. Mitchell. Coupled fluid, electrical and chemical flows in soil. *Geotechnique*, 43(1):121–134, 1993.

O.C. Zienkiewicz. *The finite element method for fluid dynamics*. PhD thesis, University of Wales, 1991.

O.C. Zienkiewicz and R.L. Taylor. *The finite element method for solid and structural mechanics*, volume 2. Butterworth-Heinemann, 2005.

Part III

Appended Publications

Paper

"Modeling of Electrokinetic Processes by Finite Element Integration of the Nernst-Planck-Poisson System of Equations"

J.M. Paz-García, B. Johannesson, L.M. Ottosen, A.B. Ribeiro & J.M. Rodríguez-Maroto

Published in: *Separation and Purification Technology, 2011*

Separation and Purification Technology 79 (2011) 183–192

Contents lists available at ScienceDirect

Separation and Purification Technology

journal homepage: www.elsevier.com/locate/seppur

Modeling of electrokinetic processes by finite element integration of the Nernst–Planck–Poisson system of equations

Juan Manuel Paz-García [a,*], Björn Johannesson [a], Lisbeth M. Ottosen [a], Alexandra B. Ribeiro [b], José Miguel Rodríguez-Maroto [c]

[a] Department of Civil Engineering, Technical University of Denmark, Brovej, Building 118, Dk-2800 Kgs. Lyngby, Denmark
[b] Department of Environmental Sciences and Engineering, Faculty of Sciences and Technology, New University of Lisbon, Campus de Caparica, 2829-516 Caparica, Portugal
[c] Department of Chemical Engineering, University of Málaga, Campus de Teatinos, 29071 Málaga, Spain

ARTICLE INFO

Keywords:
Nernst–Planck–Poisson system
Finite element method
Electrokinetics
Desalination

ABSTRACT

Electrokinetic remediation covers a variety of useful techniques for the mobilization of ionic and non-ionic species from porous materials by means of the application of an external electric field. Due to the large number of physicochemical interactions in the process, designing an electrokinetic remediation process is not simple. Mathematical models are necessary for a better understanding of its fundamentals.

In this study, a model for the electrokinetic transport phenomena based on the strongly coupled Nernst–Planck–Poisson system of equations is described. In the model presented here, the diffusion, the electromigration and the electroosmotic transport contributors are taken into account. The Poisson's equation of electrostatics is used for the calculation of the electrical potential distribution based on the global charge balance. The effect of the electrode half-reactions is included. In addition to this, water equilibrium is continuously assured and the pH value is monitored. Results from some selected test simulations of the electrokinetic desalination of a sample of porous material are presented, outlining the versatility of the model as well as showing the effect of the counterion in the removal rate of a target ion.

1. Introduction

Electrokinetic remediation (EKR) is a useful technique for the mobilization of ionic and non-ionic species from porous materials [1]. There are several applications of electrokinetic techniques in both civil and environmental engineering fields. EKR has been widely used for the remediation of heavy metal contaminated soil [2–6], the desalination of construction materials such as brick, stone or wood [4,7], the removal of heavy metals from CCA-treated wood [8,9], and the prevention of the chloride induced reinforcement corrosion and cathodic protection in concrete [10]. Apart from the elimination of contaminants, the transport of material inside the matrices has also some interesting applications [4].

The EKR technique consists in the application of a voltage difference between two electrodes limiting a region of a material [1–4]. The transport of the particles is the result of a strongly coupled flow affected by different contributions [11]. Due to the gradient of electrical potential created, ionic species will move by electromigration towards the electrode of opposite charge. Non-ionic species can also be transported due to the movement of the pore solution itself in a coupled transport phenomena known as electroosmosis [3,4,12,13]. Apart from electromigration and electroosmosis, it is typically assumed that only diffusion and advective flow can have an important influence in electrokinetic processes. Generally, the electromigration term is the most significant when considering the movement of charged particles [1,2,5,8,14,15].

Due to the large number of physicochemical interactions in the process, designing an electrokinetic remediation system is not simple. The mathematical models describing the reactive transport process are composed of strongly coupled differential equations, with terms in very different magnitude orders, which make difficult to be solved even using numerical strategies. For this reason, up to now, the most practical models for electrokinetic processes have been obtained under the hypothesis that the electromigration term is dominant in the process and, therefore, the others contributors can be neglected. Using the circuit theory, based on Kirchhoff's lattices, the Ohm's law and the molar conductivity of the different species in the system, two-dimensional models and multi-species chemical coupled models have been achieved [5,8,14,16–18]. These models have shown satisfactory results and they provide a useful tool for predicting an approximate behavior of an electrokinetic treatment in the field.

Recently, models based on the integration of the more general continuity equations that govern the process considering the

* Corresponding author. Tel.: +45 4525 5029; fax: +45 4588 3282.
E-mail address: jugra@byg.dtu.dk (J.M. Paz-García).

1383-5866/$ – see front matter © 2011 Elsevier B.V. All rights reserved.
doi:10.1016/j.seppur.2011.02.023

contribution of the different transport terms in the coupled flow [13,15,19–23] have become an interesting alternative to those models based only in the electromigration transport term. The use the numerical finite element method (FEM) can adequately solve the above described strongly coupled system of equations. Several reasons can be outlined to justify the study of these more fundamental models.

1. General computer models are not only useful for anticipating results of electrokinetic treatments in order to optimize the process, but also for increase the understanding of all the physicochemical interactions involved. One of the most important advantages of detailed EKR models is that they could predict the specific conditions in which any of the contributive terms participating in the transport process will become dominant. For example, the electrode processes produce an acid and a basic front [1–8]. The gradient of concentrations of these fronts, especially when they reach each other, is so high that the diffusion term in the transport process should not to be neglected. Similarly, from experimental results it has been shown that the other transport contributions, hydraulic gradient and the electroosmosis, can have an important role in some specific situations.
2. Kinetic rates of the equilibrium reaction of dissociation of both strong and weak acids and bases, as well as acid–base neutralization reactions are, in general, several orders of magnitude greater than transport rates [14–16]. In these and similar cases, the high difference of magnitude order between the kinetic and transport rates makes very difficult to solve numerically the continuity equation. An accepted solution has been to create a two stages procedure in which fast equilibrium reaction was re-established after each transport stage [24,25]. Nevertheless, slow reversible reactions such as some precipitation/dissolution reactions, and all irreversible chemical reactions can be better handled when their kinetic rates are taken into account and they are solved as part of the continuity equation, and not by the two sequential stages for each increment. An alternative solution is to classify the reactions in two groups, according to their relative kinetic rate with respect to the transport times [13,15]. Those reactions consider to be slow, should be solved as the generation term of the continuity equation, while fast reactions, in turn, can be considered to reach the equilibrium state immediately.

Most recent multi-species transport models are based on the Nernst–Planck–Poisson coupled system of equations [19–23,26]. The Poisson equation of electrostatics is used to calculate the electrical potential locally induced due to the charge unbalance produced when ions are migrating with a different rate. Even when there is not an external electric field applied to the system, an electrical potential distribution is expected due to the different diffusion rate of ions. This diffusion potential will produce a strong electromigration transport term driving towards the electrical neutrality of the global system despite the movement of the species.

In previous works, different ways to adapt the finite element method to the ionic multi-species transport process have been discussed. Coupled flux due to moisture transport [19] and the inclusion of a generation term in the continuity equation related to the chemical reaction [22] was studied. These works have been focused primarily on the transport phenomena itself. In the present study, a detailed description of a finite element procedure capable of solving the coupled Nernst–Planck–Poisson system is presented. Some modifications have been included with respect to previous works, in order to adapt the model for the application in electrokinetic remediation techniques, as well as to speed-up the code for increase the performance. The Nernst–Planck equations are used to calculate the concentrations of the individual ionic species, and the Poisson's equation of electrostatics is used to calculate the electrical potential with a truly coupled scheme. The electrode processes are implicitly included in the system. Based on this, a constant difference of voltage or a constant current density can be applied in the model as boundary conditions. The water chemical equilibrium is re-established as part of an iterative approach to the solution of the non-linear system of equations. This feature allows the calculation of the pH value and visualization of the acid front and basic front progress.

Some test example simulations are presented in order to evaluate the model. Experimentally, it was demonstrated that the removal rate of a specific ion depends on the counterions [7] as well as the ions of the same charge, since the electrical potential originated will be different according to the mobility of all species in the system. Test simulations were performed to evaluate how the model predicts the effect in the rate of chloride removal depending on the counterion.

2. The model

2.1. The governing equations

The model consists in the Nernst–Planck–Poisson coupled system of equations, which accounts for the mass balance equation of chemical species in a fluid medium when diffusion and electromigration are considered to be the most significant terms in the transport process. In the case of charged particles, diffusion and electromigration terms have to be taken into account even when considering free diffusion problems due to the electrical interaction between ions. Due to its relevance in electrokinetics processes, the electroosmotic flow was included in the equation. Therefore, the flow of any chemical species i in the system can be expressed as:

$$J_i = \underbrace{-D_i^{\text{eff}}\nabla n_i}_{\text{diffusion}} \quad \underbrace{-k_e n_i \nabla\phi}_{\text{electroomosis}} \quad \underbrace{-U_i^{\text{eff}} n_i \nabla\phi}_{\text{electromigration}} \tag{1}$$

where n_i is the molar concentration, D_i^{eff} is the effective diffusion coefficient and ϕ is the electrical potential, k_e is he electroosmotic permeability coefficient and U_i^{eff}, defined in (2), is the effective ionic mobility coefficient, estimated by the Einstein–Nernst relation [27].

$$U_i^{\text{eff}} = \frac{D_i^{\text{eff}} F z_i}{RT} \tag{2}$$

where R is the ideal gas constant, F is the Faraday constant, z_i is the ionic charge of the species and T is the temperature. Constant room temperature (25 °C) was assumed in the process. The value of the electroosmotic permeability uses to be in a very tight range of 10^{-5} to 10^{-4} cm^2 s^{-1} V^{-1} [28]. Let A_i be a coefficient accounting for the electromigration and the electro osmosis.

$$A_i = U_i^{\text{eff}} + k_e \tag{3}$$

For the sake of simplicity, the continuity equation of the water is not included in the system. With respect to chemical reaction phenomena, only water chemical equilibrium and the electrochemical reaction at the electrodes are considered. Therefore, the rate of generation term is also not included in the continuity equation since the high kinetic rate of this reaction with respect to the transport rates makes easier and more accurate to re-establish the equilibrium in a complementary stage, as part of the iterative solution of the non-linear system of equations. The Nernst–Planck equation (4), for each ionic species considered, is integrated over the one-dimensional region limited by the electrodes, in a truly implicit unconditionally stable time stepping scheme, to obtain the concentration profile for a given set of boundary conditions. From now, for readability reasons, the superscript related to the effective coefficient is not

used.

$$\frac{\partial n_i}{\partial t} = -\frac{\partial}{\partial x}\left(-D_i\frac{\partial n_i}{\partial x} - A_i n_i \frac{\partial \phi}{\partial x}\right) \tag{4}$$

In a system with M number of species, there will be $M+1$ state variables, depending on the time and the position: M molar concentration profiles and the electrical potential distribution ϕ. The system of equations will be form by M Nernst–Planck equations, corresponding to each one of the species, and the Poisson's equation of the electrostatics (5) used to calculate the electrical potential. This is, in fact, the Gauss' law without polarization effects and assuming that the electrical field can be expressed as the gradient of a streaming potential scalar property.

$$\varepsilon\frac{\partial^2\phi}{\partial x^2} = F\sum_{i=1}^{M} n_i z_i \tag{5}$$

where $\varepsilon = \varepsilon_r\varepsilon_o$ is the permittivity in water, ε_o is the permittivity of vacuum, ε_r is the relative electric permittivity of water.

2.2. Integration of the Nernst–Planck–Poisson system of equations

A finite element procedure [29–31] was used to solve the Nernst–Planck–Poisson coupled system described here. The one-dimensional region between the anode and the cathode used in the electrokinetic process is divided into a number of finite elements. Obviously, the higher the number of elements used, the more accurate the method will be. The problem is discretized and solved at the nodal points, by the use of algebra of matrices. A shape function is used to interpolate between the nodal points to get an approximate solution of the continuous function.

The FEM requires the use of the weak formulation of the governing differential equation to be integrated. To obtain the weak formulation from the strong formulation, the latter must be multiplied by an arbitrary function; the so-called weight function $w(x)$. Subsequently, the weak formula is integrated over the corresponding region, i.e., $0 < x < L$, being L the distance between two consecutive nodes in the one-dimensional domain considered. The elementary analysis rule for integration by parts is used for this purpose [31]. Being (4) the strong formula of the Nernst–Planck continuity equation in the one-dimensional problem considered, (6) would be the corresponding weak formula, defined in any individual finite element in which the domain has been divided.

$$\int_0^L w\frac{(n_i^t - n_i^{t-\Delta t})}{\Delta t}dx = \left[wD_i\frac{dn_i}{dx}\right]_0^L - \int_0^L \frac{dw}{dx}D_i\frac{dn_i}{dx}dx + \left[wA_i n_i^t\frac{d\phi}{dx}\right]_0^L - \int_0^L \frac{dw}{dx}A_i n_i^t\frac{d\phi}{dx}dx \tag{6}$$

At each nodal point, a linear-piecewise shape function is defined. This function will have the unit value in the node and zero value in the two neighboring points in the one-dimensional domain. This most simple kind of linear shape function gives accurate results when the number of nodal points is big enough for most kind of mass transport problems. For compatibility reasons the adopted weight functions were also defined as linear–triangular functions, according to the Galerkin assumption [31]. Let j and $j+1$ denote two consecutive nodes in the domain defining an arbitrary finite element, the approximated function could be expressed as the scalar product:

$$n_i = \mathbf{N}\mathbf{a}_i = \begin{bmatrix} N_j & N_{j+1}\end{bmatrix}\begin{bmatrix} a_j \\ a_{j+1}\end{bmatrix} = \begin{bmatrix} 1-\frac{x}{L} & \frac{x}{L}\end{bmatrix}\begin{bmatrix} a_j \\ a_{j+1}\end{bmatrix} \tag{7}$$

where $\mathbf{a}_i$ is the discrete form of the molar concentration, in the way of a column vector that contains the molar concentration of the species i, in two consecutive nodal points and $\mathbf{N}$ is a row vector depending of the shape function used for the approximation. According to this, the following standard FEM vectorial notation can be defined:

$$n_i = \mathbf{N}\mathbf{a}_i; \quad \phi = \mathbf{N}\mathbf{a}_\phi; \quad w = \mathbf{c}^T\mathbf{N}^T \tag{8}$$

where $\mathbf{a}_\phi$ is a column vector that contains the electrical potential in two consecutive nodal points and the column vector $\mathbf{c}^T$ is an arbitrary vector that has the discrete values of the meaningless weight function. The superscript T is used for denoting the transposition of the matrices. The gradients of the shape function and the weight function are easily obtained and are denoted by the vector $\mathbf{B}$.

$$\frac{dn_i}{dx} = \mathbf{B}\mathbf{a}_i; \quad \frac{d\phi}{dx} = \mathbf{B}\mathbf{a}_\phi; \quad \frac{dw}{dx} = \mathbf{c}^T\mathbf{B}^T \tag{9}$$

Using the vectorial notation in (8) and (9), the weak formula for the Nernst–Planck equation (6) can be discretized to give:

$$\int_0^L \mathbf{c}^T\mathbf{N}^T\mathbf{N}dx\frac{(\mathbf{a}_i^t - \mathbf{a}_i^{t-\Delta t})}{\Delta t} = \left[\mathbf{c}^T\mathbf{N}^T D_i\frac{dn_i}{dx}\right]_0^L - \int_0^L \mathbf{c}^T\mathbf{B}^T D_i\mathbf{B}\mathbf{a}_i^t dx + \left[\mathbf{c}^T\mathbf{N}^T n_i^t A_i\frac{d\phi}{dx}\right]_0^L - \int_0^L \mathbf{c}^T\mathbf{B}^T n_i^t A_i\mathbf{B}\mathbf{a}_\phi^t dx \tag{10}$$

The local conductivity and damping matrix can be defined as shown in (11). These matrices are called local matrices because they are defined between each two consecutive nodes. The terminology of these matrices comes from the fact that the FEM was mostly developed in the field of structure mechanics.

$$\mathbf{K}_l = \int_0^L \mathbf{B}^T\mathbf{B}dx = \frac{1}{L}\begin{bmatrix} 1 & -1 \\ -1 & 1\end{bmatrix}; \quad \mathbf{C}_l = \int_0^L \mathbf{N}^T\mathbf{N}dx = \frac{L}{6}\begin{bmatrix} 2 & 1 \\ 1 & 2\end{bmatrix} \tag{11}$$

Global matrices, that compile information of the entire domain, can be obtained from local matrices by a process called assemblage. This process requires the overlap of the local matrices in the common node between two consecutive finite elements. Eq. (12) shows the corresponding assembled form of the conductivity and damping matrices.

$$\mathbf{K} = \frac{1}{L}\begin{bmatrix} 1 & -1 & 0 & \cdots & 0 & 0 \\ -1 & 1+1 & -1 & \ddots & \ddots & \ddots \\ 0 & -1 & 1+1 & \ddots & \ddots & \ddots \\ \vdots & \ddots & \ddots & \ddots & \ddots & \ddots \\ 0 & \ddots & \ddots & \ddots & 2 & -1 \\ 0 & \ddots & \ddots & \ddots & -1 & 1 \end{bmatrix}; \quad \mathbf{C} = \frac{L}{6}\begin{bmatrix} 2 & 1 & 0 & \cdots & 0 & 0 \\ 1 & 2+2 & 1 & \ddots & \ddots & \ddots \\ 0 & 1 & 2+2 & \ddots & \ddots & \ddots \\ \vdots & \ddots & \ddots & \ddots & \ddots & \ddots \\ 0 & \ddots & \ddots & \ddots & 4 & 1 \\ 0 & \ddots & \ddots & \ddots & 1 & 2 \end{bmatrix} \tag{12}$$

Eliminating the common factor $\mathbf{c}^T$ in (10) and using the assembled notation (12), a simplified matrix Eq. (13) is obtained for each mass balance equation defined in the entire domain.

$$\mathbf{C}\frac{(\mathbf{a}_i^t - \mathbf{a}_i^{t-\Delta t})}{\Delta t} + \mathbf{K}_{D_i}\mathbf{a}_i^t + \mathbf{K}_{A_i\mathbf{a}_i}\mathbf{a}_\phi^t + \left[\mathbf{N}^T(\mathbf{J}_{Di} + \mathbf{J}_{A_i})\right]_0^{L_T} = 0 \tag{13}$$

where now, $\mathbf{a}_i$ and $\mathbf{a}_\phi$ have global definition, and are vectors containing information for each node in which the domain has been divided. The superscript t means the present time step and $t-\Delta t$ the time step before in the numerical integration. $\mathbf{K}_{D_i} = D_i\mathbf{K}$ is the conductivity matrix related to diffusion term and

$\mathbf{K}_{A_i\mathbf{a}_i} = \mathbf{a}_i A_i \mathbf{K}$ is the conductivity matrix related to the electromigration/electroosmotic term. The latter matrix induces non-linearity character to the system of equation and especial attention must be paid in the assemblage process, since the local matrix is different between elements. Terms inside the brackets are column vectors named as boundary vectors, and they represent the external flux at the boundaries of the domain, and so the superscript L_T refers to the total length of the one-dimensional domain. According to this, $\mathbf{J}_{D_i} = -D_i \nabla n_i$ refers to the diffusion flux and $\mathbf{J}_{A_i} = -n_i A_i \nabla \phi$ refers to the combination the electromigration and electroosmotic flux in the boundaries.

The corresponding local discretized expression of the Poisson equation (5) can be easily obtained following a similar analysis:

$$\sum_{i=1}^{M} \int_0^L \mathbf{c}^{\mathrm{T}} \mathbf{N}^{\mathrm{T}} F z_i \mathbf{N} \mathbf{a}_i^t dx + \int_0^L \mathbf{c}^{\mathrm{T}} \mathbf{B}^{\mathrm{T}} \varepsilon \mathbf{B} \mathbf{a}_\phi^t dx = \left[\mathbf{c}^{\mathrm{T}} \mathbf{N}^{\mathrm{T}} \varepsilon \frac{d\phi}{dx} \right]_0^L \tag{14}$$

Using the terminology defined in (8) and (9), the weak formula of (14) would be:

$$\sum \mathbf{E}_i \mathbf{a}_i^t + \mathbf{K}_\phi \mathbf{a}_\phi^t = \left[\mathbf{N}^{\mathrm{T}} \varepsilon \frac{d\phi}{dx} \right]_0^{L_T} \tag{15}$$

where $\mathbf{K}_\phi = \varepsilon \mathbf{K}$ is the conductivity matrix related to the electrical potential, $\mathbf{E}_i = F z_i \mathbf{C}$ is the free charge density matrix and the term inside the brackets represents the flux of electrical potential. The global matrix system of equation, formed by M Nernst–Planck equations and the Poisson equation is obtained in a simplified expression:

$$\mathbf{C}^{\mathrm{global}} (\mathbf{a}^t - \mathbf{a}^{t-\Delta t}) + \mathbf{K}^{\mathrm{global}} \mathbf{a}^t = \mathbf{f}^{\mathrm{global}} \tag{16}$$

where now $\mathbf{a}$ is the column vector obtained from vertical concatenation of all $\mathbf{a}_i$, discrete molar concentration of each chemical species, and $\mathbf{a}_\phi$, discrete electric potential distribution. The different terms in (16) are defined as:

$$\mathbf{C}^{\mathrm{global}} (\mathbf{a}^t - \mathbf{a}^{t-\Delta t}) = \frac{1}{\Delta t} \begin{bmatrix} \mathbf{C} & \mathbf{0} & \cdots & \cdots & \mathbf{0} \\ \mathbf{0} & \mathbf{C} & \ddots & \ddots & \mathbf{0} \\ \vdots & \ddots & \ddots & \ddots & \vdots \\ \vdots & \ddots & \ddots & \mathbf{C} & \mathbf{0} \\ \mathbf{0} & \mathbf{0} & \cdots & \mathbf{0} & \mathbf{0} \end{bmatrix} \begin{bmatrix} \mathbf{a}_1 - \mathbf{a}_1 \\ \mathbf{a}_2 - \mathbf{a}_2 \\ \vdots \\ \mathbf{a}_M - \mathbf{a}_M \\ \mathbf{a}_\phi - \mathbf{a}_\phi \end{bmatrix} \tag{17}$$

$$\mathbf{K}^{\mathrm{global}} \mathbf{a}^t = \begin{bmatrix} \mathbf{K}_{D_1} & \mathbf{0} & \cdots & \cdots & \mathbf{K}_{A_1 \bar{\mathbf{a}}} \\ \mathbf{0} & \mathbf{K}_{D_2} & \ddots & \ddots & \mathbf{K}_{A_2 \bar{\mathbf{a}}} \\ \vdots & \ddots & \ddots & \ddots & \vdots \\ \vdots & \ddots & \ddots & \mathbf{K}_{D_M} & \mathbf{K}_{A_M \bar{\mathbf{a}}} \\ \mathbf{E}_1 & \mathbf{E}_2 & \cdots & \mathbf{E}_M & \mathbf{K}_\phi \end{bmatrix} \begin{bmatrix} \mathbf{a}_1{}^t \\ \mathbf{a}_2{}^t \\ \vdots \\ \mathbf{a}_{\mathrm{M}}{}^t \\ \mathbf{a}_\phi{}^t \end{bmatrix} \tag{18}$$

$$\mathbf{f}^{\mathrm{global}} = \begin{bmatrix} -[\mathbf{N}^T (J_{D_1} + J_{A_1})]_0^{L_T} \\ -[\mathbf{N}^T (J_{D_2} + J_{A_2})]_0^{L_T} \\ \vdots \\ -[\mathbf{N}^T (J_{D_M} + J_{A_M})]_0^{L_T} \\ \left[\mathbf{N}^T \varepsilon \frac{d\phi}{dx} \right]_0^{L_T} \end{bmatrix} \tag{19}$$

where now, $\mathbf{f}^{\mathrm{global}}$ denotes the force vector. This matrix system (16) can be algebraically re-arranged in order to obtain a simplified notation, using $\mathbf{K}^*$ and $\mathbf{f}^*$ as described in (20).

$$\underbrace{(\mathbf{C} + \mathbf{K})}_{\mathbf{K}^*} \mathbf{a}^t = \underbrace{\mathbf{C} \mathbf{a}^{t-\Delta t} + \mathbf{f}}_{\mathbf{f}^*} \tag{20}$$

An system of equations with large sparse matrices is obtained. A sparse matrix is one populated primarily by zeros, and some computational advantages can be obtained when using specific sparse-matrices functions [32,33]. Sparse-matrices functions were taken into account and used when implementing the code, obtaining high-speed computational time and low memory requirements. This feature allows accurate simulations using a large number of nodal points in the discretization process.

2.3. Electrode processes

An electrokinetic process uses a voltage difference between two points of a section of a matter medium for the mobilization of particles. The voltage difference applied produces electrolysis reactions at the electrodes. Different oxidation reactions at the anode and reduction reactions at the cathode will take place, depending on the species in the media. In aqueous solutions water electrolysis is always present, and it will be the electrode reaction considered in this model.

The water oxidation reaction at the anode is described by:

$$\mathrm{H_2O} \rightleftarrows \frac{1}{2}\mathrm{O_2} + 2\mathrm{H^+} + 2\mathrm{e^-}; \quad E^\circ = -1.229\,\mathrm{V} \tag{21}$$

And the water reduction at the cathode is the reaction:

$$2\mathrm{H_2O} + 2\mathrm{e^-} \rightleftarrows \mathrm{H_2} + 2\mathrm{OH^-}; \quad E^\circ = -0.828\,\mathrm{V} \tag{22}$$

where E° is the standard redox potential of the half reaction.

An EKR system has, at least, two voltage drops in series: one due to the electrical resistance of the pore solution to the ionic current, and the other to the electrode processes [17]. The vector $\mathbf{a}_\phi$ obtained in the model represents the electric potential distribution due to the local unbalance produced when ions are migrating. By establishing a reference point in the cathodic node, the voltage drop due to the electrical resistance can be obtained. The voltage drop due to the electrode processes is not included in $\mathbf{a}_\phi$, but it can be obtained from the Nernst equation of the half reaction involved in the electrode processes [17]. In the adopted model, the partial pressures of the gases produced were assume to keep a constant value of 1 atm meaning bubbles of pure gas in the electrolytic solution, and this voltage drop was estimated from the Nernst equation applied to the electrodes global reaction:

$$E = -1.23 - 0.059(\mathrm{pH_{cathode}} - \mathrm{pH_{anode}}) \tag{23}$$

Therefore, the voltage drop between the electrodes is the sum of the voltage drop obtained from the difference between the electrical potential among the anode and the cathode nodal points, and the voltage drop calculated in (23).

The implemented model can work under conditions of constant difference of voltage or under constant current density. In experimental electrokinetic treatments, a constant current is usually applied along the sample, since it allows a better control of the removal process. The application of a constant current density in the model is done by considering that Eqs. (21) and (22) are taken place and, consequently, a flux of protons and hydroxides is established in the anodic and cathodic nodal points respectively. This can be achieved by the definition of the corresponding boundary vector (19) as boundary conditions. Alternatively, the model can be easily adapted to work under conditions of a constant difference of voltage between electrodes terminals or between the electrode surfaces. In other words, the difference of voltage can be applied to the general process, or only in the electrical resistance voltage drop

described above. When boundary conditions are applied in the electrode nodal points, additional boundary vectors are obtained. These calculated boundary vectors, denoted as $\mathbf{f}_b^*$, have the same meaning of those described in (19) but they are calculated in the model when boundary conditions are used in order to keep the physical consistency. The flux of charge into the system is due to a flux of ions, according to Eqs. (21) and (22). Therefore, calculated boundary vectors related to a flux of charge can be converted to boundary vector of protons and hydroxides in order to keep constant the difference of voltage applied.

2.4. Water chemical equilibrium

An electrokinetic process involves several chemical interactions between the different species in the system. As a first approach, only the chemical equilibrium of the dissociation reaction of water has been taken into account. After solving the global matrix system defining the process (20), if the chemical generation term has not been included in the continuity equation, an unfounded unbalance in the water acid–base equilibrium will appear due to the different migration rates of protons and hydroxides. As mentioned before, the high kinetic rate of this reaction with respect to the transport rates makes easier and more accurate to re-establish the equilibrium in a complementary stage, as part of the iterative solution of the non-linear system of equations [14–16]. The iterative method evaluates the equilibrium state in each node considered in the FEM model. Being $K_w = 10^{-14}$ the water equilibrium constant (for concentration expressed in mol/L), and x_w the number of water molecules that dissociate ($x_w > 0$) or are created ($x_w < 0$) in order to re-establish this equilibrium, and considering that the activities of the ionic species can be assumed equal to the concentration values, the process will be described by:

$$[H^+ + x_w][OH^- + x_w] = K_w \tag{24}$$

The variable x_w can be worked out in (24) where only the positive value of the square root has a physical meaning.

$$x_w = \frac{-([H^+] + [OH^-]) + \sqrt{([H^+] + [OH^-])^2 - 4([H^+][OH^-] - K_w)}}{2} \tag{25}$$

Once the equilibrium has been re-established, the concentration of protons and hydroxides will be:

$$[H^+]_{eq} = [H^+] + x_w; \quad [OH^-]_{eq} = [OH^-] + x_w \tag{26}$$

2.5. The solution procedure

The direct solution of (20) is not straightforward, due to the strong non-linearity in the equations of the coupled Nernst–Planck–Poisson system. More specifically, in (4) it can be seen that the transport terms corresponding to the electromigration and electroosmosis in the continuity equation depend on the product of the molar concentration and the electric potential distribution. For this reason, an iterative approach solution for the matrix system of equations is required.

In previous works [19–22], the solution of the non-linear problem was dealt by the use of a modified Newton–Raphson procedure, based on the Taylor expansion of the residual vector. In the present work, an alternative method has been developed in order to handle the problem due to the non-linearity and, at the same time, to take into account the electrode processes and the complementary stage for re-establishing the chemical equilibrium. The procedure is based in the hypothesis that the variation of the molar concentration in each time step of the numerical integration is considerably small. The error induced by this hypothesis is subsequently minimized, using an iterative method. According to this assumption, in order to calculate the ionic mobility conductivity matrix $\mathbf{K}_{U_i\mathbf{a}_i}$ described in (13), the concentration profile obtained in the previous time step is used. Afterwards, the matrix system of equations (20) is solved. For this purpose, a function that allows the definition of boundary conditions in the matrix system of equations has been implemented giving $\mathbf{a}^t$ and $\mathbf{f}_r^*$.

$$\mathbf{a}^t = (\mathbf{K}^*)^{-1}(\mathbf{f}^* + \mathbf{f}_r^*) \tag{27}$$

where $\mathbf{f}_r^*$ is a reactive vector calculated by the model as a result of the use of boundary conditions. These reactive vectors can be understood as the load vectors necessary to satisfy the boundary conditions established in the system. As mentioned before, $\mathbf{f}_r^*$ is especially important when establishing a constant difference of voltage as boundary condition in the system. Knowing those parameters, the numerical residual of the matrix system of equation would be calculated as:

$$\varphi = \mathbf{K}^*\mathbf{a}^t - \mathbf{f}^* - \mathbf{f}_r^* \tag{28}$$

The profile obtained $\mathbf{a}^t$ after the transport process is subjected to a complementary stage of chemical re-establishing for every node, according to (24) and (26), obtaining a chemically sound profile. Nevertheless, one should remember that this profile was obtained from an estimation of the electromigration conductivity matrix, $\mathbf{K}_{A_i\mathbf{a}_i}$. For this reason, an iterative procedure is started to minimize this error. Instead proceeding with the next step of the numerical integration, the code goes back to the time step just solved. The term $\mathbf{K}_{A_i\mathbf{a}_i}$ is upgraded using the provisional calculated profile. Despite the error induced in its calculation, the provisional profile is considered to be a better approximation of the next step than the previous profile. The same time step is solved in this connected two stages procedure, and the difference between two consecutive profiles is monitored. For small enough numerical time increments, Δt, this difference, and therefore the error, converges to zero. As acceptance criteria, it was established that the scalar product of the vector containing the difference between two consecutive profiles should be

Table 1
Model parameters.

Parameter	Value	Unit
D_{H^+}	9.311×10^{-9}	m^2/s
D_{OH^-}	5.273×10^{-9}	m^2/s
D_{Na^+}	1.334×10^{-9}	m^2/s
D_{Cl^-}	2.032×10^{-9}	m^2/s
D_{K^+}	1.957×10^{-9}	m^2/s
τ_c	1.26	–
τ_a	1.11	–

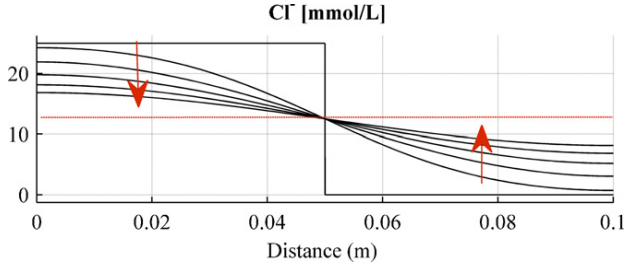

Fig. 1. Simulation 1. Free diffusion. Cl^- concentration profile.

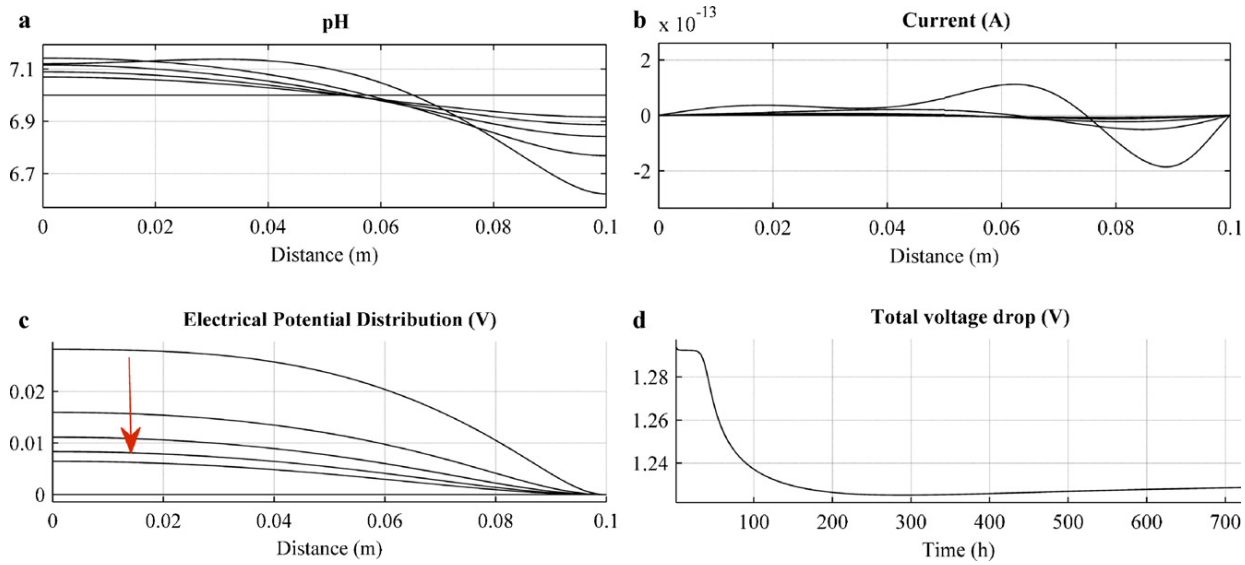

Fig. 2. Simulation 1. Free diffusion. pH profile and electrical parameters.

lower than a reference value. Experimentally, it was checked that, for concentrations expressed in mmol/L and electric potential in V, a reference value in the range of 10^{-12} assured accurate results with a moderate number of iterations.

3. Results of selected test simulations and discussions

In order to evaluate the consistency of the model, numerical simulations of the desalination process of a sample of a porous material contaminated with chloride salts has been studied. Four simulations are shown: free diffusion desalination, electrokinetic desalination under constant difference of voltage and two cases electrokinetic desalination under constant current comparing the effect of the counterion (Na^+ or K^+) on the removal rate of Cl^-.

A porosity of 30% is adopted for the material, which is a reasonable value for a typical porous construction material [7], the matrix is considered to be chemically inert, and no dissolution or precipitation of salt is expected. Pores are completely saturated with a neutral pH aqueous solution containing 25 mmol/L of a chloride salt. No changes on the moisture content on the internal pore is considered, maintain the condition of complete water saturation during the simulation. The electrodes are placed directly at the ends of the sample, making possible to consider the process like a one-dimensional problem. The cross-sectional area has a value of 125 cm^2. The chemical species considered are: H^+, OH^-, Cl^-, Na^+ and K^+ depending on the simulation. Effective diffusion coefficients are obtained by multiplying the diffusion coefficient in the infinite solution by the porosity and dividing by a geometrical tortuosity factor.

$$D_i^{\text{eff}} = \frac{p}{\tau} D_i \tag{29}$$

Mohajeri et al. [34] made some numerical calculations of the effective diffusion coefficient for charged species taking into account the effect of the surface charge of the porous structure. They proposed a different tortuosity factor for cations than for anions, depending on the geometry of the pore. Most of the matrices of interest in electrokinetic remediation has internal negative surface, such as soil, concrete, clays bricks or sandstones. Based on this, in the present work a different tortuosity factor has been defined depending on the sign of the ion. The internal porous structure is considered to be a combination of Z-shape and Ω-shape channels, and the tortuosity factor is given a value of $\tau = 1.26$ for all the cations and $\tau = 1.11$ for all the anions (Table 1).

In all cases, the domain is divided in a total of 200 finite elements. The time step used in the truly implicit numerical integration is 300 s for the free diffusion simulation. In the case of the simulations under an external applied electric field the time step is 60 s and a constant electroosmotic permeability coefficient is used, with a value of $k_e = 2 \times 10^{-9}$ m^2 s^{-1} V^{-1}. As acceptance criteria in the loop of iterative approach the reference value for the scalar product of the vector containing the difference between two consecutive profiles and the corresponding reference value for the boundary vector is 10^{-12}.

3.1. Simulation 1

Fig. 1 shows concentration profile of Cl^- in the free diffusion desalination case. A 5 cm length sample contaminated with 25 mmol/L NaCl is put in direct contact with a same geometry sam-

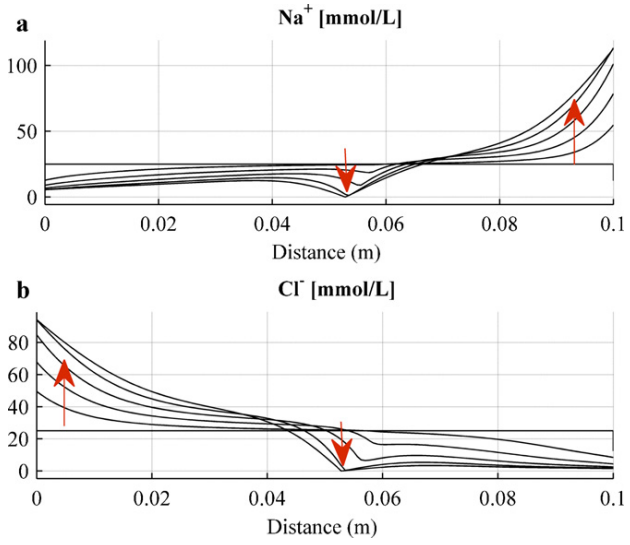

Fig. 3. Simulation 2. Constant voltage. Na^+ and Cl^- concentration profiles.

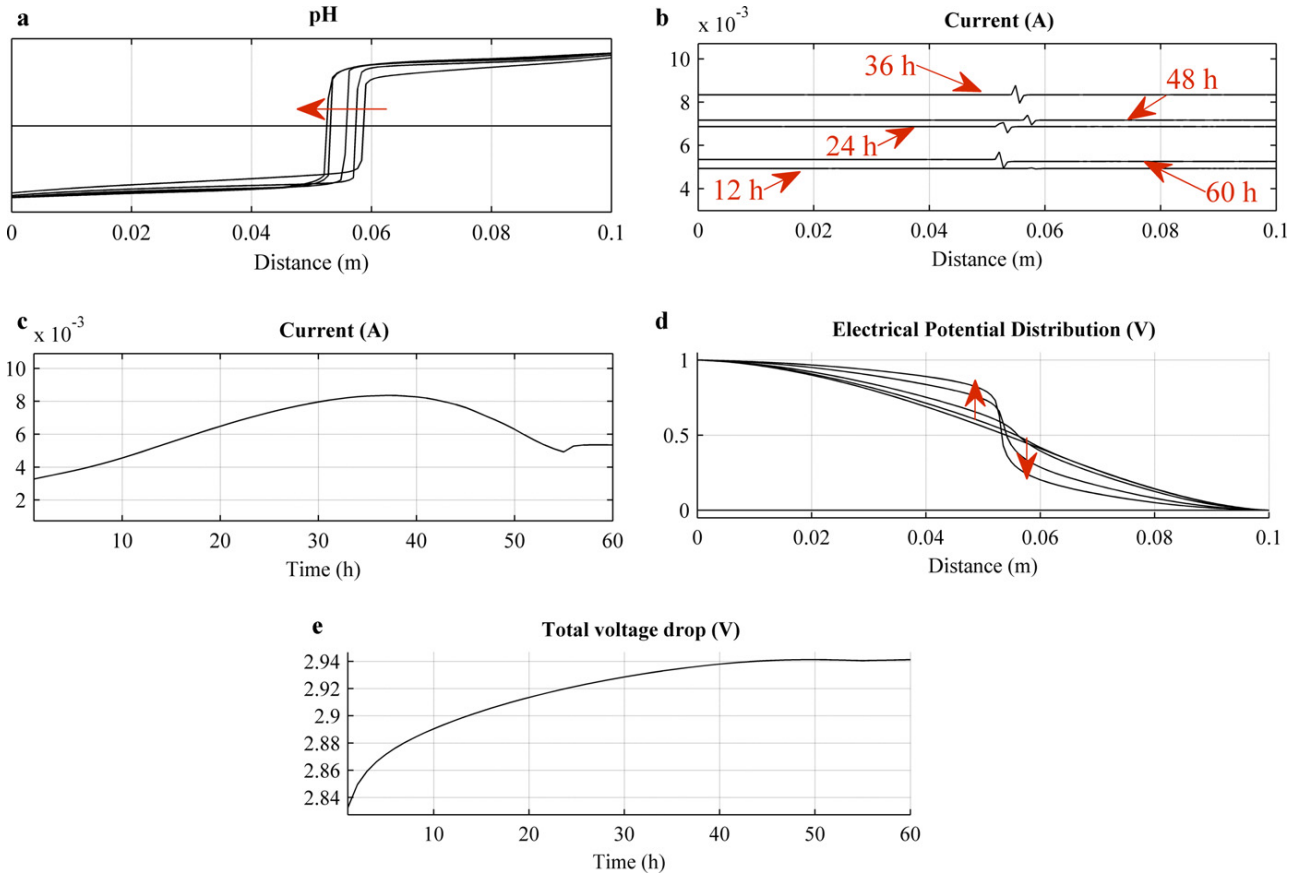

Fig. 4. Simulation 2. Constant voltage. pH profile and electrical parameters.

ple which had distilled water in the pore solution. The duration of the experiment is 720 h and only one profile each 6 days is shown. Due to the high gradient of concentration the initial effect of the diffusion is much more important in the early stages of the process. The final desalination efficiency is limited for the equilibrium state that, in this example and for symmetry reasons, would be half of the initial concentration on NaCl in the sample. The concentration profile of Na^+, not shown, is very similar to the profile of Cl^-.

Fig. 2(c) shows that the free diffusion of ions generates an electric potential distribution in the pore solution (diffusion potential). Protons and hydroxides undergo a migration following the Na^+ and the Cl^- in order to keep the electrical neutrality. Consequently, the pH profile, shown in Fig. 2(a), varies. The electrical potential distribution, Fig. 2(c), decreases when the initial high gradient of concentration is softened. The total voltage drop, Fig. 2(d), accounts for the electric resistance voltage drop between the ends of the sample, and the redox potential. In this case, the redox potential is the minimum external voltage to be applied in order to start the electrode processes. Fig. 2(b) shows some oscillations in the current along the sample, that have very low magnitude order and they are buffered when the process proceeds.

3.2. Simulation 2

Fig. 3 shows concentration profile of Na^+ and Cl^- in the electrokinetic desalination case with a constant difference of voltage of 1 V in the voltage drop corresponding to the electrical resistance in the pore solution. Electrodes are connected at the ends of a 10 cm length sample, contaminated with 25 mmol/L NaCl in the pore solution. The duration of the experiment is 60 h and only one profile each 12 h is shown. Due to the electrokinetic process, anions (OH^- and Cl^-) migrate towards the anode and cations (H^+ and Na^+) towards the cathode. A range of very low concentration of Cl^- and Na^+ is observed in the middle part of the sample. This can be related to a low conductivity cross-section that can limit the electrokinetic process. According the Ohm's law, a high electrical resistance cross-section in a system with constant difference of voltage applied would decrease the current of the whole system and, consequently, the efficiency of the electrokinetic process.

The ionic migration of chloride is higher than the one corresponding to the sodium and the different tortuosity factor should make cations to migrate slower. Nevertheless, the accumulation of sodium observed in the cathode in higher than in the accumulation of chloride in the anode, due to the electroosmotic flow established.

Fig. 4(a) shows the corresponding pH profile in the sample. Due to the electrode process, an acid front at the anode and a basic front at the cathode are developed. These fronts reach each other in a distance of approximately 2/3 from the anode in a very short time (less than 12 h of treatment according to the results shown). Accordingly to Fig. 3, this pH boundary also determines the position inside the sample where the removal and the accumulation are taken place. For example, the chloride is removed at the right side and accumulated at the left side of the mentioned pH boundary. It can be seen that the pH boundary position is not fixed, and in this case it moves slightly towards the anode. This phenomenon can be explained taken into account that the chloride has higher migration rate than sodium. The displacement of the pH boundary position keeps the electrical neutrality in the system.

Fig. 4(b) shows that the ionic current is constant along the distance, which offers high consistency to the model. It can be seen

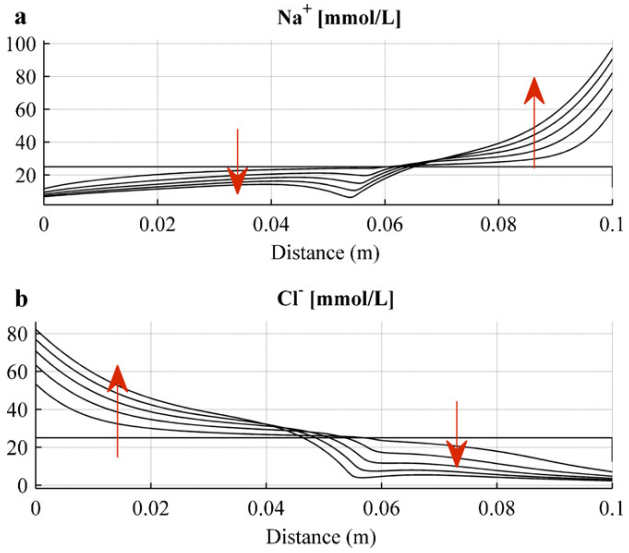

Fig. 5. Simulation 3. Constant current. Single salt. Na^+ and Cl^- concentration profiles.

that the ionic current varies in the time. Fig. 4(c) shows the variation of the ionic current in the time during the whole process. The variation of the current is related to the variation of the conductivity of the pore solution. Since the voltage is fixed constant, as the salt is removed the resistance of the pore solution is expected to increase and, as result, the ionic current should decrease. Nevertheless, the constant flux of protons and hydroxides due to the electrode processes can compensate the lost of conductivity in the pore solution.

Many important aspects related to the pH of the medium have to be considered in the electrokinetic process. Protons and hydroxides have a rather high value of the diffusion and ionic mobility coefficients as compared to most other ions typically present. In addition to this, the constant flux of those ions to the system in the electrode process produce a high concentration of both of them, with respect to the other ions presented. Consequently, most of the current applied to the system is transported by these two ions [2]. The progress of the basic and acid fronts is also important since it can

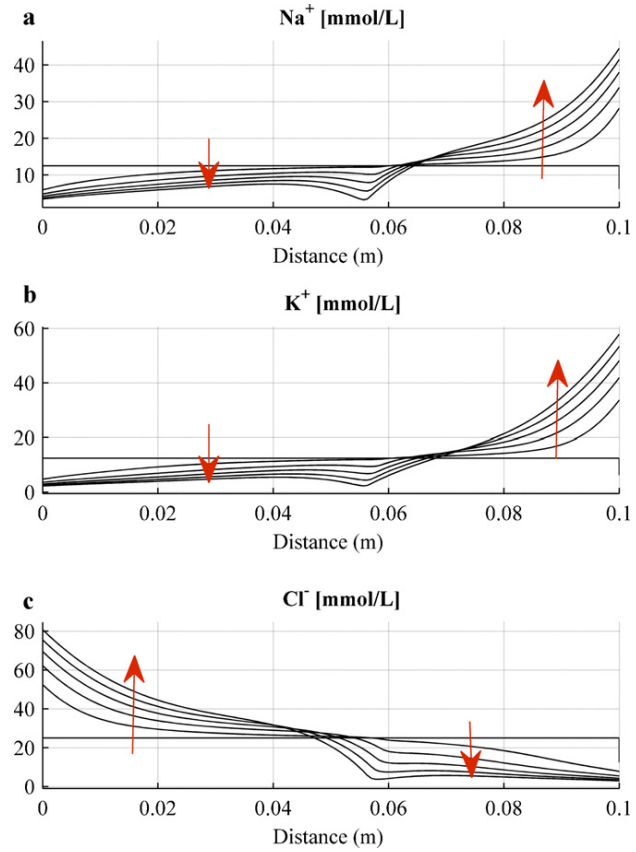

Fig. 7. Simulation 4. Constant current. Combination of salts. Na^+, K^+ and Cl^- concentration profiles.

produce changes in the speciation of the species to be removed, and even interact with the material matrix. These phenomena justify the use of different enhanced electrokinetic techniques [35].

Fig. 4(d) shows that the electric resistance in the position of the pH boundary becomes dominant. The electric resistance voltage drop matches with the low concentration section observed in

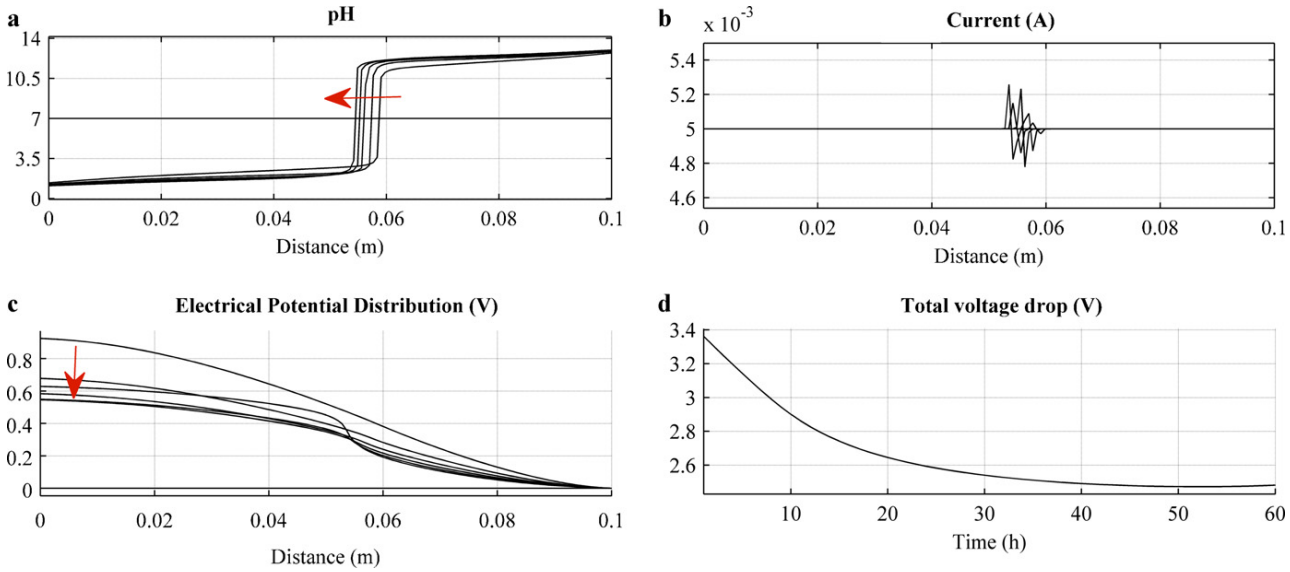

Fig. 6. Simulation 3. Constant current. Single salt. pH profile and electrical parameters.

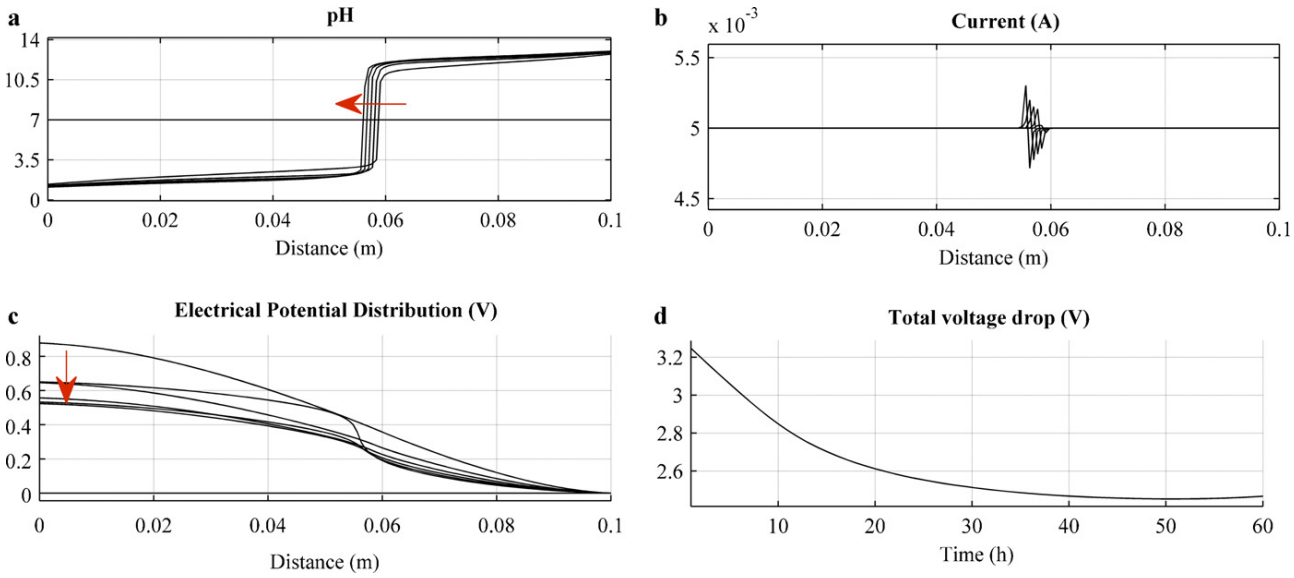

Fig. 8. Simulation 4. Constant current. Combination of salts. pH profile and electrical parameters.

Fig. 3. Consequently, a high competition between the diffusion and electromigration transport terms can be expected in this boundary. Fig. 4(e) shows the total voltage drop in the system including the redox potential.

3.3. Simulation 3

Fig. 5 shows concentration profile of Na^+ and Cl^- in the electrokinetic desalination case with a constant current of 5 mA. Electrodes were placed at the ends of the 10 cm length sample, contaminated with 25 mmol/L NaCl in the pore solution. The duration of the experiment is 60 h and only one profile each 12 h is shown. Results are very similar to those obtained in the experiment at constant voltage.

Fig. 6(b and c) shows that, in this case, the current is kept constant in both the distance and the time during the process while the voltage drop due to the electrical resistance varies. The electrical resistance in the global system initially decreases until a value between 0.5 and 0.6 V. After that, the low conductivity cross-section observed in Fig. 5 develops a high electrical resistance, what means a high voltage drop, matching with the position of the change in the pH.

3.4. Simulation 4

In this case, a similar experiment described in Section 3.3 is shown, but considering the pore solution contaminated with 0.0125 mmol/L of NaCl and KCl. Fig. 7 shows that the electrokinetic desalination process has a similar general behavior for the case of removing KCl and NaCl. The higher transport number of potassium with respect to sodium produces a lightly lower migration rate of chloride than in Section 3.3. For the same reason, the accumulation of potassium in the cathode is clearly higher than the accumulation of sodium.

Comparing Figs. 6 and 8(a) it can be seen that the position of the pH boundary moves slower than in the case of only NaCl. As explained before, it can be due to that the migration rate between the ions studied. Results show that both the free diffusion and the electromigration rate of a specific ion are affected by the counterions and the other species present in the system.

4. Conclusions

Using the Nernst–Planck–Poisson system, a general electrokinetic process has been modeled. The finite element method, combined with an iterative method that deals simultaneously with the electrode processes and the water chemical equilibrium, was used for the integration of the strongly coupled system of equations. The model presented here shows high versatility, since it is able to predict results from simple cases of electrokinetic desalination under conditions of constant electric current density or constant difference of voltage. In addition to this, the model is able to predict results for free diffusion problems, taken into account the electrical interaction between the charged particles in the transport process.

As an example of the consistency of the model, it can be outlined that the current density calculated in every time step is constant in the distance, and when a constant the current density established in the electrode processes it remains also constant in the time. In general, the model shows high consistency and efficiency in the computational time, which encourages the authors to include additional features, and the individual study of different enhanced electrokinetic treatments.

Acknowledgments

Authors acknowledge the Danish Agency of Science Technology and Innovation. This research was funded as part of the project “Fundamentals of Electrokinetics in In-homogeneous Matrices”, with project number 274-08-0386.

References

[1] Y.B. Acar, A.N. Alshawabkeh, Principles of electrokinetic remediations, Environ. Sci. Technol. 27 (1993) 2638–2647.
[2] Y.B. Acar, R.J. Gale, A.N. Alshawabkeh, R.E. Marks, S. Puppala, M. Bricka, R. Parker, Electrokinetic remediation: basics and technology status, J. Hazard. Mater. 40 (1995) 117–137.
[3] F. Garcia-Herruzo, J.M. Rodriguez-Maroto, R.A. Garcia-Delgado, C. Gomez-Lahoz, C. Vereda-Alonso, Limpieza de suelos por electrodescontaminación 1: fundamentos y aspectos básicos, Ing. Quim. 370 (2000) 209–214.
[4] L.M. Ottosen, I.V. Christensen, I. Rörid-Dalgaard, P.E. Jensen, H.K. Hansen, Utilization of electromigration in civil and environmental engineering—processes, transport rates and matrix changes, J. Environ. Sci. Health 43 (2008) 795–809.

[5] C. Vereda-Alonso, J.M. Rodriguez-Maroto, R.A. Garcia-Delgado, C. Gomez-Lahoz, F. Garcia-Herruzo, Two-dimensional model for soil electrokinetic remediation of heavy metals. Application to a copper spiked kaolin, Chemosphere 54 (2004) 895–903.
[6] L.M. Ottosen, H.K. Hansen, A.B. Ribeiro, A. Villumsen, Removal of Cu, Pb and Zn in an applied electric field in calcareous and non-calcareous soils, J. Hazard. Mater. 85 (2001) 291–299.
[7] L.M. Ottosen, I. Rödig-Dalgaard, Desalination of a brick by application of an electric DC field, Mater. Struct. 42 (7) (2009) 961–971.
[8] A.B. Ribeiro, J.M. Rodríguez-Maroto, E.P. Mateus, E. Velizarova, L.M. Ottosen, Modeling of electrodialytic and dialytic removal of Cr, Cu and As from CCA-treated wood chips, Chemosphere 66 (2007) 1716–1726.
[9] H. Sarahney, J. Wang, A. Alshawabkeh, Electrokinetic process for removing Cu, Cr, and As from CCA-treated wood, Environ. Eng. Sci. 22 (2005) 642–650.
[10] L. Bertolini, F. Bolzoni, M. Gastaldi, T. Pastore, P. Pedeferri, E. Redaelli, Effects of cathodic prevention on the chloride threshold for steel corrosion in concrete, Electrochim. Acta 54 (2009) 1452–1463.
[11] A.T. Yeung, J.K. Mitchell, Coupled fluid, electrical, and chemical flows in soil, Geotechnique 43 (1) (1993) 121–134.
[12] T Grundl, P. Michalski, Electroosmotically driven water flow in sediments, Water Res. 30 (1996) 811–818.
[13] A.B. Ribeiro, J.M. Rodríguez-Maroto, E.P. Mateus, H. Gomes, Removal of organic contaminants from soils by an electrokinetic process: the case of atrazine. Experimental and modeling, Chemosphere 59 (2005) 1229–1239.
[14] D.J. Wilson, J.M. Rodriguez-Maroto, C. Gomez-Lahoz, Electrokinetic remediation I. Modeling of simple systems, Sep. Sci. Technol. 30 (1995) 2937–2961.
[15] R.A. Jacobs, R.F. Probstein, Two-dimensional modeling of electroremediation, AIEChE J. 42 (1996) 1685–1696.
[16] D.J. Wilson, J.M. Rodriguez-Maroto, C. Gomez-Lahoz, Electrokinetic remediation II. Amphoteric metals and enhancement with weak acid, Sep. Sci. Technol. 30 (1995) 3111–3128.
[17] A.B. Ribeiro, J.M. Rodríguez-Maroto, Electrokinetic modeling of heavy metals, in: M.N.V. Prasad, K.S. Sajwan, R. Naidu (Eds.), Electroremediation of Heavy Metal-Contaminated Soils—Processes and Applications in Trace Elements in The Environment, Taylor & Francis, 2005.
[18] Y.S. Choi, R. Lui, A mathematical model for the electrokinetic remediation of contaminated soil, J. Hazard. Mater. 44 (1995) 61–75.
[19] B. Johannesson, Y. Hosokawa, K. Yamada, Numerical calculations of the effect of moisture content and moisture flow on ionic multi-species diffusion in the pore solution of porous materials, Comput. Struct. 87 (2009) 39–46.
[20] B. Johannesson, L.M. Ottosen, Modeling of electromigration salt removal methods in building materials, in: Proceedings from Salt Weathering on Building and Stone Sculptures, Copenhagen, Denmark, 2008, pp. 351–360.
[21] B.F. Johannesson, Diffusion of a mixture of cations and anions dissolved in water, Cem. Concr. Res. 29 (1999) 1261–1270.
[22] B. Johannesson, Ionic diffusion and kinetic homogeneous chemical reactions in the pore solution of porous materials with moisture transport, Comput. Geotech. 36 (2009) 577–588.
[23] E. Samson, J. Marchand, Numerical solution of the extended Nernst–Planck model, J. Colloid Interface Sci. 215 (1999) 1–8.
[24] M.D. Garcia−Gutierrez, C. Gomez−Lahoz, J.M. Rodriguez−Maroto, C. Vereda−Alonso, F. Garcia−Herruzo, Electrokinetic remediation of a soil contaminated by the pyritic sludge spill of Aznalcollar (SW, Spain), Electrochim. Acta 52 (2007) 3372–3379.
[25] C. Vereda-Alonso, C. Heras-Lois, C. Gomez-Lahoz, F. Garcia-Herruzo, J.M. Rodriguez-Maroto, Ammonia enhanced two-dimensional electrokinetic remediation of copper spiked kaolin, Electrochim. Acta 52 (2007) 3366–3371.
[26] B. Johannesson, Comparison between the Gauss' law method and the zero current method to calculate multi−species ionic diffusion in saturated uncharged porous materials, Comput. Geotech. 37 (2010) 667–677.
[27] J.S. Newman, Electrochemical Systems, Prentice Hall, Englewood Cliffs, 1991.
[28] J.K. Mitchell, Fundamentals of Soil Behavior, 2nd ed., John Wiley & Sons, New York, 1993.
[29] O.C. Zienkiewicz, R.L. Taylor, The Finite Element Method, vol 2, McGraw-Hill, London, 1989.
[30] K.J. Bathe, M.R. Khoshgoftaar, Finite element formulation and solution on nonlinear heat transfer, J. Nucl. Eng. Des. 51 (1979) 389–401.
[31] N.S. Ottosen, H. Petersson, Introduction to the Finite Element Method, Prentice Hall International (UK) Ltd, Hertfordshire, 1992.
[32] J.R. Gilbert, C. Moler, R. Schreiber, Sparse matrices in MATLAB: design and implementation, SIAM J. Matrix Anal. A 13 (1992) 333–356.
[33] G.R. Lindfield, J.E.T. Penny, Using MATLAB for sparse matrices, Int. J. Math. Educ. Sci. Technol. 28 (1997) 427–436.
[34] A. Mohajeri, G.A. Narsilio, P. Pivonka, D.W. Smith, Numerical estimation of effective diffusion coeficients for charged porous materials based on micro-scaled analyses, Comput. Geotech. 37 (2010) 280–287.
[35] F. Garcia-Herruzo, J.M. Rodriguez-Maroto, R.A. Garcia-Delgado, C. Gomez-Lahoz, C. Vereda-Alonso, Limpieza de suelos por electrodescontaminación 2: mejoras de la técnica en el movimiento de contaminantes, Ing. Quim. 369 (2000) 215–220.

Paper

"A Generalized Model for Transport of Contaminants in Soil by Electric Fields"

J.M Paz-García, K. Baek, I.D. Alshawabkeh and A.N. Alshawabkeh

Published in: *Journal of Environmental Science and Health, Part A, 2012*

Journal of Environmental Science and Health, Part A (2012) **47**, 308–318

ISSN: 1093-4529 (Print); 1532-4117 (Online)
DOI: 10.1080/10934529.2012.640911

Taylor & Francis
Taylor & Francis Group

A generalized model for transport of contaminants in soil by electric fields

JUAN MANUEL PAZ-GARCIA[1], KITAE BAEK[2], IYAD D. ALSHAWABKEH[3] and AKRAM N. ALSHAWABKEH[4]

[1]*Department of Civil Engineering, Technical University of Denmark, Copenhagen, Denmark*
[2]*Department of Environmental Engineering, Kumoh National Institute of Technology, Gumi, Gyeongbuk, Republic of Korea*
[3]*Department of Chemistry, Jerash University, Jerash, Jordan*
[4]*Department of Civil and Environmental Engineering, Northeastern University, Boston, Massachusetts, USA*

A generalized model applicable to soils contaminated with multiple species under enhanced boundary conditions during treatment by electric fields is presented. The partial differential equations describing species transport are developed by applying the law of mass conservation to their fluxes. Transport, due to migration, advection and diffusion, of each aqueous component and complex species are combined to produce one partial differential equation that describes transport of the total analytical concentrations of component species which are the primary dependent variables. This transport couples with geochemical reactions such as aqueous equilibrium, sorption, precipitation and dissolution. The enhanced model is used to simulate electrokinetic cleanup of lead and copper contaminants at an Army Firing Range. Acid enhancement is achieved by the use of adipic acid to neutralize the basic front produced for the cathode electrochemical reaction. The model is able to simulate enhanced application of the process by modifying the boundary conditions. The model showed that kinetics of geochemical reactions, such as metals dissolution/leaching and redox reactions, may be significant for realistic prediction of enhanced electrokinetic extraction of metals in real-world applications.

Keywords: Electrokinetic remediation, lead, cupper, mathematical model, reactive transport.

Introduction

A group of electrokinetic and electrochemical remediation technologies are developed to treat sites polluted with toxic heavy metals, radionuclides, and organic pollutants. The technologies are based on application of electric currents across electrodes inserted in the soil to induce electrolysis and generate an electric field. Ambient or introduced solutes migrate in response to the imposed electric field by electroosmosis and ionic migration. Electroosmosis mobilizes the pore fluid to flush solutes, usually toward the cathode, while ionic migration effectively separates anionic and cationic species, drawing them to the anode and cathode, respectively. This transport coupled with geochemical reactions, such as sorption, precipitation and dissolution, are the fundamental mechanisms of electrokinetic remediation. Contaminant extraction and removal are accomplished by electrodeposition, precipitation or ion exchange either at the electrodes or in an external extraction system.

Address correspondence to Akram N. Alshawabkeh, Department of Civil and Environmental Engineering, Northeastern University, Boston, USA; E-mail: aalsha@coe.neu.edu
Received May 26, 2011.

Electrokinetic extraction of metals and radionuclides from soils has been investigated by bench-scale tests, pilot-scale tests, and limited field applications.[1–12] The major advantages of the technology include: (a) it can be implemented in situ with minimal disruption, (b) it is well suited for fine-grained, heterogeneous media, where other techniques such as pump-and-treat can be ineffective, and (c) accelerated rates of contaminant transport and extraction may be obtained.

In electrokinetic extraction of metals, the electrical current applied is transformed to an ionic current in the pore solution by means of the electrochemical reactions taking place at the electrodes. Electrode reactions can vary depending on the chemical species present in the media. Electrolysis of water reactions, oxidation at the anode, Equation 1, and reduction at the cathode, Equation 2, are always likely to occur:

$$H_2O \rightleftarrows \frac{1}{2}O_2 + 2H^+ + 2e^- \quad (1)$$

$$2H_2O + 2e^- \rightleftarrows H_2 + 2OH^- \quad (2)$$

Water electrolysis generates an acidic medium at the anode, which can decrease the pH to below 2, and an alkaline medium at the cathode, which may increase the pH to above 10.[7] Proton (or hydronium ion, H_3O^+) mobility

under electrical field is about twice that of the hydroxyl ion (OH^-) which results in a faster advance of the acid front relative to the base front.[13]

Transport of the H_3O^+ is also enhanced by electroosmotic advection, which usually acts from the anode towards the cathode. In unamended treatments, strong pH changes are expected in the pore solution. Unless the transport of the proton is retarded by the soil buffering capacity,[14] the soil between the electrodes will be acidified. This acidification results in enhanced solubilization of contaminants susceptible to cation exchange and dissolution at lower pH. Once contaminants are dissolved or complexed to an ionized solute, they migrate to the electrode of opposite polarity under the applied electric field leading to their extraction from the soil.

Electrical neutrality of the pore fluid is maintained by transport of equivalent cations and anions in and out from a unit volume of pore fluid. Rigorous consideration of geochemical behavior is necessary due to the range of pH conditions and ion activity induced between the electrodes. Speciation, ion exchange, and dissolution-precipitation are among the reactions of potential significance. In unamended electrokinetic remediation, the protons that transport across the soil meet the hydroxyl ions close to the cathode compartment resulting in neutralization and the generation of water.

A section with high pH gradient is formed, which can affect to the chemical speciation. Some metals are amphoteric, i.e., can exist either in positive or negative ion forms e.g., Pb^{2+} or $Pb(OH)_3^-$, Cr^{3+} or $Cr(OH)_4^-$ depending on the local conditions. A change in magnitude or polarity of the charge of a complex would affect the rate and direction of migration, conceivably to the stalling the advance of the contaminant in a pH gradient zone. Additionally, in the more alkaline region metal hydroxides precipitation may decrease the concentrations of the ionic species in the pore fluid, decreasing the electrolyte strength, and creating a zone of low electrical conductivity in the soil adjacent to the cathode. The formation of this low conductivity zone results in a significant increase in the voltage gradient across the soil and a commensurate increase in the energy expenditure required to mobilize ions.

Different schemes have been proposed to enhance transport and extraction of species under electric fields, and to prevent formation of precipitates. The objective of some of these schemes is to neutralize the cathode water electrolysis reaction to avoid generation and transport of high concentrations of the OH- ion into the soil and to enhance metal electrodeposition at the cathode. In these acid-enhanced treatments, the neutralization of the cathode water electrolysis reaction will also assist in decreasing the electrical potential difference across the electrodes and consequently decrease energy expenditure. Acetic, sulfamic, and other acids could be introduced at the cathode at a controlled rate to prevent an increase in the catholyte pH.[7,10,12] Extracting agents are used in combination of the aforementioned acid enhancement, to obtain a soluble complex ion by chemical reaction between the target heavy metal and the extracting agents.[15–17]

Contaminant transport models which incorporate electrical gradients are limited.[2,18–23] Shapiro et al.[2] and Shapiro and Probstein[18] developed a one-dimensional model for transport of chemical species under electrical gradients, incorporating the electrochemical processes, extended to a two-dimensional by Jacobs and Probstein.[24] The model couples the transport equations of N chemical species together with the charge flux equation and accounts for specific chemical reactions in the soil pore fluid. A steady-state electroosmotic flux is assumed and the comparisons with experimental results display good agreement with one case of acetic acid transport. This model, however, assumes incompressible soil medium, and disregards the changes in hydraulic potential distribution. Jacobs et al.[21] improved the Shapiro and Probstein[18] model by incorporating complexation and precipitation reactions. Haran et al.[23] presented a model for the transport of hexavalent chromium under electric fields in sand. Electroosmotic flow is assumed zero as the model was implemented for a case of sandy soil.

Acar et al. presented a one-dimensional model used to estimate the pH distribution during the electrokinetic process.[20,25] Paz-Garcia et al.[22] presented a transport model based on the Poisson-Nernst-Planck system accounting for electroosmotic advection and water chemical equilibrium. Alshawabkeh and Acar[19,20] developed a numerical solution for the equations describing reactive multi-component species transport under coupled hydraulic, electrical, and chemical concentration gradients. The finite element method (FEM) is used in space discretization and the finite difference method was used for time discretization. Predicted lead profile show excellent agreement with the pilot-scale test results on a kaolinite soil samples mixed with lead. This model couples electroosmotic consolidation with species transport, which is essential when electrokinetic-induced settlement is problematic.

An engineering design/analysis package for expedient field implementation of electrokinetic and electrochemical applications in environmental restoration requires the continued development of generalized mathematical formulation and the development of a comprehensive model for multi-component, reactive transport under coupled hydraulic, electric, and chemical gradients. The present work summarizes enhancements on the model developed by Alshawabkeh and Acar.[19,20] A generalized model applicable to soils contaminated with multiple metals under enhanced boundary conditions during electrokinetic processing is presented. The enhanced model is used to simulate electrokinetic cleanup of lead and copper contaminants at an Army Firing Range.

Materials and methods

Theoretical formulation

The conceptual model of the porous medium is as a solid framework of cation exchange surfaces with the pore space occupied by chemically reactive species in aqueous solution. Chemical species consist of N_i components that can react with each other to form N_y aqueous complexes and N_p precipitated solids. The choice of independent components is arbitrary, under the restriction that each component should represents one of the elements participating in the chemical system. Aqueous complexes and precipitates are defined as function of the chosen components by a corresponding stoichiometric chemical reaction. Additionally, aqueous components and complexes may be adsorbed to the surface of N_{site} to form N_{si} adsorbed components and N_{sy} adsorbed complexes. Accordingly, the total number of aqueous species will be the sum of N_i aqueous components and N_y aqueous complexes. The total number of adsorbed species will be the sum of N_{si} and N_{sy}.

In the present formulation for modeling the transport of species under electric fields, c_i ($i = 1, 2, \ldots, N_i$) refers to concentration of the ith primary aqueous component (e.g., Pb^{2+}, Cu^{2+}), c_y ($y = 1, 2, \ldots, N_y$) is the concentration of the complex yth (e.g., $Pb(OH)^{+}$, $Cu(OH)^{+}$). Concentration of the ith adsorbed component (e.g., Pb^{2+} -N_{site}, Cu^{2+} -N_{site}) is represented by s_i ($i = 1, 2, \ldots, N_{si}$), while s_y ($y = 1, 2, \ldots, N_{sy}$) is the concentration of the adsorbed yth complex (e.g., $Pb(OH)^{+}$ -N_{site}, $Cu(OH)^{+}$ -N_{site}), and p_k ($k = 1, 2, \ldots, N_p$) is the concentration of the precipitate k (e.g., $Pb(OH)_2$(s), $Cu(OH)_2$(s)). Solute concentrations are expressed in units of moles/volume, adsorbed and precipitated concentrations are expressed in units of mass/mass of dry soil.

The partial differential equations (PDEs) describing species transport are developed by applying the law of mass conservation to their fluxes. Transport PDEs (due to migration, advection and diffusion) of each component and complex aqueous species are combined to produce one PDE that describes transport of the total analytical concentrations of component species i (T_i), which are the primary dependent variables. This formulation forces the sum of the rates describing the change in species concentration due to chemical reactions to zero, i.e., $\sum R_{iy} = 0$, where R_{iy} is the rate of change in the concentration of species i due to the rth chemical reaction, where $r = 1, 2, \ldots, N_T$, and $N_T = N_i + N_y + N_s + N_p$. This will facilitate the operator splitting formulation for transport and geochemical reactions.

The differential equations describing transport of total analytical concentrations of the components species i are derived by applying the law of conservation to mass flux through a control volume. Mass fluxes are evaluated under electric, hydraulic, and chemical concentration gradients.[20] Accordingly the mass conservation equations are given by

$$n\frac{\partial T_i}{\partial t} = L(c_i) + \sum_{y=1}^{N_y} a_{iy} L(c_y) - \lambda_i T_i; \quad i = 1, 2, \ldots, N_i \tag{3}$$

where n is the soil porosity, t is time, a_{iy} is the stoichiometric coefficient of the ith aqueous component in the yth complexed species, λ_i is the decay rate constant for the ith aqueous component, assumed first-order, and $L(c_i)$ is the flux term defined as:

$$L(C_i) = \nabla \cdot (D_i \nabla C_i + u_i c_i \nabla E + k_e c_i \nabla E + k_h c_i \nabla h) \tag{4}$$

where D_i is the effective diffusion tensor of component ith, u_i is the effective ionic mobility tensor of component ith, k_e is the electroosmotic permeability tensor, k_h is the hydraulic conductivity tensor, E is the electric potential, and h is the hydraulic head. $L(c_y)$, the flux term for the aqueous complexes, is defined similarly. The total analytical concentrations of species i (T_i) are the sum of concentrations of all forms of species i and are given by,

$$T_i = c_i + \sum_{y=1}^{Ny} a_{iy} c_y + s_i + \sum_{y=1}^{Ny} a_{iy}^{s} s_y + \sum_{k=1}^{k} a_{ik}^{p} p_k; \quad i = 1, 2, \ldots, N_i \tag{5}$$

where a_{iy}^{s} is the stoichiometric coefficient of the ith aqueous component in the yth adsorbed species, p_k is the concentration of the precipitate kth, a_{ik}^{p} is the stoichiometric coefficient of the ith aqueous component in the kth precipitated species.

Charge conservation

In the present model, ions transport under electric fields is assumed to be controlled by the electric neutrality of the free pore fluid.

$$\sum_{i=1}^{N_i} z_i c_i + \sum_{y=1}^{N_y} z_y c_y = 0 \tag{6}$$

Consequently, an equivalent positive and negative charge should pass through a unit volume in order to maintain zero net charge, assuming no electric capacitance of the porous medium. Application of Faraday's law to the flux terms defined in Equation 4 results in the following charge conservation equation:

$$C_p \frac{\partial E}{\partial t} = F\left(\sum_{i=1}^{N_i} z_i L(C_i) + \sum_{y=1}^{N_y} z_y L(C_y)\right) \tag{7}$$

where z_i is the charge of the ith component, z_y is the charge of the yth complex, F is the Faraday's constant (96,485 C/mol) and C_p is the electrical capacitance per unit soil volume (FL^{-3}). If the soil capacitance C_p is zero then Equation

7 will result in:

$$\sum_{i=1}^{N_i} z_i L(c_i) + \sum_{y=1}^{N_y} z_y L\left(c_y\right) = 0 \tag{8}$$

which means that the net change in charge per unit volume of free pore fluid due to all species (components and complexes) transport is zero. Equation 8 is used to calculate the electrical potential distribution.

Geochemical reactions

Transport of species under electric fields will be controlled by the nature and rates of geochemical reactions in the soil. Some base or acid produced by electrolysis reactions may be consumed in non-target reactions with the medium but convergence of the fronts creates locally sharp pH and concentration gradients and a challenge to robust geochemical modeling. Geochemical reactions that should be included in the geochemical model and will impact the transport include sorption, aqueous phase, redox, and precipitation/dissolution reactions. Recent developments showed that these reactions could be incorporated by a set of algebraic equations (for equilibrium reactions) and differential equations (for reaction kinetics). Mathematical treatment for some of these reactions is provided assuming instantaneous equilibrium, since aqueous chemical reaction rates are, generally, several order of magnitude faster than transport rates in most electrokinetic treatments.[22]

Aqueous phase reactions

A set of nonlinear algebraic equations may be developed from mass balance considerations of the aqueous phase reactions. In this case, any complex y is the product of ith reactant components, i.e.,

$$c_y \rightleftarrows \sum_{i=1}^{N_i} a_{iy} c_i; \quad y = 1, 2, \ldots, N_y \tag{9}$$

where a_{iy} is the stoichiometric coefficient in complex y for component i (*mole y/mole i* or *mass y / mass i*). The law of mass action implies that

$$c_y = \frac{1}{K_y^{eq}} \prod_{i=1}^{N_i} c_i^{a_{iy}}; \quad y = 1, 2, \ldots, N_y \tag{10}$$

where K_y^{eq} is the equilibrium constant for aqueous reaction *yth* described as a dissociation reaction. Precipitation/dissolution reactions must be considered in the mass transport formulation because they can affect dramatically the electrokinetic efficiency. In precipitation reactions the stoichiometric reaction is defined similarly to aqueous equilibrium reaction,

$$p_k \rightleftarrows \sum_{i=1}^{N_i} a_{ik} c_i; \quad i = 1, 2, \ldots, N_p \tag{11}$$

where p_k is the chemical formula of precipitate *kth*, a_{ik} is the stoichiometric coefficient of component *ith* in precipitate *kth* [mass/mass], and N_p is the number of precipitates. The existence of the precipitates species is conditional upon constituent solute(s) *ith* concentrations exceeding the saturation index of *kth*. The law of mass action is written as

$$\begin{cases} \prod_{i=1}^{N_i} c_i^{a_{ik}} = K_k^{sp}; & p_k \neq 0 \\ \prod_{i=1}^{N_i} c_i^{a_{ik}} < K_k^{sp}; & p_k = 0 \end{cases} \tag{12}$$

where K_k^{sp} is the solubility product equilibrium constant for the precipitate *kth* described as a dissolution reaction. The current model implementation neglects nonlinear effects of solute concentrations on ionic activity (e.g., Davies, Debye-Hückel, Pitzer or other model) and thus solubility index for precipitates. This limitation restricts model application to solutions of relatively low ionic strength and is one of our priority targets for relaxation.

Sorption reactions

Sorption reactions will provide two sets of algebraic equations: one set for adsorbed components and another set for adsorbed complexes. Assuming instantaneous equilibrium in sorption reactions and linear isotherms,

$$\frac{\partial s_i}{\partial c_i} = K_{di} \tag{13}$$

where K_{di} is the distribution coefficient (L^3M^{-1}) of species *ith*. The same procedure could be used for adsorbed components or complexes. Simple isotherm sorption models ignore the potential effects of variations in pH, solute composition and ionic strength, redox potential, or processes such as competitive adsorption. Alternative, more robust (and complicated) sorption models include ion- or ligand-exchange, mass action models, and surface complexation models as described by several research groups.[26–32] The reader could refer to some of these references for more rigorous treatment of sorption and other reactions such as redox.

Hydraulic head and soil volume change

Another variable that impacts reactive transport is the hydraulic gradient that will vary depending upon the compressibility of the porous medium. As the process is used for remediation of soft cohesive soils, the compressibility of the medium will depend on the consolidation characteristics of the soil. Volume change in the soil medium due to

consolidation is described by the following partial differential equation

$$m_v \gamma_w \frac{\partial h}{\partial t} = k_h \nabla^2 h + k_e \nabla^2 E \tag{14}$$

where m_v is the coefficient of volume compressibility ($L^2 M^{-1}$) and γ_w is the unit weight of water ($M L^{-3}$). Solution of equation 14 will provide the hydraulic gradients that will be used in species transport. Equation 14 is dependent upon the soil parameters and also on the electric field intensity, which is dependent upon the species distribution.

Complete system of equations

Nine sets of unknowns (T_i, c_i, c_y, s_i, s_y, p_k, E, h, and σ^*) could be identified in this case for modeling reactive transport of species under electric fields. The required nine sets of equations for simulating the process are equations 3, 5–7, 10, 12, 2 equations of form 13 (one for components and another one for complexes), and 14. Equation sets 3, 7, and 14 are second order partial differential equation, thus three sets of boundary and initial conditions are needed. Boundary conditions for one-dimensional contaminant transport are derived from electrolysis reactions at the electrodes.

Electrolysis reactions and enhancements at boundaries

Electrokinetic remediation can be adapted in a variety of options to enhance cleanup of the target contaminants and/or to accommodate site geology and geochemistry. In practice, much of this adaptation involves chemical conditioning or introduction of proper reactants at the electrodes. Thus, in terms of modeling, the major difference between these electrokinetic applications is the treatment of electrode boundary conditions. When inert electrodes (e.g., graphite) are used in groundwater, oxidation of water at the anode, Equation 1, produces an acid front; while reduction of water at the cathode, Equation 2, produces a basic front.

Despite the water electrolysis of the pore solution is always likely to happen, the prevailing oxidation/reduction reactions at the electrodes might vary depending upon the chemical composition, pH, and the electrochemical potentials of these reactions. Multiple electrolysis reactions may occur at the cathode or anode depending on the water composition and electrochemical potential of each reaction. In general, the overall electrolysis (cell) reaction comprises two separated half-reactions: reduction at the anode and oxidation at the cathode. Consider the following half-cell reaction:

$$a_o \mathrm{O} + n e^- \rightleftarrows a_r \mathrm{R} \tag{15}$$

where O is the oxidized form, R is the reduced form, and a_o and a_r are the stoichiometric coefficients. The Gibbs free energy (G) of this cell reaction is given by

$$\delta G = \delta G^o + RT \ln \frac{[\mathrm{R}]^{a_r}}{[\mathrm{O}]^{a_o}} \tag{16}$$

where G^o is the standard free energy, R is the universal gas constant (8.3144 $J{\cdot}K^{-1}{\cdot}mol^{-1}$), T is temperature (K), and the squared brackets represent chemical activities. Since $G = -nFE$, Equation (16) becomes:

$$E = E^0 - \frac{RT}{nF} \ln \frac{[R]^{a_r}}{[O]^{a_o}} \tag{17}$$

where E^o is the standard reduction potential versus the standard hydrogen electrode (*SHE*). Equation 17 is the Nernst Equation[33] and it provides the potential of the O/R electrode verses Natural Hydrogen Electrode (*NHE*) as a function of the activities of O and R. Equation 17 is useful for the identification of the electrolysis reactions to be expected at the electrode. The electrolysis reaction that has the highest positive redox potential, E, will occur at the cathode, while the electrolysis reaction with the most negative value of E will occur at the anode. These electrolysis reactions at the electrodes will drive continuous changes that will either enhance or retard the electrokinetic process.

Numerical strategy

Three approaches were considered in the development of a numerical solution to differential and algebraic equations posed previously. The differential and algebraic equations approach (DAEA) consists of providing a solution to the mixed differential and algebraic equations in which the transport and reaction equations are solved simultaneously.[30,34,35] The direct substitution approach (DSA) consists of direct substitution of the algebraic chemical equilibrium equations into the differential transport equations to form a highly nonlinear system of partial differential equations.[27,29,31,36] Finally, the sequential iteration approach (SIA) consists of iterating between the sequentially solved differential and algebraic equations.[26,28,32]

The primary advantages of SIA over the other schemes (DAEA and DSA, which could be considered globally implicit schemes) is the lower computational memory requirements[37] and their greater flexibility to incorporate higher-order methods to accommodate advection-dominated systems,[35] and in this case migration dominated transport. For the geochemical conditions to be simulated, DAEA and DSA offer no clear advantage to justify the memory overhead. At the same time, the two-steps SIA allows incorporating existing geochemical models in the developed system of transport rather than developing a specific geochemical model for transport under electric fields. The advantages and disadvantages of the schemes are discussed elsewhere.[32,35,37] The SIA is used in this study.

Model application

The numerical model described here was developed in conjunction with basic and applied research on the electrokinetic recovery of lead from soils. Laboratory- and field-scale evaluation of the electrokinetic extraction of lead have been conducted using contaminated soils from a small arms firing range. The experimental study was conducted by Electrokinetics, Inc. (Baton Rouge, LA), in collaboration with the U.S. Army Engineers Waterways Experiment Station (WES), Vicksburg, Mississippi.[9] Soil samples were retrieved from a firing range situated along the bank of a small ephemeral /intermittent (usually dry) stream.

Bullet fragments from several decades of operation littered the area, acting as a potential source of lead and copper contamination to surface and ground waters. Due to the low aqueous solubility of weathered lead, most fragments have remained in the bank and floodplain soils. Older small arms munitions have copper alloy jackets surrounding the lead alloy slug (solid tip of the projectile). Copper metal in electrical proximity to the lead induces galvanic (or cathodic) corrosion, accelerating the weathering and release of lead to the environment. Particulate lead also has been transported with other sediment along the creek with the seasonal flood events.

A laboratory pilot investigation was conducted in the WES Hazardous Waste Research Center (HWRC). The soil was retrieved from two depths at the contaminated firing range. A first set of samples was collected from the upper contaminated sand layer up to 30 cm depth. A second set of samples was then collected from the underlying, and relatively clean, clayey sandy layer up to a depth of 45 cm. The soil was placed in 208 L drums by a hauler. The drums were transported to WES on a flatbed truck. At WES, the soil was air dried and sieved through a 1/4 inch (6.35 mm) mesh to minimize the impact of discrete metal fragments on the investigation. However, appreciable amounts (about 8 % by weight) of bullet fragments remained in the surface soil. The lower layer did not contain any fragments.

Soil mixing and homogenizing operations were carried in batches by addition of water (20 % by weight of dry soil). Mixing was carried in a pool using a shovel. The soil was then transported to the testing area and was placed in a lined wooden container. The container inner dimensions were 76.2 cm width, 91.4 cm height, and 183 cm length (2.5 × 3 × 5 feet). A prefabricated, 80 mm thick, high density polyethylene (HDPE) liner was placed inside the containers as primary protection from any leakage. The soil was placed in layers inside the container and compacted with a hammer. The hammer used is a steel rod of 91.4 cm long, welded to a steal plate with a contact area of 15.2 cm × 15.2 cm. The gross weight of the hammer is 4.54 kg.

The soil was compacted in seven layers. Each layer was compacted by dropping the hammer 800 times on top of the soil from a height of about 90 cm. Each layer thickness was about 10 cm after compaction. The natural stratification was replicated in the setup by first compacting 4 layers of the underlying clayey sand followed by three layers of the contaminated sandy soil. Electrodes were placed in wooden compartments that are 10 cm in width. Two cathode compartments were placed at the sides of the container, while one anode compartment was placed in the middle. This arrangement provided two cells each with a center to center cathode-anode spacing of about 87 cm. The soil was divided into two cells in order to compare the results and assure the quality and repeatability of data collected, as one of the cells was used for intermediate sampling.

Anode compartment had five, 5 cm diameter, holes for five graphite electrodes. Cathode compartment had a longitudinal slot to place galvanized mesh electrodes. A composite fabric supported by geotextile grid was nailed to the side of the electrode compartment to separate the electrolyte from soil and allow free water flow. Electrode compartments were filled with tap water up to the soil surface level. The electrodes were connected to the DC power supply and current of 1.2 A was applied. The current was divided in half by passing 0.6 A through each cell, rendering a current density of about 1.8 A/m^2 (cross-sectional area of the soil is 5500 cm^2). The test was processed for 9 months.

The electrochemical treatment was amended at the cathode by the injection of adipic acid to control pH. As mention before, control of the basic front will increase the solubility and thus the mobility of the target contaminants.

Initial chemical analysis was conducted on 36 randomly collected samples from the compacted layers. Initial and final sampling was conducted on both cells, whereas intermediate samples were collected every two weeks from one cell only. The intermediate samples were collected using 2.54 cm diameter tubes at 10 cm equally spaced locations between the anode and cathode. Final sampling was performed by slicing each cell into five horizontal layers. Each layer was divided into 8 longitudinal sections and 2 lateral sections of equal size. Prior to chemical analysis, the soil sample was oven dried, crushed with a mortar and a pistol, and sieved through 2.00 mm sieve. A riffle was also used for splitting the soil into equal portions.

One-gram samples were then taken from the riffled soil. EPA SW 846 Method 3051 was used for soil digestion. Inductively Coupled Plasma-Atomic Emission Spectroscopy (ICP) was used for analysis of the leachate (EPA SW 846 Method 6010A). The soil was poorly sorted sand (an SP by the Unified Soil Classification System). Hydraulic conductivity of the soil was 9.8×10^{-5} cm/s; geotechnical properties of the soil are summarized in Table 1. Chemical analysis showed a mean lead concentration of 3041 mg/kg with a standard deviation of 887 mg/kg. Mean concentrations of other metals in the soil matrix included 589 mg/kg copper, 524 mg/kg calcium, and 96 mg/kg zinc.

Metal fragments impede the remediation process, acting as a significant internal source of contamination. Reactive transport of eight components (Pb^{2+}, Cu^{2+}, Ca^{2+}, NO_3^-, Cl^-, OH^-, A^{-2} and H^+) and four complexes ($Pb(OH)^+$,

Table 1. Soil geotechnical properties.

Depth below surface	*Contaminated sandy soil*	*Underlying clayey sand*
Initial water content w_i (%)	18.2	20.2
Initial degree of saturation S (%)	56	66
Liquid Limit	–	22.6
Plastic Limit	–	14
Plasticity index	–	8.6
Specific Gravity (G_s)	2.61	2.64
γ_d (kN/m^3)	13.8	14.5
Porosity (n)	0.46	0.44
Void Ratio (e)	0.85	0.79
Permeability (cm/s)	9.8×10^{-5}	2×10^{-7}
Unified Soil Classification System	SP	SC

$Pb(OH)_2$, $Cu(OH)^+$, and $Cu(OH)_2$) are modeled in the present simulations. A^{-2} represents the adipate ion, $O_2C(CH_2)_4CO_2^{-2}$. The system of differential equations required to implement the code for this case of lead extraction includes eight transport equations, one volume change equation and one charge conservation. Initial concentrations (e.g., total lead and copper concentrations), soil parameters (e.g., hydraulic conductivities, electroosmotic permeability), and boundary conditions must be defined. Table 2 summarizes all initial concentration of components used in the present simulations.

Only the boundaries represented by the anode ($x = 0$) and cathode ($x = L$) need be defined in the one-dimensional simulations presented here. Hydraulic head gradient is set to zero, consistent with the experimental setup, which results in the following boundary conditions for Equation 18:

$$h|_{x=0} = h|_{x=L} = 0 \tag{18}$$

Boundary conditions for charge conservation equation are developed from the current value at the boundary. The constant current applied through the experiment requires the following transport boundary conditions:

$$\left[F \sum_{i=1}^{N_i} z_i D_i \frac{\partial c_i}{\partial x} + F \sum_{y=1}^{N_y} z_y D_y \frac{\partial c_y}{\partial x} - \sigma^* \frac{\partial E}{\partial x} \right] = 0; \quad E|_{x=L} = 0 \tag{19}$$

where σ^* is the effective electric conductivity of the soil free pore fluid which is described by:

$$\sigma^* = F \sum_{i=1}^{N_i} z_i u_i c_i + F \sum_{y=1}^{N_y} z_y u_y c_y \tag{20}$$

where u_i is the effective ionic mobility of the ith component and u_y is the effective ionic mobility of the yth complex.

Boundary conditions for the given species transport equation are evaluated based on the flux of each species at the cathode and the anode. There are two components of mass fluxes at the electrode, one is due to water advection (advective component, including electroosmosis since there is no hydraulic gradient) and the other is due to electrolysis (current component). The mass fluxes of any species (component or complex) at the cathode and at the anode are given by:

$$\left| -D_i \frac{\partial c_i}{\partial x} + v_i c_i + \sum_{y=1}^{N_y} a_{iy} \left[-D_y \frac{\partial c_y}{\partial x} + v_y c_y \right] \right|_{x=0} = T_i \mathbf{J}_w + \frac{I_i}{z_i F} + \sum_{y=1}^{N_y} \frac{a_{iy} I_y}{z_y F} \tag{21}$$

$$\left| -D_i \frac{\partial c_i}{\partial x} + v_i c_i + \sum_{y=1}^{N_y} a_{iy} \left[-D_y \frac{\partial c_y}{\partial x} + v_y c_y \right] \right|_{x=L} = T_i \mathbf{J}_w + \frac{I_i}{z_i F} + \sum_{y=1}^{N_y} \frac{a_{iy} I_y}{z_y F} \tag{22}$$

where $\mathbf{J}_w$ is the advective flux at the electrodes, I_i and I_y are the partial current densities, and the v_i, is defined by:

$$v_i = -(u_i + k_e) \frac{\partial E}{\partial x} - k_h \frac{\partial h}{\partial x} \tag{23}$$

and v_y is defined similarly for the complexes. The partial current density of a component or a complex is the percentage of the total current that is employed in production the specific component or complex due to electrolysis reactions. The partial current densities are evaluated based on the electrolysis reactions of each component and complex. For example, if only water electrolysis is occurring at the electrodes, then at the anode the partial current densities are 1.0 for H^+ and zero for all other species. Similarly at the cathode the partial current densities are 1.0 for OH^- and zero for all other species.

Table 2. Initial concentration of components used in modeling pilot-scale study.

Component	*Initial concentration (M)*
Pb^{2+}	0.0449
Cu^{2+}	0.0283
Ca^{2+}	0.0400
NO_3^-	0.1120
Cl^-	0.1130
OH^-	1×10^{-4}
A^{-2}	0
H^+	1×10^{-10}

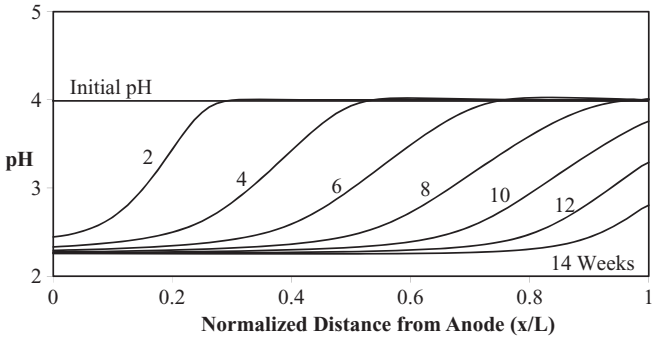

Fig. 1. Predicted pH profiles across the pilot-scale sample.

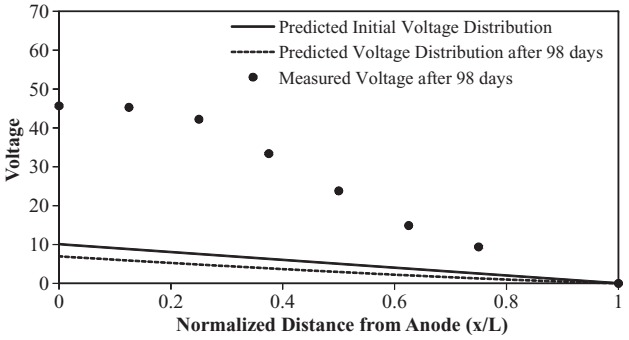

Fig. 3. Comparisons between predicted and measured voltage profiles across the soil sample.

Results and discussion

Figure 1 shows the transport of the acid front developed at the anode. The pH profile does not show an increase of the pH value at the cathode. The adipic acid added to the cathode compartments neutralized the water electrolysis reaction at this end of the setup and prevented the development of a high pH zone at the cathode. Adipic acid dissociation at the cathode neutralizes the water reduction electrolysis reaction, keeping the pH at around 4 to 5. Enough adipic acid was used for this purpose. Nevertheless, adipate anion was not found in the soil.

Figure 2 shows comparisons of the experimental and predicted pH profiles for the first pilot-scale test. The comparisons indicate that the advance of pH front is overestimated by the model.

The model results show that predicted breakthrough of pH front at the cathode occurs in 14 weeks (98 days). On the other hand, the experimental results do not show a breakthrough of the acid front even after 270 days of processing. A similar behavior is noted in prediction of lead and copper transport. This overestimation of transport of ions could be related to many reasons. Rate of transport of charged particles is a function of the electric gradient

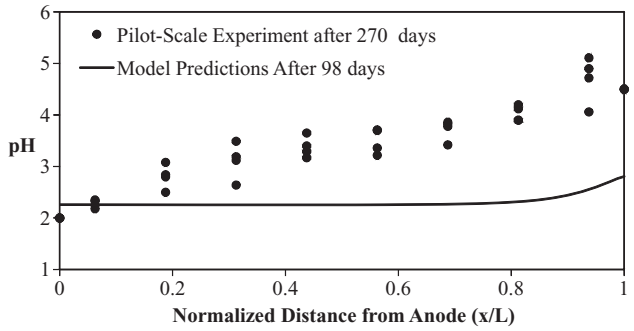

Fig. 2. Comparisons between predicted pH profile after 98 days and experimental pH profile after 270 days showing the model predictions overestimate acid transport rates.

ion mobility and pore fluid chemistry. An overestimate of ion transport could be due to overestimate of electric field strength, overestimate of effective ionic mobility, and/or improper handling of soil pore fluid chemistry. Comparisons of predicted and measured electric gradients (Fig. 3) show that the model underestimates the electric potential and electric gradient. This result is due to the fact that the predicted electric conductivity of the pore solution is higher than the measured one. This will lead to the other reason for overestimating the rate of acid transport, which is the effective ionic mobility of the species.

As described earlier, the effective ionic mobility is assumed equal to the ionic mobility at infinite dilution multiplied by soil porosity and soil tortuosity. Proper evaluation of porosity and tortuosity is important for modeling; yet, the critical factor is the use of ionic mobility coefficients at infinite dilution. It is established in electrochemistry that ionic mobilities are dependent on the ionic strength of the solution. Thus, the use ionic mobilities at infinite dilution for measuring the effective ionic mobilities, which is considered valid, needs to be further investigated. However, since the results overestimated acid transport rates and due to increased interest of electrochemical processing of soil, it is recommended that more basic research is needed to better understand ionic migration in soils.

Other important factor that will impact acid transport is pore fluid and soil chemistry. Soil buffer capacity could limit the acid advance. However, the soil used in the pilot-scale experiments is a silty sand soil with limited buffer capacity. Presence of bullet fragments and other species could result in some buffer capacity of the soil. The efficiency of electrolysis reaction at the anode also needs to be considered. It is expected that electrolysis reactions might occur at less than 100 % efficiency. This defines the boundary condition for the acid transport. Water oxidation at the anode is assumed to occur at 100 % efficiency. This might be another reason for overestimation of the rate of advance of the acid front. Efficiencies less than 100 % could be used for electrolysis reactions at the electrodes. Yet, these values will be estimated and might not represent real life conditions.

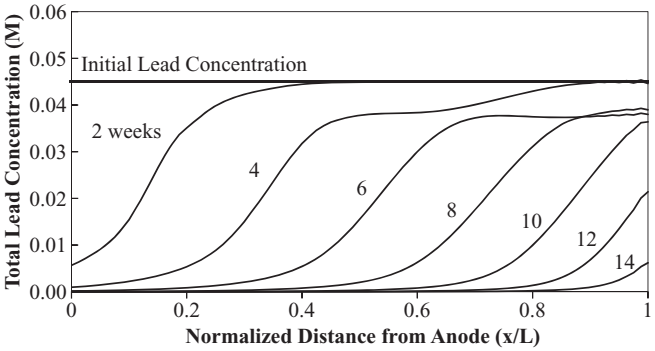

Fig. 4. Predicted lead transport in two weeks intervals.

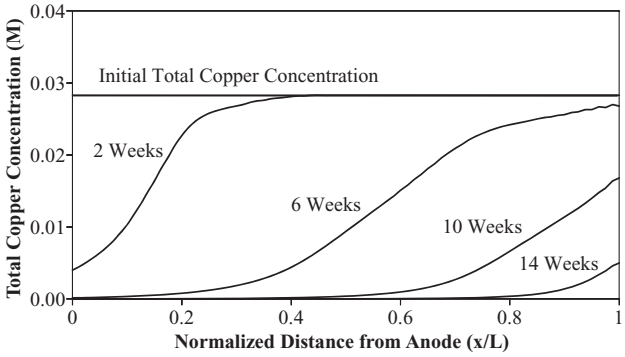

Fig. 6. Predicted Cu transport in the pilot-scale test.

Figure 4 shows predicted lead profiles in the pilot-scale study. Predicted profiles indicate that full extraction of lead could be achieved in 100 days (about 3 to 4 months). On the other hand, experimental results showed that it took about 9 months to reduce lead concentration to less than 300 mg/kg.

Figure 5 shows comparison between predicted and measured lead profiles in the soil after 2 and 14 weeks of processing. Predicted profiles show reasonable agreement with experimental results. However, comparisons after 15 weeks show that the model overestimates lead transport. Similar to the advance of the acid front, predicted rates of lead transport are faster than measured ones. This again will question the use of lead ionic mobility at infinite dilution for estimation of lead effective ionic mobility in soils. The more significant factor in predicting lead transport is the geochemistry and impact of bullet fragments on lead concentration. Initial soil pH was around 4. During processing, predicted and measured pH profiles clearly show the drop in pH to around 2, especially near the anode.

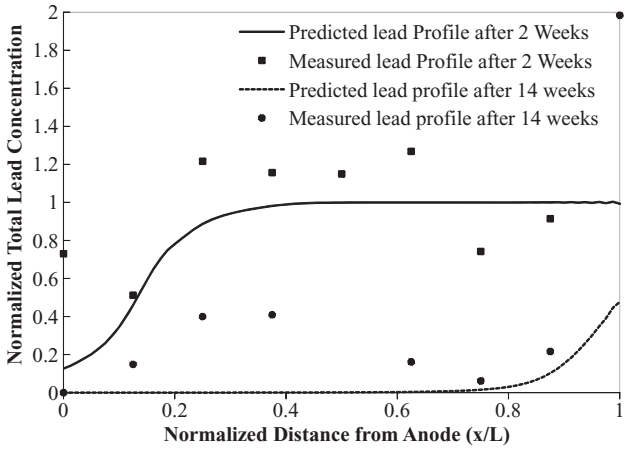

Fig. 5. Comparisons between predicted and measured lead profiles after 2 and 14 weeks.

This will lead to lead dissolution, desorption, and consequently migration. The two important factors in realistic prediction of lead transport are (a) dissolution of lead from bullet fragments and precipitates and (b) the kinetics of lead dissolution. The predicted transport did not account for presence of 8 % bullet fragments. These fragments contain significant amount of lead, copper, and zinc, which will leach in time with the advance of the acid from the anode. These fragments will act as a continuous source of lead. This is the major reason for the differences between predicted and measured lead profiles. The predicted profiles show cleanup of lead to minimal concentrations across the sample. The measured concentrations show a steady-state final lead concentration in the soil in the range of 200 to 500 mg/kg. These concentrations could be the equilibrium values of lead in solution due to its leaching from bullet fragments. The significance of the bullet fragments is observed in the case of copper transport.

Figure 6 displays predicted copper profiles, while Figure 7 displays measured final copper profiles. The predicted profiles show a decrease in copper concentration with time and complete extraction after 14 weeks. The measured final copper profiles show increase in copper concentrations

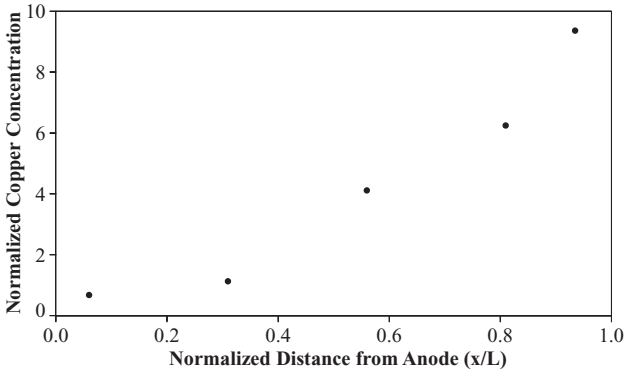

Fig. 7. Measured total Cu concentration after 39 weeks of processing.

near the cathode. In fact the measured final copper concentrations were higher than the initial concentrations. This increase is directly related to its leaching from the bullet fragments which was not incorporated in the model predictions.

One method to handle leaching of contaminants from bullet fragments is to assume a constant source in the soil. This however will require a more elaborate work on the geochemistry involved. Lead, copper, and zinc leaching rate kinetics will be of significant importance in such enhancement. An elaborate geochemical code is needed for more realistic prediction of the process. Furthermore, the results suggest that there is a need for better understandings of the basic physicochemical soil properties.

Conclusion

This article presents a generalized model for simulating contaminants transport and extraction from soils by electric fields. The model is able to simulate enhanced application of the process by modifying the boundary conditions. The model is applied for the case of lead and copper extraction from a contaminated soil sample collected from an Army Firing Range site by enhanced electrokinetic processing. While model performance was realistic in the first few weeks of processing, it showed that further understanding of physicochemical and geochemical processes is needed for proper simulation of such a complicated process in a "real world" soil.

These understandings include (a) verifying existing methods for estimating effective ionic mobilities in soils and/or development of other theoretical or experimental procedures for accurate evaluation of effective ionic mobilities in soils at variable pH and ionic strength conditions, (b) the geochemical sub-model used in this study is a limited sub-model that accounts for basic geochemical reactions, such as precipitation dissolution and/or complexation. This sub-model is shown to be appropriate for modeling lab experiments where synthetic soils are mixed with contaminants. This study showed that such basic geochemical sub-model has limitations in predicting geochemistry during enhanced EK application in real contaminated soil. The model also showed that kinetics of geochemical reactions, such as metals dissolution/leaching and redox reactions might be significant for realistic prediction of enhanced electrokinetic extraction of metals in real world applications.

Acknowledgments

Partial support of the work described is provided through Award Number P42ES017198 from the National Institute of Environmental Health Sciences. The content is solely the responsibility of the authors and does not necessarily represent the official views of the National Institute of Environmental Health Sciences or the National Institutes of Health.

References

[1] Lageman, R.; Pool, W.; Seffinga, G. Electro-reclamation: Theory and practice. Chem. Ind. **1989**, 585–590.
[2] Shapiro, A.; Renaud, P.; Probstein, R.F. Preliminary studies on the removal of chemical species from saturated porous media by electroosmosis. Physicochem. Hydrodyn. **1989**, *11*, 785–802.
[3] Hamed, J.; Gale, R.J. Pb (II) removal from kaolinite by electrokinetics. J. Geotech. Eng.-ASCE **1991**, *117*, 241–270.
[4] Probstein, R.F.; Hicks, R.E. Removal of contaminants from soils by electric fields. Science **1993**, *260*, 498–503.
[5] Runnells, D.D.; Wahli, C. In situ electromigration as a method for removing sulfate, metals, and other contaminants from ground water. Ground Water Monit. Remed. **1993**, *13*, 121–129.
[6] Lageman, R. Electroreclamation. Applications in the Netherlands. Environ. Sci. Technol. **1993**, *27*, 2648–2650.
[7] Acar, Y.B.; Alshawabkeh, A.N. Principles of electrokinetic remediation. Environ. Sci. Technol. **1993**, *27*, 2638–2647.
[8] Acar, Y.B.; Alshawabkeh, A.N. Electrokinetic remediation .1. Pilot-scale tests with lead-spiked kaolinite. J. Geotech. Eng.-ASCE **1996**, *122*, 173–185.
[9] Alshawabkeh, A.N.; Bricka, R.M.; Gent, D.B. Pilot-scale electrokinetic cleanup of lead-contaminated soils. J. Geotech. Geoenviron.-ASCE **2005**, *131*, 283–291.
[10] Kim, D.H.; Ryu, B.G.; Park, S.W.; Seo, C.I.; Baek, K. Electrokinetic remediation of Zn and Ni-contaminated soil. J. Hazard. Mater. **2009**, *165*, 501–505.
[11] Ryu, B.G.; Park, S.W.; Baek, K.; Yang, J.S. Pulsed Electrokinetic decontamination of agricultural lands around abandoned mines contaminated with heavy metals. Sep. Sci. Technol. **2009**, *44*, 2421–2436.
[12] Ryu, B.G.; Yang, J.S.; Kim, D.H.; Baek, K. Pulsed electrokinetic removal of Cd and Zn from fine-grained soil. J. Appl. Electrochem. **2010**, *40*, 1039–1047.
[13] Acar, Y.B.; Gale, R.J.; Alshawabkeh, A.N.; Marks, R.E.; Puppala, S.; Bricka, M.; Parker, R. Electrokinetic remediation: Basics and technology status. J. Hazard. Mater. **1995**, *40*, 117–137.
[14] Puppala, S.K.; Alshawabkeh, A.N.; Acar, Y.B.; Gale, R.J.; Bricka, M. Enhanced electrokinetic remediation of high sorption capacity soil. J. Hazard. Mater. **1997**, *55*, 203–220.
[15] Kim, K.J.; Kim, D.H.; Yoo, J.C.; Baek, K. Electrokinetic extraction of heavy metals from dredged marine sediment. Sep. Purif. Technol. **2011**, *79*, 164–169.
[16] Park, S.Y.; Park, G.Y.; Kim, D.H.; Yang, J.S.; Baek, K. Electrokinetic separation of heavy metals from wastewater treatment sludge. Sep. Sci. Technol. **2010**, *45*, 1982–1987.
[17] Subirés-Muñoz, J.D.; García-Rubio, A.; Vereda-Alonso, C.; Gómez-Lahoz, C.; Rodríguez-Maroto, J.M.; García-Herruzo, F.; Paz-García, J.M. Feasibility study of the use of different extractant agents in the remediation of a mercury contaminated soil from Almaden. Sep. Purif. Technol. **2011**, *79*, 151–156.
[18] Shapiro, A.P.; Probstein, R.F. Removal of contaminants from saturated clay by electroosmosis. Environ. Sci. Technol. **1993**, *27*, 283–291.
[19] Alshawabkeh, A.N.; Acar, Y.B. Removal of contaminants from soils by electrokinetics: A theoretical treatise. J. Environ. Sci. Health Pt. A **1992**, *27*, 1835–1861.
[20] Alshawabkeh, A.N.; Acar, Y.B. Electrokinetic remediation .2. Theoretical model. J. Geotech. Eng.-ASCE **1996**, *122*, 186–196.
[21] Jacobs, R.A.; Sengun, M.Z.; Hicks, R.E.; Probstein, R.F. Model and experiments on soil remediation by electric fields. J. Environ. Sci. Health A **1994**, *29*, 1933–1955.

[22] Paz-García, J.M.; Johannesson, B.; Ottosen, L.M.; Ribeiro, A.B.; Rodríguez-Maroto, J.M. Modeling of electrokinetic processes by finite element integration of the Nernst-Planck-Poisson system of equations. Sep. Purif. Technol. **2011**, *79*, 183–192.
[23] Haran, B.S.; Popov, B.N.; Zheng, G.; White, R.E. Mathematical modeling of hexavalent chromium decontamination from low surface charged soils. J. Hazard. Mater. **1997**, *55*, 93–107.
[24] Jacobs, R.A.; Probstein, R.F. Two dimensional modeling of electroremediation. AIChE J. **1996**, *42*, 1685–1696.
[25] Acar, Y.B.; Alshawabkeh, A.N.; Gale, R.J. Fundamental aspects of electrokinetic remediation of soils. Waste Manag. **1993**, *13*, 513.
[26] Kirkner, D.; Jennings, A.; Theis, T. Multisolute mass transport with chemical interaction kinetics. J. Hydrol. **1985**, *76*, 107–117.
[27] Jennings, A.A.; Kirkner, D.J.; Theis, T.L. Multicomponent equilibrium chemistry in groundwater quality models. Water Resour. Res. **1982**, *18*, 1089–1096.
[28] Kirkner, D.J.; Theis, T.L.; Jennings, A.A. Multicomponent solute transport with sorption and soluble complexation. Adv. Water Resour. **1984**, *7*, 120–125.
[29] Lewis, F.M.; Voss, C.I.; Rubin, J. Solute transport with equilibrium aqueous complexation and either sorption or ion exchange: Simulation methodology and applications. J. Hydrol. **1987**, *90*, 81–115.
[30] Lichtner, P.C. Continuum model for simultaneous chemical reactions and mass transport in hydrothermal systems. Geochem. Cosmochim. Acta **1985**, *49*, 779–800.
[31] Valocchi, A.J.; Street, R.L.; Roberts, P.V. Transport of ion-exchanging solutes in groundwater: Chromatographic theory and field simulation. Water Resour. Res. **1981**, *17*, 1517–1527.
[32] Yeh, G.T.; Tripathi, V.S. A model for simulating transport of reactive multispecies components: model development and demonstration. Water Resour. Res. **1991**, *27*, 3075–3094.
[33] Bard, A.; Faulkner, L. *Electrochemical Methods: Fundamentals and Applications*. John Wiley & Sons, Canada 1980.
[34] Miller, C.; Benson, L. Simulation of solute transport in a chemically reactive heterogeneous system: Model development and application. Water Resour. Res. **1983**, *19*, 381–391.
[35] Steefel, C.I.; Lasaga, A.C. A coupled model for transport of multiple chemical species and kinetic precipitation/dissolution reactions with applications to reactive flow in single phase hydrothermal systems. Am. J. Sci. **1994**, *294*, 529–592.
[36] Rubin, J. Transport of reacting solutes in porous media: Relation between mathematical nature of problem formulation and chemical nature of reactions. Water Resour. Res. **1983**, *19*, 1231–1252.
[37] Yeh, G.; Tripathi, V. A critical evaluation of recent developments in hydrogeochemical transport models of reactive multichemical components. Water Resour. Res. **1989**, *25*, 93–108.

Paper

"Modeling of Electrokinetic Desalination of Bricks"

J.M. Paz-García, B. Johannesson, L.M. Ottosen, A.N. Alshawabkeh, A.B. Ribeiro and J.M. Rodríguez-Maroto

Published in: *Electrochimica Acta, 2012*

G Model
EA-18833; No. of Pages 10
ARTICLE IN PRESS

Electrochimica Acta xxx (2012) xxx–xxx

Contents lists available at SciVerse ScienceDirect

Electrochimica Acta

journal homepage: www.elsevier.com/locate/electacta

Modeling of electrokinetic desalination of bricks

Juan Manuel Paz-García[a,*], Björn Johannesson[a], Lisbeth M. Ottosen[a], Akram N. Alshawabkeh[b], Alexandra B. Ribeiro[c], José Miguel Rodríguez-Maroto[d]

[a] Department of Civil Engineering, Technical University of Denmark, Kgs. Lyngby, Denmark
[b] Department of Civil and Environmental Engineering, Northeastern University, Boston, MA, USA
[c] Department of Environmental Sciences and Engineering, Faculty of Sciences and Technology, New University of Lisbon, Campus de Caparica, Caparica, Portugal
[d] Department of Chemical Engineering, University of Málaga, Campus de Teatinos, Málaga, Spain

ARTICLE INFO

Article history:
Received 25 October 2011
Received in revised form 24 May 2012
Accepted 25 May 2012
Available online xxx

Keywords:
Nernst–Planck–Poisson system
Electrokinetic desalination
Reactive transport modeling
Chemical equilibrium

ABSTRACT

A model for the reactive transport of matter through porous media induced by an externally applied electric field is discussed. The Nernst–Planck–Poisson system of equations is used for modeling multi-species electro-diffusion transport phenomena, assuming chemical equilibrium during the process. The system of equations includes the transport of water and the resulting advective flow of the aqueous species. The model takes into account transient change in porosity and its impact on transport. Test examples were performed and compared to experimental data for electrokinetic desalination treatment of yellow bricks contaminated with chloride salts.

1. Introduction

Electrokinetic phenomena consist of electrochemically induced transport of matter in porous materials due to application of an external electric DC field [1–5]. A summary of electrokinetic phenomena in different materials and its applications for different engineering disciplines [3] highlights the common physicochemical aspects of these applications. In civil engineering, the main use of the electrokinetics techniques has been the desalination of concrete. Several new applications have been developed, such as the re-impregnation of wood in structures and the removal of salts from masonry in building facades, tiles, sculptures or frescoes. In environmental engineering, electrokinetics techniques are used for the mobilization of pollutants in contaminated matrices (electrokinetic remediation, or EKR). The removal of heavy metals and/or organic contaminants from contaminated soil, sludge, fly ashes and waste wood has been widely investigated [3].

Due to the complex physicochemical interactions during the process, designing an electrokinetic treatment system is a difficult task. Transport of species through porous media is the result of several mechanisms, e.g. see [6]; including diffusion, the mass flux due to concentration gradient; electromigration, the mass flux due to electric potential gradient; and advection, the flow of the solution itself. In electrokinetics, electromigration and electroosmotic advection are assumed to be the primary transport mechanisms of ionic and non-ionic species respectively. However, other mechanisms, including diffusion and hydraulic advection, have an impact and should be included.

Strictly speaking, the term electrokinetics should only be used for the transport mechanisms which have as underlying source the interactions between the electrically charged solid surface and the pore solution, e.g. electroosmosis and electrophoresis. In this work, the term electrokinetics is used in a more general meaning, as the electrochemically induced transport through porous media, i.e. it also includes the electro-diffusion and electroosmotic advection transport mechanisms.

Mobilization of species by electrokinetics is a reactive transport phenomenon, as, during the transport, the chemical species interact with the solid matrix and with the aqueous chemical species in the pore solution, e.g. see [7,8]. When designing electrokinetic treatments, geochemical reactions, such as precipitation/dissolution, sorption/desorption, and complexation or ion exchange should be incorporated in the design and analysis [9–12].

Due to charge-mass transfer at the electrodes, different electrolysis reactions may occur, depending on the species type and concentration in the electrolytes, e.g. see [13]. Water oxidation at the anode (1) and reduction at the cathode (2) are the typical

* Corresponding author. Tel.: +45 4525 5029; fax: +45 4588 3282.
E-mail addresses: jugra@byg.dtu.dk, juanma.paz@me.com (J.M. Paz-García).

0013-4686/$ – see front matter © 2012 Elsevier Ltd. All rights reserved.
http://dx.doi.org/10.1016/j.electacta.2012.05.132

electrolytic reactions if inert electrodes are used. A common competitive reaction is the oxidation of chloride at the anode to produce gaseous chlorine (3):

$$H_2O \rightleftarrows \frac{1}{2}O_2 + 2H^+ + 2e^- \quad (1)$$

$$2H_2O + 2e^- \rightleftarrows H_2 + 2OH^- \quad (2)$$

$$2Cl^- \rightleftarrows Cl_2 + 2e^- \quad (3)$$

Irrespectively of the competitive redox reactions, water oxidation and reduction typically occur and, consequently, significant pH changes are expected. These pH changes play an important role for several reasons [2–4]. Acidic or basic environments, with high concentration of either protons or hydroxides, will result in an inefficient electrical transport process. For such cases, protons and hydroxides will carry most of the ionic current in the system instead of the target contaminants. In addition to this, inappropriate pH conditions may produce undesirable effects on the material being treated. For example, in electrokinetic desalination treatments of calcite-based building materials (marble, stone or bricks), the acid front induced by the anode reaction can produce serious damage in the solid matrix [13].

Furthermore, the pH of the pore solution affects to the speciation and the chemical stability of the solids. The target contaminants need to be in a soluble state in order to be mobilized by electromigration and/or electroosmosis. For instance, heavy metals form insoluble hydroxides in alkaline conditions [7–15]. The basic front generated at the cathode may induce the precipitation of the heavy metals, limiting the efficiency of the technique [16].

Enhanced methods have been proposed to improve the effectiveness, in terms of increasing the removal rate and reducing the energy consumption [12,17]. Enhanced techniques aim to increase the mobility of the target species by producing changes in its speciation state. Common enhanced techniques target controlling the formation of acidic and basic fronts generated by electrolysis. For example, the use of buffer substances, conjugate acids or bases, or ion-selective membranes have been investigated [10–17]. Other enhanced techniques combine the control of the pH with the use of specific extracting agents, which are added to the system to change the contaminant speciation state increasing its solubility [10]. This technique not only increases the effectiveness of the process, but also allows selective extraction of target contaminants while avoiding undesirable effects on the treated solids.

These studies reveal that the effectiveness of electrokinetic treatment depends more on the geochemical changes and interactions in the pore solution than on the external applied current or the transport process itself [4–19]. Therefore, the specific geochemical reactions must be incorporated when modeling electrokinetic desalination treatments.

For a complete understanding of the different processes taking place in any electrokinetic treatment, it is essential to study the physicochemical fundamentals that govern the process and to suggest mathematical models that describe them. The model solution, by means of computer-aided numerical methods, allows the corroboration of the assumptions and, eventually, the elaboration of some prediction tools for optimizing the different enhanced techniques and increasing the efficiency of treatments. Different approaches have been proposed for modeling of electrochemically induced transport of matter through porous media. The theoretical background has been widely described [1–6,8,20]. Based on the assumption that the electromigration is the main transport mechanism, some practical models have been proposed [7,21,22]. The detailed system of equation accounting for different transport terms has also been solved by different numerical strategies such as finite differences [23] or finite elements methods [14,24]. The advective transport is typically included in an explicit manner, but some authors have achieved the coupling between ion and moisture transport [25,26].

The Nernst–Planck–Poisson (NPP) system of equation is used to describe multi-species electro-diffusion transport in porous media. The NPP system can be used for modeling ionic and non-ionic transport in many different contexts, e.g. see: [27,28]. In macro-scale models, the Nernst–Planck–Poisson equation may be simplified with the electro-neutrality condition [29–31]. Models including the chemical effects in the electrochemically induced transport are rare, but some models have been discussed in the literature, highlighting the importance of the chemical effects in the migration rate of the target contaminants [9,23,32–34].

In the present work, a generalized model for electrokinetic reactive transport phenomena is presented, based on the strongly coupled NPP system of differential equations under the assumption of chemical equilibrium. The model is a continuation of the work described in [14] coupled with a model for chemical equilibrium calculation and extended in order to incorporate the transport of water through the porous material and the resulting advective flow of aqueous species. The reactive transport model is used to simulate the desalination of brick pieces contaminated with chloride salts, using a buffer substance enhanced technique. Results from simulations are compared with the laboratory experiments reported by Ottosen and Rödig-Dalgaard [13].

2. The model

In general, kinetic rates of aqueous reversible reactions are several orders of magnitude faster than the electromigration transport rates. Detailed models describing the reactive transport process accounting for the kinetic rates of the chemical reactions in the continuity equations in an explicit manner are extremely difficult to solve, even using the most sophisticated numerical strategies [31,33–35]. Accordingly, the reactive transport has been modeled considering the chemical equilibrium condition during the transport process.

The model for the reactive transport presented here consists of two coupled modules: one for the transport process and another one for computing chemical equilibrium. In this section, first the modeled system is described. Subsequently, the transport and the chemical modules are described separately.

2.1. Modeled system

The modeled system is based on the buffer-substance enhanced electrodesalination treatment presented and analyzed in [13], where half pieces of yellow brick samples (11.4 cm × 10.8 cm × 5.4 cm) were subjected to a constant current of 10 mA during 9 days. The yellow color was related to a high content of calcium carbonate in the raw material used for the production of the brick samples. The air-dried brick pieces were soaked in NaCl 0.26 M or KCl 0.25 M solution during 4 days prior the treatment.

Fig. 1 shows a schematic representation of the experimental setup. Two cylindrical polymethyl methacrylate electrode compartments, with an internal diameter of 8.0 cm and a length of 5.0 cm were placed at each end of the brick sample and filled with natural clay rich in $CaCO_3$ (about 17% by total mass). The buffer capacity of $CaCO_3$ is expected to neutralize the acid front developed at the anode. The calcite system is also supposed to slow down the alkaline front at the cathode due to precipitation of $Ca(OH)_2$.

Table 1 shows the solid composition of the brick and the buffering clay assumed for the simulations to match the initial measured concentration and porosity in the experiments in [13]. The buffering clay filling the electrode compartments in the experiments was

Please cite this article in press as: J.M. Paz-García, et al., Modeling of electrokinetic desalination of bricks, Electrochim. Acta (2012), http://dx.doi.org/10.1016/j.electacta.2012.05.132

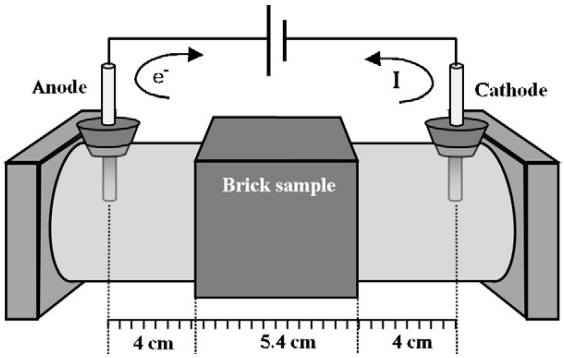

Fig. 1. Schematic representation of the experimental setup for electrodesalination of bricks using buffer clay.

from the same raw material used in the production of the investigated bricks. For the sake of simplicity, in the simulations the carbonated clay and the bricks are considered composed from a combination of SiO_2 (quartz) and $CaCO_3$ (calcite) in different proportions and the quartz is assumed chemically inert.

Similar to [13], two different contaminated brick samples are studied denoted in the simulations as Brick 1 (contaminated with KCl) and Brick 2 (contaminated with NaCl). The clay is considered to have a certain initial amount of salt, in order to assure enough conductivity in the system.

Table 2 shows the chosen set of chemical reactions taking place in the process. The equilibrium constants for the given stoichiometry were obtained from [36] and the diffusivities from [37]. Diffusivity values for those species not found in the consulted databases were given an arbitrary value equal to the component with the lower diffusivity and divided by the number of ions in the molecule.

2.2. Transport process

The Nernst–Planck–Poisson system of equations is used to describe multi-species electro-diffusion transport in porous media [14,38–40].

2.2.1. Nernst–Planck equation

The Nernst–Planck conservation of mass equation is used to describe the motion of chemical species in a fluid medium. It accounts for diffusion, electromigration and advection.

$$Awp\left(\frac{\partial c_i}{\partial t} = -\nabla \mathbf{J}_i + G_i\right); \quad \mathbf{J}_i = \underbrace{\mathbf{v}_w c_i}_{\text{advection}} \underbrace{- D_i^{eff}\nabla c_i}_{\text{diffusion}} \underbrace{- U_i^{eff} c_i \nabla\phi}_{\text{electromigration}} \tag{4}$$

where $A\,(m^2)$ is the cross sectional area, $w\,(kg_w\,m^{-3}_{pore})$ is the moisture content, i.e. the amount of water filling the pore volume, p (dimensionless) is the porosity, $c_i\,(mol_i\,kg_w^{-1})$ is the molal concentration of the ith aqueous species, $\mathbf{J}_i\,(mol_i\,m^{-2}\,s^{-1})$ and $G_i\,(mol_i\,m^{-3}\,s^{-1})$ are respectively the flux and the generation (chemical reaction) terms, $\mathbf{v}_w\,(m^2\,s^{-1})$ is the velocity of the pore solution phase, $D_i^{eff}\,(m^2\,s^{-1})$ is the effective diffusion coefficient, $U_i^{eff}\,(m^2\,V^{-1}\,s^{-1})$ is the effective ionic mobility coefficient and $\phi\,(V)$ is the electrical potential. A, w and p are introduced in the equation in order to consider the macro scale description of the process.

Table 1
Initial solid matrix composition and porosity for the electrokinetic desalination simulations.

Mineral	Brick 1	Brick 2	Carbonated clay	Units
Quartz, SiO_2	30,000	30,000	15,000	mol m^{-3}
Calcite, $CaCO_3$	500	500	3000	mol m^{-3}
Sylvite, KCl	50	0	10	mol m^{-3}
Halite, NaCl	0	44	10	mol m^{-3}
Initial porosity	0.299	0.299	0.549	mol m^{-3}

Table 2
Set of chemical species and reversible reactions for the electrokinetic desalination system. Species are sub-divided in master species, aqueous secondary species and solid secondary species. Equilibrium constants at room temperature for the given stoichiometry and diffusion coefficients in pure water are included.

	H_2O	H^+	Ca^{2+}	CO_2^{2-}	K^+	Na^+	Cl^-	$\log_{10}(K_{eq})$	$D_i \times 10^9$
H_2O	1	0	0	0	0	0	0	–	–
H^+	0	1	0	0	0	0	0	–	9.311
Ca^{2+}	0	0	1	0	0	0	0	–	1.584
CO_2^{2-}	0	0	0	1	0	0	0	–	1.846
K^+	0	0	0	0	1	0	0	–	1.957
Na^+	0	0	0	0	0	1	0	–	1.334
Cl^-	0	0	0	0	0	0	1	–	2.032
OH^-	1	−1	0	0	0	0	0	14.00	5.273
$CaCO_3$	0	0	1	1	0	0	0	−3.22	0.792
HCO_3^-	0	1	0	1	0	0	0	−10.33	1.185
CO_2	−1	2	0	1	0	0	0	−16.68	0.593
$CaHCO_3^+$	0	1	1	1	0	0	0	−11.43	0.593
$CaOH^+$	1	−1	1	0	0	0	0	12.78	0.792
$CaCl^+$	0	0	1	0	0	0	1	0.29	0.792
$NaCO_3^-$	0	0	0	1	0	1	0	−1.27	0.667
$NaHCO_3$	0	1	0	1	0	1	0	−10.08	0.593
KCl	0	0	0	0	1	0	1	0.50	0.979
NaCl	0	0	0	0	0	1	1	0.50	0.667
KOH	1	−1	0	0	1	0	0	14.46	0.979
Na(OH)	1	−1	0	0	0	1	0	14.75	0.667
$CaCO_3$ (s)	0	0	1	1	0	0	0	−8.48	–
$Ca(OH)_2$ (s)	2	−2	1	0	0	0	0	22.81	–
KOH (s)	1	−1	0	0	1	0	0	24.6	–
NaCl (s)	0	0	0	0	0	1	1	1.59	–
KCl (s)	0	0	0	0	1	0	1	0.87	–

2.2.2. Water transport equation

The NPP system is extended to include the transport of water along the porous structure and the corresponding advective transport of aqueous species. As mentioned before, the moisture content, $w\,(kg_w\,m^{-3}_{pore})$, is used as the state variable to describe water. Water transport through the porous media is assumed to be the result of two main mechanisms: moisture transport and electroosmosis. The conservation of mass and the constitutive equation for the mass flow of water are described as:

$$Ap\left(\frac{\partial w}{\partial t} = -\nabla \mathbf{J}_w + G_w\right); \quad \mathbf{J}_w = \underbrace{-D_w\nabla w}_{\text{moisture transport}} \underbrace{-k_e w\nabla\phi}_{\text{electroomosis}} \tag{5}$$

where $\mathbf{J}_w\,(kg\ m^{-2}\,s^{-1})$ and $G_w\,(kg\ m^{-3}\,s^{-1})$ are, respectively, the water flow and generation (chemical reaction) terms, $D_w\,(m^2\,s^{-1})$ is the moisture diffusivity coefficient in the solid matrix and $k_e\,(m^2\,V^{-1}\,s^{-1})$ is the electroosmotic permeability coefficient.

In the experimental treatment no hydraulic pressure was applied. The electrode reactions have a net flux of oxygen and hydrogen that are freely released out of the system, reducing the overall water content. Consequently, unsaturated conditions are expected. Thus in the present model transport due to pressure gradients is neglected. The first term of $\mathbf{J}_w$ in Eq. (5) represents the transport of water due to the gradient of moisture content. This term describes the total moisture transport in unsaturated porous media for both vapor and liquid phases as a combination of diffusion, viscous saturated flow and capillary forces, assuming isothermal conditions. This constitutive equation is sometimes named as Richards' equation; an extension of the Darcy's law applied for unsaturated porous media [39–45].

Please cite this article in press as: J.M. Paz-García, et al., Modeling of electrokinetic desalination of bricks, Electrochim. Acta (2012), http://dx.doi.org/10.1016/j.electacta.2012.05.132

Table 3
Parameters used for the characterization of the porous media in the simulations.

Parameter	Brick	Clay	Units
k'_e	1×10^{-8}	1×10^{-9}	$m^2\ s^{-1}\ V^{-1}$
$\tau_{cations}$	1.3	1.4	–
τ_{anions}	1.2	1.1	–
$D_{w,0}$	2×10^{-7}	5×10^{-7}	$m^2\ s^{-1}$

The second term of $\mathbf{J}_w$ in Eq. (5) accounts for the electroosmotic transport; i.e. the transport of water through the porous material due to the electromigration of the diffuse layer in the vicinities of the solid surface [20]. Most soils and construction materials develop negative surface charge in its pore structure balanced by a positively charged diffuse layer. Thus, the electroosmotic flow uses to be from the anode toward the cathode [8]. Consequently, in electrokinetic treatments, the transport of water by electroosmosis usually dries the material at the surroundings of the anode. This drying behavior may interrupt the ionic current and ultimately stop the process completely. Furthermore, in absence of hydraulic flow, electroosmotic advection is of major importance when considering the transport of non-charged particles such as organic contaminants in soils.

Due to the surface action, the electroosmotic flow is more significant in narrow pores. The coefficient of electroosmotic permeability has been demonstrated to be proportional to zeta potential, $\zeta(V)$, which is the electrical potential at the junction between the fixed and mobile parts of the electrical double layer. The electroosmotic velocity of a fluid of certain viscosity and dielectric constant through a surface charged porous medium subjected to an electric gradient is given by the Helmholtz–Smoluchowski (H–S) equation [20],

$$k_e = \frac{p\varepsilon}{\mu}\zeta \tag{6}$$

where $\mu\,(N\,s\,m^{-2})$ is the viscosity of the pore fluid, $\varepsilon\,(C\,V^{-1}\,m^{-1})$ is the permittivity in water. The magnitude and sign of ζ depends on the pore fluid chemistry, being strongly influenced by the pH. However, the coefficient of electroosmotic permeability varies only within one order of magnitude between 10^{-9} and $10^{-8}\,(m^2\,V^{-1}\,s^{-1})$ [6].

In the modeled system, the buffering substance maintains the pH in the range of neutral to alkaline. Thus, no reverse osmosis is expected and changes in the ζ potential are expected to be small. For the sake of simplicity, in this study a constant ζ potential is assumed, and the electroosmotic permeability is calculated from $k_e = pk'_e$ being $k'_e = \varepsilon\zeta/\mu$ a constant. Chosen k'_e values for the brick and the clay are listed in Table 3.

2.2.3. Extended Nernst–Planck equation

From the constitutive equation for $\boldsymbol{J}_w$, the velocity of the water can be expressed as:

$$\mathbf{v}_w = -(w^{-1}D_w\nabla w + k_e\nabla\phi) \tag{7}$$

As a result, Eq. (7) can be included in the advective term of the flux vector, as:

$$\mathbf{J}_i = -\left(\overbrace{\underbrace{c_i w^{-1}D_w\nabla w}_{\text{moisture transport}} + \underbrace{k_e c_i\nabla\phi}_{\text{electroomosis}}}^{\text{advection}} + \underbrace{D_i^{eff}\nabla c_i}_{\text{diffusion}} + \underbrace{U_i^{eff}c_i\nabla\phi}_{\text{electromigration}}\right) \tag{8}$$

Effective diffusion coefficients for the aqueous species are estimated from the corresponding diffusivity at infinite solution (in pure water), the porosity, the volumetric moisture content $\theta\,(m^3\,m^{-3})$ and a fitting parameter τ (dimensionless) which gathers the effect of the anisotropy of the porous media, i.e. the tortuosity and the constrictivity [46,47].

$$D_i^{eff} = \theta\frac{p}{\tau}D_i \tag{9}$$

Hydrodynamic dispersive transport, accounting for the differences in flow velocities at the pore scale due to different pore sizes and shapes, has been neglected in this work, as done in most electrokinetic theoretical models [1–6]. Electroosmosis and moisture transport terms counteract each other. Consequently, the velocity of water can be assumed slow enough and the effect of the hydraulic dispersion can be neglected. On the contrary, the ionic mobility coefficient is related to the diffusion coefficient by the Nernst–Townsend–Einstein equation:

$$U_i^{eff} = \frac{D_i^{eff}Fz_i}{RT} \tag{10}$$

where T is the absolute temperature, R is the universal gas constant, F is the Faraday constant and z_i is the ionic charge.

2.2.4. Poisson equation

The Poisson equation for electrostatics is used to complete the system of equations. The Poisson equation describes the coupling between the concentration and the electrical potential according to:

$$\varepsilon\nabla^2\phi = -F\sum_i c_i z_i \tag{11}$$

The Poisson equation relates the scalar electrical potential field with the free charge density in the ionic solution [20,48]. It is, in fact, the Gauss' law without polarization effects and assuming that the electrical field can be expressed as the gradient of a streaming potential scalar property. The strongly coupled NPP system takes into account the difference between the migration rates of the ions, which are responsible for the so-called diffusion potential [6].

2.3. Chemical reaction

A set of non linear algebraic equations is developed from the mass balance and the action mass equation describing the chemical equilibrium [47,49]. Let $i = 1, 2, \ldots, N$ and $r = 1, 2, \ldots, M$ be, respectively, the indexes for the ith chemical species, the rth secondary species; being N be the total number of species and M the number of chemical equilibrium. The set of species and the stoichiometric coefficients for the modeled system are listed in Table 2.

The variable $n_i\,(mol)$ denotes the amount species in the system. For a set of N chemical species, the M stoichiometric equations that relate them can be defined as a combination of master species by means of stoichiometric equations in the form:

$$\sum_{i=1}^{N} v_{i,r}n_i = 0, \quad r = 1, 2, \ldots, M \tag{12}$$

where $v_{i,r}$ is the stoichiometric coefficient of the ith species in the rth reaction. By definition, each rth secondary species participate only in the rth stoichiometric equation that describes it and its stoichiometric coefficient always $v_r = -1$. In a process in which N chemical species react between each other to reach the chemical equilibrium state, the mass balance equation can be written as a function of the extent of the reaction ξ. The amount of moles at the equilibrium of each species is given by:

$$n_{i,eq.} = n_{i,init.} + \sum_{r=1}^{M}\xi_r v_{i,r}, \quad i = 1, 2, \ldots, N \tag{13}$$

$f_r(\xi)$ is a function on the extent of all equilibrium reactions, and it represents the distance to the equilibrium state as a measure of the

Please cite this article in press as: J.M. Paz-García, et al., Modeling of electrokinetic desalination of bricks, Electrochim. Acta (2012), http://dx.doi.org/10.1016/j.electacta.2012.05.132

Gibbs energy of the chemical system. It is obtained from the mass action expression of each reaction:

$$\prod_{i=1} a_i^{v_{i,r}} - K_{\mathrm{eq},r} = f_r(\xi), \quad r = 1, 2, \ldots, M \tag{14}$$

where $K_{\mathrm{eq},r}$ is the equilibrium constant for the rth reaction and a_i (dimensionless) is the chemical activity. The activity is defined from the molal concentration c_i (mol kg^{-1}) and the activity factor γ_i; being the latter obtained from the Davies and the Setschenow equations for ionic and non-ionic species respectively [35,36]. Activities for the solvent and the solid species are set to a fixed value of 1. Heterogeneous precipitation/dissolution reactions are also included in the model. The equilibrium reactions for the solid species are only included in the set of chemical reactions when the saturation index predicts the existence of the precipitated phase.

Using logarithms, each mass action equations are expressed as:

$$\sum_{i=1} v_{i,r} \log(\gamma_i c_i) - K_{\mathrm{eq},r} = f_r(\xi), \quad r = 1, 2, \ldots, M \tag{15}$$

The M equilibrium equations are coupled in a matrix system of equations and solved by means of a Newton–Raphson method for non-linear matrix systems. Stoichiometric equations are consistent with the mass and charge conservation principles. As a result, using the extents of each reaction as independent variables, the electrical balance of the solution is not modified during the speciation process. This feature makes the presented algorithm suitable for problems in which a thorough control of the electrical balance is required, such as the case of strongly coupled transport model described in this work. Furthermore, a line-search approach is used in the Newton–Raphson method to assure the convergence and, at the same time, deal with the non-negative concentration constraints of all the chemical species [50].

The mineral phases are included in order to take into account the reactivity of the matrix. By taking into account the molar mass and the specific gravity of the solid species, the volume fraction of each solid phase can be calculated. The porosity value and the variations due to precipitation and dissolution process during the electrokinetic treatment are monitored. Changes of the porosity along the spatial domain affect significantly the transport process regarding both aqueous species and the water, since the effective transport coefficients are assumed dependent on the porosity of the media in the macro scale description of the process. This effect has been taken into account numerical procedure used.

3. Results and discussion

The electrochemical desalination treatment studied in [13] is focused on the removal of chloride from bricks. The effect of the counter-ion K^+ or Na^+ on the removal of chlorides was discussed there. To evaluate the salt concentration in bricks in relation to hygroscopic moisture content, concentrations were referred to the mass of solid (mg$_i$ kg$_{\mathrm{solid}}^{-1}$), and compared to the Austrian ÖNORM B3355-1 "Dehumidification of masonry – Building diagnostics and planning principles" [51]. In the present work, molal concentrations related to the water phase are used i.e. (mol$_i$ kg$_w^{-1}$), referred as (mol kg^{-1}). Table 3 shows the chosen parameters used to characterize the hydraulic properties of the solid matrix in the simulations. Based on the results from [42] and [52], the moisture diffusivity is assumed given by function of the form $D_w = \theta^2 D_{w,0}$. Constant room temperature is assumed during the process. The tortuosity values are obtained assuming combination of Z-shape and Ω-shape channels, according to the model presented in [38]. A different tortuosity value is used for cations and anions, which indirectly takes into account the effect of the surface charge of the porous structure on the ionic diffusion [14,38].

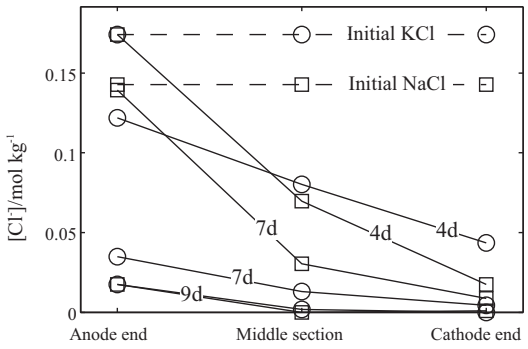

Fig. 2. Chloride concentration profiles in the brick segments after 4, 7 and 9 days from the experimental results reported in [13]. Concentrations are in mol of chloride per kilogram of water. □ KCl ○ NaCl.

3.1. Concentration profiles

Figs. 2 and 3 show, respectively, the results for the chloride concentration profiles in the experimental work and the simulations. Accumulation of chloride in the regions near to the anode is observed. Simulations results show the profiles at the electrode compartments. This information was not shown in the experimental work.

In both cases, "Brick 1" and "Brick 2" the chloride concentration profile is very similar, but the removal of Cl^- when NaCl is supplied to the brick is slightly slower than when KCl is supplied as seen in the experimental results. Comparison between experimental results and those obtained in the simulations shows that the model is capable to predict the general behavior of the electrokinetic desalination treatment. Differences between the two cases may be influenced due to the by the initial concentration of chloride, which is about 15% less in "Brick 2" case than in "Brick 1".

Fig. 4 shows the concentration profile for additional aqueous species in the simulation "Brick 1". The migration of cations toward

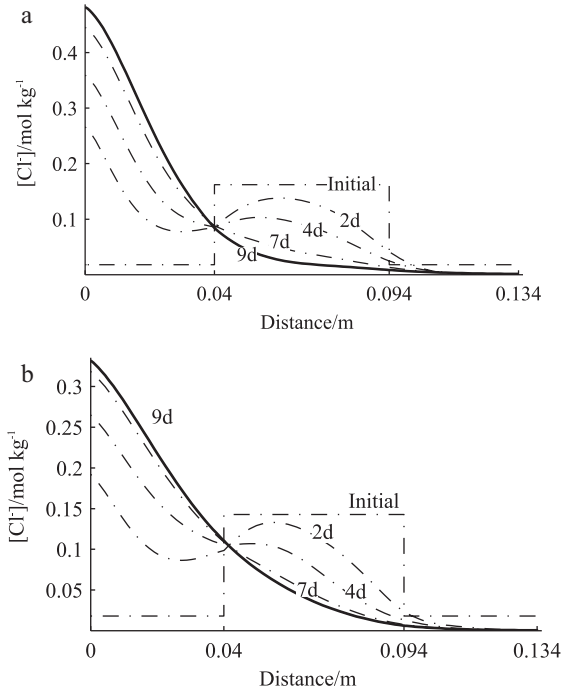

Fig. 3. Chloride concentration profiles in the brick and the electrode compartments obtained in the simulations. (a) "Brick 1" (KCl case). (b) "Brick 2" (NaCl case).

Please cite this article in press as: J.M. Paz-García, et al., Modeling of electrokinetic desalination of bricks, Electrochim. Acta (2012), http://dx.doi.org/10.1016/j.electacta.2012.05.132

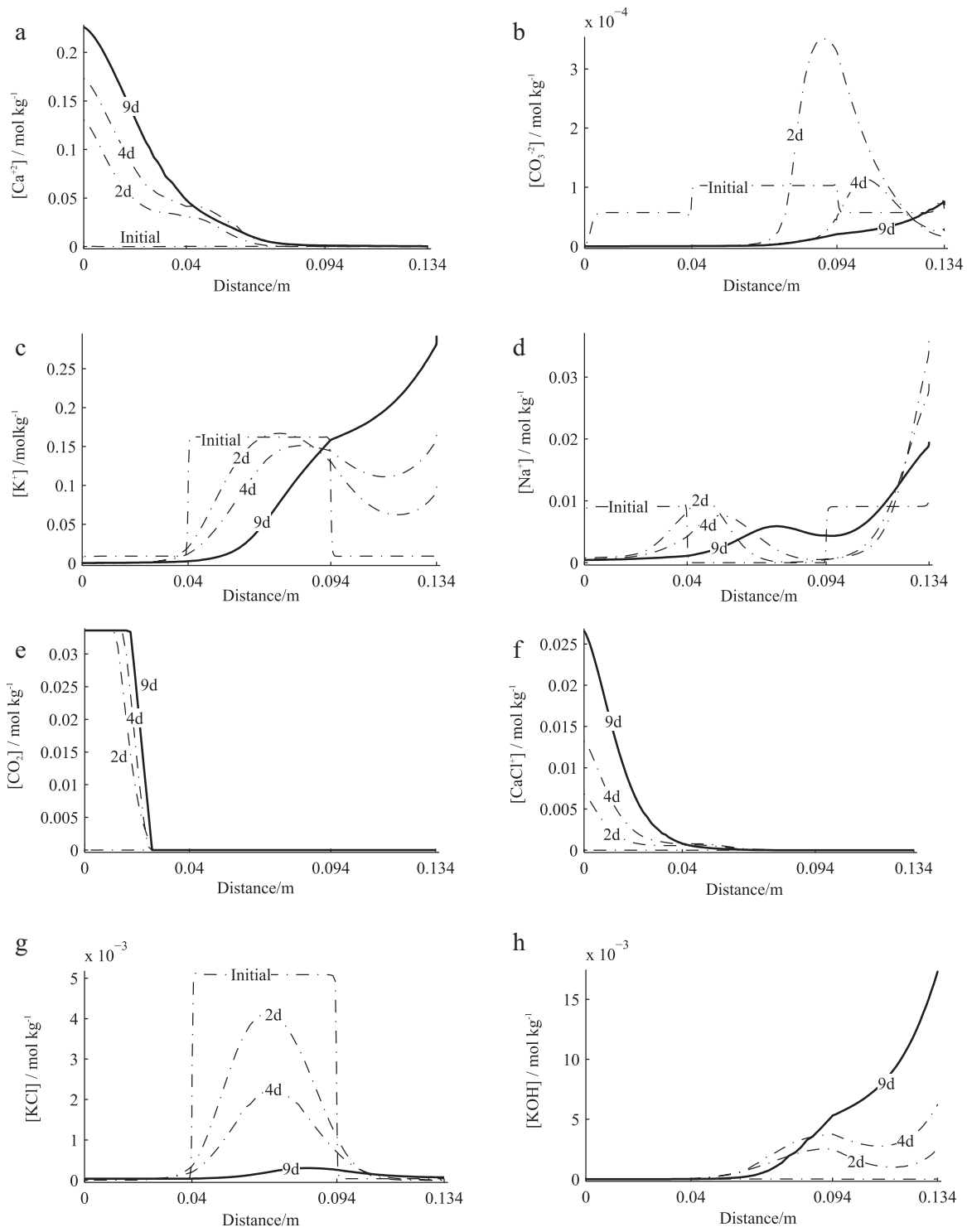

Fig. 4. Concentration profiles for different aqueous species in "Brick 1" case (KCl contaminated brick).

the cathode is clearly observed, e.g. K^+ and Na^+ in Fig. 4c and d. In the case of Ca^{+2}, it is generated in the anode compartment, due to the dissolution of calcite, and it also migrates toward the cathode. The concentration of CO_3^{2-} and CO_2 (aq) is more influenced by the chemical equilibrium than the electrokinetic transport. In the case of CO_2(aq), the saturation limit is reached at the anode end. In this point, formation and release of CO_2(g) bubbles at 1 atm is predicted. Fig. 4f shows that the formed calcium front reacts with the chloride front to form $CaCl^+$, which is a cation instead of an anion and, consequently, migrates toward the cathode retarding the migration rate of chloride. The aqueous species KCl, with high initial concentration in the brick, is removed significantly as a consequence of the migration of its ionic constituents. Slightly higher concentration of this non-ionic species is detected in the cathode compartment as the result of the electroosmotic advective flow.

Please cite this article in press as: J.M. Paz-García, et al., Modeling of electrokinetic desalination of bricks, Electrochim. Acta (2012), http://dx.doi.org/10.1016/j.electacta.2012.05.132

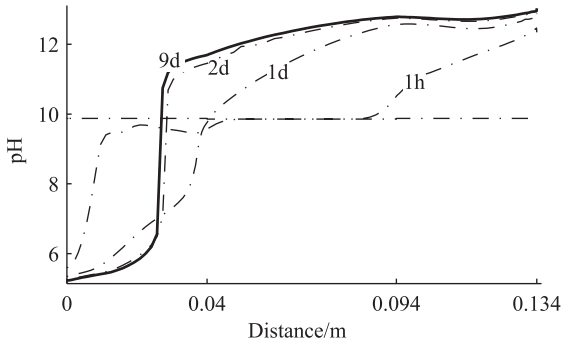

Fig. 5. pH profile in "Brick 1" case (KCl contaminated brick).

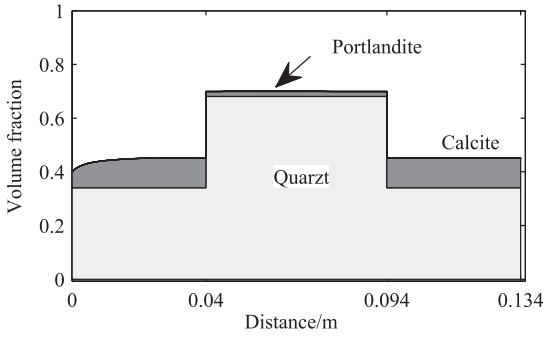

Fig. 6. Volume fraction of solids and void at the end of the desalination treatment (9 days) in "Brick 1" case (KCl contaminated brick).

3.2. pH, solid distribution and porosity

The pH profile for the "Brick 1" case is presented in Fig. 5. Relevant information is obtained from the pH profile of the sample. First, the efficiency of the buffer-substance enhanced desalination technique can be mentioned. Due to the high migration rates of proton and hydroxide, the pH profile in the simulations develops faster than the other aqueous species and reach the steady state in about 2 days. The pH in the anode compartment is buffered until a value of about 5, what means that the calcium carbonate used at the electrode compartments is able to buffer the acid front generated in the anode reaction (Figs. 6 and 7).

The alkaline front is not significantly affected by the buffer capacity of the system and severe alkaline conditions are obtained in the brick. In the experimental work, the pH measured in the brick was around 10, with a tendency to be comparable higher at the cathode end. In the simulations the same tendency is observed, but with a value of about 12. Authors consider that the differences

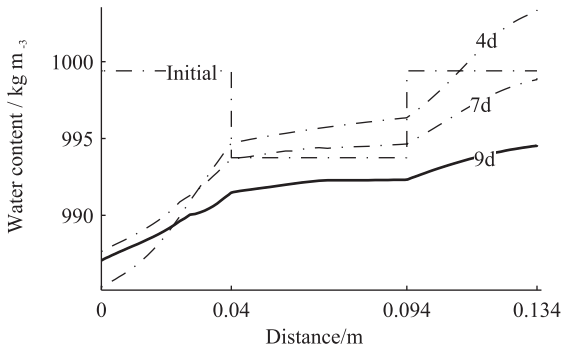

Fig. 7. Water profile in "Brick 1" case (KCl contaminated brick).

may be due to two reasons. First, the analytical method for measuring the pH in [13] may induce some dilution factors not taken into account in the presented results. Secondly, the reactivity of the assumed inert matrix can have some impact in the equilibrium condition.

A pH boundary section is formed in the anode compartment where the acid and basic fronts meet each other producing water. Sharp concentration gradients of protons and hydroxides are observed in this section. Despite the electromigration transport is the main mechanism responsible of the electrokinetic transport of ions, in this case the diffusion transport mechanism is considered to become competitive or predominant with respect to the electromigration transport.

In the simulation results presented here, the matrix is assumed to be form by chemically inert quartz material. As mentioned before, the calcite in the anode compartment dissolves due to the progress of the electrochemical reaction leading to porosity changes in that region.

Despite small amount of KOH and $Ca(OH)_2$ is predicted at the cathode compartment, the predicted production of hydroxides is not significant. The volume fraction of $Ca(OH)_2$ at the end of the simulation at the middle of the brick sample is about 5×10^{-5} and it is mainly the result of the interaction of the alkaline front meeting the calcium front originated in the dissolution of the calcite at the anode. In the experimental results, these species were not analyzed.

3.3. Water content

Results from simulations show smooth water profiles with slightly higher water content at the cathode compartment. According to the electrochemical reactions, Eqs. (1) and (2), the consumption of water at the vicinities of the cathodic electrode is double than in the anode under constant current conditions, but electroosmotic flow drives water from anode to cathode. The moisture transport term, counteract the electroosmotic transport to keep constant moisture content along the domain.

The total water content decreases with the time, as the electrode processes release gases. But the overall decrease of water content at the end of the simulation the simulation is lower than 1%. In the cathode compartment, illogical water content higher than 1000 ($kg\,m^{-3}$) is predicted. This value is temporally accepted in the model since it is auto regulated by the moisture diffusivity expression. Furthermore, in the experimental work, some leaking was observed at the cathode compartment.

3.4. Potential drop between electrodes

The total potential shown in Fig. 8a is the sum of the voltage drop due to the electrical resistance of the pore solution, and the voltage drop associated to the electrochemical reactions. For the redox potential, the Nernst equation is used assuming that the gas generated in the electrochemical reactions has a partial pressure equal to 1 atm and neglecting polarization effects [14,18].

The initial potential is about 5 V in both the experimental results and the simulations. In the simulations, the total electric potential over the sample decreases until stabilization in a value of 2 V. In the experimental results, also an initial decrease was observed at the first hours of the treatment, probably due to an increase of the conductivity due to the electrode reactions. Due to the production of protons and hydroxides in the electrochemical reactions, the conductivity increase in both compartments and the electrical resistance decreases rapidly.

In the long term, the potential calculated in the simulation underestimates that obtained experimentally. In the experimental results, an increase in the voltage drop is observed after 4 days of treatment, not observed in the simulation. This potential increase

Please cite this article in press as: J.M. Paz-García, et al., Modeling of electrokinetic desalination of bricks, Electrochim. Acta (2012), http://dx.doi.org/10.1016/j.electacta.2012.05.132

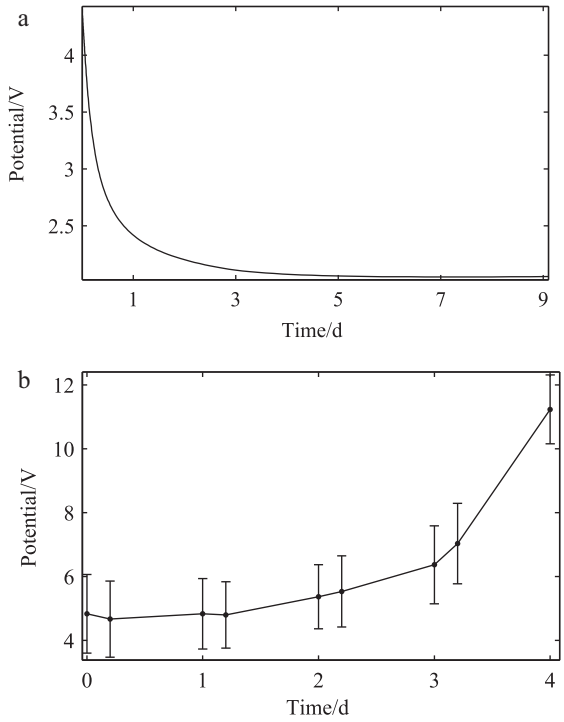

Fig. 8. (a) Total electrical potential between electrodes in "Brick 1" case (KCl contaminated brick). (b) Electrical potential between electrodes from the experimental results. Three replicates, KCl case, constant current 10 mA.

may be explained by two different phenomena: The clean-up process and the polarization effects. In the first case, the process reduces the concentration of salts in the brick, and therefore the conductivity decreases and the voltage increase. In the simulations, the pH obtained in the alkaline zone is high enough to induce high conductivity levels during the whole process, except for domains where the basic and acid fronts collide. In this short section, the solution becomes neutral, with low conductivity and the resistance increases. If the system is considered as an electrical circuit working in series and by observing that the current is constant at all spatial positions, a section with low conductivity will introduce an increase in the voltage according to the Ohm's law. In the experimental work, the duration of the experiments was 9 days because at that moment the voltage reached a value of 136 V, the maximum accepted by the power supply. Conductivity measurements showed a clear relationship between the conductivity of the pore water and the chloride concentration.

The second aspect affecting the voltage variation in time is may be related to the polarization, taking place at the surface of the electrodes. The electrochemical reactions creates bubbles of oxygen and hydrogen, and possibly other compounds such as $Cl_2(g)$ or $CO_2(g)$. The electrode compartments in the experiments where sealed with stoppers resulting in that the gas was not allow to be release freely. Formed gases may reduce the effective surface of the electrodes in contact with the solution, and increase the voltage drop.

Polarization effects are not included in the model. Additionally, in the simulations we obtain a pH value of 12, while the pH of the experiments was about 10. So, the conductivity in the simulations is always high enough to maintain the ionic current.

4. Conclusions

A model for the reactive transport of matter through porous media induced by an externally applied electric field was presented. The NPP system of equations was used for the multi-species electro-diffusion reactive transport phenomena modeled assuming chemical equilibrium during the process. The system of equations includes the transport of water, and the resulting advective flow of the aqueous species. Porosity changes are calculated during the process.

Two test examples were performed and compared to existing experimental data for electrokinetic desalination treatment of yellow construction bricks contaminated with chloride salts. Results from simulations satisfactory match with results obtained experimentally, validating the assumptions of the model. Additionally, simulations threw some light on the phenomenological behavior of the process and suggested some enhancements for the experimental technique. In this context, authors suggest that some polarization effects can be minimized by the use of non-sealed electrode compartments.

Differences between the simulations and the experimental results can be explained by different reasons, which affect both the experimental treatment and the model assumptions. First, analyses for measuring the chloride concentration are destructive. Thus, different bricks were used and the experiment was stopped and analyzed at different exposure times. Bricks used in the experimental work are originated from a non-homogeneous natural material and differences are expected between them. The analyses used in the experimental work are destructive, and so the profiles shown for 4, 7 and 9 days correspond to different samples.

The analysis of pH, conductivity and chloride concentration carried out in the experiments consist of the dilution of 5 g of dried powder of material, placed in equilibrium with 12.5 mL of distilled water. Consequently, some dilution factor can have been induced and results may differ from those obtained in the simulations. Additionally, the accumulation of gases at the electrode compartments may cause an increase of the voltage between electrodes, due to polarization effects, as well as some hydraulic flow, due to an increase of the pressure in the media. This feature has not been included in the model, where polarization effects at the electrodes were neglected, and gases are assumed freely released.

Extra reactivity of the solid matrix may be included. Silicic acid, gibbsite or aluminum hydroxides, between others, will be present in a very low concentration, but they can have some effect of the chemical equilibrium condition. Modeling of low concentration species is a challenging task for chemical equilibrium and transport models. Eventually, parameters in Table 3 are arbitrary, obtained from literature for similar materials. Uncertainly is expected from the use of those fitting parameters, and experimental work may be carried out for a better estimation of them.

Acknowledgments

Authors acknowledge The Danish Agency of Science Technology and Innovation. This research was funded as part of the project "Fundamentals of Electrokinetics in In-homogeneous Matrices", with project number 274-08-0386.

Appendix A. Finite element integration of the extended NPP system of equations

A finite element method (FEM) is used for the integration of the strongly coupled differential equations describing the electrokinetic process [14,53–56] (Table A1).

Table A1
Description of the matrices in the global matrix system of equations for the finite element formulation.

Term	Matrix	State variable	Local matrix	k
Moisture transport	$\mathbf{K}^{mt}$	w	$\mathbf{K}_e$	ApD_w
Electroosmosis	$\mathbf{K}^{eo}$	ϕ	$\mathbf{K}_e$	$Awp^2k'_e$
Moisture transport advection	$\mathbf{K}_i^{mta}$	w	$\mathbf{K}_e$	ApD_wc_i
Electroosmotic advection	$\mathbf{K}_i^{eoa}$	ϕ	$\mathbf{K}_e$	$Awp^2k'_ec_i$
Diffusion	$\mathbf{K}_i^{dif}$	c_i	$\mathbf{K}_e$	$Awp^2\tau^{-1}\theta D_i$
Electromigration	$\mathbf{K}_i^{em}$	ϕ	$\mathbf{K}_e$	$Awp^2\tau^{-1}\theta U_i$
Electric potential	$\mathbf{K}_\phi$	ϕ	$\mathbf{K}_e$	ε
Free charge density	$\mathbf{E}_i$	c_i	$\mathbf{C}_e$	Fz_i
Accumulation of water	$\mathbf{C}_w$	$\partial w/\partial t$	$\mathbf{C}_e$	Ap
Accumulation of aqueous species	$\mathbf{C}_i$	$\partial c_i/\partial t$	$\mathbf{C}_e$	Apw

The domain under consideration is divided into a number of finite elements limited by dimensionless nodal points where the state variables are discretized and solved by means of matrix algebra. Let $\mathbf{a}_w$, $\mathbf{a}_i$ and $\mathbf{a}_\phi$ be, respectively, the vectors describing the discrete form of the state variables at the nodal points for the water content, the molal concentration and the electrical potential. The following standard FEM notations are defined:

$$\begin{aligned} w &= \mathbf{N}\,\mathbf{a}_w \quad ; \quad c_i = \mathbf{N}\mathbf{a}_i \quad ; \quad \phi = \mathbf{N}\mathbf{a}_\phi \\ \nabla w &= \mathbf{B}\,\mathbf{a}_w \quad ; \quad \nabla c_i = \mathbf{B}\mathbf{a}_i \quad ; \quad \nabla\phi = \mathbf{B}\mathbf{a}_\phi \end{aligned} \tag{16}$$

where $\mathbf{N} = [1 - x/L_e, x/L_e,]$ is the shape function used in the FEM for interpolate between nodal points, where L_e(m) is the length of the element, $e = 1, 2, \ldots, N_e$ and N_e is the total number of finite elements. In the one-dimensional model presented here, linear piecewise functions are used. Gradients of the shape functions are denoted by the vector $\mathbf{B} = [-1/L_e, 1/L_e]$. A Galerkin method is used for weighting the residuals [55].

$$\begin{aligned} \mathbf{K}_e &= k\int_0^{L_e}(\mathbf{B}^{\mathrm{T}}\mathbf{B})dx = \frac{k}{L_e}\begin{bmatrix} 1 & -1 \\ -1 & 1 \end{bmatrix} \\ \mathbf{C}_e &= k\int_0^{L_e}(\mathbf{N}^{\mathrm{T}}\mathbf{N})dx = \frac{kL_e}{6}\begin{bmatrix} 2 & 1 \\ 1 & 2 \end{bmatrix} \end{aligned} \tag{17}$$

$\mathbf{K}_e$ and $\mathbf{C}_e$ are defined as the conductivity and mass matrices for the eth finite element, while $\mathbf{K}_i$ and $\mathbf{C}_i$ are the corresponding matrices for the eth species defined for the entire domain after assemblage of the local element matrices. The superscript T means the transpose of the vectors and k is a parameter with the value of a property defined for the finite element, such as the transport coefficient. Table A1 summarizes the value of the k parameter in the matrices related to each term.

Using the FEM notation and the matrices defined in Table A1, the discretized weak formulation of the NPP system results in the Eq. (18).

$$\begin{aligned} &\mathbf{C}_w\frac{(\mathbf{a}_w^t - \mathbf{a}_w^{t-\Delta t})}{\Delta t} + \mathbf{K}^{mt}\mathbf{a}_w^t + \mathbf{K}^{eo}\mathbf{a}_\phi^t + \mathbf{f}_w = 0 \\ &\mathbf{C}_i\frac{(\mathbf{a}_i^t - \mathbf{a}_i^{t-\Delta t})}{\Delta t} + \mathbf{K}_i^{mta}\mathbf{a}_w^t + \mathbf{K}_i^{dif}\mathbf{a}_i^t + (\mathbf{K}_i^{eoa} + \mathbf{K}_i^{em})\mathbf{a}_\phi^t + \mathbf{f}_i = 0 \\ &\sum_{i=1}^{N}\mathbf{E}_i\mathbf{a}_i^t + \mathbf{K}_\phi\mathbf{a}_\phi^t + \mathbf{f}_\phi = 0 \end{aligned} \tag{18}$$

In Eq. (18) the superscript $t - \Delta t$ represents the time step before the present time t considered in the numerical integration and N is the number of species included in the model. A truly implicit scheme for the discretization in the time domain is used. $\mathbf{f}_w$, $\mathbf{f}_i$ and $\mathbf{f}_\phi$ include both the load vectors (flux terms at specific nodal points of the domain) and the boundary vectors (reactive terms necessary to define boundary conditions). The electrochemical reactions taking place at the electrodes are implicitly included in the finite element transport method by means of these boundary vector terms.

Non-linearity is solved by means of an iterative numerical procedure [14]. Initially, the k parameter used in the calculation of the non-linear matrices is estimated using the corresponding value of p, D_w, w, θ or n_i from the time step before. Subsequently, matrices are updated with the new values obtained and the procedure is repeated a number of times until minimizing the error, i.e. the iterations are performed until two consecutive profiles solutions are almost similar.

In the system with N aqueous species, a global matrix system of equation is formed from Eq. (18). The matrix expression for the global coupled system of equations is:

$$\mathbf{C}(\mathbf{a}^t - \mathbf{a}^{t-\Delta t}) + \mathbf{K}\,\mathbf{a}^t + \mathbf{f} = 0 \tag{19}$$

where

$$\mathbf{C}(\mathbf{a}^t - \mathbf{a}^{t-\Delta t}) = \frac{1}{\Delta t}\begin{bmatrix} \mathbf{C}_w & 0 & \cdots & \cdots & 0 \\ 0 & \mathbf{C}_1 & \ddots & \ddots & 0 \\ \vdots & \ddots & \ddots & \ddots & \vdots \\ \vdots & \ddots & \ddots & \mathbf{C}_N & 0 \\ 0 & 0 & \cdots & 0 & 0 \end{bmatrix}\begin{bmatrix} \mathbf{a}_w^t - \mathbf{a}_w^{t-\Delta t} \\ \mathbf{a}_1^t - \mathbf{a}_1^{t-\Delta t} \\ \vdots \\ \mathbf{a}_N^t - \mathbf{a}_N^{t-\Delta t} \\ \mathbf{a}_\phi^t - \mathbf{a}_\phi^{t-\Delta t} \end{bmatrix} \tag{20}$$

$$\mathbf{K}\,\mathbf{a}^t = \begin{bmatrix} \mathbf{K}^{mt} & 0 & \cdots & \cdots & \mathbf{K}^{eo} \\ \mathbf{K}_1^{mta} & \mathbf{K}_1^{dif} & 0 & \ddots & (\mathbf{K}_1^{eoa} + \mathbf{K}_1^{em}) \\ \vdots & 0 & \ddots & \ddots & \vdots \\ \mathbf{K}_N^{mta} & \ddots & \ddots & \mathbf{K}_N^{dif} & (\mathbf{K}_N^{eoa} + \mathbf{K}_N^{em}) \\ 0 & \mathbf{E}_1 & \cdots & \mathbf{E}_N & \mathbf{K}_\phi \end{bmatrix}\begin{bmatrix} \mathbf{a}_w^t \\ \mathbf{a}_1^t \\ \vdots \\ \mathbf{a}_N^t \\ \mathbf{a}_\phi^t \end{bmatrix} \tag{21}$$

$$\mathbf{f} = \begin{bmatrix} \mathbf{f}_w \\ \mathbf{f}_1 \\ \vdots \\ \mathbf{f}_N \\ \mathbf{f}_\phi \end{bmatrix} \tag{22}$$

The global conductivity matrix shows how to couple the different transport terms from the continuity equations with the free density and charge balance terms.

References

[1] Y.B. Acar, A.N. Alshawabkeh, Environmental Science and Technology 27 (1993) 2638.

Please cite this article in press as: J.M. Paz-García, et al., Modeling of electrokinetic desalination of bricks, Electrochim. Acta (2012), http://dx.doi.org/10.1016/j.electacta.2012.05.132

[2] Y.B. Acar, R.J. Gale, A.N. Alshawabkeh, R.E. Marks, S. Puppala, M. Bricka, R. Parker, Journal of Hazardous Materials 40 (1995) 117.
[3] L.M. Ottosen, I.V. Christensen, I. Rörid-Dalgård, P.E. Jensen, H.K. Hansen, Journal of Environmental Science and Health, Part A 43 (2008) 795.
[4] F. Garcia-Herruzo, J.M. Rodriguez-Maroto, R.A. Garcia-Delgado, C. Gomez-Lahoz, C. Vereda-Alonso, Ingeniera Quimica (Madrid) 370 (2000) 209.
[5] A.T. Yeung, S. Datla, Canadian Geotechnical Journal 32 (1995) 569.
[6] A.T. Yeung, J.K. Mitchell, Géotechnique 43 (1) (1993) 121.
[7] C. Vereda-Alonso, C. Heras-Lois, C. Gomez-Lahoz, F. Garcia-Herruzo, J.M. Rodriguez-Maroto, Electrochimica Acta 52 (2007) 3366.
[8] A.N. Alshawabkeh, Y.B. Acar, ASCE Journal of Geotechnical Engineering 122 (3) (1996) 186.
[9] J.M. Paz-Garcia, K. Baek, I.D. Alshawabkeh, A.N. Alshawabkeh, Journal of Environmental Science and Health, Part A 47 (2012) 308.
[10] J.D. Subirés-Muñoz, A. García-Rubio, C. Vereda-Alonso, C. Gómez-Lahoz, J.M. Rodríguez-Maroto, F. García-Herruzo, J.M. Paz-García, Separation and Purification Technology 79 (2011) 151.
[11] A.N. Alshawabkeh, S. Puppala, Y.B. Acar, R. Gale, R.M. Bricka, ASCE Geotechnical Special Publications 71 (1997) 532.
[12] F. Garcia-Herruzo, J.M. Rodriguez-Maroto, R.A. Garcia-Delgado, C. Gomez-Lahoz, C. Vereda-Alonso, Ingeniera Quimica (Madrid) 369 (2000) 215.
[13] L.M. Ottosen, I. Rödig-Dalgaard, Materials and Structures 42 (7) (2009) 961.
[14] J.M. Paz-García, B. Johannesson, L.M. Ottosen, A.B. Ribeiro, J.M. Rodríguez-Maroto, Separation and Purification Technology 79 (2011) 183.
[15] M.D. Garcia-Gutierrez, C. Gomez-Lahoz, J.M. Rodriguez-Maroto, C. Vereda-Alonso, F. Garcia-Herruzo, Electrochimica Acta 52 (2007) 3372.
[16] Y.B. Acar, A.N. Alshawabkeh, ASCE, Journal of Geotechnical Engineering 122 (3) (1996) 173.
[17] A.T. Yeung, Y. Gu, Journal of Hazardous Materials 195 (2011) 11.
[18] A.B. Ribeiro, J.M. Rodríguez-Maroto, in: M.N.V. Prasad, K.S. Sajwan, Ravi Naidu (Eds.), Trace Elements in the Environment: Biogeochemistry, Biotechnology and Bioremediation, Taylor & Francis, CRC Press, Florida, 2006, Chapter 18.
[19] J.M. Rodríguez-Maroto, C. Vereda-Alonso, in: K.R. Reddy, C. Cameselle (Eds.), Electrochemical Remediation Technologies for Polluted Soils, Sediments and Groundwater, John Wiley & Sons, Inc., Hoboken, NJ, USA, 2009, Chapter 25.
[20] S. Pamukcu, in: K.R. Reddy, C. Cameselle (Eds.), Electrochemical Remediation Technologies for Polluted Soils, Sediments and Groundwater, John Wiley & Sons, Inc., Hoboken, NJ, USA, 2009, Chapter 2.
[21] C. Vereda-Alonso, J.M. Rodriguez-Maroto, R.A. Garcia-Delgado, C. Gomez-Lahoz, F. Garcia-Herruzo, Chemosphere 54 (2004) 895.
[22] Y.S. Choi, R. Lui, Journal of Hazardous Materials 44 (1995) 61.
[23] A.Z. Al-Hamdan, K.R. Reddy, Journal of Geotechnical and Geoenvironmental Engineering 134 (2008) 91.
[24] L.Y. Li, C.L. Page, Corrosion Science 42 (2000) 2145.
[25] E. Samson, J. Marchand, K.A. Snyder, J.J. Baudoin, Cement and Concrete Research 35 (1) (2005) 142.
[26] A. Revil, N. Linde, A. Cerepi, D. Jougnot, S. Matthäi, S. Finsterle, Journal of Colloid and Interface Science 313 (2007) 315.
[27] B. Lu, M.J. Holst, J.A. McCammon, Y.C. Zhou, Journal of Computational Physics 229 (2010) 6979.
[28] J. Lim, J. Whitcomb, J. Boyd, J. Varghese, Journal of Colloid and Interface Science 305 (2007) 159.
[29] E. Samson, J. Marchand, Journal of Colloid and Interface Science 215 (1999) 1.
[30] O.A. Prado-Rubio, S.B. Jørgensen, G. Jonsson, Journal of Membrane Science 374 (2011) 20.
[31] R.A. Jacobs, R.F. Probstein, AIChE Journal 42 (1996) 1685.
[32] E. Samson, J. Marchand, J.J. Beaudoin, Cement and Concrete Research 30 (2000) 1895–1902.
[33] D.J. Wilson, J.M. Rodriguez-Maroto, C. Gomez-Lahoz, Separation Science and Technology 30 (1995) 3111.
[34] A.B. Ribeiro, J.M. Rodríguez-Maroto, E.P. Mateus, H. Gomes, Chemosphere 59 (2005) 1229.
[35] F.M.M. Morel, J.G. Hering, Principles, Applications of Aquatic Chemistry, Wiley Interscience, New York, 1993.
[36] D.L. Parkhurst, C.A.J. Appelo, U.S. Department of the Interior, Water-Resources Investigations Reports (1999) 99.
[37] P. Vanysek, in: W.M. Haynes (Ed.), CRC Handbook of Chemistry and Physics, Internet version 2012 (92nd Edition), Taylor and Francis, 2012.
[38] A. Mohajeri, G.A. Narsilio, P. Pivonka, D.W. Smith, Computers and Geotechnics 37 (2010) 280.
[39] B. Johannesson, Y. Hosokawa, K. Yamada, Computers & Structures 87 (2009) 39.
[40] B. Johannesson, Computers and Geotechnics 36 (2009) 577.
[41] B. Johannesson, M. Janz, Building and Environment 44 (2009) 1285.
[42] M. Janz, Materials and Structures 35 (247) (2002) 141.
[43] Y. Pachepsky, D. Timlin, W. Rawls, Journal of Hydrology 272 (2003) 3.
[44] S. Roels, J. Carmeliet, H. Hens, Transport in Porous Media 52 (2003) 333.
[45] T.Q. Nguyen, J. Petkovic, P. Dangla, V. Baroghel-Bouny, Construction and Building Materials 22 (2008) 2185.
[46] J. Van Brakel, P.M. Heertjes, International Journal of Heat and Mass Transfer 17 (1974) 1093.
[47] J.B. Rawlings, J.G. Ekerdt, Chemical Reactor Analysis and Design Fundamentals, Nob Hill Publishing, Madison, WI, 2002.
[48] B. Johannesson, Computers and Geotechnics 37 (2010) 667.
[49] C. Bethke, Geochemical and Biogeochemical Reaction Modeling, Cambridge University Press, 2008.
[50] W.H. Press, B.P. Flannery, S.A. Teukolsky, W.T. Vetterling, Numerical Recipes in C: The Art of Scientific Computing, Cambridge University Press, 1992, Chapter 9.
[51] ÖNOR.M.B. 3355-1, Trockenlegung von feuchtem Mauerwerk - Teil 1: Bauwerksdiagnose und Planungsgrundlagen Berlin. ASI Austrian Standards Institute Österreichisches Normungsinstitut (Herausgeber) Deutschland, Bundesrepublik, Beuth Verlag, 2006.
[52] S. Chemkhi, F. Zagrouba, Desalination 185 (2005) 491.
[53] O.C. Zienkiewicz, R.L. Taylor, The Finite Element Method, vol. 2, McGraw-Hill, London, 1989.
[54] K.J. Bathe, M.R. Khoshgoftaar, Journal of Nuclear Engineering and Design 51 (1979) 389.
[55] N.S. Ottosen, H. Petersson, Introduction to the Finite Element Method, Prentice Hall International (UK) Ltd., Hertfordshire, 1992.
[56] N.S. Ottosen, M. Ristinmaa, The Mechanics of Constitutive Modeling, Elsevier Sciences, 2005.

Please cite this article in press as: J.M. Paz-García, et al., Modeling of electrokinetic desalination of bricks, Electrochim. Acta (2012), http://dx.doi.org/10.1016/j.electacta.2012.05.132

Paper

"Modeling of the Formation of Electric Double Layers Including Chemical Reaction Effects"

J.M. Paz-García, B. Johannesson, L.M. Ottosen, A.B. Ribeiro and J.M. Rodríguez-Maroto

Submitted , *2012*

Modeling of the Formation of Electric Double Layers Including Chemical Reaction Effects

J. M. Paz-García[a,*], B. Johannesson[a], L. M. Ottosen[a], A. B. Ribeiro[b], J. M. Rodríguez-Maroto[c]

[a] *Department of Civil Engineering, Technical University of Denmark, Lyngby, Denmark.*
[b] *CENSE-Departamento de Ciências e Engenharia do Ambiente, Faculdade de Ciências e Tecnologia, Universidade Nova de Lisboa, Campus de Caparica, 2829-516 Caparica, Portugal.*
[c] *Departamento de Ingeniería Química, Facultad de Ciencias, Universidad de Málaga, Campus de Teatinos, Málaga, Spain.*

Abstract

A model for the formation of an electric double layer between an electrolyte and a chemically active flat surface is presented. The model consists of a generalized solution of the transient Nernst-Planck-Poisson system of equations for the microscopic reactive-transport of aqueous species until the stationary state. The model works for asymmetric and multi-species electrolytes, it is not limited to any range of surface potentials and it includes chemical effects. Aqueous complexation reactions are modeled assuming instantaneous equilibrium while surface reactions at the interface are modeled taking into account their chemical kinetics. The surface potential is not a fixed constant but a calculated value and it depends on the bulk solution composition and concentration. Numerical simulations are presented, showing positively and negatively charged surfaces obtained as a function of the bulk solution pH.

Keywords: Electric double layer, Gouy-Chapman diffuse layer, Surface complexation, Chemical reaction modeling, Poisson-Nernst-Planck system

1. Introduction

1.1. Description of the electric double layer

The term electric double layer (EDL) refers to the interface between an ionic solution and a charged solid surface. Most solid materials obtain an electrical surface potential when they are brought into contact with an aqueous solution. A typical reason for this surface potential is the ionization of the chemically active surface groups resulting in the accumulation of charge at the solid surface. As a result of the surface potential, a charged region in the electrolyte near the solid surface can be identified, which balances the charge at the solid surface. Both the charged surface and the layer of liquid containing the balancing charges form the so-called electric double layer [1–5].

In general, any macroscopic sample of electrolyte is electrically neutral, i.e. the sum of all the positive charge (from the cations) equals the sum of all the negative charge (from the anions). The electrostatic charges on the solid surface attract the counter-ions and repel the co-ions in the liquid, producing the above mentioned electrical imbalance in a very narrow region at vicinities of the surface. The electric double layer is, therefore, a microscopic phenomenon. It usually ranges from a few nanometers, in high ionic strength electrolytes, to micrometers, in pure water and organic solvents.

Electric double layers are essential in many physic-chemical processes. In EDL-capacitors, the energy is accumulated in the double layer interface [6]. Double-layer forces stabilize colloids to form suspensions and they influence the function of biomolecules [7]. Furthermore, the existence of and EDL is considered the source for the electrokinetic transport phenomena, such as electrophoresis and electroosmosis [8–14].

1.2. EDL and electrokinetic phenomena

The term Electrokinetics is used to defined a number of transport phenomena in porous media that take place, simultaneously to the electro-diffusion process, under the effect of external electric fields. As mention before, the source for the electrokinetic transport is the existence of a EDL in the interface between an electrolyte and the solid surface of the porous structure or the suspended particles. Electrokinetic phenomena includes, among other, electroosmosis and electrophoresis, but it is also related to the streaming and sedimentation potentials.

Electro-diffusion is a term related to the combination of chemical diffusion and ionic migration transport, described by the Nernst-Planck continuity equation, which is used in this work to model the EDL in a microscale approach.

Under the effect of an external electric field, electromigration is considered to be the dominant transport mechanism of ionic species through porous media. In the case of uncharged species and in the absence of pressure gradients

*Corresponding author
Email address: jugra@byg.dtu.dk (J. M. Paz-García)

the main transport mechanism is assumed to be the electroosmotic advection. Electroosmosis is the motion of an electrolyte solution related to a stationary charged surface, induced by an externally applied electric field [15, 16]. It is a phenomenon strongly related to the electric double layer formed at the porous material surface. More specifically, electroosmotic is assumed to be the result of the migration of the electrically unbalanced diffuse layer towards the electrode of opposite charge.

In macroscale models, electroosmotic velocity of the fluid, $\mathbf{u}$ $\left(\mathrm{m\,s^{-1}}\right)$, is typically accepted to be proportional to the gradient of electric potential, $\phi\,(\mathrm{V})$, and the so-called electroosmotic permeability coefficient $K_{e.o.}$ $(\mathrm{m^2\,V^{-1}\,s^{-1}})$, in the form $\mathbf{u} = -K_{\mathrm{e.o.}}\nabla\phi$.

The Helmholtz–Smoluchowski (H-S) model is commonly accepted to relate the electroosmotic permeability with the zeta potential at the surface [17].

$$K_{\mathrm{e.o.}} = \frac{\varepsilon}{\mu}\zeta \tag{1}$$

where p (dimensionless) is the porosity, μ $(\mathrm{N\,s\,m^{-2}})$ is the viscosity of water, ε $(\mathrm{C\,V^{-1}\,m^{-1}})$ is the permittivity of the medium and ζ (V) is the electrokinetic potential (sometimes refereed to as ζ (or zeta) potential). Some corrections for this theory have been presented including the effect of the tortuosity of the media [18]. Experimentally, it was observed that, for most solid materials, the optimal k_e varies in a narrow range of values, within 10^{-9} and 10^{-8} $(\mathrm{m^2\,V^{-1}\,s^{-1}})$ [19, 20]. The electroosmotic flow depends on the electrolyte concentration and pH, as it does the ζ potential. In electrokinetic treatments, the pH value undergoes important changes due to the electrochemical reactions taken place at the electrodes. At a certain pH and pore fluid ionic strength, the surface charge can drop to zero rendering a null zeta potential, typically called the point of zero charge [5, 17, 21].

It is difficult to model the transport phenomena in macroscale electrokinetic treatments accounting for the microscale effects at the solid/liquid interface. There is a need for models coupling these two phenomena. In this context, one of the goals of the present research is to develop a model for the prediction of the surface potential as a function of the pH and concentration of the pore solution electrolyte.

1.3. Mathematical models for the EDL

The earliest model for electric double layers is attributed to Helmholtz, who treated the EDL as a simple capacitor [3, 22]. Helmholtz's model states that there is a single and immobile layer of strongly attached ions immediately next to the charged solid surface. Gouy and Chapman introduced a diffuse model for the EDL. In the Gouy-Chapman (GC) diffuse layer model the electric potential decreases exponentially from the compact layer to the electrically neutral bulk liquid [2, 22]. Ions in the diffuse layer are not compact as they are in the Helmholtz layer and their concentration can be expressed in terms of the concentration

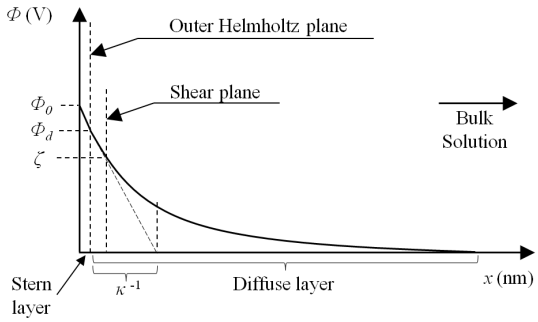

Figure 1: Stern-Gouy-Chapman model for a positively charged surface. κ^{-1} (m) is the Debye length.

of the bulk solution. The thickness of the diffuse layer is dependent on the bulk ionic concentration and composition. An important part of the diffuse layer can move under tangential stresses. The shear plane is characterized by the ζ potential, that can be measured experimentally. In fluid mechanics, the liquid velocity at the shear plane is usually set to be zero and used as a boundary condition [2]. In the case of electrokinetic transport, the electroosmosis is also related to the ζ potential.

The diffuse GC model can be described with relatively simple analytical equations that become exact at a sufficiently large distance from the surface. The Stern's compact layer enhancement is accepted as an improvement of the model, as it deals properly with experimental systems at short distances [3]. Therefore, the combined Stern-Gouy-Chapman (SGC) model is widely used.

Stern stated that modeling chemical species as dimensionless points is not valid at the vicinities of the charged surface. Stern suggested the combination of the Helmholtz and Gouy-Chapman models, defining an internal compact layer between the surface and the diffuse layer. In the Stern layer there is no free charge and the electric potential distribution decrease linearly. Stern's layer (or compact layer) has an assumed thickness approximately equal to the radius of one hydrated ion, typically about 0.5 nm [18, 22].

Stern's model is based on the concept of the specific adsorption and desorption at the surface sites. Different approaches for the Stern layer has been proposed [23]. This compact layer is theoretically divided in a number of plane surfaces. The plane where the specifically adsorbed ions reside is called the inner Helmholtz plane. Ions become specifically adsorbed when short-range interactions between them and the inter-phase become important [24]. The boundary between the compact layer and the diffuse layer is usually referred to as the outer Helmholtz plane (oHp) characterized by the potential ϕ_d (V) (see Fig. 1). Experimentally, it has been obtained that the outer Helmholtz plane and the slip plane are identical or very close. For practical purposes it is often a good

approximation to identify ϕ_d with the measurable ζ potential. Furthermore, the Stern Layer is thin compared to the diffuse layer and the surface potential, ϕ_o (V), can also be estimated from the value of the ζ potential in most cases.

In the classical definition of the GC and SGC model some general assumptions are adopted [2, 3]:

1. The EDL is in the stationary state. Ions have no macroscopic motion.
2. Chemical species, including the solvent, are effectively modeled as point charges.
3. The dielectric permittivity and the viscosity of the fluid are assumed to be constant throughout the double layer region.
4. The only significant interactions in the diffuse layer are due to electrostatic forces. The chemical effects (surface reaction and chemical equilibrium) are not taken into account in the analytical solution.
5. The system is subjected to a homogeneous surface electrical field characterized by the assumed-constant surface potential ϕ_o .

1.4. Scope of the present work

In this work, a Nernst-Planck-Poisson model is proposes for formation of the double layer in the vicinities of a chemically active flat surface. The model presented here is suitable for multi-species and asymmetric electrolytes and it accounts for heterogeneous chemical equilibrium including surface reaction. In this context, items 1, 4 and 5 of the SGC assumptions list are modified. The assumptions and features of the present model are:

1. The time-transient formation of the EDL is studied.
2. Any multi-species asymmetric electrolyte is accepted by the model. It is also not restricted to a maximum value of the surface potential.
3. Chemical species, including the solvent, are effectively modeled as point charges at the diffuse layer. The compact layer, with a defined thickness of 0.5nm, contains only surface species, defined as active sites where protons can be chemically adsorbed.
4. The dielectric permittivity and the viscosity of the fluid are assumed to be constant throughout the diffuse layer region.
5. Both electrostatic dynamic equilibrium and chemical equilibrium are assured during the transient process and at the stable state.
6. A time-dependent surface complexation model (SCM) is used for modeling the surface reaction. Moreover, the surface species are used to calculate the surface charge and surface potential.
7. Both the surface charge and the surface potential are not constant. They depends on the bulk solution composition.

A finite element method (FEM) has been implemented and used for the integration of the strongly coupled Nernst-Planck-Poisson system of equations [22, 25–28]. For the sake of readability, the finite element integration is described in an appendix.

2. Physicochemical model

2.1. Nernst-Planck-Poisson system

The Nernst-Planck-Poisson (NPP) system of equations mathematically describes the electro-diffusion transport phenomena of multi-species electrolytes in porous media [5, 25, 26, 29, 30]. The GC model is based on the Poisson-Boltzmann equation, which derives from the NPP system assuming the stationary state [2, 3].

The conservation of mass equation for the i^{th} chemical species is:

$$\frac{\partial c_i}{\partial t} = -\nabla \mathbf{J}_i + G_i \quad ; \quad (i = 1, 2, ..., N_i) \tag{2}$$

where c_i $\left(\mathrm{mol\,m^{-3}}\right)$ is the concentration, $\mathbf{J}_i$ $\left(\mathrm{mol\,m^{-2}\,s^{-1}}\right)$ is the flux term, G_i $\left(\mathrm{mol\,m^{-3}\,s^{-1}}\right)$ is the generation (chemical reaction) term and N_i is the total number of species in the system. Eq. (2) is known as the Nernst-Planck continuity equation when the flux term $\mathbf{J}_i$ includes not only the diffusion transport but also electromigration and advection. Advection is the transport of aqueous species resulting from the motion of the bulk solution itself. Advection may be originated, among other mechanisms, by hydraulic gradients, capillary forces and electroosmosis. Electromigration is a coupled transport term proportional to the concentration and the gradient of electric potential. Electromigration is essential in the ionic electro-diffusion process, since it covers the electrostatic interaction between ions [8, 11].

$$\mathbf{J}_i = \underbrace{\mathbf{u}\, c_i}_{\text{advec.}} - \underbrace{D_i \nabla c_i}_{\text{diffus.}} - \underbrace{U_i\, c_i \nabla \phi}_{\text{elec. mig.}} \tag{3}$$

D_i $\left(\mathrm{m^2\,s^{-1}}\right)$ is the diffusivity and U_i $\left(\mathrm{m^2\,V^{-1}\,s^{-1}}\right)$ is the ionic or electrochemical mobility. The latter coefficient is defined from the diffusivity by means of the so-called Nernst-Townsend-Einstein equation:

$$U_i = \frac{F z_i}{RT} D_i \tag{4}$$

z_i (dimensionless) is the ionic charge defined as mol of electrons per mol of ions, F $\left(\sim 96\,485\,\mathrm{C\,mol^{-1}}\right)$ is the Faraday constant, R $\left(\sim 8.314\,\mathrm{J\,K^{-1}\,mol^{-1}}\right)$ is the universal gas constant and T (K) the absolute temperature. According to the theory of electrostatics, the relation between the electric potential and ρ $(\mathrm{C\,m^{-3}})$, the local net charge density per unit volume at any point in the solution, is described by the Gauss's law for conservation of charge in the absence of a changing magnetic field, known as the Poisson's equation [29]:

$$\varepsilon \nabla^2 \phi = -\rho \tag{5}$$

The electroneutrality assumption, $\rho = 0$, simplifies the mathematical treatment of bulk transport in most electrochemical processes and it is accepted as an adequate approximation when considering macro-scale problems [25,

31–36]. Nevertheless, the no charge accumulation assumption is not suitable for modeling the electric double layer region. In these cases, the net charge density is better described by the charge balance:

$$\rho = F \sum c_i z_i \tag{6}$$

2.2. Mathematical solution of the GC model near a flat surface

In this section we describe the analytical solution of the GC diffuse layer formed in the vicinities of a flat charged surface. As mentioned before, the GC diffuse layer is based on the Poisson–Boltzmann equation, which derives from the NPP system described in Eq. (2) and (5). The scope of this section is to empathize the relation between the NPP system and the GC model, and identify the differences with respect to the model suggested in this work.

A charged surface is in contact with an sufficiently large liquid medium. The distance $x = \infty$ refers to the bulk solution, far enough to the solid surface placed at $x = 0$. The bulk solution does not experience the influence of the double layer and is electrically neutral Accordingly, the bulk solution boundary conditions are $\phi_{x=\infty} = \phi_\infty = 0$ and $c_{i,x=\infty} = c_{i,\infty}$.

The system is reduced to a one-dimensional problem related to the perpendicular direction to the flat surface. Additionally, when studying the microscale formation of the double layer the flow of the solution can be assumed to be slow enough to neglect the advective term. According to the above mentioned assumptions the generation term G_i is not included in the conservation equation. In the stable state, the diffusion and electromigration driving forces are in dynamic equilibrium. The simplified Nernst-Planck equation, Eq. (2) results in $\nabla \mathbf{J}_i = 0$ which can be integrated using the boundary conditions at the bulk solution ${}^{dc_i}/_{dx} \mid_{x=\infty} = 0$ and ${}^{d\phi}/_{dx} \mid_{x=\infty} = 0$, giving:

$$\frac{D_i}{c_i}\frac{dc_i}{dx} + U_i \frac{d\phi}{dx} = 0 \tag{7}$$

Integrating again, with $\phi_{x=\infty} = \phi_\infty = 0$ and $c_{i,x=\infty} = c_{i,\infty}$, one obtains:

$$c_i(x) = c_{i,\infty} \exp\left(-\frac{z_i F}{RT}\phi(x)\right) \tag{8}$$

Eq. (8) is known as the Boltzmann's distribution equation and it is sometimes expressed in terms of the Boltzmann's constant, k_B $\left(\sim 1.38 \times 10^{-23}\,\mathrm{J/K}\right)$, and the elementary charge, e $\left(\sim 1.6 \times 10^{-19}\,\mathrm{C/mol}\right)$ as $(R\,k_B = e\,F)$. By replacing Eq. (8) into the Poisson's equation, Eq. (5), one obtains:

$$\frac{d^2\phi}{dx^2} = -\frac{F}{\varepsilon}\sum_i^{N_i} z_i c_{i,\infty} \exp\left(-\frac{z_i F}{RT}\phi\right) \tag{9}$$

Eq. (9) is known as the Poisson-Boltzmann equation. It describes the electric potential at the diffuse part of the double layer as function of the distance from the surface and the bulk solution concentration. Eq. (9) is non-linear and its solution is not straightforward for the cases of multi-species and asymmetric electrolytes. Nevertheless, the analytical solution for the simple case of a binary and symmetric 1:1 electrolyte can be achieved. Thus, when there are only two significant ions with the same valence but opposite sign, such as Na^+ and Cl^-, and so $i = 1, 2$; $z = z_1 = -z_2$ and $c_{1,\infty} = c_{2,\infty} = c_\infty$, the hyperbolic sine function, $\sinh(x) = (\exp(x) - \exp(-x))/2$, can be used giving:

$$\frac{d^2\phi}{dx^2} = -\frac{2F}{\varepsilon} z\, c_\infty \sinh\left(-\frac{z\,F\,\phi}{R\,T}\right) \tag{10}$$

Let $1/\kappa$ (m) be the Debye length, shown in Fig. 1, as:

$$\kappa^2 = \frac{2\,z^2 F^2 c_\infty}{\varepsilon\,R\,T} \tag{11}$$

The Debye length is a characteristic value for the thickness of the diffuse layer associated to a decreasing exponential relaxation time (see Fig. 1). The bulk concentration can be assumed at a distance of approximately 5 times the Debye length. With κ^2 and the dimensionless electrical potential, $\psi = \phi\, z\, F\, R^{-1} T^{-1}$, one obtains the following expression of the Poisson-Boltzmann equation for a binary and symmetric electrolyte:

$$\frac{d^2\psi}{dx^2} = \kappa^2 \sinh(\psi) \tag{12}$$

where the property $\sinh(-\psi) = -\sinh(\psi)$ has been used. Furthermore, in the case of low surface potentials ($\phi < 25\,\mathrm{mV}$) the Debye-Hückel approximation may be used, which consists of the approximation of the hyperbolic sine function to a linear function [2], giving:

$$\frac{d^2\psi}{dx^2} = \kappa^2 \psi \tag{13}$$

Eq. (13) is a second order linear differential equation that can be solved using the bulk-solution boundary conditions and the constant surface potential boundary condition, $\phi_{x=0} = \phi_0$, giving the expected decreasing exponential function for the electric potential in the diffuse layer:

$$\phi(x) = \phi_0 \exp(-\kappa x) \tag{14}$$

By substituting Eq. (14) into Eq. (8) one obtains the ionic concentration profiles in the diffuse layer for the case of a binary and symmetric 1:1 electrolyte:

$$c_i(x) = c_\infty \exp\left(-\frac{zF}{RT}\phi_o \exp(-\kappa x)\right) \tag{15}$$

For the flat surface and one-dimensional system, the analytical solution of the Poisson-Boltzmann equation without using the linear approximation is also possible [2]:

$$\psi(x) = \frac{2\,F\,T}{z\,R} \ln \left[\frac{1 + \exp(-\kappa x) \tanh\left(\frac{z\,e\,\phi_0}{4\,k_B\,T}\right)}{1 - \exp(-\kappa x) \tanh\left(\frac{z\,e\,\phi_0}{4\,k_B\,T}\right)} \right] \quad (16)$$

It must be stressed that the analytical solution of the GC model described above is restricted to a binary and symmetric electrolyte, constant surface charge and no chemical effects.

2.3. Chemical reaction model

In contrast to the classical formulation of the GC theory described in the previous section, in the present work, the distribution of species is assumed to be determined not only by the electrostatic forces (due to the electric potential at the surface) but also by the chemical interactions among the species in the electrolyte and at the surface. The chemical equilibrium assumption is accepted for the aqueous species in the electrolyte. A batch reaction, chemical equilibrium and speciation model has been implemented and coupled with the finite element transport model of the NPP system described above. After each time step in the numerical integration of the transport equations, the chemical equilibrium condition is re-established in each discrete node of the domain.

The chemical equilibrium assumption is based on the concept that the kinetic rate of the reversible equilibrium reactions is faster than the transport rates in the reactive transport process. Lim et al. [22] showed, by numerical models without chemical effects, that the time-transient formation of an electric double layer in the vicinities of a surface with a predefined constant potential reach the stationary state in the order of milliseconds. Aqueous equilibrium reactions, such as auto ionization of water and strong and moderate strong acid and bases dissociation, have a kinetic rate that can be assumed in the same range or faster than this transport rates associated with the formation of the double layer [35]. On the other hand, heterogeneous reactions are usually slow compared to the electro-diffusion transport process. Aringhieri and Pardini [37] reported results for the kinetics of the protonation reaction at the surface of some clayey soil samples. The reaction rate was dependent on the specific composition of the electrolyte, and the solid matrix. In any case, the average value for the kinetic constant was in the range of $10^0 - 10^2$ s^{-1}. Hence, a more detailed double layer model should take into account separate surface reactions including chemical kinetics.

2.3.1. Chemical equilibrium

A set of non linear algebraic equations is developed from the mass balance and the action mass equations describing the chemical equilibrium [38, 39]. Let i and r be respectively the indexes for the chemical species and the chemical reactions describing the secondary species, with $i = 1, 2, ..., N_i$ and $r = 1, 2, ..., N_r$; where N_i is the total number of species, $(N_i - N_r)$ is the number of master species and N_r is the number of chemical equilibrium reactions used to defined the secondary species as function of the master species. A secondary species is a chemical species defined from a set of master species by means of a chemical equilibrium reaction.

For a set of N_i chemical species, the N_r stoichiometric equations are defined as:

$$\nu_r n_r \rightleftarrows \sum_{i=1}^{N_i} \nu_{i,r} n_i \quad (17)$$

where the extensive variable n_i (mol) denotes the total amount of the i^{th} species in the system and $\nu_{i,r}$ is the stoichiometric coefficient for the i^{th} species in the r^{th} reaction.

When a set of N_i chemical species in non-equilibrium, react with each other to reach the chemical equilibrium state, a mass conservation equation can be written as a function of the extent of the reaction ξ_r. The extent of reaction (or reaction progress) is the extensive quantity describing the progress of a chemical reaction equal to the number of chemical transformations [24]. In order to reach the chemical equilibrium state, any reversible reaction can proceed towards the products or towards the reactants, so ξ_r can be either a positive or a negative value.

According to the previous definition, the total amount of each species at the equilibrium is given by the mass balance equation along the chemical reaction path, in the form of:

$$n_{i,\text{eq.}} = n_{i,\text{init.}} + \sum_{r=1}^{N_r} \xi_r \nu_{i,r} \quad (18)$$

Let $\mathbf{x} = \left[\ \xi_1, \xi_2, \cdots, \xi_M\ \right]$ be the vector containing the reaction extents for the N_r reactions. The function $f_r(\mathbf{x})$ is defined as a measure of the Gibbs energy of the chemical system according to the thermodynamic description of the chemical potential [39] and it tends to zero when the systems approaches to the equilibrium. Thus, the function $f_r(\mathbf{x})$ represents the distance to the equilibrium state for the r^{th} reversible reaction. Using logarithms, $f_r(\mathbf{x})$ can be expressed from the action mass equation as:

$$f_r(\mathbf{x}) = \sum_{r=1}^{N_r} (\nu_{i,r} \ln a_i) - \ln K_{eq,r} \quad (19)$$

where $K_{eq,r}$ is the equilibrium constant for the r^{th} reaction and a_i (dimensionless) is the chemical activity. The activity is defined from the molal concentration b_i $\left(\text{mol kg}^{-1}\right)$ the standard concentration $b_i^{\ominus}$ $\left(\text{mol kg}^{-1}\right)$, necessary to ensure that both the activity is dimensionless, and the activity factor γ_i (dimensionless). Activity factors are obtained from the Davies and the Setschenow equations for ionic and non-ionic species respectively [40, 41]. Activities for the solvent and the solid species are set to a fixed value of 1.

Heterogeneous precipitation/dissolution reactions are also included in the model. This means that the equilibrium reaction for the solid species is only included in the set of chemical reactions when the saturation index predicts the existence of the precipitated phase. Mineral phases are included in the chemical system to define the initial concentration of the electrolyte solution. Nevertheless, in the simulations presented here, unsaturated conditions are expected.

The N_r equilibrium equations are coupled in a matrix system of equations and solved by means of a Newton-Raphson method. Stoichiometric equations are consistent with the mass and charge conservation principles. As a result, using the extents of each reaction as independent variables, the electrical balance of the solution is not modified during the speciation process. This feature makes the presented algorithm suitable for problems in which a thorough control of the electrical balance is required, such as the case of strongly coupled transport model described in this work. Furthermore, a line-search approach is used in the Newton-Raphson method to assure the convergence and, at the same time, deal with the non-negative concentration constraints of all the chemical species [42].

2.3.2. Surface reaction

The surface reaction is modeled based on a surface complexation model in which the chemical kinetic rates are considered. SCM's are discrete site models that provide molecular descriptions of surface reaction using an equilibrium approach [15, 40, 43]. Thus, SCM's define surface heterogeneous reactions with an approach similar to aqueous and solid precipitation/dissolution equilibrium models. In this context, mass balance and action mass equations are solved to minimized the Gibbs energy of the chemical system, as explained in the section before.

SCM's have been previously proposed for modeling the electric double layer interface. Dzombak and Morel [44] reported diffused-layer model parameters for the adsorption of different ions on hydrous ferric oxide. These thermodynamic data are used in some surface complexation and aqueous speciation programs, such as [40]. Davis et al. [1] listed some electrical double layer studies from different researches, focused on different electrolytes and solid matrices, such as oxides of Fe, Al, Si, Ti and Zn. Al-Hadman and Reddy [15] reported some experimentally obtained intrinsic surface equilibrium constants for the surface complexation reactions on kaolin, which will be used in this work.

In the present work, only the protonation and deprotonation reactions of the surface sites XOH are included, given by:

$$\mathrm{XOH_2}^+ \underset{k_{-1}}{\overset{k_1}{\rightleftarrows}} \mathrm{XOH} + \mathrm{H}^+ \tag{20}$$

$$\mathrm{XO}^- \underset{k_{-2}}{\overset{k_2}{\rightleftarrows}} \mathrm{XOH} - \mathrm{H}^+ \tag{21}$$

where X represents the solid matrix and the concentration of the solid species XOH, $\mathrm{XOH_2^+}$ and $\mathrm{XO^-}$ is given in $\left(\mathrm{mol\,kg^{-1}}\right)$. According to Eq. (20) and Eq. (21), the surface species $\mathrm{XOH_2^+}$ and $\mathrm{XO^-}$ are formed, as function of the proton concentration (or pH value) at the vicinities of the surface. The surface charge, σ_0 $\left(\mathrm{C\,m^{-2}}\right)$, is obtained from the charge balance of these charged surface species:

$$\sigma_0 = \left(\left[\mathrm{XOH_2^+}\right] - \left[\mathrm{XO^-}\right]\right) F\, L_0\, \rho_w \tag{22}$$

where L_0 (m) is the thickness of the compact layer and ρ_w $\left(\mathrm{kg\,m^{-3}}\right)$ is the density of the bulk solution. In the simulations presented here, low concentrations are used and the density of solution is assumed equal to the density of water at room temperature. The surface potential is obtained by assuming the charge balance at the surface as a source vector in the finite element integration (see appendix).

The intrinsic equilibrium constant for the surface reactions are:

$$\mathrm{K_{int}^+} = \frac{[\mathrm{XOH}]_{eq}\,[\mathrm{H}^+]_{eq}^{surf}}{\left[\mathrm{XOH_2^+}\right]_{eq}} = \frac{k_1}{k_{-1}} = 10^{-3.8} \tag{23}$$

and

$$\mathrm{K_{int}^-} = \frac{[\mathrm{XOH}]_{eq}}{[\mathrm{XO^-}]_{eq}\,[\mathrm{H}^+]_{eq}^{surf}} = \frac{k_2}{k_{-2}} = 10^{9.4} \tag{24}$$

Intrinsic equilibrium constants, not dependent on the surface potential, are defined from the concentration of the surface species, and the concentration of the aqueous species in equilibrium with the surface. In classical surface complexation models, the concentration of ions at the surface is estimated assuming the Poisson-Boltzmann theory described above, in the form:

$$\left[\mathrm{H}^+\right]^{\mathrm{surf}} = \left[\mathrm{H}^+\right]_\infty \exp\left(\frac{-F\,\phi_0}{RT}\right) \tag{25}$$

In the model presented here, the concentration of the ions at the surface is calculated by means of the electrodiffusion transport model. Additionally, the kinetic rate of the surface reaction is taken into account for a more realistic model of the dynamic formation of the electric double layer. $\mathrm{K_{int}^+}$ and $\mathrm{K_{int}^-}$ values are obtained from [15], assuming that the solid matrix is pure kaolin.

The kinetic constant for the surface reactions in the system considered in Eq. (20) and (21) are unknown. For this reason, for this study, some arbitrary chosen values are used, i.e. $k_{-1} = 10^5$ and $k_{-2} = 10^{-2}$, while k_1 and k_2 are obtained from the equilibrium constants. These arbitrary values for the kinetic constant give a reasonable rate for the surface reaction (in the order of seconds), according to the results presented in [37] for the protonation of kaolinite particle surface. The adopted approach allows a comparison of the relative importance of the rate in the transient formation of EDL.

Table 1: Chemical parameters for the modeled system

		H_2O	H^+	Ca^{+2}	Cl^-	$\log_{10}(K_{eq})$	z_i	$D_i \times 10^9 \left(\frac{m^2}{s}\right)$
Master	H_2O	1	0	0	0	-	0	-
	H^+	0	1	0	0	-	1	9.311
	Ca^{+2}	0	0	1	0	-	2	1.584
	Cl^-	0	0	0	1	-	-1	2.032
Secondary	OH^-	1	-1	0	0	14.00	-1	5.273
	$CaOH^+$	1	-1	1	0	12.78	1	0.792
	$CaCl^+$	0	0	1	1	0.29	1	0.792
	$CaCl_2$	0	0	1	2	0.64	0	0.528
	HCl	0	1	0	1	0.71	0	1.016
	$CaCl_2$ (s)	0	0	1	2	11.77	0	0
	$Ca(OH)_2$ (s)	2	-2	1	0	22.81	0	0

3. Results and discussions.

In this section, we present numerical results from simulations of the time-transient formation of an electrical double layer when a chemically active flat surface is placed in contact with an electrolyte solution. An asymmetric and multi-species electrolyte is used, resulting from the dissolution of $CaCl_2$ (s), $Ca(OH)_2$ (s) in HCl solution (or, in some cases, pure water) until the chemical equilibrium is reached. The complete set of chemical species in the electrolyte is listed in Table 1 together with the matrix of stoichiometric coefficients, the equilibrium constants for the given stoichiometry (from [40]), and the diffusivities (from [45]). In the case of $CaOH^+$, $CaCl^+$, $CaCl_2$(aq) and HCl(aq) their diffusivities were not found in any of the databases investigated. Thus, an arbitrary value was used, equal to the diffusivity of the slowest ion and divided by the number of ions in the molecule.

The master species are H_2O, H^+, Ca^{+2} and Cl^-. Ca^{+2} and Cl^- are the main ions in the electrolyte in neutral conditions, i.e. the ions with higher concentrations. H^+ and OH^-get more importance in acid or basic conditions respectively, when their concentration can be equal to or greater than the ions Ca^{+2} and Cl^-. Different proportions of $Ca(OH)_2$ (s) and HCl are use to modify the pH of the bulk solution.

The surface is defined with an initial concentration of $1\,\mathrm{mol\,kg^{-1}}$ of the surface compound XOH. Assuming a thickness of 0.5 nm for the compact layer, the surface concentration is equivalent to $0.5 \times 10^{-6}\,\mathrm{mol\,m^{-2}}$. Initially, both the surface and the solution are electrically neutral. The active sites XOH at the surface can dissociate or protonate to give a negative or positive surface charge respectively, as shown in Fig. 2. Protonation and dissociation intrinsic constants for the surface complexation reaction are taken from [15] assuming a kaolin solid matrix.

In all the simulations presented in this work, the one-dimensional domain for the diffuse layer is divided in 50 finite elements. The thickness of the elements in the diffuse layer decrease when approaching to the surface (or increase when approaching the bulk solution) as shown in Fig. A.10. The distance from the surface in which the concentration is assumed to be the bulk solution is estimated as approximately 5-10 times the value of Debye length for the binary and symmetric electrolyte.

Assuming constant room temperature, the Debye length described in Eq. (11) is approximated from the ionic strength, $I\ \left(\mathrm{mol\,kg^{-1}}\right)$, as [2]:

$$\frac{1}{k} \approx \frac{0.304}{\sqrt{I}}\ (\mathrm{nm}) \tag{26}$$

In the Figs. 3 - 4 and 6 - 8, dashed lines represents the time-transient profiles, and the steady state is represented with continuous lines. In some cases, a legend is included to indicate the time scale of the process. A dotted vertical line is used to indicate the boundary of the compact and diffuse layer, at 0.5 nm from the surface. 15 time-transient profiles are shown but, in most cases, some of the profiles are overlapped with the stable state and they are visually impossible to distinguish.

Fig. 3 show the results for the time-transient formation of the double layer for a selected case in which the electrolyte was an alkaline solution with pH = 8.68 and ionic strength $I = 0.01$. In this case, the surface potential at the stationary state is -16 mV. Counter-ions (the cations Ca^{+2}, $CaOH^+$, $CaCl^+$, and H^+) accumulate at the vicinities of the negative surface, while co-ions (the anions Cl^- and OH^-) are repulsed. In Fig. 3, Ca^{+2} and Cl^-, the ions in higher proportion, are shown together, while the concentrations of protons and hydroxides are implicitly included in the pH profile. The pH value at the surface is 8.38. It is slightly lower than the pH value at the bulk solution, as the H^+ are attracted and the OH^- repulsed by the charged surface.

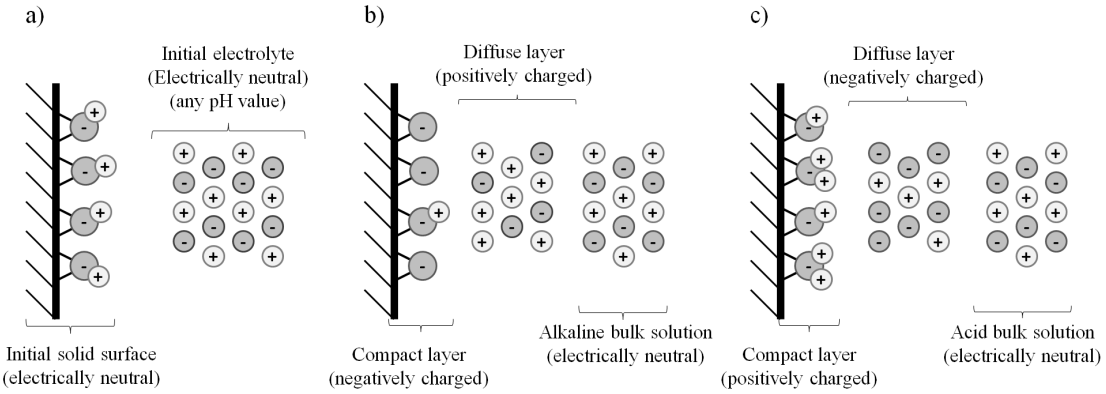

Figure 2: Scheme of the interface system modeled a) Initial conditions b) Negative charged surface c) Positive charged surface

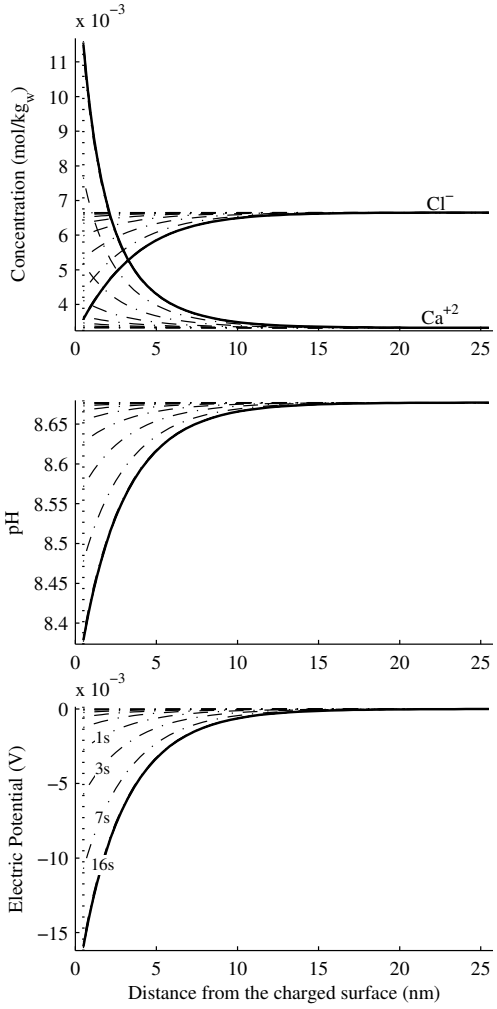

Figure 3: Main species transient profiles and electric potential in the simulation with surface reaction accounting for kinetic rates; with $I = 0.01$ and pH $= 8.68$, resulting from the dissolution of 3.33 mmol $CaCl_2$ and 0.003 mmol $Ca(OH)_2$ in 1 kg of pure water.

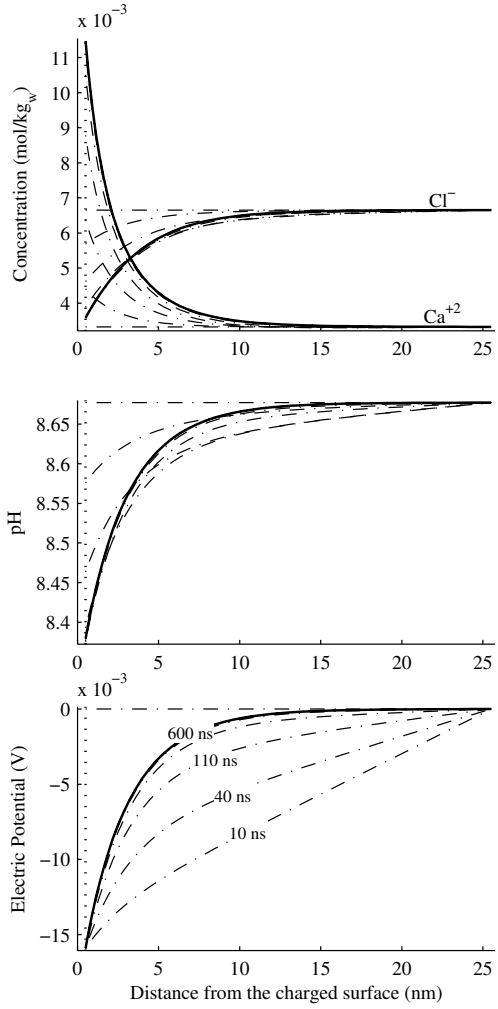

Figure 4: Main species transient profiles and electric potential in the simulation with constant surface potential and no surface reaction; with $I = 0.01$ and pH $= 8.68$, resulting from the dissolution of 3.33 mmol $CaCl_2$ and 0.003 mmol $Ca(OH)_2$ in 1 kg of pure water.

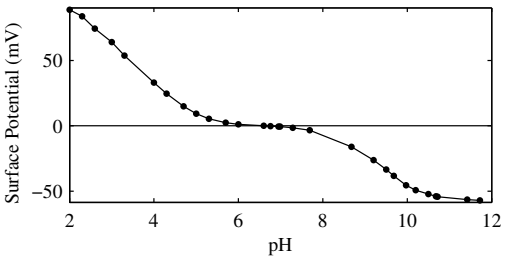

Figure 5: Surface potential dependence on the bulk solution pH for I = 0.01.

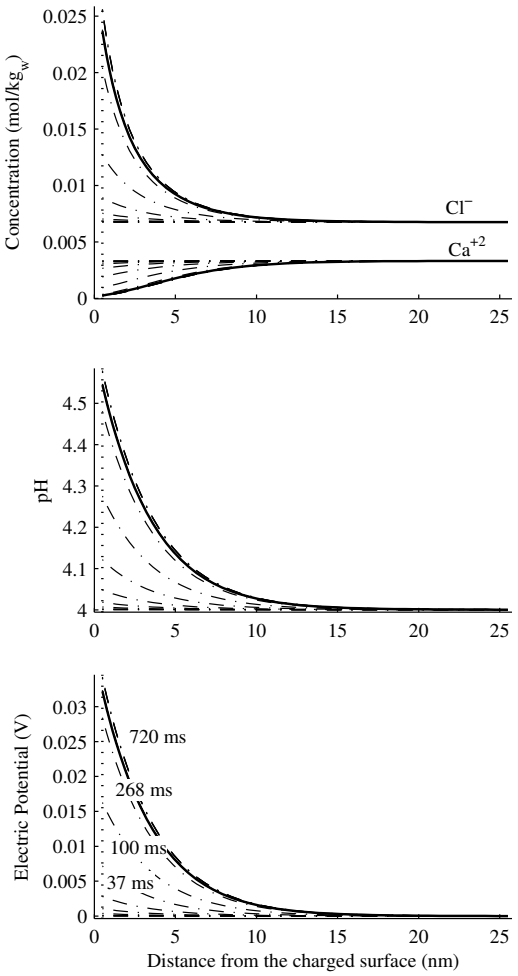

Figure 6: Main species transient profiles and electric potential in the simulation with surface reaction accounting for chemical kinetics with $I = 0.01$ and pH = 4, resulting from the dissolution of 3.33 mmol $CaCl_2$ in 1 kg of HCl solution 10^{-4} molal.

In Fig. 3 one can see that the stable state is reached in approximately 16 s. This time is several orders of magnitude slower than the simulation results reported in [22]. This difference is due to the chemical reaction kinetic rate. To demonstrate this statement, and compare the time scales of the surface reaction and the electro-diffusion process, a new simulation is performed but for a system in which the surface is assumed chemically inert (no surface reaction) and the surface potential is fixed to a constant value of -16 mV, the value obtained at the stable state in the previous simulation.

Fig. 4 show the results equivalent to those shown in Fig. 3. In this case, the Ca^{+2}, Cl^-, pH and electric potential profiles at the stationary state are very similar to those shown in (3). But the time-transient profiles follow a different path until the equilibrium. The simulations done at constant surface potential reach the stationary state in approximately 600 ns, which is considerably faster than the case including for surface reaction.

Comparing results from Figs. 3 and 4 it can be concluded that, the rate of formation of the double layer in a real case may be controlled by the kinetic rate of the surface reaction, and not for the electro-diffusion process at the vicinities of the surface. Consequently, incorporating surface complexation models and assuming instantaneous chemical equilibrium at the diffuse layer and at the surface may be inappropriate for modeling the time-transient formation of the double layer. Furthermore, the electro-diffusion process is much faster than the surface reactions. Accordingly, the surface concentration of the aqueous species can be assumed controlled and defined by this electro-diffusion process.

To study the dependence of the surface potential on the pH of the bulk solution, a set of simulations are performed in which the pH of the media is changed, but keeping constant the ionic strength of a value of $I = 0.01$. The pH of the bulk solution is modified by defining the electrolyte using different combinations of the species $CaCl_2$ (s), $Ca(OH)_2$ (s) and HCl. In the system modeled here, the surface reaction depends only on the concentration of protons, that is the pH of the media. Fig. 5 shows the dependence of the surface potential on the pH of the bulk solution. The study is limited to the range of pH 2 and 12, assigned to pure HCl and $Ca(OH)_2$ at the fixed ionic strength value. The point of zero charge is obtained in a pH = 6.6.

In Fig. 6 we show the results of a simulation in which a moderate acid media, pH = 4, is established in the bulk solution. For this case, a positive surface charge and potential is developed, and ions distribute accordingly. The stable state is reached in approximately 0.7 s. This equilibrium time is faster than compared to the simulation shown in Fig. 3, but it is still slow enough to state that the process is controlled by the kinetic rate of the surface reaction. For the same simulation at pH = 4 the transient profiles for the other aqueous species in the system are shown in Fig. 7. $CaOH^+$ and $CaCl^+$ are cations, and they are repulsed by the positively charged surface. Non-ionic species, $CaCl_2$ and HCl, undergo time-transient

variations and reach an stationary state in chemical equilibrium with the other ions in the system. In the classical GC and SGC model, non-ionic species are not affected by the electric double layer forces and so their concentration is assumed constant. In the model presented here, chemical effects produce the formation of concentration profiles for all species to satisfy the chemical equilibrium condition. As a result, the concentration profiles of these non-ionic species is indirectly related to the surface potential, which affect the ions in equilibrium with the non-ionic aqueous species.

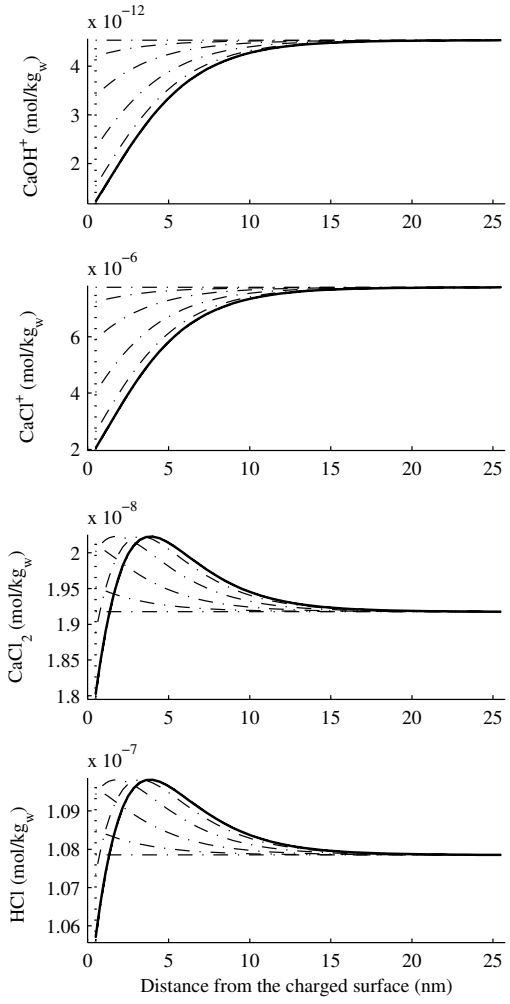

Figure 7: Minor species transient profiles in the simulation with surface reaction accounting for chemical kinetics with $I = 0.01$ and pH = 4, resulting from the dissolution of 3.33 mmol $CaCl_2$ in 1 kg of HCl solution 10^{-4} molal.

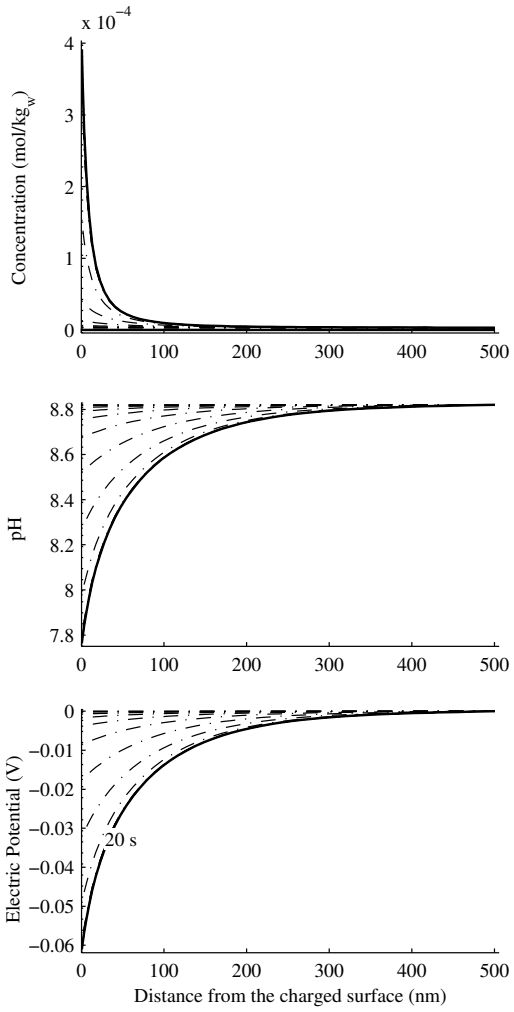

Figure 8: Ca^{+2}, pH and electric potential transient profiles in the simulation with surface reaction accounting for chemical kinetics with $I = 10^{-5}$ and pH = 8.8, resulting from the dissolution of 3.5×10^{-4} mmol $CaCl_2$ and 3×10^{-3} mmol $Ca(OH)_2$ in 1 kg of solution HCl 10^{-4} molal.

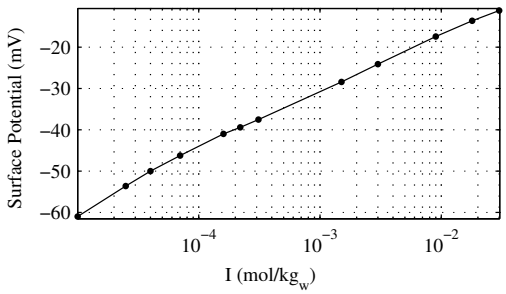

Figure 9: Surface potential at the steady state against bulk solution ionic strength in logarithm scale (pH = 8.2).

Next, the dependence of the surface potential on the concentration is studied. According to the analytical solution of the GC model, both the surface potential and the thickness of the diffuse layer increases when decreasing the ionic strength. Fig. 8 shows the results for a simulation with $I = 10^{-5}$ and pH = 8.8. In this case, the diffuse layer thickness is calculated to be 500 nm and the corresponding surface potential in the stationary state is about -60 mV. By comparing results from Fig. 3 with $I = 10^{-2}$ and Fig. 8 with $I = 10^{-5}$, it is clear that the diffuse layer is more pronounced at lower concentrations. These results are consistent with the experimental results for electrokinetic transport, when the electroosmosis becomes more important with respect to the electromigration with decreasing concentrations.

A set of simulations is performed at different ionic strengths, but constant pH value (pH = 8.2). In the results presented in Fig. 9 it can be seen that in the range of 10^{-5} to 10^{-2} there is a fairly linear tendency between the surface potential and the decimal logarithm of the ionic strength of the media.

Conclusions

A model for the formation of an electric double layer between an electrolyte and a chemically active flat surface has been described. It consists of a generalized solution of the transient Nernst-Planck-Poisson system of equations for the microscopic reactive-transport of aqueous species. The one presented here is appropriate for asymmetric and multi-species electrolytes and it is not limited to any range of surface potential. Chemical effects are included, assuming instantaneous aqueous complexation equilibrium and time dependent surface reactions.The surface charge and potential developments are the result of the surface reactions. Consequently, the surface potential is not a constant, since it depends on the bulk concentration.

The following conclusions can be drawn from the simulations performed using the work described here:

- Concentration profiles for the non-ionic species are formed at the vicinities of the charged surface as a result of the chemical interaction with the charged species in the system.

- The electro-diffusion transport process for a constant surface potential is very fast, reaching the stationary state in the order of microseconds in most cases.

- Despite the kinetic constants used in the simulations are arbitrarily chosen, they have orders of magnitude estimated from real cases. Results from simulations show that the transient formation of electric double layers may be controlled by the kinetics of the surface reactions, and not by the electro-diffusion transport process.

These conclusions obtained here are not possible to be discussed from the standard electric double layer models, which are based on the analytical solution of the Nernst-Planck-Poisson system, and their applicability is limited to stationary state problems, binary electrolytes, limited and fixed constant surface potentials and no chemical reaction effects.

Acknowledgments

Authors acknowledge The Danish Agency of Science Technology and Innovation. This research was funded as part of the project "Fundamentals of Electrokinetics in In-homogeneous Matrices", with project number 274-08-0386. José M. Rodríguez-Maroto acknowledges the financial support from the Ministerio de Ciencia e Innovación of the Spanish Government through the project ERHMES, CTM2010-16824, and FEDER funds.

AppendixA. Finite Element Integration of the NPP model

A finite element method (FEM) is used for the integration of the strongly coupled NPP system of differential equations under consideration [25, 26, 35]. The spatial domain is divided into a number of finite elements limited by dimensionless nodal points where the state variables are discretized and solved by matrix algebra [46]. Shape functions are used to interpolate between the nodal points to get an approximate solution of the unknown continuous function.

Let $\mathbf{a}_i$ and $\mathbf{a}_\phi$ be the discrete form of the state variables at the nodal points for the molal concentration and the electrical potential respectively and let w be the arbitrary weight function. The Galerkin method is used for weighting the residuals [47]. The following standard FEM vectorial notations are defined.

$$\begin{array}{ccccc} c_i = \mathbf{N}\mathbf{a}_i & , & \phi = \mathbf{N}\mathbf{a}_\phi & , & w = \mathbf{w}^{\mathrm{T}}\mathbf{N}^{\mathrm{T}} \\ \nabla c_i = \mathbf{B}\mathbf{a}_i & , & \nabla\phi = \mathbf{B}\mathbf{a}_\phi & , & \nabla w = \mathbf{w}^{\mathrm{T}}\mathbf{B}^{\mathrm{T}} \end{array} \quad \text{(A.1)}$$

where $\mathbf{N} = [1 - {}^{x}/_{L_e},\ {}^{x}/_{L_e}]$ is the linear piecewise shape function used to interpolate between nodal points. L_e (m) is the length of the one-dimensional finite element, with $e = 1, 2, ..N_e$ and N_e is the total number of finite elements. The gradient of the shape function is given by $\mathbf{B} = [{}^{-1}/_{L_e},\ {}^{1}/_{L_e}]$. The superscript T is used to indicate the transpose of the vectors. $\mathbf{K}_e$ and $\mathbf{C}_e$ are defined as the conductivity and mass matrices for the e^{th} element as:

$$\mathbf{K}_e = \int_0^{L_e} \mathbf{B}^{\mathrm{T}}\mathbf{B}dx = \frac{1}{L_e}\begin{bmatrix} 1 & -1 \\ -1 & 1 \end{bmatrix} \quad \text{(A.2)}$$

and

Table A.2: Terminology for the discrete NPP system

Related term	Terminology	State variable	$k_{e,i}$ parameter
Accumulation	$\mathbf{C}_i$	$\partial c_i/\partial t$	$L_e/6$
Diffusion	$\mathbf{K}_i^{\text{diff}}$	c_i	D_i/L_e
Electromigration	$\mathbf{K}_i^{\text{em}}$	ϕ	$c_i z_i D_i F/\left(RTL_e\right)$
Free charge density	$\mathbf{E}_i$	c_i	$Fz_iL_e/6$
Electric potential	$\mathbf{K}^{\phi}$	ϕ	ε/L_e

$$\mathbf{C}_e = \int_0^{L_e} \mathbf{N}^{\mathrm{T}}\mathbf{N}dx = \frac{L_e}{6}\begin{bmatrix} 1 & 2 \\ 2 & 1 \end{bmatrix} \tag{A.3}$$

In the present model, the elements in the one-dimensional domain have different length in order to include a higher number of shorter elements in those regions where sharper profiles are expected, i.e. near the surface (see Fig. A.10). This method has shown accurate results with a lower number of elements.

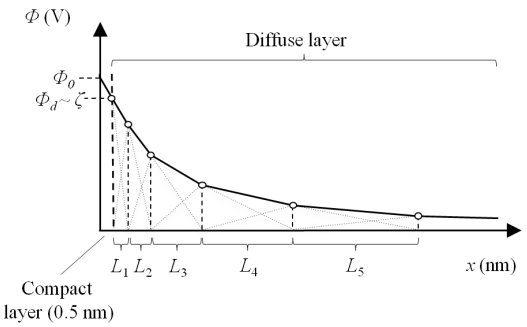

Figure A.10: Scheme for the discretization of the region near the charged surface. The thickness of the first element is fixed to 0.5 nm. The thickness of the elements increases when approaching to the bulk solution.

Since the time-transient process modeled here tends to the stationary state, the system tends to experience lower changes when approaching to the equilibrium. For this reason, the time increment for the numerical integration, Δt, increases when approaching to the stable state. This numerical strategy resulted in a significant reduction of the computational time.

$\mathbf{K}_i$ and $\mathbf{C}_i$ are the respectively the conductivity and mass matrices for the i^{th} species, defined for the entire one-dimensional domain. They result from the assemblage of the local matrices $\mathbf{K}_e$ and $\mathbf{C}_e$. Eq. (A.4) illustrates the assemblage of $\mathbf{K}_i$. The assemblage of $\mathbf{C}_i$ is done in a similar way. The property k_e is a parameter with a specific element value, shown in Table A.2.

$$\mathbf{K}_i = \begin{bmatrix} k_1 & -k_1 & 0 & \cdots & 0 \\ -k_1 & (k_1+k_2) & -k_2 & \ddots & \vdots \\ 0 & -k_2 & \ddots & \ddots & 0 \\ \vdots & \ddots & \ddots & (k_{N_e-1}+k_{N_e}) & -k_{N_e} \\ 0 & \cdots & 0 & -k_{N_e} & k_{N_e} \end{bmatrix} \tag{A.4}$$

The NPP system of equations is non-linear. In the microscale, the non-linearity comes from the electromigration term, which depends on both the concentration and the gradient of electrical potential. In this model, the latter is used as a state variable when obtaining the discrete formulation. The concentration is assumed as a characteristic element value, included in the parameter during the assemblage of the conductivity matrices. In the macroscale, non-linearity can also be due to the advection term or the the porosity [26]. According to this, matrices $\mathbf{K}_i$ and $\mathbf{C}_i$ are recalculated and reassembled during the transient process as part of a general procedure to solve the non-linear system. This solution procedure is based on a general iterative algorithm [25, 26], which requires the updating of the matrices $\mathbf{K}_i$ and $\mathbf{C}_i$ with the new specific element value k_e.

The one-dimensional Nernst-Planck and Poisson equations are multiplied by the arbitrary weight function w and integrated between the limits of the linear element. The integration-by-parts technique and the terminology in Eq. (A.1) and in Table A.2 is used to get the discretized Nernst-Planck and Poisson equations as:

$$\mathbf{C}_i\frac{\partial \mathbf{a}(t)}{\partial t} + \mathbf{K}_i^{\text{diff}}\mathbf{a}_i(t) + \mathbf{K}_i^{\text{e.m.}}\mathbf{a}_\phi(t) + \mathbf{f}_i = 0 \tag{A.5}$$

and

$$\sum_{i=1}^{N_i}\mathbf{E}_i\mathbf{a}_i(t) + \mathbf{K}^{\phi}\mathbf{a}_\phi(t) + \mathbf{f}_\phi = 0 \tag{A.6}$$

where $\mathbf{f}_i$ and $\mathbf{f}_\phi$ are the flux vectors of species $\left(\mathrm{mol\,m^{-2}\,s^{-1}}\right)$ or charge $\left(\mathrm{V\,m^{-2}}\right)$ respectively. For a system with N_i chemical species, $N_i + 1$ equations are coupled to form the global matrix system:

$$\underbrace{\begin{bmatrix} \mathbf{C}_1 & 0 & \cdots & 0 \\ 0 & \ddots & \ddots & \vdots \\ \vdots & \ddots & \mathbf{C}_{N_i} & 0 \\ 0 & \cdots & 0 & 0 \end{bmatrix}}_{\mathbf{C}} \frac{\partial}{\partial t} \underbrace{\begin{bmatrix} \mathbf{a}_1 \\ \vdots \\ \mathbf{a}_{N_i} \\ \mathbf{a}_\phi \end{bmatrix}}_{\frac{\partial \mathbf{a}(t)}{\partial t}} + \underbrace{\begin{bmatrix} \mathbf{K}_1^{\text{diff}} & 0 & \cdots & \mathbf{K}_1^{em} \\ 0 & \ddots & \ddots & \vdots \\ \vdots & \ddots & \mathbf{K}_{N_i}^{\text{diff}} & \mathbf{K}_{N_i}^{em} \\ \mathbf{E}_1 & \cdots & \mathbf{E}_{N_i} & \mathbf{K}^\phi \end{bmatrix}}_{\mathbf{K}} \underbrace{\begin{bmatrix} \mathbf{a}_1 \\ \vdots \\ \mathbf{a}_{N_i} \\ \mathbf{a}_\phi \end{bmatrix}}_{\mathbf{a}(t)} + \underbrace{\begin{bmatrix} \mathbf{f}_1 \\ \vdots \\ \mathbf{f}_{N_i} \\ \mathbf{f}_\phi \end{bmatrix}}_{\mathbf{f}} = 0 \tag{A.7}$$

which can be expressed in a simplified notation in the way:

$$\mathbf{C}\frac{\partial \mathbf{a}(t)}{\partial t} + \mathbf{K}\,\mathbf{a}(t) + \mathbf{f} = 0 \tag{A.8}$$

where the absence of subscripts means the global matrices and vectors for the entire coupled system.

Linear finite elements are used for the discretization in the time. A truly implicit unconditionally stable scheme is used, which is equivalent to consider that the time derivative is obtained by an incremental form:

$$\frac{\partial \mathbf{a}(t)}{\partial t} = \frac{\mathbf{a}_{t_0+\Delta t} - \mathbf{a}_{t_0}}{\Delta t} \tag{A.9}$$

where t_0 is the present time and $t_0+\Delta t$ is the next time step in the numerical integration. Accordingly, Eq. (A.8) can be rearranged to give the following:

$$\underbrace{\left(\frac{\mathbf{C}}{\Delta t} + \mathbf{K}\right)}_{\mathbf{K}^\star} \mathbf{a}_{t_0+\Delta t} = \underbrace{\frac{\mathbf{C}}{\Delta t}\mathbf{a}_{t_0} - \mathbf{f}}_{\mathbf{f}^\star} \tag{A.10}$$

which is solved by means of a left division operation with forced boundary conditions [47]. As mention before, the surface potential is obtained by using as boundary condition the charge balance at the surface calculated in Eq. (22) as the source vector, $\mathbf{f}_\phi$ in the Poisson equation. Also, constant concentration and electroneutrality are the boundary conditions for the last node of the one-dimensional domain, assigned to the bulk solution.

References

[1] J. Davis, R. James, J. Leckie, Surface ionization and complexation at the oxide/water interface: I. computation of electrical double layer properties in simple electrolytes, J. Colloid Interf. Sci. 63 (3) (1978) 480–499.

[2] L. Dongqing, Basics of electrical double layer, in: Electrokinetics in microfluidics, Academic Press, 2004, Ch. 2.

[3] J. Lyklema, Fundamentals of interface and colloid science, Vol. 5, Academic Press, 2005.

[4] H. Ohshima, Diffuse double layer equations for use in surface complexation models: Approximations and limits, in: J. Lützenkirchen (Ed.), Surface Complexation Modelling, Academic Press, 2006, Ch. 3.

[5] S. Pamukcu, Electrochemical transport and transformations, in: K. R. Reddy, C. Cameselle (Eds.), Electrochemical Remediation Technologies for Polluted Soils, Sediments and Groundwater, Wiley Online Library, 2009, pp. 29–64.

[6] S. Shiraishi, Chapter 27 - electric double layer capacitors, in: E. ichi Yasuda, M. Inagaki, K. Kaneko, M. Endo, A. Oya, Y. Tanabe (Eds.), Carbon Alloys, Elsevier Science, Oxford, 2003, pp. 447 – 457.

[7] D. Leckband, J. Israelachvili, Intermolecular forces in biology, Q. Rev. Biophys. 34 (02) (2001) 105–267.

[8] J. Mitchell, K. Soga, Fundamentals of soil behavior, Wiley New York, 1976.

[9] Y. Acar, R. Gale, A. Alshawabkeh, R. Marks, S. Puppala, M. Bricka, R. Parker, Electrokinetic remediation: Basics and technology status, J. Hazard. Mater. 40 (2) (1995) 117–137.

[10] A. Yeung, J. Mitchell, Coupled fluid, electrical and chemical flows in soil, Geotechnique 43 (1) (1993) 121–134.

[11] A. Yeung, S. Datla, Fundamental formulation of electrokinetic extraction of contaminants from soil, Can. Geotech. J. 32 (4) (1995) 569–583.

[12] T. Grundl, P. Michalski, Electroosmotically driven water flow in sediments, Water Res. 30 (4) (1996) 811–818.

[13] A. Delgado, F. Gonzalez-Caballero, R. Hunter, L. Koopal, J. Lyklema, Measurement and interpretation of electrokinetic phenomena, J. Colloid Interf. Sci. 309 (2) (2007) 194–224.

[14] L. Bertolini, L. Coppola, M. Gastaldi, E. Redaelli, Electroosmotic transport in porous construction materials and dehumidification of masonry, Constr. Build. Mater. 23 (1) (2009) 254–263.

[15] A. Al-Hamdan, K. Reddy, Surface speciation modeling of heavy metals in kaolin: implications for electrokinetic soil remediation processes, Adsorption 11 (5) (2005) 529–546.

[16] L. Ottosen, I. Christensen, I. Rorig-Dalgaard, P. Jensen, H. Hansen, Utilization of electromigration in civil and environmental engineering - Processes, transport rates and matrix changes, J. Environ. Sci. Health, Part A 43 (8) (2008) 795–809.

[17] A. Alshawabkeh, R. Bricka, Basics and applications of electrokinetic remediation, Environ Sci. Pollut. Control Series (2000) 95–112.

[18] J. Shang, Zeta potential and electroosmotic permeability of clay soils, Can. Geotech. J. 34 (4) (1997) 627–631.

[19] F. Herruzo, J. Maroto, R. Delgado, C. Lahoz, C. Alonso, Limpieza de suelos por electrodescontaminacion (I), Ing. Quim. 32 (369) (2000) 215–222.

[20] A. Ribeiro, J. Rodriguez-Maroto, E. Mateus, H. Gomes, Removal of organic contaminants from soils by an electrokinetic process: the case of atrazine. Experimental and modeling, Chemosphere 59 (9) (2005) 1229–1239.

[21] R. Hunter, H. Wright, The dependence of electrokinetic potential on concentration of electrolyte, J. Colloid Interf. Sci. 37 (3) (1971) 564–580.

[22] J. Lim, J. Whitcomb, J. Boyd, J. Varghese, Transient finite element analysis of electric double layer using Nernst-Planck-Poisson equations with a modified stern layer, J. Colloid Interf. Sci. 305 (1) (2007) 159–174.

[23] J. Westall, H. Hohl, A comparison of electrostatic models for the oxide/solution interface, Adv. Colloid Interface Sci. 12 (4) (1980) 265–294.

[24] A. McNaught, A. Wilkinson, Compendium of Chemical Terminology: Iupac Recommendations, 2nd Edition, Blackwell Science, 1997.

[25] J. Paz-Garcia, B. Johannesson, L. Ottosen, A. Ribeiro, J. Rodriguez-Maroto, Modeling of electrokinetic processes by

finite element integration of the Nernst-Planck-Poisson system of equations, Sep. Purif. Technol. 79 (2) (2011) 183–192.
[26] J. Paz-García, B. Johannesson, L. Ottosen, A. Alshawabkeh, A. Ribeiro, J. Rodríguez-Maroto, Modeling of electrokinetic desalination of bricks, Electrochim. Acta.
[27] A. Javadi, M. Al-Najjar, Finite element modeling of contaminant transport in soils including the effect of chemical reactions, J. Hazard. Mater. 143 (3) (2007) 690–701.
[28] B. Johannesson, Y. Hosokawa, K. Yamada, Numerical calculations of the effect of moisture content and moisture flow on ionic multi-species diffusion in the pore solution of porous materials, Comput. Struct. 87 (1-2) (2009) 39–46.
[29] B. Johannesson, Development of a generalized version of the Poisson-Nernst-Planck equations using the hybrid mixture theory: Presentation of 2D numerical examples, Transport porous med. 85 (2) (2010) 565–592.
[30] B. Li, B. Lu, Z. Wang, J. McCammon, Solutions to a reduced Poisson-Nernst-Planck system and determination of reaction rates, Physica A 389 (7) (2010) 1329–1345.
[31] J. Paz-García, K. Baek, I. Alshawabkeh, A. Alshawabkeh, A generalized model for transport of contaminants in soil by electric fields, J. Environ. Sci. Health, Part A 47 (2) (2012) 308–318.
[32] A. Alshawabkeh, Y. Acar, Electrokinetic remediation II: Theoretical model, J. Geotech. Eng-ASCE 122 (3) (1996) 186–196.
[33] C. Vereda-Alonso, J. Miguel Rodriguez-Maroto, R. Garcia-Delgado, C. Gómez-Lahoz, F. Garcia-Herruzo, Two-dimensional model for soil electrokinetic remediation of heavy metals: Application to a copper spiked kaolin, Chemosphere 54 (7) (2004) 895–903.
[34] C. Vereda-Alonso, C. Heras-Lois, C. Gomez-Lahoz, F. Garcia-Herruzo, J. Rodriguez-Maroto, Ammonia enhanced two-dimensional electrokinetic remediation of copper spiked kaolin, Electrochim. Acta 52 (10) (2007) 3366–3371.
[35] R. Jacobs, R. Probstein, Two-dimensional modeling of electroremediation, AIChE J. 42 (6) (1996) 1685–1696.
[36] E. Samson, J. Marchand, Numerical solution of the extended Nernst-Planck model, J. Colloid Interf. Sci. 215 (1) (1999) 1–8.
[37] R. Aringhieri, G. Pardini, Protonation of soil particle surfaces: Kinetics, Can. J. Soil Sci. 65 (4) (1985) 677–686.
[38] J. Rawlings, J. Ekerdt, Chemical reactor analysis and design fundamentals, Vol. 67, Nob Hill Publishing, 2002.
[39] C. Bethke, Geochemical and biogeochemical reaction modeling, 2nd Edition, Cambridge University Press, 2008.
[40] D. Parkhurst, C. Appelo, User's guide to PHREEQC (version 2) - A computer program for speciation, batch-reaction, one-dimensional transport, and inverse geochemical calculations, U.S. Department of the Interior, Water-Resources Investigations Reports (99-4259) (1999).
[41] W. Stumm, J. Morgan, Aquatic Chemistry; An Introduction Emphasizing Chemical Equilibria in Natural Waters by Werner Strumm and James J. Morgan, 2nd Edition, New York, Wiley-Interscience, 1970.
[42] W. Press, S. Teukolsky, W. Vetterling, B. Flannery, Root finding and nonlinear sets of equations, in: Numerical recipes in C: The art of Scientific Computing, Cambridge University Press, 1992, Ch. 9.
[43] M. Borkovec, J. Westall, Solution of the poisson-boltzmann equation for surface excesses of ions in the diffuse layer at the oxide-electrolyte interface, J. Electroanal. Chem. Interf. Electrochem. 150 (1-2) (1983) 325–337.
[44] D. Dzombak, F. Morel, Surface complexation modeling: Hydrous ferric oxide, Wiley-Interscience, 1990.
[45] R. Weast, M. Astle, W. Beyer, CRC handbook of chemistry and physics, Vol. 69, CRC Press Boca Raton, FL, 1988.
[46] O. Zienkiewicz, R. Taylor, The finite element method for solid and structural mechanics, Vol. 2, Butterworth-Heinemann, 2005.
[47] N. Ottosen, H. Petersson, Introduction to the finite element method, Prentice-Hall, 1992.

Paper

"Computing Chemical Equilibrium Systems with an Algorithm Based on the Reaction Extents"

J.M. Paz-García, B. Johannesson, L.M. Ottosen, A.B. Ribeiro and J.M. Rodríguez-Maroto

Submitted , *2012*

Computing Chemical Equilibrium Systems with an Algorithm Based on the Reaction Extents

J. M. Paz-García[a,*], B. Johannesson[a], L. M. Ottosen[a], A. B. Ribeiro[b], J. M. Rodríguez-Maroto[c]

[a] *Department of civil Engineering, Technical University of Denmark, Brovej, Building 118, Dk 2800 Kgs. Lyngby, Denmark.*
[b] *Department of Environmental Sciences and Engineering, Faculty of Sciences and Technology, New University of Lisbon, Caparica, Portugal*
[c] *Department of Chemical Engineering, Faculty of Sciences, University of Malaga, Campus de Teatinos, Malaga, Spain.*

Abstract

A mathematical model for the solution of a set of chemical equilibrium equations in a multi-species and multiphase chemical system is described. The computer-aid solution of model is achieved by means of a Newton-Raphson method enhanced with a line-search scheme, which deals with the non-negative constrains. The residual function, representing the distance to the equilibrium, is defined from the Gibbs energy of the chemical system. Local minimums are potentially avoided by the prioritization of the aqueous reactions with respect to the heterogeneous reactions. The formation and release of gas bubbles is taken into account in the model, limiting the concentration of volatile aqueous species to a maximum value, given by the Henry constant.

The reaction extents are used as state variables for the numerical method. As a result, the accepted solution satisfies the charge and mass balance equations and the model is fully compatible with general reactive transport models.

Keywords: Chemical equilibrium, Speciation, Reaction extent, Reactive transport

1. Introduction

1.1. Computing chemical equilibrium

Computing chemical equilibrium consists of the computer-aided mathematical calculation of the concentrations of a number of chemical species in chemical equilibrium state.

Chemical species in equilibrium are, indeed, in a dynamic equilibrium state; i.e. the reaction takes place at equal rates in its direct and reverse directions, so that the concentrations of the reacting substances (reactants and products) do not change with time. The chemical equilibrium assumption is equivalent to consider that all the species in the system have time enough to reach the equilibrium state. As a result, the time derivative of the chemical equations becomes zero and a set of non-linear algebraic equation (equilibrium equations) can be used to mathematically describe such a system.

The chemical equilibrium condition is restricted to a system described with a set of reversible reactions; i.e. no irreversible reactions take place in the chemical system, being handled in a specific manner. Naturally, the reliability of the chemical equilibrium assumption depends on the time scale for the speciation problem in which the reactions take place.

Mathematical models describing the equilibrium distribution of aqueous multi-species systems are common tools, for example, when fitting experimental data to chemical equilibrium state in a numerical speciation process. Speciation analysis is the analytical method of identifying and/or measuring the quantities of one or more individual chemical species in a chemical system [1]. When quantitative analytical methods for tracers are not accurate enough, chemical equilibrium models can be used to estimate concentrations of trace components based on analytical measurements of species with significantly higher concentrations. Other interesting applications are the study of the response of a chemical system in equilibrium with respect to external changes, the study of weathering mechanisms in geochemical systems and the chemical interactions between the pore solution and the solid matrix in porous materials such as concrete or others construction materials [2]. In all the above mentioned cases, the time scale is usually accepted to be large enough to justify the equilibrium assumption.

The model for computing chemical equilibrium presented here can be used in any of the aforementioned applications, but it is specifically designed to be used together with a more general reactive-transport model through porous media including electrode processes. In this kind of models, the rates of the main transport mechanisms in the process (diffusion, electromigration and electroosmosis) are slow enough for making the equilibrium assumption for the aqueous reactions in the pore solution electrolyte [3, 4]. According to Morel and Hering [5] aqueous reversible reactions (such as acid and bases dissociation or the wa-

*Corresponding author
Email address: jugra@byg.dtu.dk (J. M. Paz-García)

ter auto-ionization) have high values for the kinetic rates in both reaction directions (towards the products and towards the reactants) and, consequently, these kind of reactions can reach the equilibrium in the order of microseconds or faster. Aqueous complexation reactions are typically slower, but still in the range from micro- to milliseconds. In the case of heterogeneous reactions, such as adsorption/desorption or precipitation/dissolution, the kinetic rates decrease significantly compared to the above mentioned aqueous complexation reactions. Heterogeneous reactions kinetic rates may be in the same order of magnitude than the transport rates or even slower.

Models for reactive-transport in porous media have been presented taking into consideration the kinetics of the chemical system [6–9]. Nevertheless, models for reactive-transport under the chemical equilibrium assumption are more extensively used [10–18]. Combined models, including a set of feasible reactions able to reach the equilibrium in the time scale of the transport process and a parallel solution of the kinetic equations of slow or irreversible reactions, are considered the most realistic approach.

Thermodynamic equilibrium computer programs are available for the numerical speciation problem of chemical systems under the assumption of chemical equilibrium. Some of the most used are PHREEQC [19], PHREEQCi [20], WATEQ4F [21], MINTEQ [22], EQ3/6 [23] or GEMS [24]. It is not straightforward to couple these kind of stand-alone programs with more general codes for different purposes, such as reactive-transport or simulations of industrial scale processes. Exporting and importing data between different programs is a common solution, but in these cases the computational time increases to levels in which simulations become unfeasible. Consequently, the implementation of tailor-made codes is almost always necessary for more complex problems [18].

In [2] and [25], a detailed compilation of different proposed models for the mathematical solution of chemical equilibrium problems can be found. For the sake of simplicity, this literature review will not be repeated here.

Numerical strategies for computing chemical equilibrium problems are typically separated in two main groups: nonstoichiometric algorithms, in which a direct minimization of the Gibbs energy functions is used, and stoichiometric algorithms, based on the solution of the set of nonlinear equilibrium equations with mass balance constrains [25–27]. Evidently, the thermodynamic definition of chemical equilibrium states that stoichiometric methods are indirectly minimizing the Gibbs energy as well, which is the property measuring the distance to the equilibrium for a chemical system. In the present work, a stoichiometric method will be discussed. However, the thermodynamic definition of the chemical potential (and consequently the Gibbs energy of the chemical system) is used, showing the connection between the above mentioned models.

1.2. Main difficulties and limitations

Modeling of multiphase and multi-species chemical equilibrium problems is not a straightforward task. Apart from the time scale issue, which is the first limitation to be addressed in order to accept the equilibrium condition, some extra difficulties have to be taken into account.

1. Except for extremely simple cases, the high number of non-linear equations requires the use of numerical approaches. The Newton-Raphson (NR) method for non-linear equations is the most commonly used in this kind of problems [28, 29], and it is also the one used here.
2. Important difficulties arise when considering heterogeneous systems, since solids, gaseous, ionic and non-ionic aqueous species have different physical and chemical behavior, e.g. different chemical activities.
3. For a detailed solution of the problem, chemical activities have to be considered, accounting for the deviation from the ideal solution case. Theories to calculate the chemical activity are limited to a range of concentrations, which makes difficult to implement a general algorithm. Furthermore, for concentrated solutions, where the deviation from the ideal solution is more important, most of the activity theories fails leading to erroneous results.
4. The mathematical system of equations is limited to a number of physical constrains, e.g. concentrations are restricted to non-negative values, which has to be meticulously handled in the implementation.
5. Concentrations of the species vary over many orders of magnitude [2]. Most programming languages have difficulties to handle data with different orders of magnitude.
6. Low concentration values can lead to erroneous results or information losses. The machine epsilon (or eps, macheps) for a given programming language indicates the upper bound of the relative error due to rounding in floating point arithmetic[30]. A typical value for machesp is $2^{-52} \approx 2.22 \times 10^{-16}$. This means that the program will automatically round small values losing some information. For example, let y be the concentration of a trace species and $y < eps$. If, for any reason, the computer model have to sum the concentration of y with another value in the range of unity, the result will be rounded off in the form: $1 + y = 1$.

1.3. Compatibility with transport equations

The most accepted mathematical algorithm for chemical equilibrium calculations is based on the Morel's Tableau method [5, 18, 31]. This is an stoichiometric method in which the set of chemical species is divided in a number of master species (or components) and secondary species. Secondary species are defined as a combination of master species by means of stoichiometric equations (chemical equilibrium equations).

In the Morel's Tableau method, the concentration of master species is used as independent variable, and the residual function to be minimized in the numerical procedure is the mass balance for the chosen master species and the saturation index of the existing solid components. In most cases, the mass balance of protons is replaced by the charge balance equation. This is done for two reasons: to avoid considering the water as a chemical species in the setup and, to assure charge neutrality in the equilibrated solution.

The Morel's Tableau method has shown accurate results and it has been the base for many chemical equilibrium models. Unfortunately, difficulties arise when coupling the Nernst-Planck-Poisson system of transport equations with the above described method, since the small variations in the charge balance could produce oscillations in the electrical potential profile. The Nernst-Planck-Poisson system of equations can accurately describe the transport of chemicals through porous media in micro- and macroscale applications [16, 32–35]. A consequence of the above described standard calculation procedure is that the charge balance is slightly modified when calculating the electrical neutrality of the system. This means that, even though the electrical balance is assured to be lower than a predefined value, there will be some differences between the initial and final solutions in terms of the global charge. Transport terms depending on the electrical potential may be affected in an unrealistic and dramatic manner.

For this reasons, an alternative approach is proposed which has shown accurate results when coupled with both micro- and macroscale finite element reactive-transport models based on the Nernst-Planck-Poisson system of equation, where a thorough control of the mass balance and charge conservation principles is required. In this work, the Tableau concept is also used. But, instead of the concentration of master species, the extent of the reactions will be used as state variables and the reaction path from a non-equilibrium to the equilibrium state will be followed. The numerical implementation of the model is meticulously described in order to facilitate the reproducibility of the model.

2. Mathematical model

2.1. Stoichiometry of the chemical system

The analytical solution of the chemical equilibrium problem is performed by a set of non-linear algebraic equations, formulated from the mass balance and the action mass equations describing the chemical system [2, 36].

The total number of species, N, is divided into $(N - M)$ master species (or components) and M secondary species (or chemical reactions). For a given set of chemical species, the master species are freely chosen. The only condition is that any master species should represents one element in the chemical system [18].

For a set of N chemical species, the M stoichiometric equations are defined as:

Table 1: Terminology for the set of chemical species

Index	Meaning
$i = 1, 2, ..., N$	Chemical species
$j = 1, 2, ..., (N - M)$	Master species
$r = 1, 2, ..., M$	Equilibrium reactions

$$\sum_{i=1}^{N} \nu_{i,r} n_i = 0 \quad , \quad r = 1, 2, ..., M \tag{1}$$

where n_i (mol) denotes the total amount of the i^{th} species in the system and $\nu_{i,r}$ is the stoichiometric coefficient for the i^{th} species in the r^{th} reaction. The stoichiometric coefficients of the reactants, when they are written as products, are given negative values.

In the model presented here, stoichiometric equations have to be written in the form of dissociation or dissolution reactions with only one reactant. By definition, each secondary species participate only in the r^{th} stoichiometric equation that describes it and its stoichiometric coefficient is always $\nu_r = 1$, which becomes negative when defining the stoichiometric matrix. Accordingly, Equation (1) is rewritten as a function of the master and secondary species in the form:

$$\nu_r n_r \rightleftarrows \sum_{j=1}^{(N-M)} \nu_{j,r} n_j \quad , \quad r = 1, 2, ..., M \tag{2}$$

where now, n_j (mol) is used for the master species and n_r (mol) for the secondary species and $\nu_{j,r}$ is the stoichiometric coefficient for the j^{th} master species in the r^{th} reaction.

As mentioned before, stoichiometric equations have to be written in the form of dissociation or dissolution reactions with only one reactant. If a chemical equation has two or more reactants, one of them has to be chosen as the secondary species defined by the equation and the other reactants expressed as products of the reaction with negative stoichiometric coefficients. For example, in the auto-ionization reaction of water it is common to use water and the proton as master species and the hydroxide ion as a secondary species. Accordingly, the equilibrium reaction, typically written as:

$$H^+ + OH^- \rightleftarrows H_2O \tag{3}$$

is rewritten as:

$$OH^- \rightleftarrows H_2O - H^+ \tag{4}$$

where, for this stoichiometry, the master species H^+ has a negative stoichiometric coefficient. Equilibrium constants must be defined accordingly to the chosen stoichiometry.

Table 2: Chemical system resulting from the dissolution of $CaCO_3$ (s), $CaCl_2$ (s) and $Ca(OH)_2$ (s) in pure water or HCl solutions. Equilibrium constants for the given stoichiometry are obtained form [19].

Reaction	$\log(K_{eq})$
$OH^- \rightleftarrows H_2O - H^+$	14.00
$CaOH^+ \rightleftarrows H_2O - H^+ + Ca^{+2}$	12.78
$CaCl^+ \rightleftarrows Ca^{+2} + Cl^-$	0.29
$CaCl_2 \rightleftarrows Ca^{+2} + 2Cl^-$	0.64
$HCl \rightleftarrows H^+ + Cl^-$	0.71
$CaCO_3 \rightleftarrows Ca^{+2} + CO_3^{-2}$	-3.22
$CO_2^* \rightleftarrows -H_2O + 2H^+ + CO_3^{-2}$	-16.68
$HCO_3^- \rightleftarrows H^+ + CO_3^{-2}$	-10.33
$CaHCO_3^+ \rightleftarrows Ca^{+2} + H^+ + CO_3^{-2}$	-11.43
$CaCO_3$ (s) $\rightleftarrows Ca^{+2} + CO_3^{-2}$	-8.48
$CaCl_2$ (s) $\rightleftarrows Ca^{+2} + 2Cl^-$	11.77
$Ca(OH)_2$ (s) $\rightleftarrows 2H_2O - 2H^+ + Ca^{+2}$	22.81

In the following, we will used the chemical system resulting form the dissolution of $CaCO_3$ (s), $CaCl_2$ (s) and $Ca(OH)_2$ (s) in HCl solution, summarized in Table 2 as an example to illustrate the speciation model. In Section (4), test examples simulations are shown based on the chemical system described here.

The species CO_2 (g) is not included in the set of equations. The species CO_2^* (aq) represents the combination of carbonic acid H_2CO_3 (aq) and real CO_2 (aq) [37]. In aqueous solution carbonic acid exists in equilibrium with carbon dioxide, and the concentration of H_2CO_3 is much lower than the concentration of CO_2. It is very difficult to analytically distinguish both species, and individual equilibrium constant are not reliable. Consequently, the equilibrium constant used is based on the combination of both species into a single one [19].

The numerical method proposed here is based on the solution of a matrix system of non-linear equations. A matrix of stoichiometric coefficients (denoted as stoichiometric matrix) with M rows and $(N - M)$ columns is formed from the set of stoichiometric equations describing the system. Figure 1 shows the stoichiometric matrix, denoted as $\mathbf{M}$, for the example listed in Table 2. The full stoichiometric matrix must be extended with an identity matrix, symmetric with M rows and columns, with the negative stoichiometric coefficient of the secondary species defined for the chemical reactions.

2.2. Mass action equation

The chemical potential, μ_i $\left(\mathrm{J\,mol^{-1}}\right)$, is defined as the Gibbs energy of the species i, per mole unit, at a given temperature and pressure [2, 38]:

$$\mu_i = \mu_i^{\Theta} - RT \ln a_i \tag{5}$$

where a_i (dimensionless) is the chemical activity, μ_i^{Θ} is the standard chemical potential, R $\left(\approx 8.314\,\mathrm{J\,K^{-1}\,mol^{-1}}\right)$ is

	H_2O	H^+	Ca^{+2}	CO_3^{-2}	Cl^-
OH^-	1	-1	0	0	0
$CaOH^+$	1	-1	1	0	0
$CaCl^+$	0	0	1	0	1
$CaCl_2$	0	0	1	0	2
HCl	0	1	0	0	1
$CaCO_3$	0	0	1	1	0
CO_2^*	-1	2	0	1	0
HCO_3^-	0	1	0	1	0
$CaHCO_3^+$	0	1	1	1	0
$Ca(OH)_2$ (s)	2	-2	1	0	0
$CaCl_2$(s)	0	0	1	0	2
$CaCO_3$ (s)	0	0	1	1	0

Figure 1: Stoichiometric matrix for the chemical system summarize in Table 2. A squared identity matrix with the negative stoichiometric coefficients related to the defined secondary species must be added.

the universal gas constant and T (K) is the absolute temperature. The total chemical potential μ_r (or Gibbs energy $\Delta G_r = \mu_r$) for the r^{th} chemical reaction, is obtained from the summation along the reactants and products using the corresponding stoichiometric coefficient (with negative coefficients for reactants).

$$\mu_r = \sum_{i=1}^{N} \nu_{i,r} \mu_i^{\Theta} + RT \sum_{i=1}^{N} \nu_{i,r} \ln a_i \tag{6}$$

At the equilibrium, the Gibbs energy tends to zero. Defining the Standard Gibbs energy for the r^{th} reaction as:

$$\Delta G_r^{\Theta} = \sum_{i=1}^{N} \nu_{i,r} \mu_i^{\Theta} \tag{7}$$

and the equilibrium constant for the r^{th} chemical reaction, $K_{\text{eq},r}$, as:

$$K_{\text{eq},r} = \exp\left(-\frac{\Delta G_r^{\Theta}}{RT}\right) \tag{8}$$

the mass action equation or equilibrium equation (9) is easily obtained:

$$\prod_{i=1}^{N} a_{i,\text{eq}}^{\nu_{i,r}} = K_{\text{eq},r} \tag{9}$$

where $a_{i,\text{eq}}$ is the activity for the concentrations at the equilibrium state.

2.3. Extent of the reaction

When N chemical species in non-equilibrium react with each other to reach the chemical equilibrium state, a mass conservation equation can be described as a function of the extent of the reaction x_r. The extent of reaction (or reaction progress) is the extensive quantity describing the

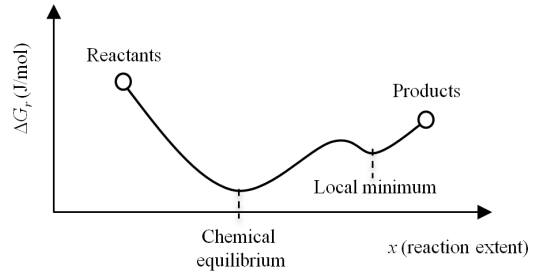

Figure 2: Chemical equilibrium as a function of the reaction extent

progress of a chemical reaction equal to the number of chemical transformations [1]. In order to reach the chemical equilibrium state, any reversible reaction can proceed towards the products or towards the reactants, meaning that x_r can be either a positive or a negative value.

The total amount of each species at the equilibrium is given by the mass balance equation along the chemical reaction path, in the form of:

$$n_{i,\text{eq.}} = n_{i,\text{init.}} + \sum_{r=1}^{M} x_r \nu_{i,r} \quad ; \quad i = 1,\, 2,\, ...,\, N \tag{10}$$

In matrix notation, this equation is:

$$\mathbf{n}_{eq.} = \mathbf{n}_{\text{init.}} + \mathbf{x}\mathbf{M} \tag{11}$$

where $\mathbf{n} = \left[\ n_1,\, n_2,\, \cdots,\, n_N\ \right]$ is a vector containing the molar quantities of all species and $\mathbf{x} = \left[\ x_1,\, x_2,\, \cdots,\, x_M\ \right]$ is the vector containing the reaction extents for the M considered reactions. The vector $\mathbf{x}$ will be used as the independent state variable in the numerical method.

2.4. The non-equilibrium equation

When the concentration of species in the system is not at chemical equilibrium state ($a_i \neq a_{i,\text{eq}}$), equation (9) will not be satisfied, that is:

$$\prod_{i=1}^{N} a_i^{\nu_{i,r}} \neq K_{\text{eq},r} \quad ; \quad r = 1, 2, ..., M \tag{12}$$

The residual function $f_r(\mathbf{x})$ is defined as a measure of the Gibbs energy of the chemical system according to the thermodynamic description of the chemical potential [2]. The residual function tends to zero when the system approaches to the equilibrium. Thus, the function $f_r(\mathbf{x})$ represents the distance to the equilibrium state for the r^{th} reversible reaction. Using logarithms, $f_r(\mathbf{x})$ can be expressed from the equation (12) as:

$$f_r(\mathbf{x}) = \sum_{r=1}^{M} (\nu_{i,r} \ln a_i) - \ln K_{\text{eq},r} \tag{13}$$

The vector-function $\mathbf{f}(\mathbf{x})$ compiles the value of $f_r(\mathbf{x})$, defined in equation (13), for the complete set of M reactions. $\mathbf{f}(\mathbf{x})$ is the function to minimize by the numerical method. The goal is to obtain a vector $\mathbf{x}$ that approaches the system to the equilibrium, e.i. $\mathbf{f}(\mathbf{x}) = 0$. In this context, the minimization of $\|\mathbf{f}(\mathbf{x})\|$, scalar value resulting from the norm of the vector $\mathbf{f}(\mathbf{x})$, is addressed, which is equivalent to a least square minimization technique.

$$\mathbf{f}(\mathbf{x}) = \begin{bmatrix} f_1(\mathbf{x}) \\ f_2(\mathbf{x}) \\ \vdots \\ f_M(\mathbf{x}) \end{bmatrix} \tag{14}$$

Let $\mathbf{a}$ and $\mathbf{k}$ be the vectors resulting from the natural logarithm of the activity and equilibrium constant of the M chemical reactions in the system.

$$\mathbf{a}(\mathbf{x}) = \begin{bmatrix} \ln a_1(\mathbf{x}) \\ \ln a_2(\mathbf{x}) \\ \vdots \\ \ln a_M(\mathbf{x}) \end{bmatrix} \tag{15}$$

$$\mathbf{k} = \begin{bmatrix} \ln K_{\text{eq},1} \\ \ln K_{\text{eq},2} \\ \vdots \\ \ln K_{\text{eq},M} \end{bmatrix} \tag{16}$$

Using the vectors $\mathbf{f}$, $\mathbf{a}$ and $\mathbf{k}$, equation (13) can be expressed in matrix notation as:

$$\mathbf{f}(\mathbf{x}) = \mathbf{M}\,\mathbf{a}(\mathbf{x}) - \mathbf{k} \tag{17}$$

For the numerical procedure both decimal and natural logarithm can be used. Nevertheless, even though the decimal logarithm is a more intuitive choice when defining the equilibrium constants, the natural logarithm is usually computed faster than the decimal logarithm in most programming languages. For this reason, equilibrium constants are converted to the natural logarithm scale for the model.

2.5. Aqueous equilibrium

The activity value of each species is obtained from the amount $n_i(\mathbf{x})$ calculated in each numerical iteration step. The activity is defined from the molal concentration c_i $\left(\text{mol}\,\text{kg}^{-1}\right)$, the standard concentration $c_i^{\ominus}$ $\left(\text{mol}\,\text{kg}^{-1}\right)$ necessary to ensure that the activity is dimensionless with a standard value of unity, and the activity factor γ_i (dimensionless) [19, 38].

$$a_i = \gamma_i \frac{c_i}{c_i^{\ominus}} \tag{18}$$

For convenience, the first species in the set of chemical species is reserved for the water, and its chemical activity is always set to the unity value. The concentrations for aqueous species are obtained by referring the amount of moles n_i to the mass of water, as

$$c_i = \frac{n_i}{m_{\mathrm{H_2O}}\, n_{\mathrm{H_2O}}} \tag{19}$$

where $m_{\mathrm{H_2O}} = 18 \times 10^{-3}\ \left(\mathrm{kg\,mol^{-1}}\right)$ is the molecular mass of water.

Activity coefficients of ionic aqueous species are calculated using the Davies equation (20), which is an empirical extension of the Debye-Hückel equation [38]. The Davies equation is considered to be a reasonable approximation even at relatively high ionic concentrations.

$$\ln \gamma_i = A z_i^2 \left(\frac{\sqrt{I}}{1+\sqrt{I}} - 0.3I \right) \tag{20}$$

where $A = -1.172\ (\mathrm{kg\,mol^{-1}})^{1/2}$ is a constant with the given value when the natural logarithm is used and the concentrations are expressed in molality units, $z_i\ \left(\mathrm{mol\,mol^{-1}}\right)$ is the ionic charge of the i^{th} ion and $I\ \left(\mathrm{mol\,kg^{-1}}\right)$ is the ionic strength of the electrolyte media, calculate by:

$$I = \frac{1}{2} \sum_{i=1}^{N} c_i z_i^2 \tag{21}$$

For the case of non-ionic aqueous species, the activity factor is obtained using the Setschenow relation, as

$$\ln \gamma_i = b_i\, I \tag{22}$$

where b_i is the Setschenow coefficient. In this work, $b_i = 0.1$ is used for all non-charged aqueous species, as done in [19].

The validity of the Davies and Setschenow equations is limited to values of ionic strength equal to or lower than 0.5 [2]. Over this limit, spurious results may be obtained. Different approaches, such as the Specific Ion Interaction Theory (SIT) [39] and the Pitzer activity coefficients [40] can be used to increase the range of validity of the activity coefficients.

3. Numerical implementation

3.1. Newton-Raphson method for non-linear system of equations with line-search enhancement

The value of the reaction extents vector $\mathbf{x}$ that assures global equilibrium is obtained by an iterative procedure based on a NR method with a line-search technique to satisfy the non-negative constrain [29]. The numerical procedure is summarized in the pseudo-code shown in appendix (1).

The NR method for non-linear matrix system of equations indicates the next iteration value for the unknowns, $\mathbf{x}_{\mathrm{new}}$, obtained from the present value, $\mathbf{x}_{\mathrm{old}}$, by adopting a numerical increment, $\delta\mathbf{x}$, towards the direction that decreases the global residual function.

$$\mathbf{x}_{\mathrm{new}} = \mathbf{x}_{\mathrm{old}} + \delta\mathbf{x} \tag{23}$$

The Taylor's series expansion of the residual function $\mathbf{f}(\mathbf{x})$ is used.

$$\mathbf{f}\left(\mathbf{x}_{\mathrm{new}}\right) = \mathbf{f}\left(\mathbf{x}_{\mathrm{old}}\right) + \mathbf{J}\delta\mathbf{x} + \mathbf{O}\left(\delta\mathbf{x}\right)^2 \tag{24}$$

where $\mathbf{O}(\delta\mathbf{x})^2$ represents the error related to terms with order greater than 2 and $\mathbf{J}$ is the Jacobian matrix of partial derivatives defined as:

$$\mathbf{J} = \left[\begin{array}{ccc} \frac{\partial \mathbf{f}}{\partial x_1} & \cdots & \frac{\partial \mathbf{f}}{\partial x_M} \end{array} \right] = \left[\begin{array}{ccc} \frac{\partial f_1}{\partial x_1} & \cdots & \frac{\partial f_1}{\partial x_M} \\ \vdots & \ddots & \vdots \\ \frac{\partial f_M}{\partial x_1} & \cdots & \frac{\partial f_M}{\partial x_M} \end{array} \right] \tag{25}$$

Ignoring the term $\mathbf{O}(\delta\mathbf{x})^2$, equation (24) becomes:

$$\mathbf{f}\left(\mathbf{x}_{\mathrm{new}}\right) = \mathbf{f}\left(\mathbf{x}_{\mathrm{old}}\right) + \mathbf{J}\,\delta\mathbf{x} \tag{26}$$

The next step in the NR method adopted will be given from the fact that the target is to obtain $\mathbf{f}\left(\mathbf{x}_{\mathrm{new}}\right) = \mathbf{0}$. Therefore, the increment in the extent of all considered reactions is obtained as:

$$\delta\mathbf{x} = -\mathbf{J}^{-1}\mathbf{f}\left(\mathbf{x}_{\mathrm{old}}\right) \tag{27}$$

As mentioned before the vector $\delta\mathbf{x}$ indicates the direction in which the residual decreases but it carries no information about the magnitude of the increment in the extent of the reactions.

The system of equations considered is constrained to non-negative values for the concentrations of all species. For this reason, a line-search enhancement is used in the NR method described above. Line-search iterative methods usually require an important computational effort [29] what means a long run time, due to a large number of iterations until convergence. But they are indispensable in order to satisfy the non-negative constrain of the physical problem in any iteration. This is not only because of the uncertainty in the solution, but also for the limitation of using logarithm functions which will not allow the use of negative values.

A scalar factor λ is used to control the magnitude of the increment calculated by the NR method. Equation (28) is used instead of equation (23).

$$\mathbf{x}_{\mathrm{new}} = \mathbf{x}_{\mathrm{old}} + \lambda\delta\mathbf{x} \tag{28}$$

The optimal λ value is obtained by a try-and-error algorithm, following a decreasing sequence given by the geometric progression according to equation (29), with an initial value of $\lambda_0 = 1$.

$$\lambda_{\mathrm{new}} = \lambda_{\mathrm{old}}/10 \tag{29}$$

3.2. Computing the Jacobian

The analytical calculation of the Jacobian matrix is difficult due to the non-linearity of the system of equations. A numerical procedure is used based on a central differences vector differentiation.

$$\frac{\partial \mathbf{f}(\mathbf{x})}{\partial x_r} = \frac{\mathbf{f}(\mathbf{x} + \Delta x_r) - \mathbf{f}(\mathbf{x} - \Delta x_r)}{2\Delta x_r} \tag{30}$$

The increment Δx_r used in the calculation of the Jacobian plays an important role in the convergence capability of the problem. The reaction extent of the different equilibrium equations may differ significantly, and therefore a constant Δx_r find unwanted local minimums which may ruin the iterative approach. In order to elude this problem, the value Δx_r used is scaled to the value of the vector $\mathbf{x}$ during any iteration:

$$\Delta x_r = \begin{cases} \Delta h_{\min} & if\ |x_r| = 0 \\ |x_r|\,\Delta h & if\ |x_r| > 0 \end{cases} \tag{31}$$

where $\Delta h_{\min}$ is 10^{-30}, and Δh is a value between 10^{-10} and 10^{-20}. The value Δh is decreased ten times in the "Converge strategies" function when the model is not able to minimize the residual.

The numerical calculation of the Jacobian matrix typically requires significant amount of computational time. In the algorithm presented in appendix (2) we propose a vectorized implementation for computing the numerical Jacobian. In this context, vectorized implementation means that no loops are used for the calculation of the Jacobian. Instead, only matrix algebra operators are used. As the Jacobian matrix is computed several times during the process, using a vectorized algorithm, as the one proposed here, one can make the the calculation between 10 to 100 times faster than compared to using computational "for" or "while" loops.

3.3. Precipitation/dissolution heterogeneous equilibrium

Heterogeneous precipitation and dissolution reactions have some key differences with respect to the aqueous complexation. The former kind of reactions require specific care in the numerical implementation.

For example, the activity of solids is, by definition, set to unity. Consequently, in the mass action equation for precipitation/dissolution reactions, the excess of solids in saturated solutions does not affect the concentration of aqueous species.

The existence of solid species is limited by the saturation index, which determines if the electrolyte solution is saturated or undersaturated with respect to the solid defined by a precipitation/dissolution reaction. Indeed, the equilibrium constant for a precipitation/dissolution reaction is typically denoted as solubility product, $K_{eq,\,r}$. The value of the residual function $f_r(\mathbf{x})$ can be used as an indicator of the saturation index, in the form:

$$\begin{cases} f_r(\mathbf{x}) < 0 & undersaturated \\ f_r(\mathbf{x}) \geq 0 & saturated \end{cases} \tag{32}$$

In undersaturated solutions, for an specific precipitation/dissolution reaction, the solid is completely dissolved and it does not participate in the equilibrium process. Therefore, its chemical equilibrium equation must be ignored. The numerical procedure, for any iteration, consists of

1. Identifying the reactions that are undersaturated, i.e. $f_r(\mathbf{x}) < 0$
2. Forcing the reaction extent for undersaturated reactions to be the maximum (complete dissolution).
3. Ignoring the contribution of $f_r(\mathbf{x}) < 0$ to the calculation of the global residual $\|\mathbf{f}(\mathbf{x})\|$.

In conditions close to the equilibrium state, the property $f_r(\mathbf{x})$ can oscillate around the value of zero, and so the reaction can oscillate around the saturated/under-saturated status during the speciation process. Consequently, this strategy has to be followed in any iteration.

Using the density and the molecular mass, the volume fraction occupied by the solution and the solids can be measured. As a result, the porosity of the porous media can be calculated, which is a very important parameter in the case of reactive-transport modeling [16].

3.4. Local minimum and precipitation/dissolution kinetics

As mention before, the NR method can fail in obtaining a correct solution when the initial estimation of the independent variable is far from the final solution. In chemical equilibrium systems, the failure in the convergence occurs because the solution drops into a local minimum state, as illustrated for example by Brassard et al.[27].

In some situations, an specific reaction should proceed towards the contrary direction suggested by the NR method, i.e. it has to proceed towards an increase of its residual function $f_r(\mathbf{x})$ in order to decrease the global residual $\mathbf{f}(\mathbf{x})$. An illustrative example of this problem could be the dissolution of kaolin:

$$Al_2Si_2O_5(OH)_4 + 6H^+ \rightleftarrows H_2O + 2H_4SiO_4 + 2Al^{+3} \tag{33}$$

Equation (33) shows the dissolution reaction of kaolinite as a function of the master species H^+, H_2O, H_4SiO_4 and Al^{+3}. According to this stoichiometry, and the Le Châtelier´s principle, an external increment in the pH in the system containing kaolinite should produce the precipitation of the mineral, what is characterized with a release of protons which will counteract the pH change. On the other hand, the pH also affects to the species H_4SiO_4 and Al^{+3}. H_4SiO_4 is an acid and can dissociate releasing protons, and Al^{+3} reacts with hydroxides to form different aluminum hydroxides. Consequently, the kaolin is forced to precipitate, due to the pH increase, but it also is forced

to dissolved to counteract the consumption of H_4SiO_4 and Al^{+3}, due to the same pH change. This kind of situations can in some instances lead to the development of a local minimum.

If one takes into account the kinetic rates of the reaction, it can be assured that the aqueous complexation reactions of H_4SiO_4 and Al^{+3} are faster than the precipitation/dissolution reaction. So, these two aqueous species would react first in order to counteract the pH changes, and so the kaolinite would be forced to the dissolution. This is congruent with the experimental results shown in [41].

According to this concept, the "Convergence strategies" function, listed in algorithm (1), included a mechanism to ignore all solids reactions under certain conditions.

3.5. Convergence strategies

The main disadvantage of using the reaction extent as the state variable is that there is a moderate high risk to fall into a local minimum (or relative minimum), as illustrated in Figure 2. The probability of finding local minimums is proportional to the distance to the equilibrium from the initial set of concentrations. In order to minimize this problem, an initial estimation of the state variable $\mathbf{x}$ is needed. In a dynamic problem, such as a reactive transport process, if the time increment for the numerical integration is short enough, the distance to the equilibrium is small and a initial estimation of $\mathbf{x} = \mathbf{0}$ uses to be valid.

In order to reduce the risk of finding local minimums, some extra considerations has been taken. In this context, the "Convergence strategies" function, listed in algorithm (1), acts as following:

1. If the residual $\|\mathbf{f}(\mathbf{x})\|$ is not minimized for a certain number of iterations, the incremental parameter for the numerical calculation of the Jacobian is reduced ten times, i.e. $\Delta h_{\text{new}} = \Delta h_{\text{old}}/10$
2. If using the value Δh_{new} the residual $\|\mathbf{f}(\mathbf{x})\|$ is not reduced, it would be accepted that the system has found a local minimum. For the next iteration, all solids reactions would be ignored, allowing the aqueous complexation reactions to get equilibrium without the influence of the solids. This is equivalent to distinguish between the kinetic rate of the precipitation/dissolution reactions and the aqueous complexation reactions.
3. If the value Δh_{min} is reached and, even though, the residual $\|\mathbf{f}(\mathbf{x})\|$ is not reduced, the local minimum is accepted as a valid result. A better initial estimation of the vector $\mathbf{x}$ or a shorter distance from the initial set of concentrations to the equilibrium is needed to decrease the residual to the absolute minimum.

3.6. Vapor-liquid heterogeneous equilibrium

The activity for the i^{th} gaseous species (fugacity) is defined from the partial pressure, $P_{i(\text{g})}$ (atm) in the unique gas phase.

$$a_i = \gamma_i \frac{P_i}{P_i^{\Theta}} \tag{34}$$

Henry's law states that, at a constant temperature, the amount of a given gas dissolved in a volume of liquid is directly proportional to the partial pressure of that gas in equilibrium with that liquid, by means of the so-called Henry´s constant.

$$P_{i(\text{g})} = K_{\text{H}}\, c_{i(\text{aq})} \tag{35}$$

For example, the concentration of gaseous carbonic acid would be given by:

$$\text{P}_{\text{CO}_2(\text{g})} = K_{\text{H}}\, c_{\text{CO}_2(\text{aq})} \tag{36}$$

This kind of approach is used to calculate the concentration of gaseous species in equilibrium with the liquid system in many geochemical speciation models, e.g. [19]. Nevertheless, vapor-liquid heterogeneous reactions are difficult to coupled with the previously described aqueous complexation and mineral dissolution reactions, because many extra assumptions are necessary.

For the case of chemical equilibrium models designed to be coupled with reactive-transport in porous media, some extra considerations have to be taken. For example, depending on the time scale of the speciation problem, assuming vapor-liquid equilibrium between the atmospheric species and the aqueous species can lead to unrealistic results. This is the case of the carbonic acid equilibrium. If we consider a porous material in contact with the atmosphere, being the atmospheric partial pressure of the carbon dioxide a constant value, the concentration of the species $CO_2(aq)$, HCO_3^-, CO_3^{-2} among others, would be fixed. Consequently, the system would be strongly buffered by the carbonic acid equilibrium. Rate constants for the reversible reaction between the gaseous and aqueous CO_2 equilibrium is slow with respect to the aqueous complexation reactions. Thus, the buffered capacity of the atmospheric $CO_2(aq)$ in the porous system would be overestimated if the equilibrium assumption is accepted.

According to this, a different approach is taken in this model. First, the system is assumed to be at constant pressure (normally 1 atm). Henry's equation is used to determine the partial pressure of the gaseous species in the system from the corresponding volatile aqueous species. If the partial pressure predicted by the Henry's equation is lower than the total pressure, these bubbles do not tend to scape from the porous structure. Consequently, they remain in the aqueous system or they are reabsorbed in form of the volatile aqueous species. In any case, the concentration of these gaseous species is considered together with the volatile aqueous species. On the other hand, if the concentration of aqueous species is such that the predicted bubbles have a partial pressure equal to or greater than the total pressure, bubbles release from the system, traveling

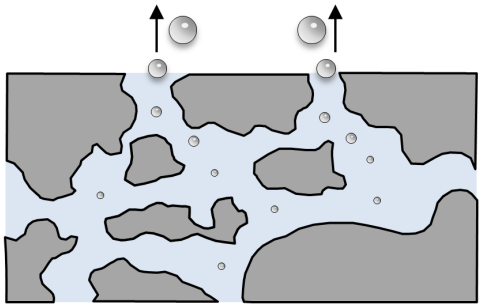

Figure 3: Release of bubbles from the porous system

trough the porous material and escaping, irreversibly, to the atmosphere, as shown in Figure (3).

Mathematically, this assumption is equivalent to consider a maximum limit value for the aqueous concentration of volatile compounds. For the case of CO_2 (g) at room temperature, the maximum CO_2(aq) concentration would be given by:

$$c_{\mathrm{CO_2(aq)}}\big|_{max} = \frac{1}{K_{\mathrm{H}}} = 3.36 \times 10^{-2} \left(\mathrm{mol\,kg^{-1}}\right) \qquad (37)$$

4. Test examples

A test example is shown based on the chemical system described in Table 2. In this test example, the concentration in equilibrium of calcite and portlandite in 1 kg of hydrochloric acid (HCl) solution at different concentrations is computed. For the simulations, the minerals are assumed in equilibrium with 1 kg of pure water. Hydrochloric acid is progressively dropped in the solution, to cover a a range from 0 until 0.6 mol per kg of water. The equilibrium concentration of aqueous species, the amount of precipitated solids and the pH are shown with respect to the amount of acid added to the system.

In Figure 4, the simultaneous dissolution of a mixture of 0.1 mol (10 g) of calcite ($CaCO_3$) and 0.1 mol (7.4 g) of portlandite ($Ca(OH)_2$) is shown. In Figure 5 and Figure 6, the individual dissolution of 0.2 mol of mineral is shown. In any case, a total of 1000 simulations are done to meet the entire range of HCl concentrations.

The chosen test example shows some of the main features of the model presented. It shown the concentration at the equilibrium in a very common multi-species and multiphase system. Two different solid phases are coexisting which dissolves in a different range of pH. Furthermore, moderate high concentrations are used to reach the saturation value of aqueous carbon dioxide associated with the release of gaseous carbon dioxide bubbles.

In Figure 4d, the amount of solids is shown with respect to the molal concentration of the hydrochloric acid solution. It can be seen that the dissolution process occurs in a sequential stage. Portlandite is more soluble than calcite. In pure water, about 20% of the initial portlandite was dissolved, while most of the calcite stays in mineral phase. When increasing the concentration of the acid, portlandite tends to dissolve. The mineral is completely dissolved when concentration of the acid is around 0.2 mol/kg. Afterward, calcite starts to dissolve to counteract the addition of extra acid in the media.

The dissolution of calcite and portlandite leads to high concentrations of ionic calcium, Ca^{+2}, as shown in Figure 4b. When both minerals are completely dissolved, the concentration of Ca^{+2} reaches a maximum. After that moment, increasing the hydrochloric acid concentration leads to the formation of the complexes $CaCl^+$ and $CaCl_2$ with a slightly decrease of the aqueous Ca^{+2}. Figure 4b also shows the limit value assigned to the aqueous carbon dioxide as a consequence of the restriction of maximum concentration. In this conditions, formation of bubbles of CO_2(g) is predicted when the concentration of acid is equal to or higher than approximately 0.28 mol/kg.

The pH value, shown in Figure 4a, stays approximately constant while there are mineral phases, showing the buffer capacity of the two solids considered. Portlandite keeps the media in alkaline conditions, as typically seen in cement-based materials. Calcite maintains the media in a slightly acid environment (pH = 5), as seen in calcareous materials. From Figure 5, it can be seen that the equilibrium pH of calcite in pure water is close to 10. The slightly acid environment (pH = 5) is obtained when the calcite is buffering a strong acid environment, such as the induced by the hydrochloric acid.

When any of the mineral phases completely dissolves, a pH drop is observed. In Figures 5 and 6, the individual dissolution of the minerals shown the same pH values than in the simultaneous dissolution. According to the results, when coexisting portlandite and calcite, the pH is determined by the portlandite equilibrium.

Figure 4c shows the concentration of the other aqueous species of interest in the system. According to the results shown here, when coexisting portlandite and calcite, the main secondary aqueous species, apart from OH^-, is the complex $CaOH^+$. When only calcite is precipitated, there are bicarbonate complexes in the system. As mentioned before, $CaCl^+$, $CaCl_2$ and HCl increases their concentration in the process, and they are the main secondary species when the mineral phases are completely dissolved.

Results from Figure 5b and Figure 6b are congruent with those obtained in Figure 4c. As mentioned before, results suggest that during the simultaneous dissolution of calcite and portlandite, the concentration of aqueous species and pH is determined by the portlandite while both minerals exist in precipitated form, i.e. in alkaline conditions.

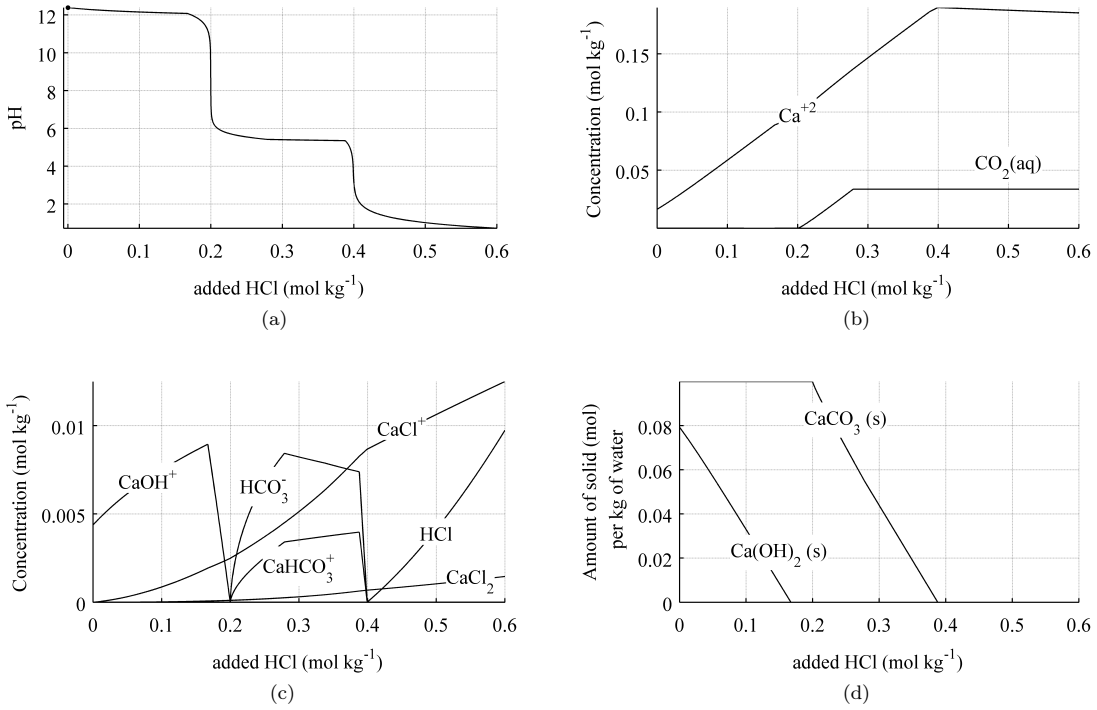

Figure 4: Simultaneous dissolution of portlandite and calcite versus added HCl

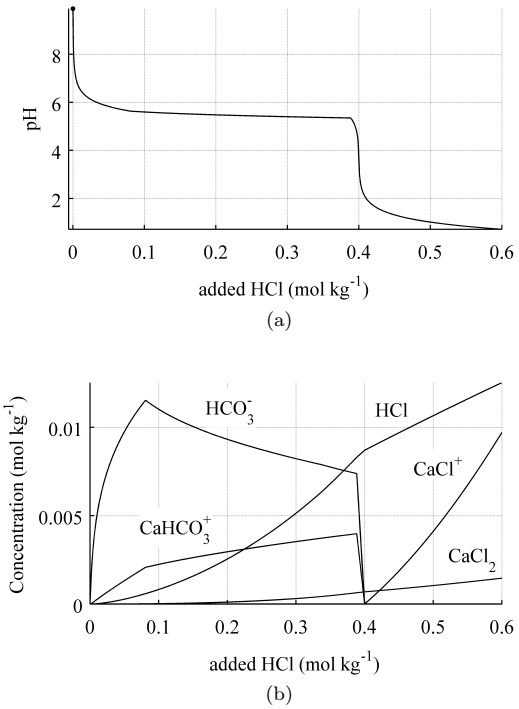

Figure 5: Dissolution of calcite versus added HCl

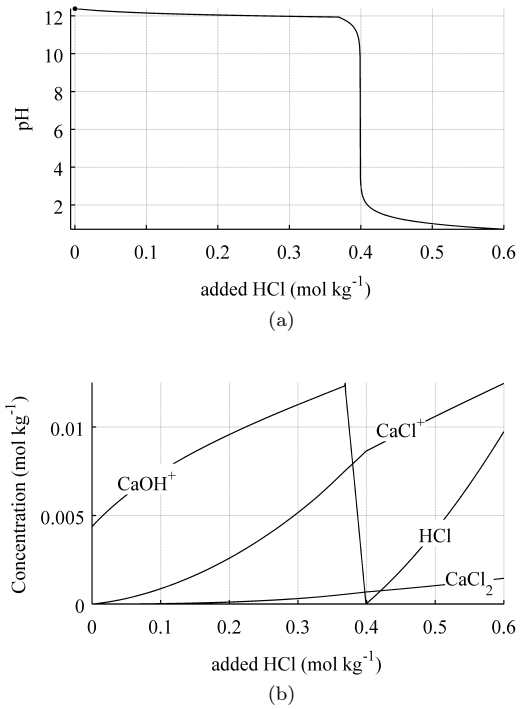

Figure 6: Dissolution of portlandite versus added HCl

Conclusions

A method for computing chemical equilibrium speciation problems has been described, based on the extent of each chemical reaction of the system. The numerical solution method is based on NR iterations in which the Jacobian matrix is formed by a numerical technique rather than being calculated analytically. Furthermore, a vectorized implementation of the Jacobian matrix is proposed in order to significantly reduce the computational time. A line search approach is used to deal with the non-negative concentrations constraint of all the chemical species.

The presented algorithm is designed to work in a multi-species and multiphase chemical systems under the assumption of chemical equilibrium. Problems associated with local minimums are potentially avoided by the prioritization of the aqueous reactions with respect to the solid dissolution or precipitation reactions. This prioritization method is based on the assumption that that the kinetic rates of reactions involving only aqueous species are faster than those involving solid mineral phases.

The formation of gaseous species is included in the model by allowing free release of gas bubbles of gaseous species when those bubbles have a higher pressure than the surrounding liquid media and vapor phase. This feature limits the concentration of volatile aqueous species to a maximum value given by the Henry constant.

A test example has been used to illustrate the main features of the model presented here. The use of the extent of the reactions as the state variable makes the presented algorithm suitable for more general problems, in which a thorough control of the electrical balance is required, such as the process of coupled chemical reaction and ionic transport through porous media by the Nernst-Planck-Poisson system of equations.

Acknowledgments

Authors acknowledge The Danish Agency of Science Technology and Innovation. This research was funded as part of the project "Fundamentals of Electrokinetics in In-homogeneous Matrices", with project number 274-08-0386. J.M. Rodríguez-Maroto acknowledges the financial support from the Ministerio de Ciencia e Innovación of the Spanish Government through the project ERHMES, CTM2010-16824, and FEDER funds.

AppendixA. Pseudo-codes

Algorithm 1 Pseudo-code for computing heterogeneous chemical equilibrium based on a Newton-Raphson scheme including a line-search technique iterating on the reaction extents. Concentrations and activity factors for the solvent and the solids are set to the unity for the calculation of the activity.

While $(\|\mathbf{f}(\mathbf{x}_{\text{new}})\| \geq \mathbf{f}_{\text{min}})$

1. Compute the Jacobian matrix
   - See Algorithm (2)
2. Newton-Raphson with boundary conditions
   - $\delta\mathbf{x} = -\mathbf{J}^{-1}\mathbf{f}(\mathbf{x}_{\text{old}})$
3. **While** $(\|\mathbf{f}(\mathbf{x}_{\text{new}})\| \geq \|\mathbf{f}(\mathbf{x}_{\text{old}})\|)$ or $(n_i < 0)$
   (a) Line-Search step
   - $\mathbf{x}_{\text{new}} = \mathbf{x}_{\text{old}} + \lambda\delta\mathbf{x}$

   (a) Compute the molar amounts
   - $\mathbf{n}_{\text{eq.}} = \mathbf{n}_{\text{init.}} + \mathbf{xM}$

   (b) Compute the concentrations
   - $c_i = \frac{n_i}{m_{H_2O}\, n_{\text{H}_2\text{O}}}$ — for aqueous species
   - $c_i = 1$ — for the solvent and the solids

   (c) Compute the activity factors
   - $I = \frac{1}{2}\sum_{i=1}^{N} c_i z_i^2$
   - $\ln\gamma_i = A z_i^2 \left(\frac{\sqrt{I}}{1+1.5\sqrt{I}} - 0.3I\right)$ — for ions
   - $\ln\gamma_i = b_i\, I$ — for uncharged species
   - $\ln\gamma_i = 1$ — for the solvent and the solids

   (d) Compute the activities
   - $a_i = c_i\gamma_i$
   - $\mathbf{a}(\mathbf{x}) = \begin{bmatrix} \ln a_1(\mathbf{x}) \\ \ln a_2(\mathbf{x}) \\ \vdots \\ \ln a_M(\mathbf{x}) \end{bmatrix}$

   (e) Compute the residual value $\|\mathbf{f}(\mathbf{x}_{\text{new}})\|$
   - $\mathbf{f}(\mathbf{x}) = \mathbf{M}\,\mathbf{a}(\mathbf{x}) - \mathbf{k}$
   - $\|\mathbf{f}(\mathbf{x}_{\text{new}})\|^2 = \mathbf{f}(\mathbf{x}_{\text{new}}) \cdot \mathbf{f}(\mathbf{x}_{\text{new}})$

   (f) Compute λ_{new}
   - $\lambda_{\text{new}} = \lambda_{\text{old}}/10$
4. **end (while loop)**
5. $\mathbf{x}_{\text{old}} = \mathbf{x}_{\text{new}}$
6. Convergence Strategies

end

Algorithm 2 Pseudo-code for the vectorized numerical calculation of the Jacobian matrix

1. Create a matrix $\mathbf{X}^{+\Delta\mathbf{X}}$ (size M by M) including the current value of the state variable $\mathbf{x}$ summed to a diagonal matrix with the finite increment for the numerical calculation of the derivatives:
   - $\mathbf{X}^{+\Delta\mathbf{X}} = \mathbf{X} + \mathrm{diag}(\Delta\mathbf{X})$

   where
   - $\mathbf{X}^{+\Delta\mathbf{X}} = \begin{bmatrix} x_1 + \Delta x_1 & \cdots & x_M \\ x_1 & \ddots & x_M \\ \vdots & \ddots & \vdots \\ x_1 & \cdots & x_M + \Delta x_M \end{bmatrix}$
2. Compute a matrix $\mathbf{N}$ (size M by N) with the molar amount of species, as a function of $\mathbf{X}^{+\Delta\mathbf{X}}$:
   - $\mathbf{N}_{eq.} = \mathbf{N}_{\text{init.}} + \mathbf{X}^{+\boldsymbol{\Delta}\mathbf{X}}\,\mathbf{M}$

   where $\mathbf{M}$ is the stoichiometric matrix (size M by N)
3. Compute the matrix $\mathbf{A}$ (size N by M) formed from the activities, using the matrix $\mathbf{N}_{eq.}$ and the same agreements for the concentrations and activity factors.
   - $\mathbf{A} = \begin{bmatrix} \mathbf{a}(\mathbf{x} + \Delta x_1) & \cdots & \mathbf{a}(\mathbf{x} + \Delta x_M) \end{bmatrix}$
4. Compute the residual matrix function, $\mathbf{F}\left(\mathbf{X}^{+\Delta\mathbf{X}}\right)$ (size M by M), as:
   - $\mathbf{F}\left(\mathbf{X}^{+\Delta\mathbf{X}}\right) = \mathbf{M}\,\mathbf{A} - \mathbf{K}$

   where $\mathbf{K} = \begin{bmatrix} \mathbf{k} & \mathbf{k} & \cdots & \mathbf{k} \end{bmatrix}$ is a matrix (size M by M) including M horizontal concatenations of $\mathbf{k}$, the vector of equilibrium constants.
5. Repeat the steps 1 to 4 with the value
   - $\mathbf{X}^{-\Delta\mathbf{X}} = \mathbf{X} - \mathrm{diag}(\Delta\mathbf{X})$
6. Compute the Jacobian matrix as:
   - $\mathbf{J} = \frac{\mathbf{F}\left(\mathbf{X}^{+\boldsymbol{\Delta}\mathbf{X}}\right) - \mathbf{F}\left(\mathbf{X}^{-\boldsymbol{\Delta}\mathbf{X}}\right)}{2\,\Delta\mathbf{X}}$

   where the latter division is done "term-by-term" instead of by standard matrix division, using the full matrix of increments in the form:
   - $\Delta\mathbf{X} = \begin{bmatrix} \Delta x_1 & \cdots & \Delta x_M \\ \vdots & \ddots & \vdots \\ \Delta x_1 & \cdots & \Delta x_M \end{bmatrix}$

References

[1] A. McNaught, A. Wilkinson, Compendium of Chemical Terminology: Iupac Recommendations, 2nd Edition, Blackwell Science, 1997.

[2] C. Bethke, Geochemical and biogeochemical reaction modeling, 2nd Edition, Cambridge University Press, 2008.

[3] R. Jacobs, R. Probstein, Two-dimensional modeling of electroremediation, AIChE J. 42 (6) (1996) 1685–1696.

[4] F. Herruzo, J. Maroto, R. Delgado, C. Lahoz, C. Alonso, Limpieza de suelos por electrodescontaminacion (I), Ing. Quim. 32 (369) (2000) 215–222.

[5] F. Morel, J. Hering, Principles and applications of aquatic chemistry, Wiley-Interscience, 1993.

[6] P. Lichtner, Continuum model for simultaneous chemical reactions and mass transport in hydrothermal systems, Geochim. Cosmochim. Acta 49 (3) (1985) 779–800.

[7] B. Johannesson, Ionic diffusion and kinetic homogeneous chemical reactions in the pore solution of porous materials with moisture transport, Comput. Geotech. 36 (4) (2009) 577–588.

[8] A. Ribeiro, J. Rodriguez-Maroto, E. Mateus, H. Gomes, Removal of organic contaminants from soils by an electrokinetic process: the case of atrazine. Experimental and modeling, Chemosphere 59 (9) (2005) 1229–1239.

[9] C. Steefel, P. Van Cappellen, A new kinetic approach to modeling water-rock interaction: The role of nucleation, precursors, and ostwald ripening, Geochim. Cosmochim. Acta 54 (10) (1990) 2657–2677.

[10] J. Rubin, Transport of reacting solutes in porous media: Relation between mathematical nature of problem formulation and chemical nature of reactions, Water Resour. Res 19 (5) (1983) 1231–1252.

[11] A. Javadi, M. Al-Najjar, Finite element modeling of contaminant transport in soils including the effect of chemical reactions, J. Hazard. Mater. 143 (3) (2007) 690–701.

[12] D. Wilson, J. Rodríguez-Maroto, C. Gómez-Lahoz, Electrokinetic remediation II. Amphoteric metals and enhancement with

a weak acid, Sep. Sci. Technol. 30 (16) (1995) 3111–3128.
[13] C. Vereda-Alonso, C. Heras-Lois, C. Gomez-Lahoz, F. Garcia-Herruzo, J. Rodriguez-Maroto, Ammonia enhanced two-dimensional electrokinetic remediation of copper spiked kaolin, Electrochim. Acta 52 (10) (2007) 3366–3371.
[14] C. Vereda-Alonso, J. Miguel Rodriguez-Maroto, R. Garcia-Delgado, C. Gómez-Lahoz, F. Garcia-Herruzo, Two-dimensional model for soil electrokinetic remediation of heavy metals: Application to a copper spiked kaolin, Chemosphere 54 (7) (2004) 895–903.
[15] J. Paz-García, K. Baek, I. Alshawabkeh, A. Alshawabkeh, A generalized model for transport of contaminants in soil by electric fields, J. Environ. Sci. Health, Part A 47 (2) (2012) 308–318.
[16] J. Paz-García, B. Johannesson, L. Ottosen, A. Alshawabkeh, A. Ribeiro, J. Rodríguez-Maroto, Modeling of electrokinetic desalination of bricks, Electrochim. Acta.
[17] A. Al-Hamdan, K. Reddy, Electrokinetic remediation modeling incorporating geochemical effects, J. Geotech. Geoenviron. 134 (2008) 91–105.
[18] J. Rodriguez-Maroto, C. Vereda-Alonso, Electrokinetic modeling of heavy metals, in: K. Reddy, C. Camesselle (Eds.), Electrochemical Remediation Technologies for Polluted Soils, Sediments and Groundwater, Wiley Online Library, 2009, Ch. 25, pp. 537–562.
[19] D. Parkhurst, C. Appelo, User's guide to PHREEQC (version 2) - A computer program for speciation, batch-reaction, one-dimensional transport, and inverse geochemical calculations, U.S. Department of the Interior, Water-Resources Investigations Reports (99-4259) (1999).
[20] S. Charlton, C. Macklin, D. Parkhurst, Phreeqci—a graphical user interface for the geochemical computer program phreeqc, Water Resources Investigation Report 97 (1997) 4222.
[21] J. Ball, D. Nordstrom, G. S. (US), User's manual for wateq4f, with revised thermodynamic data base and test cases for calculating speciation of major, trace, and redox elements in natural waters.
[22] S. Peterson, C. Hostetler, W. Deutsch, C. Cowan, Minteq user's manual, Tech. rep., Pacific Northwest Lab., Richland, WA (USA); Nuclear Regulatory Commission, Washington, DC (USA). Div. of Waste Management (1987).
[23] T. Wolery, L. L. N. Laboratory, U. S. D. of Energy, EQ3/6: A software package for geochemical modeling of aqueous systems: package overview and installation guide (version 7.0), Lawrence Livermore National Laboratory, 1992.
[24] N. Remy, Geostatistical earth modeling software: User's manual, Stanford Center for Reservoir Forecasting (SCRF), Stanford University, California, USA.
[25] M. Reed, Calculation of multicomponent chemical equilibria and reaction processes in systems involving minerals, gases and an aqueous phase, Geochim. Cosmochim. Acta 46 (4) (1982) 513–528.
[26] J. Carrayrou, R. Mosé, P. Behra, New efficient algorithm for solving thermodynamic chemistry, AIChE J. 48 (4) (2002) 894–904.
[27] P. Brassard, P. Bodurtha, A feasible set for chemical speciation problems, Computers & Geosciences 26 (3) (2000) 277–291.
[28] T. Wolery, L. Walters, Calculation of equilibrium distributions of chemical species in aqueous solutions by means of monotone sequences, Mathematical Geology 7 (2) (1975) 99–115.
[29] W. Press, S. Teukolsky, W. Vetterling, B. Flannery, Root finding and nonlinear sets of equations, in: Numerical recipes in C: The art of Scientific Computing, Cambridge University Press, 1992, Ch. 9.
[30] C. Moler, Numerical computing with MATLAB, Society for Industrial Mathematics, 2004.
[31] F. Morel, J. Morgan, Numerical method for computing equilibriums in aqueous chemical systems, Environmental Science & Technology 6 (1) (1972) 58–67.
[32] J. Paz-Garcia, B. Johannesson, L. Ottosen, A. Ribeiro, J. Rodriguez-Maroto, Modeling of electrokinetic processes by finite element integration of the Nernst-Planck-Poisson system of equations, Sep. Purif. Technol. 79 (2) (2011) 183–192.
[33] B. Johannesson, Diffusion of a mixture of cations and anions dissolved in water, Cem. Concr. Res. 29 (8) (1999) 1261–1270.
[34] B. Johannesson, Y. Hosokawa, K. Yamada, Numerical calculations of the effect of moisture content and moisture flow on ionic multi-species diffusion in the pore solution of porous materials, Comput. Struct. 87 (1-2) (2009) 39–46.
[35] B. Lu, M. Holst, J. Andrew McCammon, Y. Zhou, Poisson-Nernst-Planck equations for simulating biomolecular diffusion-reaction processes I: Finite element solutions, J. Comput. Phys. 229 (19) (2010) 6979–6994.
[36] J. Rawlings, J. Ekerdt, Chemical reactor analysis and design fundamentals, Vol. 67, Nob Hill Publishing, 2002.
[37] N. Greenwood, A. Earnshaw, Knovel, Chemistry of the Elements, Pergamon press Oxford etc., 1984.
[38] W. Stumm, J. Morgan, Aquatic Chemistry; An Introduction Emphasizing Chemical Equilibria in Natural Waters by Werner Strumm and James J. Morgan, 2nd Edition, New York, Wiley-Interscience, 1970.
[39] E. Guggenheim, J. Turgeon, Specific interaction of ions, Trans. Faraday Soc. 51 (1955) 747–761.
[40] K. Pitzer, Thermodynamics of electrolytes I. Theoretical basis and general equations, J. Phys. Chem. 77 (2) (1973) 268–277.
[41] S. Carroll, J. Walther, Kaolinite dissolution at 25, 60, and 80 c, Am. J. Sci 290 (7) (1990) 797–810.

Paper

"Simulation-based Analysis of the Differences in the Removal Rate of Chlorides, Nitrates and Sulfates by Electrokinetic Desalination"

J.M. Paz-García, B. Johannesson, L.M. Ottosen, A.B. Ribeiro and J.M. Rodríguez-Maroto

Submitted , *2012*

Simulation-based Analysis of the Differences in the Removal Rate of Chlorides, Nitrates and Sulfates by Electrokinetic Desalination Treatments

J. M. Paz-García[a,*], B. Johannesson[a], L. M. Ottosen[a], A. B. Ribeiro[b], J. M. Rodríguez-Maroto[c]

[a] *Department of Civil Engineering, Technical University of Denmark, Lyngby, Denmark.*
[b] *CENSE-Departamento de Ciências e Engenharia do Ambiente, Faculdade de Ciências e Tecnologia, Universidade Nova de Lisboa, Campus de Caparica, Portugal.*
[c] *Departamento de Ingeniería Química, Facultad de Ciencias, Universidad de Málaga, Málaga, Spain.*

Abstract

Due to their abundance in the natural environment, chlorides, nitrates and sulfates salts are considered the main responsible for the salt-induced decay processes in building materials and sculptures. Electrokinetic desalination techniques have been successfully applied for the prevention of salt-induced deterioration problems of masonry and other construction materials. It has been experimentally proved that the removal rate of sulfates is considerably slower than chloride and nitrate during electro-desalination treatments when a enhanced desalination technique is used where carbonated clay buffer poultice is placed between the surface of the stone and the electrodes.

A physicochemical model for electrochemically-induced reactive-transport processes is described and used for a theoretical analysis of the influence of the chemical interactions on the removal rate of the target ions. Simulations for the electro-desalination of a brick sample contaminated with a combination of these target ions are shown. Results from simulations show that the lower removal efficiency of sulfates is related to the formation of precipitated gypsum inside the porous body.

Keywords: Electrokinetic desalination, Salt-decay, Reactive-transport modeling, Poisson-Nernst-Planck system

1. Introduction

1.1. Salt-decay on building materials and sculptures

Salt-induced decay of porous construction materials is a severe cause of damage on buildings and sculptures. All over the world historic buildings, monuments, sculptures and frescoes are, in some degree, affected by this kind of material weathering. Most of the problems caused by salt-induced decay are merely visual. Nevertheless, in some cases, salt decay lead to structural problems, as e.g. loss of strength and bearing capacity, related to internal cracks and surface detachment. In the case of cultural heritage, the loss of surface is unacceptable [1–3]. Some other types of damage are the detachment of covering paint or plaster and the increase of hygroscopic moisture content.

Related to seasonal wetting and drying cycles and temperature changes taking place at the masonry external environment, precipitation/dissolution processes cause the deterioration of the porous structures. Salt weathering is the result of the crystallization pressure against the pore walls when salts nucleate and grow in the confined porous space [4]. When the precipitation occurs due to water evaporation at the external surface of the pore structure during a drying process, salts precipitate on the material surface, forming a layer of salt which can be easily removed by brushing. This phenomenon is known as efflorescence, and it normally causes no problems except for aesthetic issues. On the contrary, sub-florescence refers to the kind of crystallization occurring within the pores below the stone surface, and it is responsible for the aforementioned salt-decay detachment of the external surface [5–7].

Hygroscopic salts, which absorb water molecules in their solid structure forming hydrated salts, are especially responsible for the crystallization pressure formed in the pore structure, leading to salt-decay. Hydrated salts generally have lower density than the non-hydrated salts. Therefore, drastic volume changes are resulted from the hydration process. In general, limestone is considered the most susceptible material to salt-decay problems. Lime mortars, plasters, calcareous sandstones and other materials containing calcium carbonate are equally susceptible [5].

1.2. Salts responsible for salt-decay

Due to their abundance in the nature, chlorides, nitrates and sulfates salts are considered the main responsible for these weathering processes in buildings materials and sculptures [3, 8]. Laboratory analysis of salt contaminated masonry samples typically yields to a combination of carbonates, sulphates, nitrates and chlorides of sodium, potassium, magnesium and calcium in varying concentrations. These ions, which dissociate harmlessly in solution,

*Corresponding author
Email address: jugra@byg.dtu.dk (J. M. Paz-García)

may crystallize to form several salt types [2, 5, 9]. As mentioned before, the formation of the hydrated phases of the previous salts, as e.g. Glauber's salt $Na_2SO_4{\cdot}10H_2O$, is of particular importance [9].

Natural and artificial porous media become contaminated with salts in different ways. Rain water is a constant source of carbonates and bicarbonates. Sea salt can cause dramatic decay depending on the masonry substrate and it is crucial for reinforced concrete durability [10]. Fertilizers, road de-icing salts, and acid gases from various atmospheric pollutants are all sources of potentially damaging soluble salts [4, 11]. Salts in the soil and groundwater migrate through the masonry with rising capillary moisture, typically visible as a mark of staining above ground level [5]. In addition to this, some materials, such as cement-based materials, inherently contain salts. Portland cement is a typical potential source of sulphates, which significantly contribute to the decay of stonework and sculptures [5, 12].

1.3. Desalination techniques

Use of poultice materials to reduce the salt content in contaminated monuments is an established conservation technique. In general, the application methodology for poulticing is relatively simple: a wet poultice material is applied to the surface of the treated body and it is kept in place for some period of time before being removed. Ions migrate from the wall into the poultice by advection and diffusion transport [13].

Electrokinetic desalination (EKD) techniques have been proposed as an alternative treatment. EKD has ben successfully applied for the prevention of salt-induced deterioration processes and the remediation of masonry and other construction materials [8, 14–16]. The technique is based on the transport of the damaging salts out of the porous material in an externally applied electric DC field, resulting in a high removal efficiency of salts with a significant decrease of the operational time with respect to the aforementioned poulticing treatments. Experimentally, the enhancement of the technique using a buffer substance between the electrodes and the surface of the treated body has shown some advantages, in terms of increasing the removal rate and reducing the energy consumption. Furthermore, the buffer substance enhancement avoids undesirable side effects on the material being desalinated, such as the dissolution of the solid matrix due to the sharp pH changes produced at the electrodes due to electrolysis of water [17].

1.4. Scope of the present research

Despite the fact that the ionic mobility coefficients of chlorides, nitrates and sulfates ions are very similar, experimental results for electrokinetic desalination treatments have shown different removal efficiency for each species [18]. In laboratory experiments, chlorides and nitrates are easily eliminated within a few days of applied current. In the case of chlorides, it can even reach efficiencies to almost 100%. In the case of sulfates, experimental results show that the technique yields to low removal efficiency compared to the other anions. These differences in the transport rates are due to their different chemical behavior, i.e. the solubility of the salts they can form and the chemical affinity to give positively-charged or neutral aqueous complexes.

Most of the experimental analysis for measuring the concentration of the different ions in the porous system are destructive, i.e. the samples are destroyed for the chemical analysis. In this process, samples are powdered, dried, weighted and dissolved into a defined volume of solvent for the analytical measurement of the soluble ions [15]. The analytical results give information about the total amount of the measured ions in the system, based on the analyzed soluble fraction, without distinguishing between the aqueous species nor the solid phases they may be forming part during the process. Therefore, the speciation between the analyzed samples and the actual pore solution may differ.

According to this, it is not easy to explain the differences in the removal rate of chlorides, nitrates and sulfates, based on the current experimental results. For this reason, in the present work a theoretical study is carried based on EKD simulations.

In previous work [19, 20], a one-dimensional model for reactive-transport processes in electrokinetic desalination treatments was described and simulations were compared with experimental results of chloride removal from bricks. In the present work, a model similar to that described in [20] is used to analyze the influence of the chemical effects on the electro-desalination rate of chlorides, nitrates and sulphates.

Numerical simulations are shown for an EKD treatment of a brick sample contaminated with salts containing a wide combination of the most common cations and anions, i.e. H^+, Na^+, K^+, Mg^{+2}, Ca^{+2}, OH^-, CO_3^{-2}, Cl^-, NO_3^- and SO_4^{-2}, including most of the minerals and aqueous complexes that this set of common ions can form. Additionally, competitive electrochemical reactions at the electrodes are discussed, which may be also a reason for the different behavior of the target contaminants. In the modeled system, a enhanced desalination treatment based on a buffer carbonated poultice between the electrodes and the surfaces is used.

This theoretical study is used to analyze the chemical interactions taking place during the EKD in the process, understand the influence of chemistry on the different removal rates for the target contaminants and suggest ideas for the optimization of the experimental technique.

2. Physicochemical model

The model for the reactive transport in electrokinetic processes has been designed as a combination of two strongly coupled modules: One for the transport process and the

other for chemical equilibrium calculations [21]. A brief summary of the coupled model described in details in [20] is included in sections 2.1 and 2.3.

Some modifications are proposed in the present work with respect to the previous model. A generalized relation for the calculation of the effective transport coefficients is explained in section 2.2 and a new approach for modeling the competitive electrode reactions at the anode is presented in section 2.4.

2.1. Transport phenomena

The transport process is modeled based on the Nernst-Planck-Poisson (NPP) system of equations [19, 22, 23]. The transport of mass within the unsaturated porous media is described by means of the corresponding mass continuity equation of each chemical species involved in the system:

$$\frac{\partial p\theta c_i}{\partial t} = -\nabla \mathbf{J}_i + p\theta G_i \tag{1}$$

where the c_i $\left(\mathrm{mol\,m^{-3}}\right)$ is the concentration of each chemical species i, θ (dimensionless) is the volumetric moisture content referred to the volume of available pore, i.e. the saturation degree, p (dimensionless) is the porosity, G_i $\left(\mathrm{mol\,m^{-3}\,s^{-1}}\right)$ is generation (chemical reaction) term and $\mathbf{J}_i$ $\left(\mathrm{mol\,m^{-2}\,s^{-1}}\right)$ is the flux term. The volume of available pore is not a constant parameter, as the porosity may vary along the domain due to precipitation/dissolution processes. The volume of available pore is calculated as the difference between the total volume and the volume occupied by the solids.

The flux term is described as:

$$\mathbf{J}_i = p\theta \mathbf{u}\, c_i - D_i^* \nabla c_i - U_i^* c_i \nabla \phi \tag{2}$$

where $\mathbf{u}$ $\left(\mathrm{m\,s^{-1}}\right)$ is the velocity of the fluid, D_i^* $\left(\mathrm{m^2\,s^{-1}}\right)$ is the effective ionic diffusion coefficient, U_i^* $\left(\mathrm{m^2\,V^{-1}\,s^{-1}}\right)$ is the effective ionic mobility coefficient and ϕ (V) is the electric potential in the electrolyte.

Coupling between ionic and moisture transport in unsaturated media is modeled by including a mass balance equation for the transport of water.

$$\frac{\partial p\theta}{\partial t} = -\nabla \mathbf{J}_\theta + p\theta G_\theta \tag{3}$$

where $\mathbf{J}_\theta$ $\left(\mathrm{m^3\,m^{-2}\,s^{-1}}\right)$ is the flux term in units of cubic meters of water per squared meter of cross-sectional area and G_θ $\left(\mathrm{s^{-1}}\right)$ is the generation term.

The flow of moisture through the unsaturated media is modeled as a combination of capillary forces [23–28] and electroosmotic flow [20, 22].

$$\mathbf{J}_\theta = -D_\theta^* \nabla\theta - K_{e.o.}^* \nabla\phi \tag{4}$$

where D_θ^* $\left(\mathrm{m^2\,s^{-1}}\right)$ is the effective moisture diffusivity and $K_{e.o.}^*$ $\left(\mathrm{m^2\,V^{-1}\,s^{-1}}\right)$ is the effective electroosmotic permeability.

Water and ionic balance equations are coupled by defining the velocity of the fluid media as:

$$\mathbf{u} = \frac{\mathbf{J}_\theta}{p\theta} \tag{5}$$

The Poisson's equation in electrostatics, Eq. (6), is used to complete the strongly coupled system of equations.

$$\varepsilon \nabla^2 \phi + F \sum_{i=1}^{N} c_i z_i = 0 \tag{6}$$

where F $\left(\sim 96\,485\,\mathrm{C\,mol^{-1}}\right)$ is the Faraday constant, ε $\left(\mathrm{C\,V^{-1}\,m^{-1}}\right)$ is the permittivity in water and z_i $\left(\mathrm{mol\,mol^{-1}}\right)$ is the ionic charge.

Poisson's equation couples the ionic charge balance in the electrolyte with the electric potential. The strongly coupled character of the above described equations assures the electroneutrality condition in a macroscale global system [22, 29].

2.2. Constitutive equations

Effective diffusion coefficients for the aqueous species are estimated from the corresponding diffusivity at infinite solution (in pure water) as:

$$D_i^* = D_i \frac{p\,\theta}{\tau} \tag{7}$$

where τ (dimensionless) is a fitting parameter that gathers the hindering effects of the porous media on the flow rate, i.e. the tortuosity and the constrictivity. Flow of water is assumed sufficiently slow to neglect the effects of the hydrodynamic dispersion in the diffusion coefficients [20, 30].

The effective ionic mobility coefficient are defined from the effective diffusivity by means of the so-called Nernst-Townsend-Einstein equation :

$$U_i^* = \frac{F\,z_i}{R\,T} D_i^* \tag{8}$$

where R $\left(\sim 8.314\,\mathrm{J\,K^{-1}\,mol^{-1}}\right)$ is the universal gas constant and T (K) the absolute temperature.

The moisture diffusivity is modeled as:

$$D_\theta^* = \frac{p\,\theta^\vartheta}{\tau} D_\theta \tag{9}$$

where D_θ $\left(\mathrm{m^2\,s^{-1}}\right)$ is the water diffusivity coefficient which is material characteristic [20, 31]. The moisture diffusivity coefficient is strongly non-linear with respect to the saturation degree.

Electroosmotic permeability coefficient is calculated assuming the Helmholtz–Smoluchowski (H–S) equation:

$$K_{e.o.} = -\frac{\varepsilon}{\mu}\zeta \tag{10}$$

where μ $\left(\mathrm{N\,s\,m^{-2}}\right)$ is the viscosity of water and ζ (V) is the zeta potential. The minus sign indicates that negative surface potential produces direct electroosmotic flow,

i.e. from anode to cathode. Effective electroosmotic permeability is modeled assuming the same effects than the other transport coefficients, as:

$$K^*_{e.o.} = -\frac{p\theta}{\tau}\frac{\varepsilon}{\mu}\zeta \tag{11}$$

The zeta potential depends in the chemical concentration and composition of the pore electrolyte and the nature of the solid surface. In [32], a linear dependence between the logarithm of the ionic strength and the surface potential was theoretically discussed. In [33], a microscale model for the formation of the double layer supported the linear dependence.

In the simulations shown here, the ionic strength is high and, as a result, the electroosmotic effects are very small. Nevertheless, the electroosmotic transport is included in the system for a detailed and generalized description of the physicochemical process. The following relation is used, which is consistent with the experimental and theoretical observations [32–34]:

$$\zeta = -5 \times 10^{-3} \log I \tag{12}$$

The electroosmotic flow is assumed from anode to cathode, without reverse osmosis. Consequently the zeta potential calculated in Eq. (12) is limited to a value equal to or lower than zero.

2.3. Chemical equilibrium

A set of non linear algebraic equations is developed from the mass balance and the action mass equations describing the chemical equilibrium [35, 36].

Let i and r be respectively the indexes for the chemical species and the chemical reactions describing the secondary species, with $i = 1, 2, ..., N$ and $r = 1, 2, ..., M$; where N is the total number of species, $(N - M)$ is the number of master species and M is the number of chemical equilibrium reactions used to defined the secondary species as function of the master species.

For a set of N chemical species, the M stoichiometric equations are defined as:

$$\nu_r n_r \rightleftarrows \sum_{i=1}^{N} \nu_{i,r} n_i \tag{13}$$

where the extensive variable n_i (mol) denotes the total amount of the i^{th} species in the system and $\nu_{i,r}$ is the stoichiometric coefficient for the i^{th} species in the r^{th} reaction. In this model, stoichiometric equations have to be written in the form of dissociation or dissolution reactions with only one reactant. By definition, each r^{th} secondary species participates only in the r^{th} stoichiometric equation that describes it and its stoichiometric coefficient is always $\nu_r = 1$.

When N chemical species in non-equilibrium react with each other to reach the chemical equilibrium state, a mass conservation equation can be written as a function of the extent of the reaction ξ_r. The reaction extent is the extensive quantity describing the progress of a chemical reaction equal to the number of chemical transformations [37]. In order to reach the chemical equilibrium state, any reversible reaction can proceed towards the products or towards the reactants, so ξ_r can be either a positive or a negative value.

According to the previous definition, the total amount of each species at equilibrium is given by the mass balance equation along the chemical reaction path, in the form of:

$$n_{i,\text{eq.}} = n_{i,\text{init.}} + \sum_{r=1}^{M} \xi_r \nu_{i,r} \tag{14}$$

Let $\mathbf{x} = \left[\ \xi_1, \xi_2, \cdots, \xi_M\ \right]$ be the vector containing the reaction extents for the M reactions. The function $f_r(\mathbf{x})$ is defined as a measure of the Gibbs energy of the chemical system according to the thermodynamic description of the chemical potential [36] and it tends to zero when the systems approaches to the equilibrium. Thus, the function $f_r(\mathbf{x})$ represents the distance to the equilibrium state for the r^{th} reversible reaction.

Using logarithms, $f_r(\mathbf{x})$ can be expressed as:

$$f_r(\mathbf{x}) = \sum_{r=1}^{M} (\nu_{i,r} \ln a_i) - \ln K_{eq,r} \tag{15}$$

where $K_{eq,r}$ is the equilibrium constant for the k^{th} reaction and a_i (dimensionless) is the chemical activity.

In the simulations presented in this work, the ionic strength of the media is too high for the theories for accurately estimating the chemical activity. Furthermore, the uncertainly induced by the empirical coefficients used to describe the constitutive transport equations is much higher than the losses of assuming ideal conditions for the chemical activities. Consequently, the activity is defined equal to the molal concentration $\left(\text{mol}\,\text{kg}^{-1}\right)$ for aqueous species and, in the case of the solvent and the solid species, activities are set to a fixed value of 1.

Heterogeneous precipitation/dissolution reactions are included in the model. This means that the equilibrium reaction for the solid species is only included in the set of chemical reactions when the saturation index predicts the existence of the precipitated phase.

For kinetics considerations, the model does not assume equilibrium between the electrolyte and the surrounding atmosphere. Nevertheless, free release of pure bubbles with 1 atm pressure is assumed when concentration of volatile aqueous species reach a saturation level determined by its Henry's constant.

The M equilibrium equations are coupled in a matrix system of equations and solved by means of a Newton-Raphson method, enhanced with a line-search approach which assures the convergence and deals with the non-negative concentration constraints of all the chemical species [38].

The mathematical and numerical method for chemical equilibrium calculations used here is detailed described in [21].

2.4. Electrode reactions

Nernst equation is used to calculate the redox potential for each electrochemical half reaction, as:

$$E = E^0 - \frac{RT}{\nu F} \ln Q \tag{16}$$

where Q is the reaction quotient, defined as the product of the activities of the chemical species to the power of their stoichiometric coefficients, for non-equilibrium conditions. In the special case that the reaction is at equilibrium the reaction quotient is equal to the equilibrium constant. ν, in this case, is the stoichiometric coefficient of the electrons in the redox equation, i.e. the number of electrons exchanged during the oxidation or reaction process.

E (V) is the redox potential in the reduction sense and E^0 (V) is the standard redox potential, which is measured under standard conditions which are 25°C, 1 M concentration for each ion participating in the reaction, a partial pressure of 1 atm for each gas that is part of the reaction and metals in their pure state. The standard reduction potential is defined relative to a standard hydrogen reference electrode (SHE), which is arbitrarily given a potential of 0 V [39].

At the cathode, cations are attracted and reduction reactions can happens according to:

$$2H_2O + 2e^- \rightleftarrows H_2\,(g) + OH^- \quad ; \quad E^0 = -0.83 \tag{17}$$

$$Na^+ + e^- \rightleftarrows Na^0 \quad ; \quad E^0 = -2.71 \tag{18}$$

$$K^+ + e^- \rightleftarrows K^0 \quad ; \quad E^0 = -2.93 \tag{19}$$

$$Ca^{+2} + 2e^- \rightleftarrows Ca^0 \quad ; \quad E^0 = -2.87 \tag{20}$$

$$Mg^{+2} + 2e^- \rightleftarrows Mg^0 \quad ; \quad E^0 = -2.37 \tag{21}$$

The redox potential of alkali and alkaline earth metals is too high to be competitive to water in aqueous media. Consequently, it seems reasonable to assume that only water reduction is taking place at the cathode if only alkali and alkaline earth metals are present in the system.

Anions are attracted to the anode where oxidation reaction occur. The reactions assumed at the anode are:

$$4H^+ + 4e^- + O_2\,(g) \rightleftarrows 2H_2O \quad ; \quad E^0 = 1.23 \tag{22}$$

$$2e^- + Cl_2\,(g) \rightleftarrows 2Cl^- \quad ; \quad E^0 = 1.36 \tag{23}$$

CO_3^{-2} , NO_3^- and SO_4^{-2} can not participate in the anode reaction, because they are in their highest oxidation state. They might be reduced at the cathode, but it is not favored since they are migrating towards the anode.

Despite the redox potential of gaseous chlorine is greater than the gaseous oxygen, the redox potential of the half reactions may be competitive depending on the partial pressure of the gases. Consider the redox potential for both reactions, defined from the Nernst equation, as:

$$E_{O_2} = \left(E^0_{O_2} + \psi_{O_2}\right) - 0.059\,\mathrm{pH} + \frac{0.059}{4} \log\left(P_{O_2}\right) \tag{24}$$

$$E_{Cl_2} = \left(E^0_{Cl_2} + \psi_{Cl_2}\right) - 0.059 \log\left[Cl^-\right] + \\ + \frac{0.059}{2} \log\left(P_{Cl_2}\right) \tag{25}$$

where room temperature is assumed, and decimal logarithms are used instead of natural logarithms, for a more intuitive study of the dependence of the redox potential on the pH.

The term ψ (V) represents the concentration polarization effects or over-potential, i.e. the variations in E that arise from the difficulty of the transfer between the initial and final components of a reaction occurring at the electrode [40]. It is related, for example, to the ease of the produced bubbles of O_2 or Cl_2 to be desorbed and released from the surface of the electrode.

The overpotential depends, among other factors, on the nature of the electrode used and can favor in some cases one specific electrochemical reactions increasing its efficiency. In normal conditions, water electrolysis reaction has lower redox potential and it is the main predominant reaction at the anode. Most of the published models assume an efficiency of 100 % with respect to the water electrolysis reaction. Nevertheless, seawater electrolysis treatments showed that the efficiency of water electrolysis with respect to the chlorine depends on the material used as electrode [41, 42]. Bennett [41] reported an efficiency of about 66 % on gaseous chloride formation using graphite electrodes in a continuous seawater electrolysis system.

In condition of low pH, high concentration of chloride at the anode and low partial pressure of gaseous chlorine with respect to the gaseous oxygen, the redox potential of the reactions in Eq. (24) and Eq. (25) may become competitive. In the present model, it will be assumed that both reactions are continuously and simultaneously taken place. Consequently, they will have the same redox potential at any time.

$$E_{O_2} = E_{Cl_2} \tag{26}$$

It will also be assumed that mixed bubbles of Cl_2 and O_2 are released form the system, with a total partial pressure of 1 atm.

$$P_{O_2} + P_{Cl_2} = 1 \tag{27}$$

For a given pH and chloride concentration, these assumptions lead to a known value of the partial pressures of the gases. From the partial pressure, the efficiency of the water electrolysis reaction with respect to the chloride reaction can be calculated.

$$P_{Cl_2} = \frac{-1 + \sqrt{1 + 4\alpha}}{2\alpha} \tag{28}$$

where

$$\frac{0.059}{4}\log(\alpha) = \left(E^0_{Cl_2} + \psi_{Cl_2}\right) - \left(E^0_{O_2} + \psi_{O_2}\right) + \\ + 0.059\left(\mathrm{pH} - \log\left[Cl^-\right]\right) \quad (29)$$

Eq. (29) is plotted in Fig. 1 for a range of very acid pH and high chloride concentration. It can be seen that, for an inert electrode and ignoring polarization effects, the efficiency of the water electrolysis reactions is very high with respect to the chloride, leading to bubbles with a partial pressure of chlorine lower than 1 %. To be consistent with the experimental efficiencies of 66 % for graphite electrolyte, some polarization effects have to be included. Fig. 1b shows the results of the Eq. (29) but using some arbitrary values for the overpotential factors ψ_{Cl_2} and ψ_{O_2} to illustrate the material affinity. Results from Fig. 1b are used in the simulations presented in this investigation.

In an ideal system, with Faraday efficiency of 100 %, the electric current through the conductors ha the same magnitude than the ionic current through the electrolyte. The relation between the electric and ionic current, and so the magnitude of the ionic charge flux injected into the porous system at the electrode processes is obtained from the Faraday's law of electrolysis.

$$I = F\sum_{i=1}^{N} g_i\, z_i \quad (30)$$

where I (A) is the electric current and the extensive property g_i $\left(\mathrm{mol}\, s^{-1}\right)$ indicates the flux of ions entering or leaving the chemical system as a consequence of the electrochemical reactions.

In an electrochemically-induced desalination treatment under constant electric current, the fraction of ionic current resulting from the reactions in Eq. (22) and Eq. (23) may be related to the partial pressure of the reactant gases, as quantified in:

$$g_{Cl^-} = \frac{I}{F\, z_{Cl^-}}\left(\frac{1}{2}\frac{P_{Cl_2}}{(1-P_{Cl_2})}\right) \quad (31)$$

$$g_{H^+} = \frac{I}{F\, z_{H^+}}\left(1 - \frac{1}{2}\frac{P_{Cl_2}}{(1-P_{Cl_2})}\right) \quad (32)$$

where the factor 1/2 comes from the stoichiometric proportion of equations 22 and 23, since one mole of reduced Cl_2 generates half moles of electrons than the case of O_2.

3. Results and discussion

3.1. The modeled system

The desalination of a single brick contaminated with a combination of the most common salts is studied. Fig. 2 shows a schematic representation of the experimental setup for the modeled system. The physical system is based on the setup used in the experimental electro-desalination

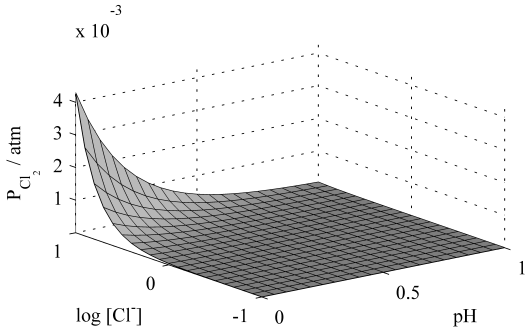

(a) $\left(E^0_{Cl_2} + \psi_{Cl_2}\right) - \left(E^0_{O_2} + \psi_{O_2}\right) = 0.13$

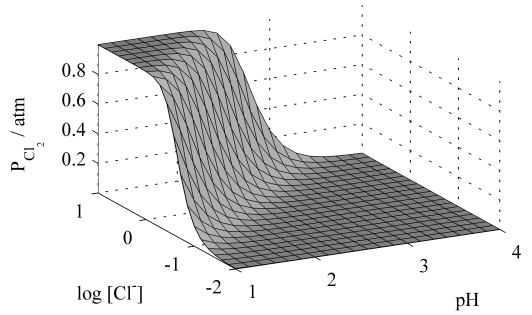

(b) $\left(E^0_{Cl_2} + \psi_{Cl_2}\right) - \left(E^0_{O_2} + \psi_{O_2}\right) = -0.1$

Figure 1: Partial pressure of gaseous chloride in the bubbles released from the anode reactions, assuming continuous competition between water and chloride electrolysis.

treatments done in the experimental studies in [14, 15] and the one modeled in [20].

Here, a modification to the standard procedure is proposed. To avoid accumulation of gases at with the corresponding hydraulic pressures and surface polarization effects at the electrodes, in the modeled system no sealers are used at the electrode compartments. It is assumed the free release of Cl_2, O_2 and H_2 gas bubbles, produced in the electrochemical reactions (see section 2.4 and Fig. 2) or the release of CO_2 resulting from the acid dissolution of the calcite mineral [21].

A cubic brick piece of 10 cm length is subjected to a constant current of 10 mA during 11 days. A buffering substance enhanced EKD treatment is assumed, based on the buffer capacity of $CaCO_3$ [17]. Cylindrical electrode compartments filled with a clay poultice rich in $CaCO_3$ are placed at each end of the brick sample. The cylinders are 5 cm long and 8 cm of internal diameter. The distance between the electrode surfaces and the brick surface is 3.5 cm.

The brick is assumed a porous inert matrix with a certain amount of minerals. Table 1 collects the initial solid composition of the brick and the clay in the simulations. The pore structure is completely saturated with pure wa-

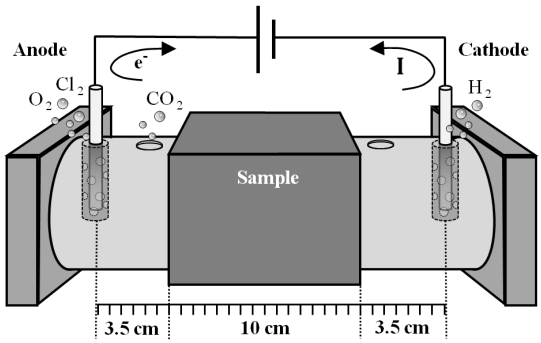

Figure 2: Scheme for the modeled experimental setup.

Table 1: Initial composition of the brick and the carbonated clay. Units in mol per cubic meter of heterogeneous porous matrix.

	Carbonated clay	Brick
SiO_2 (inert)	15000	30000
$CaCO_3$	3000	400
$MgCO_3$	-	50
NaCl	5	50
KNO_3	5	50
$CaSO_4{\cdot}2H_2O$	-	50

ter in equilibrium with 10^{-5} mol kg^{-1} of carbonic acid coming from atmospheric CO_2 (g). Small amount of salt is initially included in the clay poultice to assure enough ionic conductivity.

Table 2 shows the set of reversible chemical reactions selected for the simulations. Equilibrium constants are taken from ThermoChimie, the ANDRA thermodynamic database released as sit.dat with the PHREEQC code [43]. Equilibrium constants are congruent with a stoichiometry referred to the chosen master species collected in Table 2.

Diffusion coefficients are taken from [44] and water diffusivity values are estimated from [31]. Diffusion coefficients not found in the databases, indicated with a superscripted star, are given an arbitrary value equivalent to the diffusivity of the slower ion of the molecule and divided by the number of ions in the molecule. This added uncertainly is assumed not too relevant since species which required estimation of the transport coefficients are traces or with lower concentration than the free ions.

3.2. Removal rate of the target ions

In this section, results from simulations obtained from the 11 days at 10 mA constant current EKD treatment on the modeled system are shown. In figs. 3,4 and 5, transient profiles are marked with a legend indicating the time in days. For readability reasons, only selected transient profiles are shown. The final profile, corresponding with the 11$^{\text{th}}$ day of treatment is distinguished with a bold line, and the initial with a dashed line.

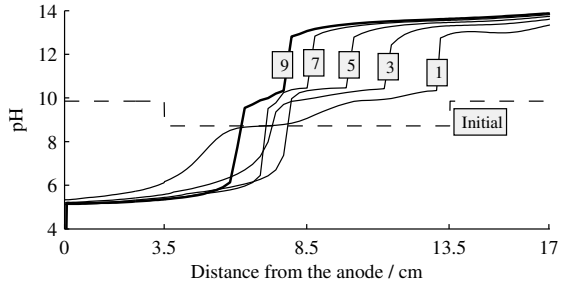

Figure 3: Selected transient pH profiles

Fig. 3 shows the transient pH profiles in the system. Simulations show that the carbonated clay system is able to buffer the acidic front generated in the anode electrode due to the water oxidation. A slightly acid environment, with pH value around 5, is maintain in the anode compartment while calcite is not completely consumed. On the other hand, the basic front is not significantly buffered, and it reaches a very alkaline environment with pH value between 13 and 14. In the brick, there is a step of slightly alkaline pH between 10 and 11, which is related to the buffer capacity of the magnesium, with precipitates forming brucite, $Mg(OH)_2$, as observed in Fig. 6.

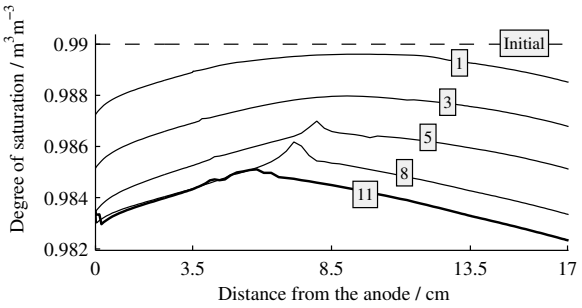

Figure 4: Selected transient profiles for the degree of saturation

Fig. 4 shows the transient profile for the volumetric water content during the simulation. The overall amount of water in the system decreases because of the continuous release of oxygen and hydrogen from the electrochemical reactions at the electrodes. In the middle of the brick sample, where the acidic and alkaline fronts collide, water is formed by chemical reaction. Due to the electroosmosis, the water content is lower in the anode compartment than

Table 2: Chemical Species in the modeled system and physicochemical properties. D (meaning D_i for aqueous species and D_θ for water) is given in $\left(\mathrm{m^2\,s^{-1}}\right)$.

Master Species	$D \times 10^9$	Aqueous species	log K_{eq}	$D \times 10^9$	Solid species	log K_{sp}
H_2O (brick)	200	OH^-	14.00	5.273	KOH (s)	24.60
H_2O (clay)	500	$MgOH^+$	11.68	0.706*	$Mg(OH)_2$ (s)	17.10
H^+	9.311	$CaOH^+$	12.78	0.792*	$Ca(OH)_2$ (s)	22.81
Na^+	1.134	CO_2	−16.68	1.846	Na_2CO_3 (s)	−0.83
K^+	1.957	HCO_3^-	−10.33	1.185	$MgCO_3$ (s)	−8.91
Mg^{+2}	1.584	$NaHCO_3$	−10.08	0.593*	$CaCO_3$ (s)	−8.48
Ca^{+2}	1.412	$MgHCO_3^+$	−11.37	0.593*	NaCl (s)	1.59
CO_3^{-2}	1.84	$CaHCO_3^+$	−11.43	0.593*	KCl (s)	0.87
Cl^-	2.032	$NaCO_3^+$	−1.27	0.667*	$MgCl_2{\cdot}6H_2O$ (s)	4.46
NO_3^-	1.902	$MgCO_3$	−2.99	0.706*	$CaCl_2{\cdot}6H_2O$ (s)	3.94
SO_4^{-2}	2.130	$CaCO_3$	−3.22	0.792*	$NaNO_3$ (s)	1.09
		$MgCl^+$	−0.35	0.706*	KNO_3 (s)	−0.10
		$CaNO_3^+$	−0.60	0.792*	$Mg(NO_3)_2{\cdot}6H_2O$ (s)	2.58
		$Ca(NO_3)_2$	−0.50	0.528*	$Ca(NO_3)_2{\cdot}6H_2O$ (s)	5.98
		HSO_4^-	−1.98	1.385	$Na_2SO_4{\cdot}10H_2O$ (s)	−1.23
		$NaSO_4^-$	−0.73	0.667*	K_2SO_4 (s)	−1.85
		KSO_4^-	−0.88	0.979*	$MgSO_4{\cdot}7H_2O$ (s)	−1.88
		$MgSO_4$	−2.23	0.706*	$CaSO_4{\cdot}2H_2O$ (s)	−4.61
		$CaSO_4$	−2.31	0.792*		

in the cathode compartment. Porosity changes due to calcite dissolution also contribute to the lower water content at the anode.

Fig. 5 shows the corresponding transient profiles of the target contaminants including all the possible species (aqueous and solids) that can be formed. Since water content, cross-sectional area and porosity along the one dimensional domain vary, specially at the interfaces between the carbonated clay and the brick sample, concentrations in Fig. 5 are referred to the assumed constant volume of heterogeneous matrix, and so expressed as total amount of mol. This reference makes easier to monitoring the migration of the total amount of target contaminant during the process.

Results from simulations are congruent with the experimental results, as those reported in [1, 14–16, 18, 45]. After 11 days of treatment, chlorides are efficiently removed from the brick, reaching very low concentrations in all of their possible species. The removal efficiency of nitrates is slightly lower than the case of chloride. Differences between the migration of chloride and nitrate may be explained because a fraction of dissolved nitrates are forming part of the aqueous complexes $CaNO_3^+$ and $Ca(NO_3)_2$. These aqueous complexes are not negative but positive and charge-neutral respectively. Therefore, calcium nitrate complexes do not migrate towards the anode as nitrate ions does. At the end of the treatment, simulations indicate that there is still some amount of nitrates at the anode end of the brick, which is mainly in the form of the aforementioned calcium aqueous complexes.

Another difference between the migration rate of chloride and nitrate is that chloride amount in the anode com-

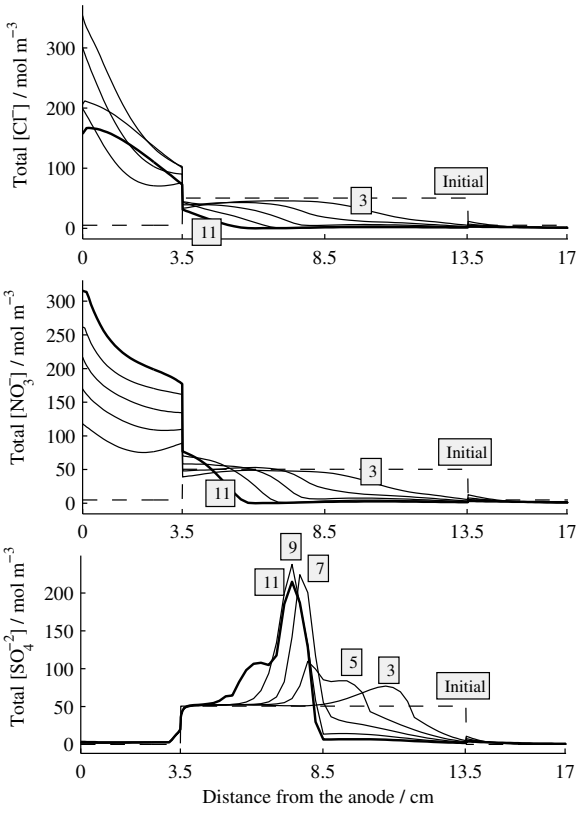

Figure 5: Transient profiles for target contaminants, including all possible chemical species. Profiles for 3, 5, 7, 9 and 11 days of treatment.

partment decreases after the fifth day of treatment because the release of gaseous chlorine as a result of the electrochemical reactions. In the simulations shown here, polarization effects are assumed to favor chloride with respect to water oxidation, as shown in Fig. 1b to match the experimental observation when chorine formation is detected by smell. The release of gaseous chlorine reduces the diffusion driving force assigned to the accumulation at the anode and it enhances the electromigration transport.

Simulations show low overall removal of global SO_4^{-2} from the sample. Sulfates are removed only from the right end (cathode end) of the brick. Sulfates are not collected at the anode compartment, but they accumulate at the left (anode) end of the brick sample. Furthermore, a peak of concentration appears very close to the middle point of the sample. Sulfate is mainly in a precipitated phase. Consequently, the migration of sulfate is better explained with the results shown in Fig. 6.

Most of the salts included in the set of chemical reactions do not precipitate during the process. Only calcium and magnesium carbonates and hydroxides and gypsum are predicted in the simulations. Salts of sodium and potassium are very soluble and they appear only when increasing the concentration by evaporation.

In the process, the gypsum in the cathode end of the brick dissolves, but it precipitates again in the middle part of the brick. This located precipitation can be explained as the sulfates dissolved at the cathode end, migrating towards the anode, collide with the calcium front that travels towards the cathode.

The calcite at the anode compartment dissolves due to the acid production at the electrode. The dissolution of calcite seems to be an effective buffering technique for the produced acid. On the other hand, calcium hydroxide is very soluble and it does not buffer the alkaline front in a significant manner. The presence of magnesium seems to be an important factor determining the buffer capacity for the alkaline front, since magnesium hydroxide is much more insoluble than the calcium one. As the alkaline front proceed, magnesite, $MgCO_3$, dissolves while brucite, $Mg(OH)_2$, precipitates. Some portlandite precipitation is also observed at the middle of the sample brick, at the end of the treatment.

In the long term, the treated material will absorb atmospheric CO_2 which will neutralize the portlandite to give calcite and water. This process, typically denoted as carbonation, is very common in cement based materials. Carbonation is very dangerous in reinforced concrete, since it promotes the corrosion by reducing the pH of the media. In the case of non-reinforced materials, carbonation effects are assumed beneficial. Despite the possibility of crystallization pressures, the precipitation of calcite normally increases the strength of the material. Furthermore, the material will act as a drain of atmospheric CO_2 (g), fixing part of the CO_2 (g) released during the treatment.

Simulations predict important porosity changes at the anode compartment as the result of the calcite dissolution.

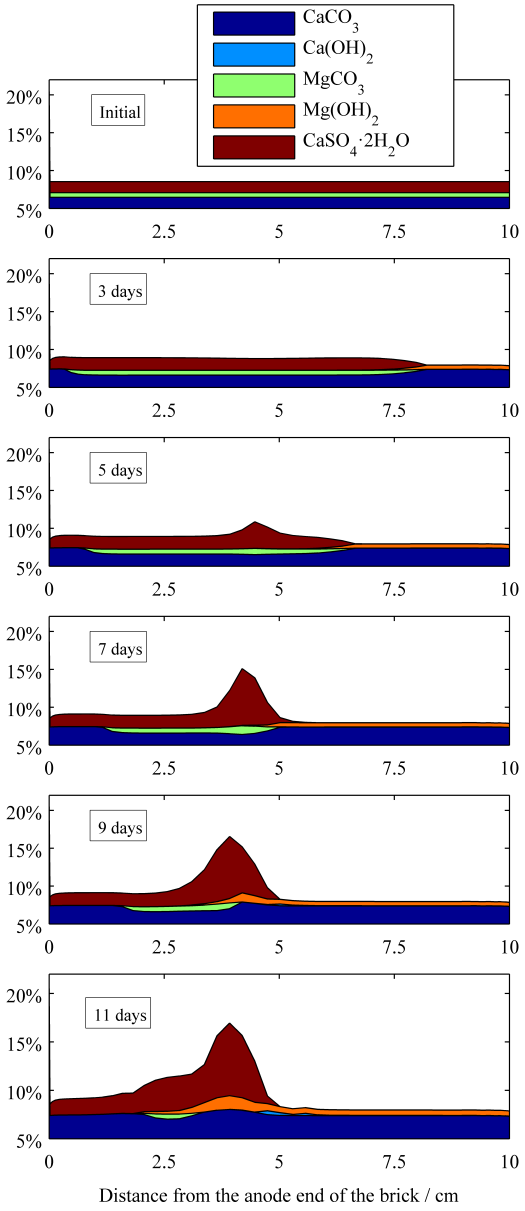

Figure 6: Volume fraction of precipitated solids referred to the available volume fraction. Available volume fraction, about 25 %, is calculated as the total volume fraction minus the volume fraction occupied by inert solid.

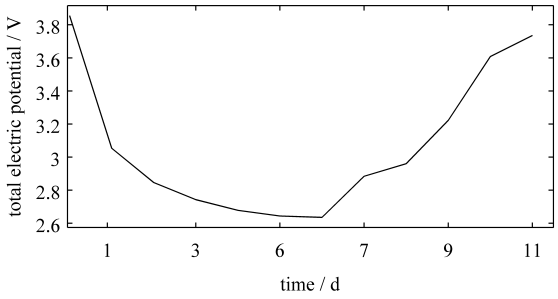

Figure 7: Total electric potential

Simulations also show that the precipitation of gypsum and hydroxides inside the brick porous structure involves a slightly decrease of its porosity. This results suggest that the application of the carbonated clay enhanced electro-desalination treatment of a contaminated material with high sulfate concentrations and very low porosity can be harmful, since the located precipitation can produce crystallization pressure.

Nevertheless, the simulations presented here may overestimate the effect of the dissolution of carbonates at the cathode end of the brick, and the precipitation of material in the middle part of the sample due to chemical kinetic considerations, as the results are based on the assumption of chemical equilibrium during the process.

3.3. Electric potential

The electrokinetic desalination treatment simulated here is carried out under constant current conditions. The total potential, shown in Fig. 7, is the sum of the electric potential drop in the electrolyte between anode and cathode, calculated from the coupled Nernst-Planck-Poisson system of equations, and the electrochemical potential at the electrodes, calculated from the Nernst equation, Eq. (16). The brick solid structure is assumed as a perfect electrical insulator.

The total electric potential drop between electrodes decreases at the beginning of the treatment, stabilizes in a range between 2 and 4 during a few days, and then it starts to increase. These results are congruent with the experimental electro-desalination processes [14, 15, 45]. The increase of the electric potential with time is related to a decrease of conductivity in the brick sample as a consequence of the desalination process. As the process causes removal of salts from the brick, the conductivity in the middle of the sample tends to reduce while the separation of anions and cations is taking place.

4. Conclusions

Electro-desalinations of construction materials, enhanced with a carbonated poultice to buffer the acid front, is a technique that allows the removal of salts from the porous structure minimizing the undesirable side effects of injecting acid into the solid matrix.

During the physicochemical process, protons produced at the anode are neutralized by the dissolution of the calcite surrounding the electrode. In the dissolution of the mineral, carbonic acid is formed and CO_2 (g) is released together with the gases produced in the electrochemical reactions: O_2, H_2 and Cl_2. Therefore, a setup for the application of the technique in both laboratory and pilot scale should take into account this release of gaseous species.

A calcium front traveling from anode to cathode is an inevitable side-effect of the carbonated clay buffering system. The calcium front is the result of the substitution of hydroxides ions for calcium ions in the dissolution of the calcite during the buffering process, by:

$$H^+ + CaCO_3 \rightleftarrows Ca^{+2} + HCO_3^- \tag{33}$$

Apart for preventing acid attack of the treated material, this phenomenon improves the efficiency in terms of energy consumption, since the ionic mobility of calcium is significantly slower than protons. In acid environments, protons carry most of the ionic current in the aqueous system due to their high ionic mobility.

Apparently, from the simulations and the published experimental results, the alkaline front is not buffered in a significant manner by this enhanced technique. Instead, the presence of magnesium in the sample, seems to be a determining factor for the alkaline buffering capacity. According to this, the use of a magnesium based poultice at the cathode compartment is proposed to be theoretically and experimentally investigated as a modification on the existing technique.

Simulation results show that the EKD treatment is highly efficient for the removal of chlorides and nitrates. Both ions form soluble salts and have low chemical affinity with calcium. In the case of sulfates, the presence of calcium, both the initial and the induced during the aforementioned buffering process, strongly limits the mobility of the anion. Calcium and sulfate precipitate in the form of mineral gypsum, $CaSO_4{\cdot}H_2O$. As most of the sulfate in the system is precipitated gypsum, it migrates in a very low rate, controlled by the precipitation/dissolution equilibrium reaction.

Furthermore, it is observed the precipitation of calcium sulfate in a narrow region located at the anode half but close to the middle of the treated sample. The calcium front, migrating towards the cathode, acts as a barrier for the sulfates. When the calcium front collides with the small fraction of dissolved sulfate migrating towards the anode, more calcium sulfate mineral precipitates in form of gypsum. This located precipitation may have important consequences related to porosity changes, and they have to be taking into account when designing EKD treatments to avoid inducing extra crystallization pressure.

To conclude, simulation results show that, after the

treatment, the material pore solution stays with a saturated solution of magnesium hydroxides (if present) and very high concentration of calcium hydroxide. A decrease of the moisture content or variations in the temperature will lead to the precipitation of portlandite and brucite inside the pore structure or in the form of efflorescence.

Acknowledgments

Authors acknowledge The Danish Agency of Science Technology and Innovation. This research was funded as part of the project "Fundamentals of Electrokinetics in In-homogeneous Matrices", with project number 274-08-0386. J.M. Rodríguez-Maroto acknowledges the financial support from the Ministerio de Ciencia e Innovación of the Spanish Government through the project ERHMES, CTM2010-16824, and FEDER funds.

Part of this work was carried out at the Departamento de Ingeniería Química y Ambiental, in Universidad Técnica Federico Santa María (UTFSM) Valparaíso, Chile. We would like to thank our host at the UTFSM, Prof. Henrik Hansen, for all his useful comments and final review of this manuscript. Authors acknowledge the finantial support from the project FP7-PEOPLE-2010-IRSES-269289-ELECTROACROSS which sponsored these secondments.

References

[1] L. Ottosen, A. Pedersen, I. Rörig-Dalgaard, Salt-related problems in brick masonry and electrokinetic removal of salts, Journal of Building Appraisal 3 (2007) 181–194.

[2] N. Kuchitsu, T. Ishizaki, T. Nishiura, Salt weathering of the brick monuments in ayutthaya, thailand, Developments in Geotechnical Engineering 84 (2000) 319–327.

[3] A. Goudie, H. A. Viles, Salt weathering hazards, Wiley, 1997.

[4] C. Cardell, F. Delalieux, K. Roumpopoulos, A. Moropoulou, F. Auger, R. Van Grieken, Salt-induced decay in calcareous stone monuments and buildings in a marine environment in sw france, Constr. Build. Mater. 17 (3) (2003) 165–179.

[5] R. J. Schaffer, T. Yates, The weathering of natural building stones, Donhead, 2004.

[6] M. Koniorczyk, Salt transport and crystallization in non-isothermal, partially saturated porous materials considering ions interaction model, International Journal of Heat and Mass Transfer 55 (4) (2012) 665–679.

[7] R. M. Espinosa-Marzal, G. W. Scherer, Advances in understanding damage by salt crystallization, Acc. Chem. Res. 43 (6) (2010) 897–905.

[8] L. Ottosen, I. Christensen, I. Rorig-Dalgaard, P. Jensen, H. Hansen, Utilization of electromigration in civil and environmental engineering - Processes, transport rates and matrix changes, J. Environ. Sci. Health, Part A 43 (8) (2008) 795–809.

[9] J. Ruedrich, S. Siegesmund, Salt and ice crystallisation in porous sandstones, Environ Geol 52 (2) (2007) 225–249.

[10] M. Castellote, C. Andrade, C. Alonso, Electrochemical removal of chlorides: Modelling of the extraction, resulting profiles and determination of the efficient time of treatment, Cem. Concr. Res. 30 (4) (2000) 615–621.

[11] C. Rodriguez-Navarro, E. Doehne, Salt weathering: influence of evaporation rate, supersaturation and crystallization pattern, Earth Surf. Process. Landforms 24 (1999) 191–209.

[12] W. Kloppmann, P. Bromblet, J. M. Vallet, V. Vergès-Belmin, O. Rolland, C. Guerrot, C. Gosselin, Building materials as intrinsic sources of sulphate: A hidden face of salt weathering of historical monuments investigated through multi-isotope tracing (b, o, s), Sci. Total Environ. 409 (9) (2011) 1658–1669.

[13] L. Pel, K. Kopinga, H. Brocken, Moisture transport in porous building materials, Technische Universiteit Eindhoven, 1995.

[14] L. Ottosen, I. Rörig-Dalgaard, Electrokinetic removal of Ca(NO3)2 from bricks to avoid salt-induced decay, Electrochim. Acta 52 (10) (2007) 3454–3463.

[15] L. Ottosen, I. Rörig-Dalgaard, Desalination of a brick by application of an electric dc field, Mater. Struct. 42 (7) (2009) 961–971.

[16] I. Rörig-Dalgaard, L. Ottosen, H. Hansen, Diffusion and electromigration in clay bricks influenced by differences in the pore system resulting from firing, Constr. Build. Mater. 27 (1) (2012) 390–397.

[17] I. Rörig-Dalgaard, L. Ottosen, Method and device for removing an ionic impurity from building structures.

[18] L. Ottosen, I. Rörig-Dalgaard, A. Villumsen, Electrochemical removal of salts from masonry - experiences from pilot scale, in: Salt Weathering on Buildings and Stone Sculptures, 2008, pp. 341–250.

[19] J. Paz-Garcia, B. Johannesson, L. Ottosen, A. Ribeiro, J. Rodriguez-Maroto, Modeling of electrokinetic processes by finite element integration of the Nernst-Planck-Poisson system of equations, Sep. Purif. Technol. 79 (2) (2011) 183–192.

[20] J. Paz-García, B. Johannesson, L. Ottosen, A. Alshawabkeh, A. Ribeiro, J. Rodríguez-Maroto, Modeling of electrokinetic desalination of bricks, Electrochim. Acta.

[21] J. Paz-Garcia, B. Johannesson, L. Ottosen, A. Ribeiro, J. Rodriguez-Maroto, Computing chemical equilibrium systems with an algorithm based on the reaction extents, Comput. Chem. Eng.

[22] S. Pamukcu, Electrochemical transport and transformations, in: K. R. Reddy, C. Cameselle (Eds.), Electrochemical Remediation Technologies for Polluted Soils, Sediments and Groundwater, Wiley Online Library, 2009, pp. 29–64.

[23] B. Johannesson, Y. Hosokawa, K. Yamada, Numerical calculations of the effect of moisture content and moisture flow on ionic multi-species diffusion in the pore solution of porous materials, Comput. Struct. 87 (1-2) (2009) 39–46.

[24] B. Johannesson, M. Janz, A two-phase moisture transport model accounting for sorption hysteresis in layered porous building constructions, Build. Environ. 44 (6) (2009) 1285–1294.

[25] M. Janz, Methods of measuring the moisture diffusivity at high moisture levels, Ph.D. thesis, University of Lund (1997).

[26] Y. Pachepsky, D. Timlin, W. Rawls, Generalized Richards' equation to simulate water transport in unsaturated soils, J. Hydrol. 272 (2003) 3–13.

[27] S. Roels, J. Carmeliet, H. Hens, Modelling unsaturated moisture transport in heterogeneous limestone, Transport porous med. 52 (3) (2003) 333–350.

[28] T. Nguyen, J. Petkovic, P. Dangla, V. Baroghel-Bouny, Modelling of coupled ion and moisture transport in porous building materials, Constr. Build. Mater. 22 (11) (2008) 2185–2195.

[29] B. Johannesson, Comparison between the Gauss' law method and the zero current method to calculate multi-species ionic diffusion in saturated uncharged porous materials, Computers and Geotechnics 37 (5) (2010) 667–677.

[30] A. Yeung, J. Mitchell, Coupled fluid, electrical and chemical flows in soil, Geotechnique 43 (1) (1993) 121–134.

[31] S. Chemkhi, F. Zagrouba, Water diffusion coefficient in clay material from drying data, Desalination 185 (1) (2005) 491–498.

[32] L. Dongqing, Basics of electrical double layer, in: Electrokinetics in microfluidics, Academic Press, 2004, Ch. 2.

[33] J. Paz-Garcia, B. Johannesson, L. Ottosen, A. Ribeiro, J. Rodriguez-Maroto, Modeling of the formation of electric double layers including chemical reaction effects, AIChE J.

[34] J. Lyklema, Fundamentals of interface and colloid science, Vol. 5, Academic Press, 2005.

[35] J. Rawlings, J. Ekerdt, Chemical reactor analysis and design fundamentals, Vol. 67, Nob Hill Publishing, 2002.

[36] C. Bethke, Geochemical and biogeochemical reaction modeling,

2nd Edition, Cambridge University Press, 2008.
[37] A. McNaught, A. Wilkinson, Compendium of Chemical Terminology: Iupac Recommendations, 2nd Edition, Blackwell Science, 1997.
[38] W. Press, S. Teukolsky, W. Vetterling, B. Flannery, Root finding and nonlinear sets of equations, in: Numerical recipes in C: The art of Scientific Computing, Cambridge University Press, 1992, Ch. 9.
[39] R. Chang, J. Overby, General chemistry - The essential concepts, McGraw-Hill, New York, 2011.
[40] P. Marcus, Corrosion mechanisms in theory and practice, 3rd Edition, CRC Press, Taylor & Francis Group, Boca Raton, 2011.
[41] J. Bennett, Electrodes for generation of hydrogen and oxygen from seawater, Int. J. Hydrogen Energy 5 (4) (1980) 401–408.
[42] R. Balaji, B. S. Kannan, J. Lakshmi, N. Senthil, S. Vasudevan, G. Sozhan, A. K. Shukla, S. Ravichandran, An alternative approach to selective sea water oxidation for hydrogen production, Electrochem. Commun. 11 (8) (2009) 1700–1702.
[43] D. Parkhurst, C. Appelo, User's guide to PHREEQC (version 2) - A computer program for speciation, batch-reaction, one-dimensional transport, and inverse geochemical calculations, U.S. Department of the Interior, Water-Resources Investigations Reports (99-4259) (1999).
[44] R. Weast, M. Astle, W. Beyer, CRC handbook of chemistry and physics, Vol. 69, CRC Press Boca Raton, FL, 1988.
[45] L. Ottosen, C. Ferreira, I. Christensen, Electrokinetic desalination of glazed ceramic tiles, J. Appl. Electrochem. 40 (6) (2010) 1161–1171.

Paper

"Feasibility Study of the Use of Different Extractant Agents in the Remediation of a Mercury Contaminated Soil from Almaden"

J.D. Subires-Muñoz, A. García-Rubio, C. Vereda-Alonso, C. Gómez-Lahoz, J.M. Rodríguez-Maroto, F. García-Herruzo, J.M. Paz-García

Published in: *Separation and Purification Technology, 2011*

Separation and Purification Technology 79 (2011) 151–156

Contents lists available at ScienceDirect

Separation and Purification Technology

journal homepage: www.elsevier.com/locate/seppur

Feasibility study of the use of different extractant agents in the remediation of a mercury contaminated soil from Almaden

J.D. Subirés-Muñoz [a], A. García-Rubio [a], C. Vereda-Alonso [a], C. Gómez-Lahoz [a], J.M. Rodríguez-Maroto [a,*], F. García-Herruzo [a], J.M. Paz-García [b]

[a] Departamento de Ingeniería Química, Facultad de Ciencias, Universidad de Málaga, 29071-Málaga, Spain
[b] Civil Engineering Department, Technical University of Denmark, Brovej, Building 118, Dk-2800 Kgs. Lyngby, Denmark

ARTICLE INFO

Keywords:
Soil flushing
Sequential extraction procedure
Risk assessment
Fate of pollutants
Remediation feasibility studies

ABSTRACT

The soil of Almaden mining district in Spain has a high concentration of mercury (1000 mg kg^{-1}), therefore decontamination activities are necessary. This paper studies the effectiveness of some chelant agents (thiosulfate, EDTA, iodide and HNO_3) for the remediation of this soil which has been polluted for several millennia. The risk assessment of the contamination and the feasibility study (RA-FS) of the remediation were based on a standard sequential extraction procedure (SEP) together with lixiviation tests. Results obtained from these RA-FSs allow the prediction of the mercury removal reached in bench scale tests of the flushing technique.

In addition the SEP was performed before and after treatments, and it was found that in some cases the remaining mercury concentration after treatment is associated to the more mobile fractions, indicating that additional treatments would be required. It also indicates that an important additional removal would be obtained if acid extraction is carried out after the first treatment.

Finally, the reliability of the standard SEP used was tested to determine if the very high total metal concentration of this contaminated site affects the fractionation results. This was done by the repetition of each sequential extraction step before moving to the next one. Results indicate that both procedures give almost identical results for mercury but some important differences can be observed for iron.

1. Introduction

The Almaden mining district constitutes one of the major concentrations of mercury on Earth. Located in south-central Spain is estimated to contain about a third of the known global mercury resources before mining (250,000 t) [1,2]. The mining activities began more than 2000 years ago, and as could be expected the soils of the Almaden district are highly contaminated, with some zones displaying Hg concentration values well above 1000 mg kg^{-1}. High concentrations of Hg in aquatic organisms commonly used in biomonitoring programs of metal pollution have been detected and preliminary studies have revealed high levels of mercury absorption by plants [3]. These facts put forward the need for soil remediation.

An exhaustive study of the characteristics of mercury in the soil is provided by Higueras et al. [3,4]. They indicated that, in the soils of the Almaden district, mercury has been introduced via geological and anthropogenic dispersion. The geological dispersion is probably due to erosion of minerals such as cinnabar. Taking into account the low solubility of HgS (10^{-54} mol dm^{-3}) [5] it is predictable that this Hg is mainly associated to the less-mobile fractions of the speciation analysis [6]. Hg with origin in anthropogenic dispersion is generated by the mining activity (transport and stockpiling, and metallurgical activities), and will probably be associated to the semi-mobile fractions [6].

Nowadays, it is well known that the total concentration of heavy metals is not enough for a sound risk assessment [7–10]. The distribution, mobility and bioavailability of these metals depend on the association form in the solid phase to which they are bound [9,11]. The target of the most used speciation analyses is not to identify nor quantify one or more individual chemical species [10,12]. It is rather a fractionation in which the total content of the element is associated to different fractions according to the agents that would mobilize the toxic [7,9]. Therefore, speciations are sometimes known better as fractionations.

In this work, different extractant agents are evaluated to establish their efficiency in the removal of the total Hg concentration of the Almaden soil. Furthermore, a speciation analysis is used to compare the mobility of mercury before and after the use of each extractant. Some authors highlight the lack of consensus about the information that can be obtained from a speciation analysis of mer-

* Corresponding author. Tel.: +34 952 131915.
E-mail addresses: cvereda@uma.es (C. Vereda-Alonso), maroto@uma.es (J.M. Rodríguez-Maroto).

1383-5866/$ – see front matter © 2011 Elsevier B.V. All rights reserved.
doi:10.1016/j.seppur.2011.01.032

Table 1
Characteristics of the soil used in this study.

Particle size distribution (%)	Sand	64.6	Total concentration (mg kg^{-1})	
	Silt	30	Hg	6100 ± 800
	Clay	5.4	Fe	45,900 ± 1700
Specific gravity (g cm^{-3})		2.24	Zn	96 ± 10
Porosity (%)		36	Cu	31 ± 8
Hydraulic conductivity (cm s^{-1})		2.1×10^{-6}	Pb	29 ± 5
Organic matter (%)		0.90	Cd	0.60
pH (distilled water) (1/2.5, w/w)		8.5	As	17
CEC (cmol kg^{-1})		14.0 ± 1.2	SO_4^{2-}	92 ± 6
Humidity (%)		<1	CO_3^{2-}	68,000 ± 4000

cury for any solid sample [8,10,13,14]. This is not surprising since the speciation is only a simple procedure in which only few fractions are obtained.

As speciation analysis we have chosen the one proposed by the Community Bureau of Reference (BCR, in French language) [14,15] which consists basically on a sequential extraction procedure (SEP) that split the total metal content into four fractions. In addition to the standard BCR, we have also performed some changes to explore the reliability of the results in soils with a high concentration of Hg and other metals.

After the evaluation of the best extractant agent for the remediation, we have explored its possible application for soil flushing [16–18]. In this technology, an extraction solution is circulated through the contaminated zone extracting the pollutants. Then the solution reaches the extraction wells where it is recovered for treatment of the contaminant and possible reuse of the extractant agent. The use of the SEP for the feasibility studies of other remediation technologies applied to real soils contaminated by several heavy metals was successfully shown previously [19].

2. Experimental methods

Soil samples were collected and kindly provided by Prof. Higueras from a zone close to the metallurgical plant of Almadenejos in the Almaden mining district. Table 1 presents the main characteristics of the soil. The textural analysis shows a sandy loam soil, with low hydraulic conductivity, low organic matter content and an alkaline pH. The metal concentrations presented were determined by microwave assisted acid digestion according to EPA method 3051, using an OI Analytical microwave digestion system and an AAS Varian SpectrAA-110. Mercury and iron show the highest concentrations (Table 1).

2.1. Metal fractionation

The BCR fractionation technique [15] provides four fractions, which here are denominated weak acid soluble (WAS), reducible, oxidizable and residual, in each of which the metals are quantified by AAS. In this procedure, the solid residue of each extraction is used to obtain the next fraction. Acetic acid, hydroxylamine, and acid-stabilized hydrogen peroxide are respectively the sequential extraction solutions for the first three fractions. The residual fraction is obtained by microwave assisted acid digestion of the sample that has already been submitted to the three previous steps.

The BCR method is normally applied to soils and sediments with values of the heavy metal concentration about a few tens of milligram per kilogram. However, when these concentrations are in the order of several thousands mg kg^{-1}, the assumption of a "complete" metal extraction could be erroneous. In addition to the normal BCR, a modified BCR procedure was also performed. This modification basically consisted in the introduction of a specific number of successive repetitions of the extraction performed in each BCR step before proceeding to the next one. The influence of the number of those successive repetitions of the extraction on the percentage of metal recovered in each BCR step is studied.

The presence of Hg in the soils of Almaden is mainly as sulfides and sulfates [3,4]. It can be assumed that the sulfates can be associated to the soluble and reducible fractions. Nevertheless we did not know if the sulfides could be associated to the oxidizable fraction or to the residual one. Therefore we designed a simple experiment to clarify this point. A kaolin sample was spiked with HgS (red and black) and $HgSO_4$ by mixing the powders of those products with the kaolin. The final ratio of mercury from HgS (red), HgS (black), and $HgSO_4$ was 2000:2000:2000 mg of Hg per kg of soil to achieve a final concentration of Hg similar to the one of the Almaden soil. The spiked soil was also analyzed by the BCR method in order to assess the fractions to which sulfides and sulfates are associated.

2.2. Batch chelant extraction experiments

A kinetic study was performed in batch extraction assays to determine both the adequate extractant agent and its optimal concentration for the flushing experiments. These assays were triplicated and basically consist of the mixture of 1 g of the initial soil with 25 mL of an extraction solution in 50 mL polypropylene screw-cap vials. For each extractant, 18 of these vials were placed in a rotary shaker at a temperature of 22 ± 1 °C. At selected times three of these vials were taken out from the shaker for pH and Hg concentration measurements in the supernatant liquid. The extractants tested were NaCl (0.01 M and 0.1 M), EDTA (0.01 M, 0.1 M and 1 M), HNO_3 (0.01 M and 0.1 M), KI (5×10^{-3}, 0.01 M, 0.1 M and 1 M) and $Na_2S_2O_3$ (0.01 M, 0.1 M and 1 M). At the end of some of the extractions (with EDTA 1 M, KI 0.1 M and $Na_2S_2O_3$ 0.01 M, 0.1 M and 1 M), normal and modified BCR fractionations were performed for the resultant soil.

2.3. Flushing experiments

In the flushing experiments, a potassium iodide solution (0.1 M) is pumped through a methacrylate column (8 cm i.d. and 20 cm length), assembled from 10 rings, that holds approximately 2 kg of water saturated soil. Iodide is used as chelating agent because high recovery rates of mercury were obtained from the batch experiments described above. The annular disposition allows, first, an easy way of filling the column, since each individual compartment is carefully filled vertically before placing the next one, avoiding air bubbles and achieving good settlement and a reproducible hydraulic conductivity. Second, an easy disassembly of the soil column can be accomplished, so that each of the 10 transversal sections can be neatly separated and analyzed once the experiment is over.

Two different flow rates of the extraction solution were used, corresponding with pore velocities of about 20 and 2 cm h^{-1}. During each assay, samples of the solution leaving the column were taken at selected time steps for pH and Hg concentration measurements. At the end of each assay, the soil is recovered from each of the 10

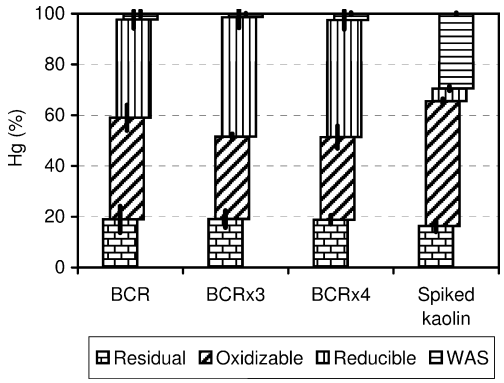

Fig. 1. Mercury fractionation analysis of the initial soil and of the spiked kaolin.

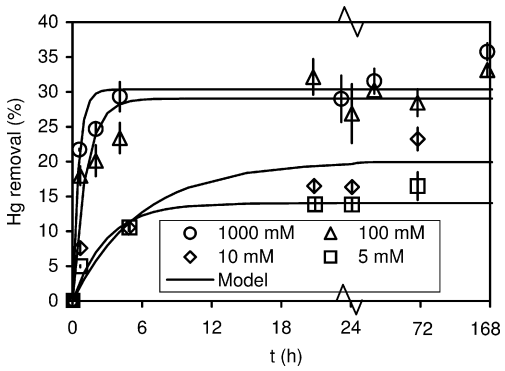

Fig. 2. Kinetic iodide extraction in the batch experiments. Error bars are for standard deviations of triple assays.

transversal sections. The pH, water content, metal concentrations and BCR fractionation are determined in each of these slices.

Since iodide is an expensive reagent, a recycling procedure of the iodide solution was also tested. Thus, two types of replicated flushing experiments were performed to evaluate the feasibility of using the recycled extraction solution. The first one uses fresh KI extraction solutions, while the effluent solutions from these first assays are used as extraction solution in the second type of experiments once it was treated in presence of iron powder at low temperature (50 °C) to recover the extractant. Klasson et al. [20] give a detailed description of this low thermal treatment for the recovery of the iodide extraction solution. In this work, the recovery procedure is performed in 1.5 L batch reactor that treats batches of about 10 L of homogenized effluent.

3. Results and discussion

3.1. Metal fractionation

The fractionation results when a normal BCR procedure is performed in the initial soil indicate that almost no metal is present in the weak acid soluble fraction probably because these metals have already been washed down by the rainwater infiltration. The distribution of the mercury among the BCR fractions in the initial soil is shown in Fig. 1. As can bee seen, about 40% of mercury is present in the reducible fraction, usually associated to the Fe/Mn oxides, and another 40% is present in the oxidizable fraction, normally associated to the organic matter and the sulfides, whereas the remaining is found under the residual form.

Nevertheless, several drawbacks have been reported about the SEPs [10,14,21–23]. Thus, Filgueiras et al. [9] indicate that substantial amounts of the metal bound to the organic matter could be recovered in the reducible fraction and, consequently, the reducible fraction may be overestimated at the expense of the oxidizable fraction. Those authors also indicate that another important drawback in the oxidizable fraction is that H_2O_2 does not completely leach the metals associated with sulfides and therefore those are recovered in the residual fraction.

The modified BCR (BCRx3 and BCRx4) procedure was performed to check if the above-mentioned problems occur. Fig. 1 shows a comparison of the results obtained for mercury from both the normal and modified BCR procedures, the results of the spiked kaolin are shown too.

The distribution of the mercury among the BCR fractions does not change significantly from the normal BCR results to the ones obtained by the modified BCR methods (Fig. 1). However, iron distribution among the BCR fractions changes significantly from the normal BCR to the modified BCR methods (BCRx3 and BCRx4) (not shown). Thus, the percentage of iron in the reducible fraction increases with the number of repetitive extractions performed in each BCR step, indicating that probably the extraction solution reaches saturation in the first extractions.

Finally, the results obtained for the spiked kaolin indicate that the Hg from the sulfate is probably associated mainly to the WAS fraction, whereas the Hg from the sulfides is associated to the oxidizable and residual fractions. As can be seen, the sum of the oxidizable and residual fractions is almost double of the sum of the WAS and reducible fractions, which is the ratio sulfide–sulfate used in the spiking of the kaolin.

3.2. Batch chelant extraction experiments

The results corresponding to the batch chelant extraction experiments indicate that iodide, thiosulfate and the 1 M solution of EDTA yield the best mercury removal percentages among the five chelants tested (NaCl, EDTA, HNO_3, KI and $Na_2S_2O_3$). Chloride solutions and the lower EDTA concentration solutions extracted less than 2% of the initial concentration of Hg in the soil. No mercury was extracted by the nitric acid solution. The low mercury removals obtained for the lower concentrations of the EDTA solutions were probably due to the competition for EDTA of the other metals present in the soil in large concentrations (such as Ca or Fe).

Figs. 2 and 3 show the kinetic results corresponding to the four concentrations of the iodide solutions tested and to the three concentrations of the thiosulfate solutions respectively. The higher the iodide concentration the higher the removal percentage of Hg (Fig. 2). Nevertheless, this happens approaching an upper limit of removal efficiency, and no significant differences exist between 100 and 1000 mM iodide solutions (Fig. 2). As a result, 100 mM iodide

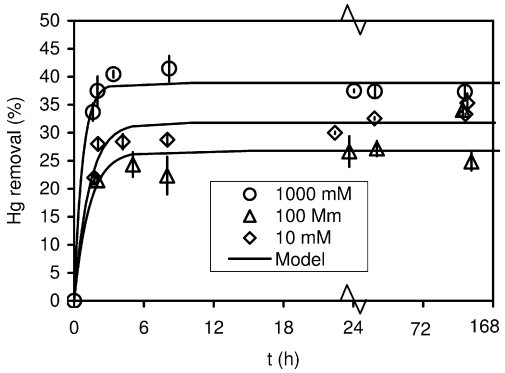

Fig. 3. Kinetic thiosulfate extraction in the batch experiments. Error bars are for standard deviations of triple assays.

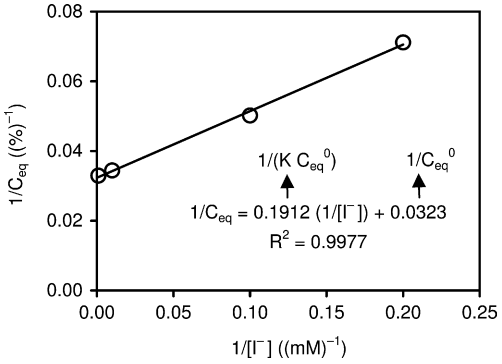

Fig. 4. Experimental and regression values (solid line) for C_{eq}.

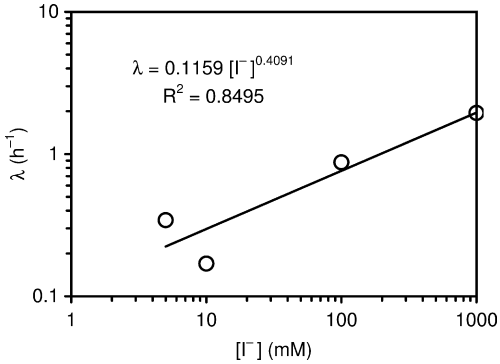

Fig. 5. Experimental and regression values (solid line) for λ.

solution was chosen for the flushing experiments. It is more difficult to make a decision about which thiosulfate concentration should be used for a flushing experiment, without performing a more exhaustive extraction stage.

The removal percentage of mercury approaches an asymptotic value that is different for each extractant concentration. That behavior is usually described by the following kinetic expression:

$$\frac{dC}{dt} = \lambda(C_{eq} - C) \tag{1}$$

where C is the instantaneous concentration of Hg in the aqueous phase, C_{eq} is the Hg concentration in the aqueous phase when the equilibrium is reached and λ is a kinetic parameter. The integration of that expression yields

$$C = C_{eq}(1 - e^{-\lambda t}) \tag{2}$$

In the present work, the removal percentage of Hg is equivalent to a normalized concentration because the solid–liquid ratio used in all assays is constant (1 g/25 mL). Thus, the values of the parameters λ and C_{eq} for each extractant concentration are obtained fitting the integrated expression (Eq. (2)) to the experimental results. The solid curves that are showed in Figs. 2 and 3 correspond to the fitting results. The correlation indexes were higher than 0.88 in all cases except for the results corresponding to the 0.1 M iodide concentration in which the value was 0.7.

The representation of the C_{eq} values against the iodide concentration requires an equation that describes that at low total iodide concentrations the maximum mercury aqueous concentration (C_{eq}) is proportional to [I⁻]. On the other hand, as this iodide concentration increases the mercury extraction becomes independent of [I⁻]. Such behavior can be expressed by

$$C_{eq} = \frac{C_{eq}^0 K[\mathrm{I}^-]}{1 + K[\mathrm{I}^-]} \tag{3}$$

The values of the parameters C_{eq}^0 and K can be obtained by the regression of Eq. (4) (the linearized expression of Eq. (3)) to the C_{eq} values obtained above for each iodide concentration. Results are presented in Fig. 4.

$$\frac{1}{C_{eq}} = \frac{1}{KC_{eq}^0}\frac{1}{[\mathrm{I}^-]} + \frac{1}{C_{eq}^0} \tag{4}$$

Regarding the kinetic coefficient (λ), the values obtained were fitted to the expression

$$\lambda = \lambda_0[\mathrm{I}^-]^m \tag{5}$$

where λ_0 and m are constant. The results are shown in Fig. 5.

As a result, the kinetic of the Hg extraction by iodide solution can be described by a set of three expressions that depend only on four parameters whose values can be easily obtained by the batch assays described in this work. That set of equations becomes a useful tool for the initial selection of the operative conditions that should be used in the remediation of the soil by the flushing technique.

Regarding the distribution of Hg among the BCR fractions after the batch chelant extraction experiments, Fig. 6 shows the BCR and BCRx4 results after the extractions with both potassium iodide 0.1 M and EDTA 1 M, together with the BCR of the initial soil. Two remarks arise from this figure: First, as previously indicated by the BCR results of the initial soil, there are not important differences between the Hg distribution obtained with the normal and modified BCR. Second, the Hg associated to the reducible fraction is efficiently removed. The oxidizable fraction for iodide undergoes also a significant decrease, which is not as important for EDTA. In addition, the mobility of mercury in the soil after the treatment increases, but this effect is much higher for iodide. Therefore, although a fraction of Hg is removed from the soil, an increase of the hazards of the site could be derived from the remediation procedure if it is not completely finished. This was previously observed for other cases [24,25]. Nevertheless, the mercury associated to the WAS fraction can be easily recovered by other techniques, such as acid-enhanced electroremediation [19].

Fig. 7 shows the BCR and BCRx4 results at the end of the batch chelant extraction experiments performed with thiosulfate. Again, no important differences are found between the Hg distributions obtained by BCR and BCRx4 procedures. The distribution of mercury that remains in the soil after thiosulfate extraction undergoes several changes; the most remarkable is the decrease of the percentage of the reducible fraction with respect to the initial soil for all thiosulfate concentrations. An increase of weak acid soluble fraction is also observed, but in a lower extent than that observed for the 0.1 M iodide solution. Only the results for the highest concentration of thiosulfate show an increase of the WAS fraction similar

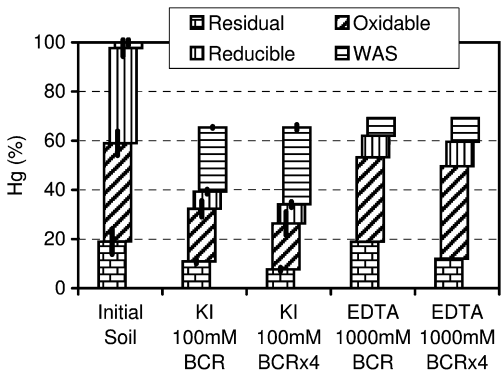

Fig. 6. Mercury fractionation with normal and modified BCR procedure of the resultant soil in batch extractions experiments with potassium iodide 0.1 M.

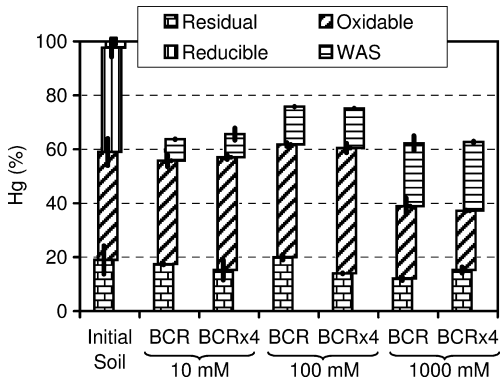

Fig. 7. Mercury fractionation with normal and modified BCR procedure of the resultant soil in batch extractions experiments with thiosulfate in different concentrations.

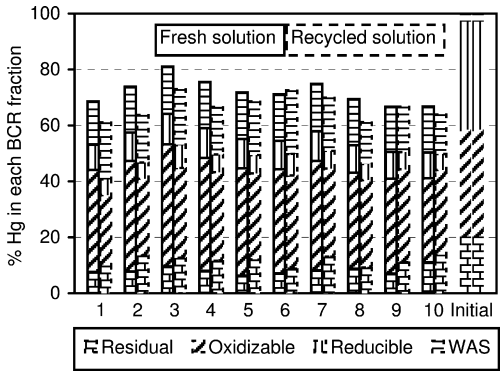

Fig. 9. Mercury fractionation with normal BCR method of the resultant soil in flushing experiments.

to the iodide one. Finally, oxidizable and residual fractions remain practically unchanged except for the 1 M thiosulfate solution, in which the oxidizable fraction decreases.

3.3. Flushing experiments

The results obtained for the two types of flushing experiments, with fresh and recovered extraction solutions of 0.1 M KI, are shown in Fig. 8, where the Hg concentration values in the column effluent and the percentage of mercury removed from the soil are plotted versus the effluent volume.

Approximately a 35% of the mercury can be removed at an acceptable rate (Fig. 8). A higher recovery ratio can be expected but only with a very low concentration of Hg in the effluent, probably due to mass-transfer kinetic limitations, in agreement with the batch chelant extraction results. These kinetic limitations were confirmed by two tests that were conducted in some of the assays. The first one was performed in one of the duplicated fresh solution assay, in which the pumping was stopped for 66 h after the circulation of 26 L, when the effluent concentration was tailing. The concentration rebound observed after this no-flow period confirms the mass-transfer limitations. In the second test, the pore velocity decreased from 20 to 2 cm h^{-1}. In this case, the maximum Hg concentration for the low velocity experiment triples the one for the high velocity, indicating again that local equilibrium between the stationary and the mobile phases was not reached for the high velocity and therefore the efficiency is limited by mass-transfer kinetics.

Regarding the use of the recycled iodide solutions, the flushing results obtained for the recovered solution follow a similar trend

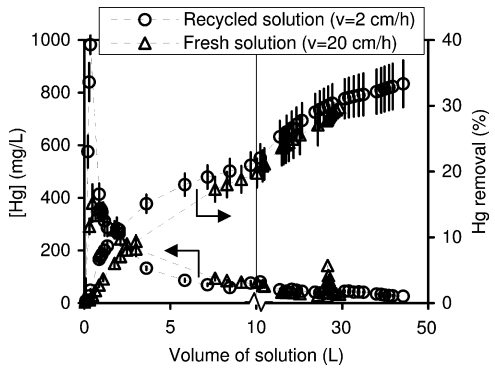

Fig. 8. Results of flushing experiments. Error bars are for standard deviations of duplicate assays.

to those obtained for the fresh solution. This indicates that the low temperature thermal treatment in presence of iron powder [20] is adequate for the recovery of the used iodide solution. The Hg concentration in each of the 10 L homogenized effluent solutions before the recovery treatment ranged from 40 to 200 mg L^{-1}. The determination of Hg concentrations in the solution after the treatment indicates that about 80% of the Hg is removed from the used extractant solution. In addition, Fig. 8 shows that the remaining 20% of Hg does not significantly affect the efficiency of the flushing technique. The recovery of the extraction solution is an important issue because the amount of iodide used for the flushing remediation of the soil is about two moles per kilogram of soil.

The analyses of the soil after treatment indicate that there are no significant changes for the values of pH and moisture from the initial ones. Fig. 9 shows the Hg concentration profile along the column length, normalized to its initial value, and its distribution in the different fractions according to the BCR method at the end of the two types of the flushing experiments. The speciation results for the initial soil are also shown. As can been seen, the results are similar to the ones obtained in the batch chelant extraction experiments: the weak acid soluble fraction increases compared to the initial soil and the reducible fraction undergoes the most important reduction, as could be expected.

4. Conclusions

The most effective chelants for mercury removal (30%) from the soil are iodide, EDTA, and thiosulfate. However, the weak acid soluble fraction in the soil after each treatment is much higher than before treatment. This may result in an increase of the environmental risks because this is the most mobile fraction. Also, this mobile fraction is easier to be treated by another remediation technique such as acid-enhanced electrokinetic remediation.

The BCR method in conjunction with the batch chelant extraction experiments give reliable results about the fractionation of the mercury in the soil remediated by the flushing technique. On the other hand, iron concentration is large enough to give different results when each step of the SEP is repeated before moving to the next sequential extraction, indicating that the standard procedure would give erroneous results.

Acknowledgements

This research was funded by Project CTM2006-13091-C02-01/TECNO (Spanish Ministry of Education and Science) and Project 148/2004/3 (Ministry for Environment).

References

[1] A. Hernández, M. Jébrak, P. Higueras, R. Oyarzun, D. Morata, J. Munhá, The Almaden mercury mining district, Spain, Miner. Deposita 34 (1999) 539–548.

[2] F. Garcia-Herruzo, A. Garcia-Rubio, C. Gomez-Lahoz, C. Vereda-Alonso, J.M. Rodriguez-Maroto, El mercurio. Situación actual, problemas y soluciones, Ing. Quim. 480 (2010) 84–91.

[3] P. Higueras, R. Oyarzun, J. Lillo, J.C. Sánchez-Hernández, J.A. Molina, J.M. Esbrí, S. Lorenzo, The Almaden district (Spain): anatomy of one of the world's largest Hg-contaminated sites, Sci. Total Environ. 356 (2006) 112–124.

[4] P. Higueras, R. Oyarzun, H. Biester, J. Lillod, S. Lorenzo, A first insight into mercury distribution and speciation in soils from the Almaden mining district, Spain, J. Geochem. Explor. 80 (2003) 95–104.

[5] H.E.L. Palmieri, H.A. Nalini Jr., L.V. Leonel, C.C. Windmöller, R.C. Santos, W. de Brito, Quantification and speciation of mercury in soils from the Tripuí Ecological Station, Minas Gerais, Brazil, Sci. Total Environ. 368 (2006) 69–78.

[6] R. Fernández-Martínez, J. Loredo, A. Ordóñez, M.I. Rucandio, Physicochemical characterization and mercury speciation of particle-size soil fractions from an abandoned mining area in Mieres, Asturias (Spain), Environ. Pollut. 142 (2006) 217–226.

[7] F.M.G. Tack, M.G. Verloo, Chemical speciation and fractionation in soil and sediment heavy metal analysis: a review, Int. J. Environ. Anal. Chem. 59 (1995) 225–238.

[8] H. Biester, G. Nehrke, Quantification of mercury in soils and sediments – acid digestion versus pyrolysis, Fresen. J. Anal. Chem. 358 (1997) 446–452.

[9] A.V. Filgueiras, I. Lavilla, C. Bendicho, Chemical sequential extraction for metal partitioning in environmental solid samples, J. Environ. Monit. 4 (2002) 823–857.

[10] N. Issaro, C. Abi-Ghanem, A. Bermonda, Fractionation studies of mercury in soils and sediments: a review of the chemical reagents used for mercury extraction, Anal. Chim. Acta 631 (2009) 1–12.

[11] A.M. Ure, C.M. Davidson, R.P. Thomas, Single and sequential extraction schemes for trace metal speciation in soil and sediment, in: Ph. Quevauviller, E.A.B. Maier, B. Griepin (Eds.), Quality Assurance for Environmental Analysis, Elsevier Science B.V., Amsterdam, 1995, pp. 505–523.

[12] D.M. Templeton, F. Ariese, R. Cornelis, L.G. Danielsson, H. Muntau, H.P. Van Leeuwen, R. Łobinski, Guidelines for terms related to chemical speciation and fractionation of elements. Definitions, structural aspects, and methodological approaches (IUPAC Recommendations 2000), Pure Appl. Chem. 72 (8) (2000) 1453–1470.

[13] D.M. Sánchez, A.J. Quejido, M. Fernández, C. Hernández, T. Schmid, R. Millán, M. González, M. Aldea, R. Martín, R. Morante, Mercury and trace element fractionation in Almaden soils by application of different sequential extraction procedures, Anal. Bioanal. Chem. 381 (2005) 1507–1513.

[14] N.S. Bloom, E. Preus, J. Katon, M. Hiltner, Selective extractions to assess the biogeochemically relevant fractionation of inorganic mercury in sediments and soils, Anal. Chim. Acta 479 (2003) 233–248.

[15] A.M. Ure, P. Quevauviller, H. Muntau, B. Griepink, Speciation of heavy metals in soils and sediments. An account of the improvement and harmonization of extraction techniques undertaken under the auspices of the BCR of the commission of the European Communities, Int. J. Environ. Anal. Chem. 5 (1–4) (1993) 135–151.

[16] D.S. Roote, In Situ Flushing, Ground Water Remediation Technologies Analysis Center, 1997.

[17] PRC Environmental Management, Inc., Recent Developments for In Situ Treatment of Metal Contaminated Soil, PRC Environmental Management, Inc., 1997.

[18] R.A. García-Delgado, J.M. Rodríguez-Maroto, C. Gómez-Lahoz, C. Vereda-Alonso, F. García-Herruzo, Soil flushing with EDTA solutions: a model for channeled flow, Sep. Sci. Technol. 33 (6) (1998) 867–886.

[19] M.D. Garcia-Gutierrez, C. Gomez-Lahoz, J.M. Rodriguez-Maroto, C. Vereda-Alonso, F. Garcia-Herruzo, Electrokinetic remediation of a soil contaminated by the pyritic sludge spill of Aznalcollar (SW, Spain), Electrochim. Acta 52 (2007) 3372–3379.

[20] K.T. Klasson, L.J. Koran, D.D. Gates, P.A. Cameron, Removal of Mercury from Solids Using the Potassium Iodide/Iodine Leaching Process, Department of Energy, US, 1997.

[21] Z. Mester, C. Cremisini, E. Ghiara, R. Morabito, Comparison of two sequential extraction procedures for metal fractionation in sediment samples, Anal. Chim. Acta 359 (1998) 133–142.

[22] L.M. Ottosen, H.K. Hansen, P.E. Jensen, Relation between pH and desorption of Cu, Cr, Zn, and Pb from industrially polluted soils, Water Air Soil Pollut. 201 (2009) 295–304.

[23] G.M. Kirkelund, L.M. Ottosen, A. Villumsen, Investigations of Cu, Pb and Zn partitioning by sequential extraction in harbour sediments after electrodialytic remediation, Chemosphere 79 (2010) 997–1002.

[24] A.B. Ribeiro, J.T. Mexia, A dynamic model for the electrokinetic removal of copper from a polluted soil, J. Hazard. Mater. 56 (3) (1997) 257–271.

[25] A.B. Ribeiro, J.M. Rodriguez-Maroto, Electroremediation of heavy metal contaminated soils. Processes and application, in: M.N.V. Prasad, K.S. Sajwan, R. Naidu (Eds.), Trace Elements in the Environment: Biogeochemistry, Biotechnology, and Bioremediation, CRC Press, Boca Raton, 2006, pp. 341–368 (Chapter 18).

Conference Contribution

"Numerical Simulations of Electrokinetic Processes Comparing the Use of a Constant Voltage Difference or a Constant Current as Driving Force"

J.M. Paz-García, B. Johannesson, L.M. Ottosen, A.B. Ribeiro and J.M. Rodríguez-Maroto

Poster presented in: *Annual meeting of the Danish Electrochemical Society - Conference on Electrochemical Science and Technology, Technical University of Denmark, Lyngby (Denmark), Sep 30 - Oct 1, 2011*

Annual meeting of the Danish Electrochemical Society
Conference on Electrochemical Science and Technology

Authors:

Juan Manuel Paz-Garcia*, Björn Johannesson, Lisbeth M. Ottosen
Department of Civil Engineering
Technical University of Denmark
Brovej, building 118
2800 Kgs. Lyngby
Denmark

Title:

Numerical Simulations of Electrokinetic Processes Comparing the Use of a Constant Voltage Difference or a Constant Current as Driving Force

Abstract:

Electrokinetic techniques are characterized by the use of a DC current for the removal of contaminants from porous materials. The method can be applied for several purposes, such as the recuperation of soil contaminated by heavy metals or organic compounds, the desalination of construction materials and the prevention of the reinforced concrete corrosion.

The electrical energy applied in an electrokinetic process produces electrochemical reactions at the electrodes. Different electrode processes can occur. When considering inert electrodes in aqueous solutions, the reduction of water at the cathode is usually the dominant in the process. On the other hand, the electrode processes at the anode depend on the ions present in its vicinity. Oxidation of water and chloride are typically assumed to be the most common processes taking place. Electrons produced in the electrode processes are transported from the anode to the cathode through the closed electrical circuit of the cell. In the solution, the electrical current is carried by the ions, which move towards the electrode with different charge. Therefore, different authors have studied the system using the circuit theory. Assuming that it is possible to study the region limited by the electrodes as a one-dimensional problem, the system consisting of electrolyte, electrodes, conductors and power supply can be considered as an electrical circuit connected in series. According to the Ohm's law, the voltage and the electrical current would be related to the conductivity of the media. This conductivity will vary as the electrokinetic process proceeds.

For a better control of the electrokinetic process, a constant difference of voltage or a constant current density between the electrodes is typically used. Most authors argued that fixing the current density results in more efficient electrokinetic experiments with less operative problems. Nevertheless, in long term treatments, maintaining a constant current density can be difficult due to limitations of the power supply.

Numerical Simulations of Electrokinetic Processes Comparing the Use of a Constant Voltage Difference or a Constant Current as Driving Force

Juan Manuel Paz-García, Björn Johannesson, Lisbeth M. Ottosen

Civil Engineering Department, Technical University of Denmark

Introduction

The **Electrokinetic techniques** are characterized by the use of a DC current for the removal of contaminants from porous materials. As driving force of the process, a constant difference of voltage or a constant electrical current is typically applied, obtaining different results. Most authors argued that establishing a constant current results in more efficient electrokinetic experiments with less operative problems.

In the present study, a theoretical comparison between these two working conditions is discussed. Numerical simulation of the process are used for illustrate the problem.

The Model

A finite element method has been developed and used for modeling the electrokinetic desalination process. The method is based on the integration of the mass continuity equations of each specie in the system and completed with a continuous charge balance equation in order to calculate the electrical potential.

$$\frac{\partial C_i}{\partial t} = -\nabla J_i + R_i$$

Equation 1: *Nernst-Planck equation; C_i is the molar concentration of the species i, J_i is the flux and R_i is the generation (chemical reaction) term.*

$$\varepsilon_o \frac{\partial^2 \phi}{\partial x^2} = \mathrm{F}\sum_i C_i z_i$$

Equation 2: *Poisson equation of electrostatics; ε_o is the permittivity, Φ the electrical potential, F is the Faraday constant and z_i the charge.*

Electrons transport the electricity through the conductors and the power supply. But, in the solution, the electrical current is transported by the ions, which move towards the electrode with different charge by a transport process denoted as electromigration. The movement of ions is mainly due to the gradient of electrical potential (electromigration) but is significantly affected for the gradient of concentration (diffusion).

$$J_i = -D_i \nabla C_i - U_i C_i \nabla \phi$$

Equation 3*: Ionic flux [mol·L·s]. D_i is the diffusion coefficient and U_i the ionic mobility coefficient.*

The electrical energy is transformed to an ionic current by means of the electrode processes. At the electrodes, redox half-reaction occurs, and a local charge unbalance is generated. In general, the electromigration term is dominant in the process. Nevertheless, large gradients of concentration could lead to the equilibrium and stop the process.

The Modeled system

In the present work, numerical simulations of the pH-buffered enhanced electrokinetic desalination process of a brick sample contaminated with high concentration of KCl are shown. As buffered substance, a kaolinite clay with high content of $CaCO_3$ is used. The experimental setup is shown in figure 1.

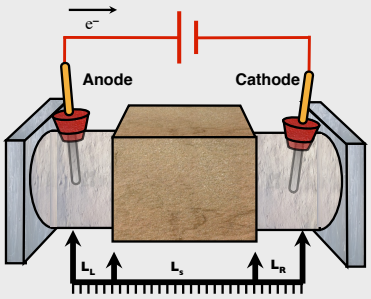

Figure 1: *Schematic representation of the 5.4 cm length brick sample, and the 4 cm length electrode compartments. Electrodes are assume to be inert. The pore solution of the sample initially contains* 0.15 M of KCl.

The following redox reactions are considering in this study:

Anode:

$$H_2O \rightleftarrows \frac{1}{2}O_2(\uparrow) + 2H^+ + 2e^-$$

$$2Cl^- \rightleftarrows Cl_2(\uparrow) + 2e^-$$

Cathode:

$$H_2O + 2e^- \rightleftarrows H_2(\uparrow) + 2OH^-$$

The model offers a general and complete description of the transport process. Nevertheless, results can be analyzed considering a electrical behavior. Considering the one-dimensional region between the electrodes, the system can be easily understood by means of the circuit theory. The Ohm's law related the voltage and the current with the conductivity of the pore solution. The following simplified system can be considered, showing the evolution of the current and the distance.

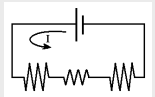

Stage 1: (fast) *The electrode compartments have low conductivity and are responsible of the main resistance. In a short period, the electrode processes increase the conductivity of the electrode compartments*

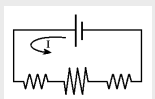

Stage 2: *While the conductivity does not change drastically, both voltage and current will keep an approximate constant value.*

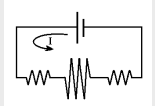

Stage 3: end of the treatment *When the KCl is been almost completely removed, the conductivity in the sample (and as a consequence, in the whole system) decreases.*

In addition to this, the voltage drop related to the electrode processes (redox potential) should also be considered. Due to the polarization effects, this voltage drop is very difficult to predict and quantify.

Results

Simulation 1: Constant voltage difference (1 V)

Results from the simulations are shown. Vertical lines indicate the interface between the clay and the brick sample.

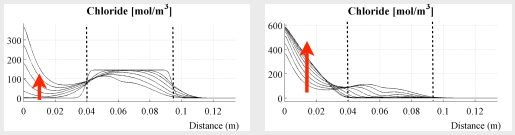

Figure 2: *Chloride concentration: a) First 3 days of treatment b) Subsequent 4 days. The chloride is considered the contaminant of interest in this process.*

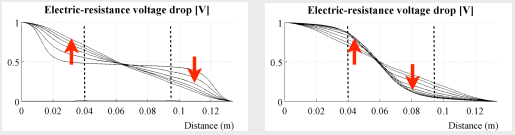

Figure 3*: Electrical potential. a) First 3 days of treatment b) Subsequent 4 days.*

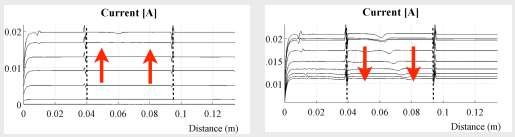

Figure 4: *Electrical current. a) First 3 days of treatment b) Subsequent 4 days.*

Simulation 2: Constant current (5 mA)

Results from the constant current treatment are quite similar to those obtained under constant voltage. Only the electrical potential distribution is shown, since it is the only parameter that vary as result of changes in the conductivity. The electrical current is, in this case, constant in the time and the distance.

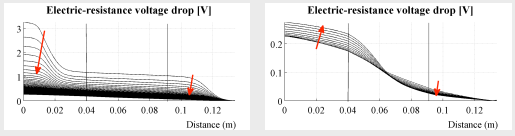

Figure 5: *Electrical potential. a) First 3 days of treatment b) Subsequent 4 days.*

Conclusions

Based on the theoretical analysis and the results from the simulations, it can be outlined the following conclusions:

- Establishing a constant current allows a **better control of the electrical conditions** in the sample. The voltage drop due to the electrode compartments and the electrode processes can not be easily predicted. By using a constant current, it can be assured that at least one of the electrical parameters is known in the main target of the treatment. On the other hand, the electrical potential undergoes important variations, since it is the only parameter that vary as result of changes in the conductivity. In addition to this, a constant current also forces the **electromigration transport** term to be **dominant with respect to the diffusion**, since the electrical current is given by the ionic flux, as explained in Equation 3.

- A standard power supply, working as a current source, has a maximum value of voltage to be given. (typically around 125 V) In fact, it acts as a voltage source what modify the voltage in order to supply the desired current. When the maximum voltage is reached, a power supply switches to constant voltage and keep this maximum value. For that reason, there is a **limitation with respect to long term treatments with constant current conditions**.

Conference Contribution

"Mathematical Modeling of the Role of Chemical Speciation on Electrokinetic Transport of Chemicals in Soil"

J.M. Paz-García, A.N. Alshawabkeh, L.M. Ottosen

Poster presented in: *Sustainable Remediation 2012 - State of the Practice, University of Massachusetts, Amherst, Massachussetts (US), Jun 1-3, 2011*

Sustainable remediation 2011 - State of the Practice
University of Massachusetts, Amherst, Massachusetts, US

Mathematical Modeling of the Role of Chemical Speciation on Electrokinetic Transport of Chemicals in Soil

J.M. Paz-García[1,2], A.N. Alshawabkeh[2], L.M. Ottosen[2]

[1]*Department of Civil Engineering, technical University of Denmark, Lyngby, Demark*
[2]*Deparment of Civil and Environmental Engineering, Northeastern University, Boston, Massachusetts, US*

Abstract

The efficiency of the electrokinetic remediation treatment of heavy metal polluted soil has been demonstrated to be dependent upon the chemical reactivity of the target contaminant rather than the migration rate of the target ions. The contaminants have to be in a soluble species, preferable an ionic form, in order to be mobilized under the gradient of electrical potential induced in the system.

In the present work, a mathematical model for chemical equilibrium calculation is developed and used for the analysis of the interactions between the species in the pore solution and the solid matrix in lead contaminated soil. The model is based on the simultaneous solution of a non-linear set of reversible aqueous and precipitation/dissolution chemical reactions. A line search Newton-Raphson method, iterating on the extent of each reaction, is used for the chemical equilibrium calculations.

Simulations are presented in order to show the behavior of the chemical system with respect to the buffering capacity of the soil and the pH changes of the pore solution induced by the electrode reactions in the electrochemical treatment. In addition to this, the role of some extracting agents in the speciation of lead is discussed. Results from simulations bring light of the effect of the speciation of lead in soil in the transport process, and can be useful for a correct design of enhanced electrokinetic remediation treatments.

Keywords:

Chemical equilibrium, Reaction extent, Lead speciation

Poster awarded with the first price student competition.

Mathematical Modeling of the Role of Chemical Speciation on Electrokinetic Transport of Chemicals in Soil

Juan Manuel Paz-Garcia[1, 2], Akram N. Alshawabkeh[2], Lisbeth M. Ottosen[1]

1: Civil Engineering Department, Technical University of Denmark; 2 Civil and Environmental Engineering; Northeastern University

Introduction

Electrokinetic (EK) transport of pollutants from soil consists of the mobilization of species by the application of an external electric DC field.

In EK processes (Fig. 1) the electric current is transported by the ions in the pore solution, which move towards the electrode of different charge (electromigration). Non-ionic species are also mobilized due to electroosmotic advection, i.e. the transport of the pore solution itself under the gradient of electrical potential. In certain conditions, the chemical diffusion can play an important role in the transport process.

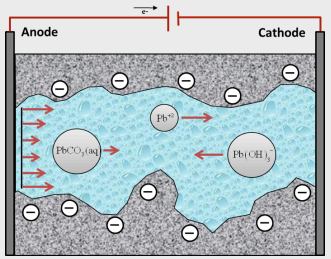

Figure 1: Electrokinetic transport process.

The efficiency of the EK soil remediation treatments was demonstrated to be dependent upon the chemical reactivity of the target pollutants rather than their migration rates. The contaminants have to be in a soluble species, preferably as ionic form, in order to be mobilized under the gradient of electrical potential induced in the system. Heavy metals easily precipitate as insoluble minerals (Fig. 2). In those conditions, the removal rate decreases while the energy consumption increases.

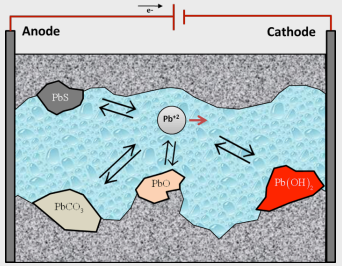

Figure 2: Feasible precipitation/dissolution equilibria for lead minerals during electrokinetic treatments.

Materials and Methods

In the present work, a mathematical model for chemical equilibrium calculation is developed and used for the analysis of the interactions between the species in the pore solution and the solid matrix in lead contaminated soil. The model is based on the simultaneous solution of a set of non-linear equations describing the reversible aqueous and precipitation/dissolution chemical reactions. A tailor-made line-search Newton-Raphson method, iterating on the extent of each reaction, is used to minimize the residual function; defined as the distance to the equilibrium state in the mass action equation of each chemical reaction included in the system.

Table 1: Solubility products of some lead minerals

Stoichiometric reaction	$\log_{10}(K_{SP})$*
$PbS\ (s) \rightleftarrows Pb^{+2} + HS^- - H^+$	-14,84
$PbO \rightleftarrows Pb^{+} + H_2O - 2H^+$	12,62
$Pb(OH)_2\ (s) \rightleftarrows Pb^{+2} + 2H_2O - 2H^+$	8,15
$PbCl_2\ (s) \rightleftarrows Pb^{+2} + 2Cl_2^-$	-4,81
$PbCO_3\ (s) \rightleftarrows Pb^{+2} + CO_3^{-2}$	-13,29

Table 2: Equilibrium constants of some lead aqueous compounds

	$\log_{10}(K_{eq})$* as function of x			
	1	2	3	4
$Pb^{+2} + xOH^- \rightleftarrows Pb(OH)_x^{2-x}$	-7,51	-16,95	-27,20	-38,90
$Pb^{+2} + xCO_3^{2-} \rightleftarrows Pb(CO_3)_x^{2-x}$	7,00	10,13	-	-
$Pb^{+2} + HCO_3^{2-} \rightleftarrows PbHCO_3^+$	13,20	-	-	-
$Pb^{+2} + xNO_3^- \rightleftarrows Pb(NO_3)_x^{2-x}$	1,06	1,48	-	-
$Pb^{+2} + x\text{Acetate}^- \rightleftarrows Pb(\text{Acetate})_x^{2-x}$	2,78	4,08	3,59	3,40
$Pb^{+2} + x\text{Citrate}^{-3} \rightleftarrows Pb(\text{Citrate})_x^{2-3x}$	7,27	6,53	-	-
$Pb^{+2} + xCl^- \rightleftarrows Pb(Cl)_x^{2-x}$	1,44	2,00	1,69	1,40

The electric current applied is transformed to an ionic current by means of the electrochemical reactions at the electrodes. Electrolysis of water reactions are always likely to happen. Consequently, sharp pH profiles are expected in EK treatments.

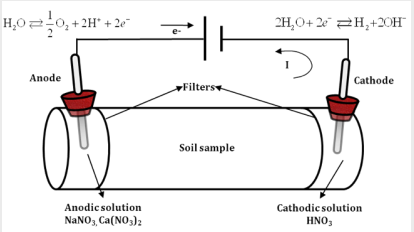

Figure 3: Typical experimental setup for a lab-scale acid-enhanced electrokinetic remediation treatment of a soil sample in horizontal column.

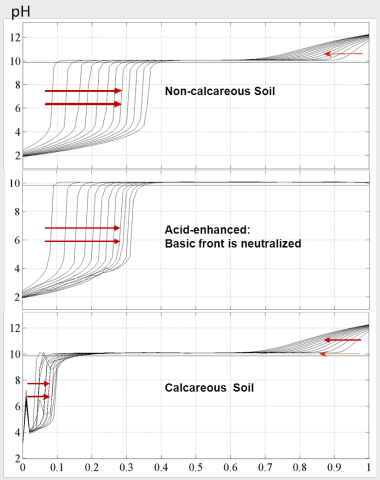

Figure 4: pH profiles from simulations with a Poisson-Nernst-Planck transport model. Constant current 1 mA. 12 hours treatment, one profile per hour. a) non-calcareous soil b) Acid enhanced treatment c) calcareous soil.

I. The acid front that is developing at the anode promotes the desorption and mobilization of most heavy metals during the remediation process.

II. Hindering the basic front developed in the cathode assures acid media in the whole domain and promotes a better mobilization of the contaminants.

III. The buffer capacity of the soil, typically due to the carbonate content, significantly affects the advance of the acid front. Additionally, the formation of insoluble carbonates, such as $PbCO_3$ may be an important type of retention of the heavy metals in calcareous soils.

Extracting agents are used to increase the solubility of the target contaminant, by balancing the equilibrium to the formation of aqueous complexes. The technique can be combined with the acid-enhanced procedures for an efficient and more selective removal of contaminants.

Different extracting agents have been tested to enhance the electrokinetic removal of lead, such as EDTA, acetic acid, citric acid and nitric acid (Table 2).

Results

Simulations presented (Table 3) show the behavior of the chemical system with respect to the buffering capacity of the soil and the pH changes of the pore solution induced by the electrode reactions. Additionally, the role of some extracting agents in the speciation of lead is discussed. Simulations consist of computing the concentration of aqueous species by considering the equilibrium state of pure water (or the specified electrolyte at 0.01 M) and a solid matrix containing enough mineral, that dissolves until over-saturated equilibrium conditions.

Table 3: Simulation results. a) Non-calcareous soil. b) calcareous soil.

		pH	Pb^{+2} [mol/L]	Lead compounds [mol/L]	
				Ionics	Non-ionics
a)	PbS	7.00	1.4783×10^{-11}	1.9347×10^{-11}	1.6568×10^{-14}
	PbS + HAc	468	2.4619×10^{-9}	2.5024×10^{-9}	1.2887×10^{-14}
	PbO	7.48	9.2789×10^{-8}	1.8020×10^{-7}	9.6887×10^{-10}
	PbO + KCl	7.38	1.0076×10^{-7}	1.0076×10^{-7}	6.2621×10^{-19}
	PbO + HAcetate	5.82	9.5024×10^{-6}	9.8358×10^{-6}	9.3012×10^{-11}
	PbO + H_3Citrate	5.92	1.0059×10^{-5}	3.0733×10^{-5}	7.7083×10^{-11}
b)	PbS	9.90	4.4489×10^{-13}	4.4489×10^{-13}	2.4307×10^{-19}
	PbS + HAc	5.68	2.1850×10^{-11}	2.1850×10^{-11}	2.4307×10^{-19}
	$PbCO_3$	8.14	2.2960×10^{-9}	1.2141×10^{-8}	6.9923×10^{-10}
	$PbCO_3$ + KCl	8.12	8.8100×10^{-9}	5.3683×10^{-8}	5.1436×10^{-7}
	$PbCO_3$ + HAcetate	8.12	8.9228×10^{-9}	5.4088×10^{-8}	5.1436×10^{-7}
	$PbCO_3$ + H_3Citrate	6.35	4.4241×10^{-8}	5.6458×10^{-6}	8.4370×10^{-10}

Results from simulations shown that acid enhanced methods, combined with the used of some extracting agents will increase the efficiency of the treatment. In calcareous soil, the buffer capacity limits the acid enhanced applicability.

Conclusion

In the present study a mathematical model for the solution of a set of simultaneous reactions in a multicomponent-multiphase chemical system under the assumption of chemical equilibrium is described. The model used here can be included in a more general model for electrokinetic transport accounting for the chemical reactivity.

Simulations shown the effect of the pH, the initial speciation of the target contaminant, and the influence of the different extracting agents and the soil buffering capacity on the aqueous concentration of the contaminant in the pore solution, which determine the efficiency of the treatment (in terms of the removal rate and the energy consumption).

Acknowledgments

This program is supported by Award Number P42ES017198 from the National Institute of Environmental Health Sciences, USA. Juan Manuel Paz-Garcia acknowledges the Danish Agency of Science Technology and Innovation, for the economical support in the project 274-08-0386 "Fundamentals of Electrokinetics in In-homogeneous Matrices".

Conference Contribution

"Coupling the transport of water and aqueous species in finite elements modeling of electrokinetics"

J.M. Paz-García, B. Johannesson, L.M. Ottosen, A.N. Alshawabkeh, A.B. Ribeiro and J.M. Rodríguez-Maroto

Poster presented in: *12th Mediterranean Congress of Chemical Engineering, Barcelona (Spain), Nov 12-15, 2011*

COUPLING THE TRANSPORT OF WATER AND AQUEOUS SPECIES IN FINITE ELEMENT MODELING OF ELECTROKINETICS

J.M. Paz-García[1], L.M. Ottosen[1], B. Johannesson[1], A.N. Alshawabkeh[2], A.B. Ribeiro[3] and J.M. Rodríguez-Maroto[4]

[1] Department of Civil Engineering, Technical University of Denmark, jugra@byg.dtu.dk
[2]Department of Civil and Environmental Engineering, Northeastern University, USA
[3]Department of Environmental Sciences and Engineering, New University of Lisbon, Portugal
[4]Department of Chemical Engineering, University of Málaga, Spain

Scientific topics: Environmental Technology

The electrokinetic transport of ionic and non-ionic species through a porous media under the effect of an external electric field can be mathematically described by the Nernst-Planck-Poisson (NPP) system of equations. The Nernst-Planck mass balance equation describes the transport of aqueous species by a combination of the diffusion and electromigration terms. Since the ions themselves contribute to the local electric potential, Poisson's equation of electrostatics, that relates the electrostatic potential to local ion concentrations, is solved simultaneously to describe this effect. This strongly coupled non-linear system has been satisfactory solved by finite element integration, and combined to additional physicochemical aspects such as the electrode processes and the chemical interaction between the species in the system for modeling of electrokinetic transport processes.

Proper models of the electrokinetic phenomena have to take into account the transport of the pore solution itself. Water is suggested to electroosmotic flow under electric fields. Electroosmotic advection is of mayor importance when considering the transport of non-charged particles such as organic contaminants from soil. The transport of water may dry the material at the anode surroundings, what may interrupt the ionic current and stop the process. Capillary forces and hydraulic gradient, between others, can also affects to the transport of water in the porous media.

In the present work, the NPP system has been extended in order to include the water transport equation, and to calculate the advective flow contribution on the ionic transport. In this model, the transport of water is assumed to be a combination of hydraulic gradient, capillary suction forces and electroosmotic flow. In the model presented here, the advective term has been implicitly included in the Nernst-Planck equation of each individual aqueous species. Thus, this coupling strategy between the water and the ionic transport together with a numerical procedure for solving the non-linearity character, allows a simplified finite element analysis.

References

J.M. Paz-García, B. Johannesson, L.M. Ottosen, A.B. Ribeiro, and J.M. Rodríguez-Maroto, "Modeling of electrokinetic processes by finite element integration of the Nernst-Planck-Poisson system of equations". Separation and Purification Technology, 2011, 79, 183-192.

COUPLING THE TRANSPORT OF WATER AND AQUEOUS SPECIES IN FINITE ELEMENT MODELING OF ELECTROKINETICS

J.M. Paz-García[1], B. Johannesson[1], L.M. Ottosen[1], A.N. Alshawabkeh[2], A.B. Ribeiro[3] and J.M. Rodríguez-Maroto[4]

[1] Department of Civil Engineering, Technical University of Denmark;
[2]Department of Civil and Environmental Engineering, Northeastern University, Boston, USA;
[3]Department of Environmental Sciences and Engineering, New University of Lisbon, Portugal;
[4]Department of Chemical Engineering, University of Málaga, Spain

Introduction

The electrokinetic transport of ionic and non-ionic species through a porous media under the effect of an external electric field can be mathematically described by the Nernst-Planck-Poisson (NPP) system of equations.

Mass balance equation for the transport of water:

$$Ap\left(\frac{\partial\theta}{\partial t}=-\nabla\mathbf{J}_\theta+G_\theta\right);\quad \mathbf{J}_w=\underbrace{-D_\theta\nabla\theta}_{\text{Moisture transport}}\ \underbrace{-k_h\nabla h}_{\text{Hydraulic transport}}\ \underbrace{-\theta k_e\nabla\phi}_{\text{Electroomosis}}$$

Nernst-Planck equation:

$$Ap\theta\left(\frac{\partial n_i}{\partial t}=-\nabla\mathbf{J}_i+G_i\right);\quad \mathbf{J}_i=\underbrace{\mathbf{v}_w n_i}_{\text{Advection}}\ \underbrace{-D_i^{eff}\nabla n_i}_{\text{Diffusion}}\ \underbrace{-U_i^{eff}n_i\nabla\phi}_{\text{Electromigration}}$$

Poisson's equation:

$$\varepsilon\nabla^2\phi=F\sum_{i=1}^{M}n_i z_i$$

where:

- **Advection**
  - $\mathbf{v}_w n_i$ — Movement of the species in the solution due to the fluid's bulk motion.
- **Diffusion** (Fick's law)
  - $-D_i^{eff}\nabla n_i$ — Movement of species due to a gradient of chemical potential.
- **Electromigration**
  - $-U_i^{eff}n_i\nabla\phi$ — Movement of charged species in an electric field.
- **Total Moisture transport** (Richards' equation)
  - $-D_\theta\nabla\theta$ — Motion of water in unsaturated porous media.
- **Hydraulic flow** (Darcy's law)
  - $-k_h\nabla h$ — Movement of water in saturated porous media, due to gradient of hydraulic gradients.
- **Electroosmotic flow**
  - $-\theta k_e\nabla\phi$ — Motion of the liquid induced by an applied electric potential.

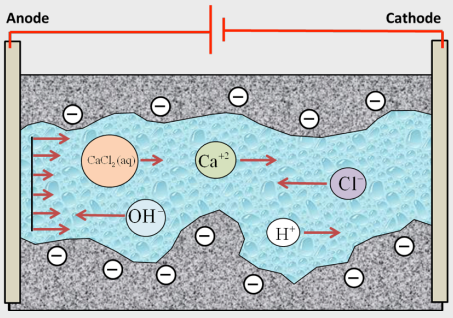

Figure 1: Electrokinetic transport phenomena

1. Electromigration is the main mechanism affecting ionic transport. Electroosmotic advection is important for the transport of non-charged particles.
2. Richards' equation describes the movement of both vapor and liquid water on the basis of a single variable, the moisture content. Capillary forces are assumed the main transport mechanism.
3. The moisture diffusivity is assumed to be non-linear function of the water content and the nature of the porous material.
4. Fully saturated conditions are rare. Hydraulic flow may be negligible with respect to the other transport contributors. Unsaturated conditions are assumed in the proposed numerical model.

Terminology

Table 1: Terminology for the mathematical description of the model

Term:	
$\theta\left(kg_w m_{pore}^{-3}\right)$	Moisture content
$n_i\left(mol_i\, kg_w^{-1}\right)$	Molal concentration
$\phi(V)$	Electrical potential
z_i	Ionic charge
h	Hydraulic head
A	Cross-sectional area
p	Porosity
i	Index for the i^{th} species
M	Total number of aqueous chemical species
$\mathbf{J}$	Flux term
G	Generation term
$\mathbf{v}_w$	Water velocity
D_i^{eff}	Effective diffusivity
U_i^{eff}	Effective ion mobility
D_θ	Total moisture diffusivity
k_e	Electroosmotic permeability coefficient
k_h	Hydraulic conductivity
F	Faraday constant

Table 2: Terminology for the matrices in the Finite Element Formulation.

FEM Matrix	State variable	k parameter
$\mathbf{K}^{mt}$	θ	ApD_θ
$\mathbf{K}^{eo}$	ϕ	$A\theta pk_e$
$\mathbf{K}_i^{mta}$	θ	$ApD_\theta n_i$
$\mathbf{K}_i^{eoa}$	ϕ	$A\theta pk_e n_i$
$\mathbf{K}_i^{dif}$	n_i	$A\theta pD_i^{eff}$
$\mathbf{K}_i^{em}$	ϕ	$A\theta pU_i^{eff}$
$\mathbf{K}_\phi$	ϕ	ε
$\mathbf{E}_i$	n_i	Fz_i
$\mathbf{C}_\theta$	$\frac{\partial\theta}{\partial t}$	$\frac{Ap}{\Delta t}$
$\mathbf{C}_i$	$\frac{\partial n_i}{\partial t}$	$\frac{Ap\theta}{\Delta t}$

Chemical Generation

Water participates in several chemical reactions along the domain of the treated body as, for example, precipitation, dissolution and hydration of salts. In electrokinetics, electrolysis reactions may occur at the electrodes as a consequence of the applied current. And so, water is consume at the vicinities of the electrodes.

$$H_2O \rightleftarrows \frac{1}{2}O_2 + 2H^+ + 2e^-$$

$$2H_2O + 2e^- \rightleftarrows H_2 + 2OH^-$$

Somewhere in the middle of the treated body, these H^+ and OH^- fronts can meet each other producing water.

Numerical Model

The strongly coupled non-linear NPP system can be satisfactory solved by finite elements integration. It can also be combined to additional physicochemical aspects such as the electrode processes and the chemical interaction between the species in the system for modeling of electrokinetic transport processes.

Let the vector $\mathbf{a}$ be the discrete form at the state variables at the nodal points, and $\mathbf{f}$ the load vectors for the state variables indicated with the corresponding subscript. Generation terms are implicitly included in the load vectors. The weak formula for the extended NPP system in the finite element method is:

Mass balance equation for the transport of water:

$$\mathbf{C}_\theta\left(\mathbf{a}_\theta^t-\mathbf{a}_\theta^{t-\Delta t}\right)+\mathbf{K}^{mt}\mathbf{a}_\theta^t+\mathbf{K}^{eo}\mathbf{a}_\phi^t+\mathbf{f}_\theta=0$$

Nernst-Planck equation:

$$\mathbf{C}_i\left(\mathbf{a}_i^t-\mathbf{a}_i^{t-\Delta t}\right)+\mathbf{K}_i^{mta}\mathbf{a}_\theta^t+\mathbf{K}_i^{dif}\mathbf{a}_i^t+\left(\mathbf{K}_i^{eoa}+\mathbf{K}_i^{em}\right)\mathbf{a}_\phi^t+\mathbf{f}_i=0$$

Poisson's equation:

$$\sum_{i=1}^{M}\mathbf{E}_i\mathbf{a}_i^t+\mathbf{K}_\phi\mathbf{a}_\phi^t+\mathbf{f}_\phi=0$$

A global matrix system of equations is obtained by:

$$\mathbf{C}\left(\mathbf{a}^t-\mathbf{a}^{t-\Delta t}\right)+\mathbf{K}\mathbf{a}^t+\mathbf{f}=0$$

Where:

$$\mathbf{C}=\begin{bmatrix}\mathbf{C}_\theta & 0 & \cdots & \cdots & 0\\ 0 & \mathbf{C}_1 & \ddots & \ddots & 0\\ \vdots & \ddots & \ddots & \ddots & \vdots\\ \vdots & \ddots & \ddots & \mathbf{C}_M & 0\\ 0 & 0 & \cdots & 0 & 0\end{bmatrix};\quad \mathbf{a}^t=\begin{bmatrix}\mathbf{a}_\theta^t\\ \mathbf{a}_1^t\\ \vdots\\ \mathbf{a}_M^t\\ \mathbf{a}_\phi^t\end{bmatrix};\quad \mathbf{f}=\begin{bmatrix}\mathbf{f}_\theta\\ \mathbf{f}_1\\ \vdots\\ \mathbf{f}_M\\ \mathbf{f}_\phi\end{bmatrix};$$

$$\mathbf{K}=\begin{bmatrix}\mathbf{K}^{mt} & 0 & \cdots & \cdots & \mathbf{K}^{eo}\\ \mathbf{K}_1^{mta} & \mathbf{K}_1^{dif} & 0 & \ddots & \left(\mathbf{K}_1^{eoa}+\mathbf{K}_1^{em}\right)\\ \vdots & 0 & \ddots & \ddots & \vdots\\ \mathbf{K}_M^{mta} & \ddots & \ddots & \mathbf{K}_M^{dif} & \left(\mathbf{K}_M^{eoa}+\mathbf{K}_M^{em}\right)\\ 0 & \mathbf{E}_1 & \cdots & \mathbf{E}_M & \mathbf{K}_\phi\end{bmatrix}$$

The proposed system can be used for simulating reactive transport of water and aqueous species in porous material under the effect of an externally applied electric field, as well as for free diffusion problems.

Conclusions

Petrov-Galerkin (PG) or Galerkin least square (PLS) are assumed standard for convection dominated problems, but they required a complicated formulation which usually implies high computation time. By means of the proposed coupled system, including the advective term directly in the Nernst-Planck equation of each aqueous species apart from in the water transport equation itself, the convenience Galerkin method of weighted residuals can be used for the solution of the non-linear coupled transport of water and aqueous species in porous media.

Acknowledgments

Rodriguez-Maroto acknowledges the financial support of the Ministerio de Ciencia e Innovación of the Spanish Government through the project ERHMES, CTM2010-16824. Paz-García acknowledges the Danish Agency of Science Technology and Innovation for the economic support through the project 274-08-0386 "*Fundamentals of Electrokinetics in in-homogeneous matrices*".

Conference Contribution

"Influence of the Chemical Interactions on the Removal Rate of Different Salts in Electrokinetic Desalination Processes"

J.M. Paz-García, B. Johannesson, L.M. Ottosen, A.B. Ribeiro and J.M. Rodríguez-Maroto

Peer-reviewed full conference paper in: *SWBSS2011 - Salt Weathering on Building ans Stone Scupltures, Limassol (Cyprus), 2011*

Influence of the Chemical Interactions on the Removal Rate of Different Salts in Electrokinetic Desalination Processes

Paz-García J.M.[1*], Johannesson B.[1], Ottosen L.M.[1], Ribeiro A.B.[2] and Rodriguez-Maroto J.M.[3]
[1] Department of Civil Engineering, Technical University of Denmark, Denmark
[2] Department of Environmental Sciences and Engineering, Faculty of Sciences and Technology, New University of Lisbon, Caparica, Portugal
[3] Department of Chemical Engineering, University of Málaga, Málaga
*Corresponding author´s email: jugra@byg.dtu.dk

ABSTRACT

Electrokinetic desalination techniques have been successfully applied for the prevention of salt-induced deterioration problems of masonry and other construction materials. A mathematical model for electrochemical desalination treatments is described, based on the Poisson-Nernst-Planck system of equations and accounting for the chemical interactions between the species in the pore solution and the solid matrix. Due to their high abundance in the natural environment, chlorides, nitrates and sulfates are considered the main ions responsible to the salt decay processes in buildings materials and sculptures. Simulations of the desalination treatment of brick samples contaminated with these target contaminants are shown. The influence of the chemical interactions on the efficiency is highlighted in the results.

Keywords: Electrokinetic desalination, chemical equilibrium, extent of the reaction, reactive transport, Poisson-Nernst-Planck system

1 INTRODUCTION

Due to their abundance in the natural environment, chlorides, nitrates and sulfates are considered the main responsible for salt-decay weathering processes in buildings materials and sculptures (Ottosen et al. 2008a, Goudie & Viles 1997). Electrokinetic desalination techniques have been successfully applied for the prevention of salt-induced deterioration processes in masonry and other construction materials. The technique consists of the transport of the damaging salts out of the porous material in an externally applied electric DC field. Experimentally, the enhancement of the technique using a buffer substance at the electrode compartments has been shown to raise the effectiveness, in terms of increasing the removal rate and reducing the energy consumption. Furthermore, the buffer substance enhancement avoids undesirable side effects on the material being desalinated, such as the dissolution of the solid matrix due to the sharp pH changes produced at the electrodes (Ottosen & Rodig-Dalgaard 2009).

Despite the fact that the ionic mobility coefficients of chlorides, nitrates and sulfates ions are very similar, experimental results for electrokinetic desalination treatments have shown different removal efficiency for each species (Ottosen et al. 2008b). These differences can be

explained by the chemical interactions taking place between the species in the pore solution and the solid matrix. Therefore, the specific chemical reactions that can take place during the process must be taken into account when optimizing or modeling electrokinetic desalination treatments (Ottosen et al. 2008a; Ribeiro & Rodriguez-Maroto 2005). Some aspects affecting related to the chemical reactivity of the system during the electrokinetic treatment are:

- Species in the system migrate with different transport rates. As consequence, a displacement in the chemical equilibrium is produced. For instance, protons move faster than hydroxide ions, and the water auto-ionization reaction will proceed to keep the equilibrium. This feature has to be taken into account even in free diffusion models.
- The electrical current is transformed into an ionic current by means of the electrochemical reactions taking place at the electrodes. Due to water electrolysis reactions, in non-amended treatments severe pH changes are expected with serious implications on the chemical speciation in both the pore solution and the solid matrix.
- Ions migrate towards the electrode with opposite charge producing fronts with sharp gradient of concentration. When fronts collide, located precipitation may occur.

In this work, a model for the reactive transport in electrokinetic processes is described. Numerical simulations of the electrokinetic desalination of a brick sample contaminated with salts containing those target ions are shown. In the modeled system, the electrode compartments are considered filled with clay rich in pure calcite. The model includes the competition of different electrochemical reactions at the electrodes, as well as a feasible set of chemical equilibrium reactions describing the chemical reactivity.

Results from simulations demonstrate the influence of the chemical interactions affecting the target ions on the removal rate of those common salts. It can, therefore, be useful when designing full-scale desalination treatments.

2 MATERIALS AND METHODS

The model for the reactive transport in electrokinetic processes presented here has been designed as the combination of two strongly coupled modules: One for the transport process and another one for chemical equilibrium calculations. Both modules are described separately.

2.1 The transport process

In electrokinetic processes, ionic and non-ionic species migrate through the porous structure by a combination of different transport contributors (Ribeiro & Rodriguez-Maroto 2005). The transport process is modeled based on the Nernst-Planck-Poisson (NPP) system of equations (Pamukcu 2009, Johannesson & Ottosen 2008). A detailed description of the finite element integration of the NPP system of equations can be found in (Paz-Garcia et al. 2011a). The system presented here has been extended in order to include the transport of water due to electroosmotic and capillary suction forces and the corresponding advective flow of the species in the pore solution. In addition to this, the system has been coupled with a chemical equilibrium module, in order to take into account the chemical reactions during the transport process. Porosity changes due to the precipitation and dissolution reactions during the process

are monitored, and the effective transport coefficients are calculated taking into account the variation of the porosity along the material.

The transport of mass along the porous media is described by means of the corresponding mass continuity equation of each chemical species involved in the system:

$$\frac{\partial n_i}{\partial t} = -\nabla \mathbf{J}_i + G_i \tag{1}$$

where the $n_i \equiv [\text{mol} \cdot \text{kg}_\text{w}^{-1}]$ is the molal concentration of each chemical species i, G_i is the generation term and $\mathbf{J}_i$ is the flux term, described as:

$$\mathbf{J}_i = -\left(\overbrace{\underbrace{n_i w^{-1} D_w \nabla w}_{\text{total moisture transport}} + \underbrace{k_e n_i \nabla \phi}_{\text{electroomosis}}}^{\text{advection}} + \underbrace{D_i^{eff} \nabla n_i}_{\text{diffusion}} + \underbrace{U_i^{eff} n_i \nabla \phi}_{\text{electromigration}} \right) \tag{2}$$

where D_i^{eff} is the effective diffusion coefficient, ϕ is the electrical potential, U_i^{eff}, is the effective ionic mobility coefficient, $w \equiv [\text{kg}_\text{w} \cdot \text{m}_\text{pore}^{-3}]$ is the porous moisture content i.e. the amount of water filling the pore structure and k_e is the electroosmotic permeability coefficient. D_w is the moisture diffusivity coefficient in the solid matrix under consideration and it represents the transport of water due to the gradient of moisture content. This term describes the total moisture transport in both vapor and liquid phases, as a combination of diffusion, viscous saturated flow and capillary transport, assuming isothermal conditions (Johannesson & Janz 2009)

Effective diffusion coefficients are calculated from the corresponding diffusivity at infinite solution and the porosity, p, and tortuosity, τ, of the porous media and the Nernst-Townsend-Einstein relation relates the ionic mobility coefficient to the diffusivity (Paz-Garcia et al. 2011a). The Poisson's equation in electrostatics is used to complete the strongly coupled NPP system of equations.

$$\varepsilon \frac{\partial^2 \phi}{\partial x^2} = F \sum_{i=1}^{M} n_i z_i \tag{3}$$

where $\varepsilon = \varepsilon_r \varepsilon_o$ is the water permittivity, ε_o is the vacuum permittivity and ε_r is the water relative permittivity, F the Faraday constant and z_i is the ionic charge. The Poisson's equation acts as a charge balance, used to calculate the electrical potential from the charge density in each point of the solution. The strongly coupled character of the system assures the electroneutrality condition in the global system.

2.2 Chemical equilibrium

During the transport process, chemical species may react with other species in the solution and with the solid matrix. Modeling of this reactive transport accounting for chemical reaction has severe numerical difficulties, mainly due to the huge difference of orders of magnitude of reactions and transport rates. In general, it can be assumed that most of the reversible chemical reactions taking place in the process are fast enough to reach the equilibrium. According to this, for a selected set of reversible chemical reactions, the reactive transport can be modeled under

the assumption of instantaneous chemical equilibrium. Only irreversible, slow reversible reactions and the electrochemical reactions at the electrodes are considered time dependent.

In the present work, the Newton-Raphson method for re-establishing the chemical equilibrium condition described in (Paz-Garcia et al. 2011b) has been coupled with the transport module. The model deals simultaneously with aqueous and precipitation/dissolution reactions, accounting for the saturation index of the solids in each iteration and each point. In addition to this, the difference between the rate of precipitation/dissolution reactions and those involving only aqueous species has been taken into account. A line search approach is used in the Newton Raphson method to assure the convergence and, the same time, deal with the non-negative concentration constraints of all the chemical species.

2.3 The modeled system

The desalination of a single brick contaminated with a combination of KCl, KNO_3 and K_2SO_4 is studied. Figure 1 shows a schematic representation of the experimental setup, based on the cases studied in Ottosen & Rodig-Dalgaard 2009 and Ottosen et al. 2008b. A brick piece of 10 cm length and 125 cm^2 cross sectional area is suggested to a constant current of 10 mA during 7 days. A buffer substance enhanced electrokinetic treatment is assumed, based on the buffer capacity of $CaCO_3$. Cylindrical electrode compartments filled with clay poultice rich in $CaCO_3$ are placed at each end of the brick sample. The cylinders are 5 cm length and 8 cm of internal diameter. The distance between the electrodes and the brick surface is 4 cm.

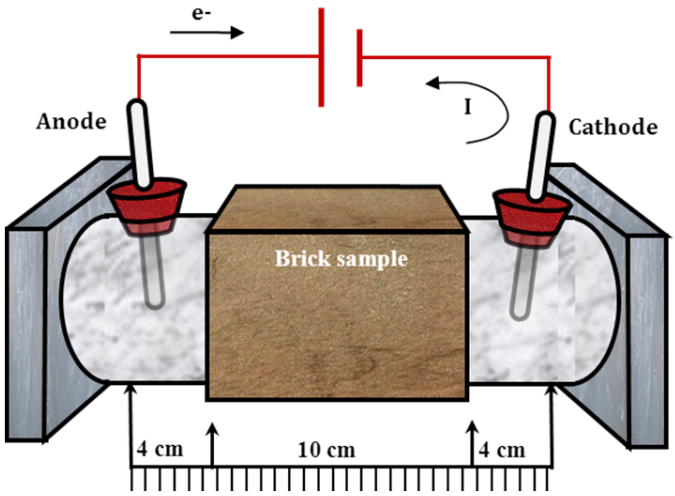

Figure 1: Schematic representation of the experimental setup for the electrodesalination of a brick.

The brick is considered as a porous inert matrix with a certain amount of $CaCO_3$ per unit volume (yellow brick). The carbonated clay in the electrode compartments initially has 1 mol/m^3 of each salt, which gives the pore solution sufficient conductivity in order to develop the necessary ionic current in the electrokinetic process. Table 1 collects the initial solid composition of the brick and the clay in the simulations. The units are referred to the considered constant volume of the heterogeneous matrix, i.e. volume of solid plus pore.

Table 1. Characteristics of the solid matrices

Property	Brick	Clay
Inert solids	17500 mol/m^3	5000 mol/m^3
$CaCO_3$ (s)	100 mol/m^3	10000 mol/m^3
KCl (s)	50 mol/m^3	1 mol/m^3
KNO_3 (s)	50 mol/m^3	1 mol/m^3
K_2SO_4 (s)	50 mol/m^3	1 mol/m^3
Initial porosity	0.2963	0.4307
Cross sectional area	125 cm^2	50 cm^2
Length	10 cm	2 × 4 cm

Table 2 shows the set of reversible chemical reactions selected for the simulation and Table 3 shows the set of dissolution/precipitation reactions that completes the system. The equilibrium constants or solubility products, obtained from (Parkhurst & Appelo, 1999), were adapted in order to be consistent with the given stoichiometric. For the sake of simplicity, only potassium is considered as a common counterion for the target contaminants. Nevertheless, the use of the $CaCO_3$ forces to consider calcium as a secondary counterion.

Table 2. Set of aqueous chemical reactions

	$\log_{10}(K_{eq})$		$\log_{10}(K_{eq})$
$OH^- \rightleftarrows H_2O - H^+$	14.00	$CaCl^+ \rightleftarrows Ca^{+2} + Cl^-$	0.29
$CaCO_3 \rightleftarrows Ca^{+2} + CO_2^{-2}$	-3.22	$CaSO_4 \rightleftarrows Ca^{+2} + SO_4^{-2}$	-2.31
$HCO_3^- \rightleftarrows H^+ + CO_3^{-2}$	-10.33	$KCl \rightleftarrows K^+ + Cl^-$	0.50
$CO_2 + H_2O \rightleftarrows H^+ + HCO_3^-$	-16.68	$KNO_3 \rightleftarrows K^+ + NO_3^-$	0.15
$CaHCO_3^+ \rightleftarrows Ca^{+2} + H^+ + CO_3^{-2}$	-11.43	$KSO_4^- \rightleftarrows K^+ + SO_4^{-2}$	-0.88
$CaOH^+ \rightleftarrows Ca^{+2} + H_2O - H^+$	12.78	$KOH \rightleftarrows K^+ + H_2O - H^+$	14.46
$CaNO_3^+ \rightleftarrows Ca^{+2} + NO_3^-$	-0.60	$HSO_4^- \rightleftarrows H^+ + SO_4^{-2}$	-1.98
$Ca(NO_3)_2 \rightleftarrows Ca^{+2} + 2NO_3^-$	-0.50		

Table 3. Set of precipitation/dissolution chemical reactions

Solid reactions	$\log_{10}(K_{sp})$
$CaCO_3(s) \rightleftarrows Ca^{+2} + CO_2^{-2}$	-8.48
$KCl(s) \rightleftarrows K^+ + Cl^-$	0.87
$CaCl_2 \cdot 6H_2O(s) \rightleftarrows Ca^{+2} + 2Cl^- + 6H_2O$	3.94
$KNO_3(s) \rightleftarrows K^+ + NO_3^-$	-0.10
$Ca(NO_3)_2(s) \rightleftarrows Ca^{+2} + 2NO_3^-$	5.98
$K_2SO_4(s) \rightleftarrows 2K^+ + SO_4^{-2}$	-1.85
$CaSO_4 \cdot 2H_2O(s) \rightleftarrows Ca^{+2} + SO_4^{-2} + 2H_2O$	-4.61
$KOH(s) \rightleftarrows K^+ + H_2O - H^+$	24.6
$Ca(OH)_2(s) \rightleftarrows Ca^{+2} + 2H_2O - 2H^+$	22.81

3 RESULTS AND DISCUSSION

Figure 2 shows the concentration profile of the target contaminants (Cl^-, NO_3^- and SO_4^{-2}) in the desalination treatment. As expected from the experimental results (Ottosen et al. 2008b) the transport of the target anions towards the anode differs. The concentration of SO_4^{-2} in the brick seems to decrease faster than the other ions. Nevertheless, the accumulation of SO_4^{-2} in the anode compartment is significantly lower than the other two anions.

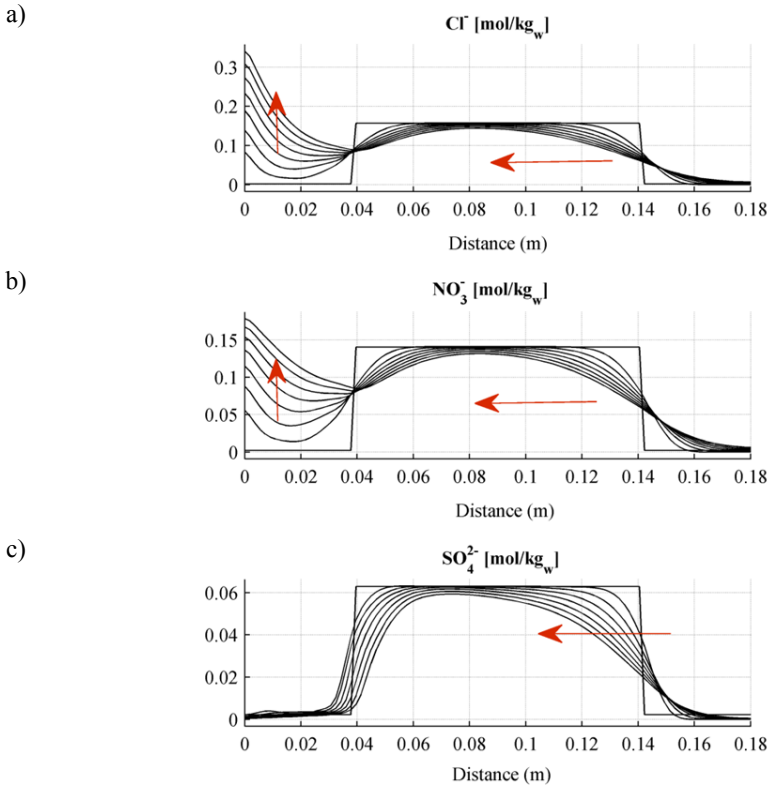

Figure 2. Concentration profile of the target ions along the sample. One profile every 24 h.

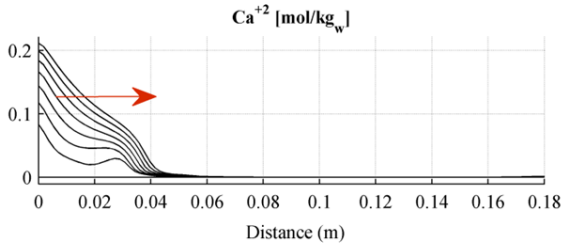

Figure 3. Calcium front developed in the cathode compartment. One profile every 24 h.

Figure 3 shows the calcium front developed at the anode compartment as result of the calcite dissolution in the buffering process. As a cation, calcium migrates towards the cathode going through the brick. Calcium may react with the different species in the system during its migration.

Table 2 and Table 3 collect a number of chemical reactions involving calcium and the target ions. Depending on the saturation index, some precipitates can be formed, being gypsum ($CaSO_4 \cdot H_2O$) the more insoluble in the set of reactions defined. Figure 4 shows the final distribution of solids, in volume fraction units; being the porosity the difference the rest of the volume not occupied by the solids. It can be seen that the electrolysis reaction at the anode produces a strong dissolution of the calcite at the electrode compartment, which matches with the calcium front shown in figure 3. The simulation does not predict the precipitation of calcium hydroxide in the cathode compartment. Furthermore, a significant precipitation of gypsum is observed in the region near nearby the anode compartment and the brick interface, where the calcium front and the sulfate front collide.

According to the results from the simulation presented here, the chemical interaction of calcium with respect the target anions can be assumed the main responsible of the differences between the removal rate of SO_4^{-2} compared to Cl^- and NO_3^-.

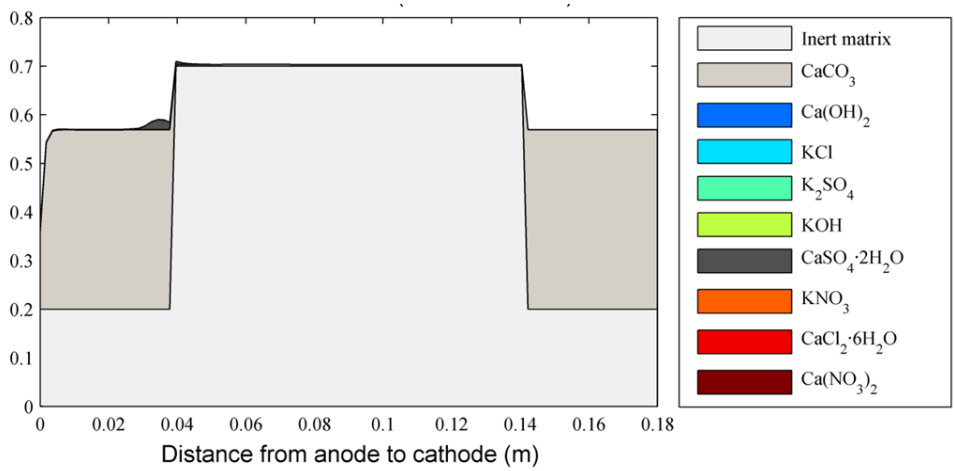

Figure 4. Distribution of solids (volume fraction) after 7 days of treatment.

4 CONCLUSIONS

A model for the reactive transport in electrokinetic desalination treatments has been described. Results from simulations show that the efficiency of the electrokinetic desalination treatments is different for each target ions, Cl^-, NO_3^- and SO_4^{-2}, using K^+ as counterion. Chloride is the fastest anion to be removed, whereas the sulfate is significantly slower. These differences are explained by the specific chemical reactivity of the ions.

In the case of the electrodesalination treatment modeled here, the enhancement by using calcium carbonate as buffer substance in the electrode compartments is considered. As result, the acid

front developed in the anode compartment is to some extent replaced by a calcium front that may proceed towards the cathode by electromigration. The reactivity of calcium with the target anions is consistent with the results obtained in the simulations. Calcium forms insoluble salts with sulfates that can limit the removal process, but also be hazardous for the material if a sharp precipitation is produced in the section where the calcium front matches the sulfates inside the sample, that could add to the salt decay of the material itself. Thus, this point is investigated experimentally at present.

REFERENCES

GOUDIE A.S. & VILES H.A. 1997. Salt Weathering Hazards, John Wiley and Sons, Chichester.

JOHANNESSON B. & OTTOSEN L.M. 2008. Modeling of electromigration salt removal methods in building materials. In: Salt Weathering on Building and Stone Sculptures: Technical University of Denmark, (351-360 p.)

JOHANNESSON B. & JANZ M. 2009. A two-phase moisture transport model accounting for sorption hysteresis in layered porous building constructions, *Building and Environment* 44, 1285-1294.

OTTOSEN L.M., CHRISTENSEN I.V., RORIG-DALGARD I., JENSEN P.E. & HANSEN H.K. 2008. Utilization of electro migration in civil and environmental engineering - Processes, transport rates and matrix changes, *Journal of Environmental Sciences and Health*, 43, 795-809.

OTTOSEN L.M., RORID-DALGAARD I., VILLUMSEN A. 2008. Electrochemical removal of salts from masonry – Experiences from pilot scale. In: Salt Weathering on Building and Stone Sculptures: Technical University of Denmark, (341-350 p.)

OTTOSEN L.M., RORID-DALGAARD I. 2009. Desalination of a brick by application of an electric DC field, *Materials and Structures*, 42, 961-971.

PAMUKCU S. 2009. Electrochemical Transport and transformations, in KRISHNA R.R. & CAMESELLE C. 2009, Electrochemical Remediation Technologies for Polluted Soils, Sediments and Groundwater.

PARKHURST D.L. & APPELO C.A.J. 1999, User's guide to PHREEQC (version 2) - A computer program for speciation, batch-reaction, one-dimensional transport, and inverse geochemical calculations, U.S. Department of the Interior, Water-Resources Investigations Reports, 99-4259.

PAZ-GARCIA J.M., JOHANNESSON, B., OTTOSEN L.M., RIBEIRO A.B., RODRIGUEZ-MAROTO J.M., 2011. Modeling of electrokinetics by finite element integration of the Nernst-Planck-Poisson system of equations, *Separation and Purification Technology*, 79(2), 183-192.

PAZ-GARCIA J.M., JOHANNESSON, B., OTTOSEN L.M., RIBEIRO A.B., RODRIGUEZ-MAROTO J.M., 2011b. Computing Chemical Equilibrium Systems with an Algorithm Based on the Extend of the Reactions, *Separation and Purification Technology, submitted.*

RIBEIRO A.B. & RODRIGUEZ-MAROTO J.M. 2005. Electrokinetic Modeling of Heavy Metals, in: PRASAD M.N.V., SAJWAN K.S. & NAIDU R., Electroremediation of Heavy Metal - Contaminated Soils - Processes and Applications in Trace Elements in The Environment, Taylor & Francis.

Conference Contribution

"Modelling of Electrokinetic Processes in Civil and Environmental Engineering Applications"

J.M. Paz-García, B. Johannesson, L.M. Ottosen, A.B. Ribeiro and J.M. Rodríguez-Maroto

Peer-reviewed full conference paper in: *Proceedings of the Thirteenth International Conference on Civil, Structural and Environmental Engineering Computing, 2011*

Paper 128

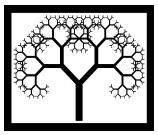

Proceedings of the Thirteenth International Conference on
Civil, Structural and Environmental Engineering Computing,
B.H.V. Topping and Y. Tsompanakis, (Editors),
Civil-Comp Press, Stirlingshire, Scotland

Modelling of Electrokinetic Processes in Civil and Environmental Engineering Applications

J.M. Paz-Garcia[1], B. Johannesson[1], L.M. Ottosen[1]
J.M. Rodriguez-Maroto[2] and A.B. Ribeiro[3]
[1] Department of Civil Engineering
Technical University of Denmark, Kgs. Lyngby, Denmark
[2] Department of Chemical Engineering, University of Málaga, Spain
[3] Environmental Sciences and Engineering Department
New University of Lisbon, Caparica, Portugal

Abstract

Electrokinetic mobilization is used for the transport of ionic and non-ionic species through the pore solution of porous materials, induced by an externally applied electric field. Several electrokinetic techniques have been proposed and successfully applied for different purposes in the fields of Civil and Environmental Engineering. A mathematical model for the electrokinetic phenomena is described, based on a finite element integration of the extended Poisson-Nernst-Planck system of equations coupled with a Newton-Raphson method for chemical equilibrium calculations. Numerical simulations of some representative test examples are shown.

Keywords: Poisson-Nernst-Planck system, chemical equilibrium, electrokinetic soil remediation, electrokinetic desalination.

1 Introduction

Electrokinetic techniques are used for several purposes in the fields of Civil and Environmental Engineering. The electrokinetic phenomena consist of the mobilization of species within the pore solution of porous materials, induced by an externally applied electric field. One of the main advantages of the electrokinetic remediation techniques is that they allow for considerable fast transport of matter through materials with a low hydraulic permeability, where other techniques are ineffective [1,2].

Ottosen et al. [3] collected a complete list of different electrokinetic applications techniques in both engineering fields, outlining the physicochemical aspects that these applications have in common or differ. In Civil Engineering, the main use of the electrokinetics techniques is been focused on the desalination of concrete. Recently, several applications are been developing for different purposes, such as the re-impregnation of wood in structures and the removal of salts from masonry in

building facades, tiles, sculptures or frescoes. In the field of Environmental Engineering, electrokinetics techniques are mainly used for the mobilization of pollutants out of contaminated matrices (electrokinetic remediation, or EKR). In this context, the removal of heavy metals and/or organic contaminants from contaminated soil, sludge, fly ashes and waste wood has been widely investigated.

Designing an electrokinetic treatment requires the consideration of many different physicochemical aspects, depending on the aim of the application, the nature of the target species to be transported and the possible side effects of the technique in the treated body [1]. In most cases, the effectiveness of an electrokinetic remediation treatment depends on the chemical interactions among the different species in the pore solution, and the interactions of species in the pore solution and the solid matrix, more than the electric conditions applied [4-6]. Therefore, the specific chemical reactions taking place must be taken into account when optimizing electrokinetic desalination treatments.

The first chemical aspect to be considered is the effect of the electrode processes. The electrical current applied to the material is transformed into an ionic current by mean of the electrochemical reactions taking place at the electrodes. Different electrochemical reactions can occur, depending on the species present in the vicinities of the electrodes. Water oxidation at the anode (1) and water reduction at the cathode (2) are always likely to happen.

$$H_2O \rightleftarrows \frac{1}{2}O_2 + 2H^+ + 2e^- \quad ; \quad E^o = -1.229\ V \tag{1}$$

$$2H_2O + 2e^- \rightleftarrows H_2 + 2OH^- \quad ; \quad E^o = -0.828\ V \tag{2}$$

Depending on the specific system, competitive reactions have to be included at the electrodes. One of the more commons could be the oxidation of chloride at the anode to produce gaseous chlorine:

$$2Cl^- \rightleftarrows Cl_2 + 2e^- \quad ; \quad E^o = 1.36\ V \tag{3}$$

Irrespective the competitive redox reactions, water oxidation and reduction will be always present. The electrolysis of water injects in the system a flux of protons and hydroxides and, as consequence, electrokinetic remediation techniques are suggested to important pH changes in the domain during the process. These pH changes play an important role in the applicability of the technique for several reasons [1-4]

- Non-neutral pH environments, with high concentration of either protons or hydroxides, will result in very inefficient electrical processes. The loose of effectiveness is due that protons and hydroxides have very high ionic mobility and the will carry most of the ionic current applied to the system instead of the target contaminants.

- Severe acid or basic conditions generally produce undesirable side effects on the material being cleaned. For example, in electrokinetic desalination treatments of calcite-based building materials, such as marble or some bricks, the acid front originated in the anode reaction can produce severe damage in the matrix.

- The pH also affect to the speciation of the target contaminants. For example, heavy metals are known to form insoluble hydroxides in basic environment. As consequence, the basic front originated in the cathode will produce the precipitation of the heavy metals, and will limit the technique, since it is an essential condition to be at least the aqueous phase to be mobilized in the transport process.

Different enhancements for the application of the electrokinetics have been proposed to raise the effectiveness, in terms of increasing the removal rate and reducing the energy consumption. Enhanced techniques are utilized for increase the mobility rate of the target species with respect to the other species in the pore solution by producing changes in the speciation state. Most common enhanced techniques have been described for the control of the aforementioned acid and basic pH fronts generated in the electrode reactions. In this group we can consider the use of different buffer substances at the electrode compartments [7], the neutralization of the fronts by means of injection of a conjugate acid or base in the system [8] or the use of selective membranes in electrodialytic procedures [9]

Modern enhanced techniques combine the control of the pH changes with the use of specific extractant agents, which are added to the system to react with the target contaminant changing its speciation state and increasing the solubility [10]. This kind of enhanced techniques increases noticeably the effectiveness of the process, but also allows a selective extraction of target contaminants, avoiding side effects on the treated matrix.

2 The Model

The model for the reactive transport in electrokinetic processes presented here can be better understood as the combination of two strongly coupled modules: One module for the transport process and another one for the chemical equilibrium condition. Both modules are described separately.

2.1 The transport process module

The transport of mass along the porous media is described by means of the corresponding mass continuity equation of each chemical species involved in the system:

$$\frac{\partial n_i}{\partial t} = -\nabla \mathbf{J}_i + G_i \tag{4}$$

where $n_i \equiv \left[\text{mol} \cdot \text{kg}_\text{w}^{-1}\right]$ is the concentration of each chemical species, G_i is the generation term and $\mathbf{J}_i$ is the flux term. The flux term of the mass balance equation (4) is described as:

$$\mathbf{J}_i = \underbrace{v_w n_i}_{advection} - \underbrace{D_i^{eff} \nabla n_i}_{diffusion} - \underbrace{U_i^{eff} n_i \nabla \phi}_{electromigration} \tag{5}$$

where D_i^{eff} is the effective diffusion coefficient, ϕ is the electrical potential, U_i^{eff}, is the ionic mobility coefficient and v_w is the velocity of the pore solution. The effective diffusion coefficient can be estimated from the corresponding diffusivity at infinite solution, and the porosity, p, and tortuosity, τ, of the porous media.

$$D_i^{eff} = \frac{p}{\tau} D_i \tag{6}$$

The ionic mobility coefficient can be related to the diffusion coefficient by the Nernst-Townsend-Einstein equation [11]:

$$U_i^{eff} = \frac{D_i^{eff} F z_i}{RT} \tag{7}$$

where T is the temperature, R is the gas constant, U_i^{eff} is the Faraday constant and z_i is the charge of the ion.

When considering the transport of ionic species, the mass balance equation is usually denoted as Nernst-Planck equation. In this equation, the flux of matter under the effect of the gradient of concentration is coupled with the flux under the gradient of electrical potential. The different migration rate of ions is responsible of the so-called diffusion potential [12] which will force the other charged particles in the system to follow or slow down the motion of a specific ion. As can be seen in (5), the transport of chemical species is strongly coupled with the electrical potential, both externally applied or due to diffusion potential, as well as the transport of the solution itself.

For describing the advection term, accounting for the transport of the aqueous species in the fluid due to the fluid's motion, a mass continuity equation for the water transport is included in the system. Let $w \equiv \left[\text{kg}_\text{w} \cdot \text{m}_\text{pore}^{-3}\right]$ be the porous moisture content i.e. the amount of water filling the pore structure. For the sake of simplicity, dilute solutions will be considered, and the density of the solution will have a constant value equivalent to the density of pure water at room temperature.

One of the main advantages of the EKR techniques is that they allow for considerable fast transport of matter through materials with a low hydraulic permeability, where other techniques are ineffective. In this model, no external

hydraulic pressure is considered. As result, the flux of water is considered determined by:

$$\mathbf{J}_w = \underbrace{-D_w^{\,eff}\nabla w}_{moisture\,gradient}\ \underbrace{-k_e^{\,eff} w\nabla\phi}_{electroomosis} \tag{8}$$

where D_w is a permeability coefficient of water in the solid matrix under consideration and k_e is he electroosmotic permeability coefficient. In this case, the effective coefficient $k_e^{\,eff}$ has been modelled considered inversely proportional to the porosity of the media, while D_w is assumed independent on the porosity.

$$k_e^{eff} = \frac{k_e}{p} \tag{9}$$

The first term in (8) represents the transport of water due to the gradient of the saturation degree, showing the tendency of the water to fill the porous material by geochemical suction. The second term accounts for the electroosmotic transport. Electroosmosis is the transport of water through the porous material due to the bulk movement of the ions in the vicinities of the solid surface [11,13]. Generally, the solution is electrically neutral. However the electrostatic charges on the solid surface attract the counterions in the liquid, and so, the counterion concentration near the solid surface is higher than that in the bulk liquid. As a result of the externally applied electric field, the electric double layer moves as a bulk towards the electrode of difference charge, producing the movement of the solution. Most soils and construction materials have a negative surface charge, undergoing electroosmotic flows from the anode towards the cathode.

The ζ potential is the electrical potential at the junction between the fixed and mobile parts of the electrical double layer. The electroosmotic velocity of a fluid of certain viscosity and dielectric constant through a surface charged porous medium of zeta or electrokinetic potential (ζ), under an electric gradient, is given by the H-S equation [13] as follows:

$$k_e = \frac{\zeta\varepsilon}{\mu} \tag{10}$$

where, μ is the viscosity of the pore fluid, $\varepsilon = \varepsilon_r\varepsilon_o$ is the permittivity in water, ε_o is the permittivity of vacuum and ε_r is the relative electric permittivity of water. The magnitude and sign of the ζ potential depends on the pore fluid chemistry, being strongly influenced by the pH [13]. However, the electroosmotic permeability coefficients are in a short range between 10^{-9} and 10^{-8} [$m^2 \cdot V^{-1} \cdot s^{-1}$] [12-14].

Taking into account the flow term of determining the water transport, described in equation (8), the velocity of the water is given by:

$$v_w = -\left(\frac{D_w^{\,eff}\nabla w}{w} + k_e\nabla\phi\right) \tag{11}$$

As result, equation (11) can be included in the advective term of the flux vector defined (5) for the extended Nernst-Planck equation of each aqueous species giving:

$$\mathrm{J}_i = -\left(\overbrace{\underbrace{\frac{n_i}{w} D_w^{\,eff} \nabla w}_{moisture\,gradient} + \underbrace{k_e^{\,eff} n_i \nabla \phi}_{electroomosis}}^{advection} + \underbrace{D_i^{\,eff} \nabla n_i}_{diffusion} + \underbrace{U_i^{\,eff} n_i \nabla \phi}_{electromigration} \right) \tag{12}$$

Finally, the Poisson's equation in electrostatics, eq (13), is used to complete the strongly coupled system. The Poisson's equation acts as a charge balance. It allows the calculation of the electrical potential from the charge density in the solution. The electrical neutrality is not directly forced in the system. Instead, the strongly coupled character of the system, mainly induced by the electromigration transport term, will assure a correct electrical behaviour [15].

$$\varepsilon \frac{\partial^2 \phi}{\partial x^2} = F \sum_{i=1}^{M} n_i z_i \tag{13}$$

A finite element method is used for the integration of the strongly couple differential equations describing the electrokinetic remediation transport phenomena of different enhanced techniques used in civil and environmental engineering. A detailed description of the finite element integration of the Poisson-Nernst-Planck system of equations can be found in [16]. The system presented here has been extended in order to include the transport of water through the material, the corresponding advective flow and the porosity changes due to the precipitation and dissolution reactions.

It should be outlined that traditional finite element analysis of convection-advection dominated systems typically required the use of specific weighting residuals functions, resulting in asymmetric conductivity and mass matrices [17,18]. In this work, the advective transport terms are calculated in the water mass balance equation as well as in the Nernst-Planck equation of each individual aqueous species, as described in the equation (12). As result, the finite element procedure does not require the use of convection-dominated integration techniques.

As explained in [16], the electrochemical reactions taking place at the electrodes, are directly included in the finite element transport method by means of the boundary vectors terms [19]. The model is able to predict electrokinetic treatments under different working conditions: constant voltage, constant electrical current, constant current density and free diffusion problems. The Faraday constant, magnitude of electric charge per mole of electrons, relates the electrical balance in the electrode processes. When an external electric current applied a flux of positive or negative charge can be defined at the electrodes nodal points in order to simulate the electrode processes. In the model, different electrode reactions are likely to occur. The redox potential is evaluated in each iteration to determine with electrochemical reaction is taking place during the current step, being the water oxidation and reduction always likely to happen.

2.2 The chemical equilibrium module

As mentioned before, electrokinetic remediation phenomena are dependent on the chemical interactions among the different species in the pore solution, and the interactions of species in the pore solution and the solid matrix. In most cases, chemical equilibrium kinetic rates are several order of magnitude higher that the transport rates. This can be assured in almost all reversible chemical reactions involving only aqueous species, and for some fast precipitation/dissolution reaction, such as those involving carbonates [20,21]. Accordingly, the reactive transport has been modelled considering the chemical equilibrium condition during the transport process.

In [16] the equilibrium condition was already included considering only the water chemical equilibrium of the solvent. In the present work, A Newton-Raphson method has been implemented and used for the solution of this specific set of chemical reactions. This set of feasible reversible stoichiometric reactions is described as function of the chemical species in the system. The selected reactions have to be a few magnitude orders faster than the transport rates in order to be included in the chosen set, so the established chemical system can be considered to satisfy the chemical equilibrium condition during the process. In addition to this, the difference between the rate of precipitation/dissolution reactions and those involving only aqueous species has been taken into account. Problems associated with local minimums are potentially avoided by the prioritization of the aqueous reactions with respect to those in which at least one solid species is involved.

The Newton-Raphson method used iterates on the extent of each individual chemical reaction [22]. The stoichiometric equations are consistent with the mass and charge conservation principles. As result, when using the extents of each reaction as independent variables, the variations on the electrical balance with respect to the initial estimation are minimized in an explicit manner. For that reason, the electrical balance of the solution is not modified during the speciation process. This feature makes the presented algorithm suitable for problems in which a thorough control of the electrical balance is required, such as the strongly coupled transport model described in this work.

A line search approach is used in the Newton Raphson method to assure the convergence and, the same time, deal with the non-negative concentration constraints of all the chemical species [23]. The residual function to be minimized is obtained from the action mass equation of each chemical reaction in the chosen set, accounting for the weight of the chemical activity as function of the ionic strength of the media. Davies and Setschenow equations are used to calculate the activity factors for ionic and non-ionic aqueous species respectively [20,24].

Despite the fact that in the transport process module previously described only the aqueous species and the solvent have been considered, in the chemical equilibrium stage the amount of solids have to be included in order to take into account the reactivity of the solid matrix as well as to evaluate the possible changes of the matrix. Let $s_i^* \equiv \left[\mathrm{mol}_i \cdot \mathrm{m}_{\mathrm{Tot}}^{-3} \right]$ be the amount of the solid *i* per volume unit.

The superscript * means that the concentration is referred to the assumed-constant volume of heterogeneous matrix. For the stoichiometric mass balance equations, the concentration of aqueous species and the water are converted to the same units of the solid species, by means of the porosity of the media.

$$n_i^* \equiv n_i \cdot w \cdot p \equiv \left[\mathrm{mol}_i \cdot \mathrm{m}_{\mathrm{Tot}}^{-3} \right] \tag{14}$$

$$w^* \equiv w \cdot p \equiv \left[\mathrm{kg}_{\mathrm{w}} \cdot \mathrm{m}_{\mathrm{Tot}}^{-3} \right] \tag{15}$$

Taken into account the molar mass and the specific gravity of the solid species, the volume occupied by the total amount of solids referred to the control volume of heterogeneous matrix can be calculated. As result, the expected porosity changes due to precipitation and dissolution process during the electrokinetic treatment [3,11] can be monitored.

Changes on the porosity along the domain affect significantly to the transport process of both aqueous species and the water, since the effective transport coefficients described in (8) and (12) depends on the porosity of the media. This effect has been taken into account in the finite element procedure described above, and the conductivity matrices calculated from the effective coefficients are updated each numerical iteration.

3 Simulations

Results from simulations of test examples are presented. Two types of enhanced methods are compared: The electrokinetic desalination of a brick sample, using carbonated clay to hinder the acid penetration; and an acid-enhanced electrokinetic soil remediation process, where the basic front is neutralized in order to avoid the precipitation of hydroxides of the target heavy metal.

3.1 Simulation 1: Desalination of a brick using a buffer substance

Ottosen et al. [7,25] presented the desalination of a brick samples contaminated with different salts combinations. In the present work, the desalination of a brick sample contaminated with KCl is simulated, based on the results reported in [7].

Not amended electrokinetic treatments on masonry materials can produce severe damage on the matrix structure, due to dissolution of the solid matrix at low pH environments. For that reason, a buffer substance enhanced electrokinetic treatment is used. Two cylindrical electrode compartments, filled with kaolinite clay rich in calcium carbonate, are placed in both ends of the brick sample. The cylinders are 5 cm length and 8 cm diameter. The clay in the electrode compartments has two main functions. First, it acts as a porous wet matrix to increase the contact between the electrodes and the target sample. Secondly, the reactivity of the calcium carbonate is expected to buffer the strong pH changes originated in the anode, due to the aforementioned water oxidation.

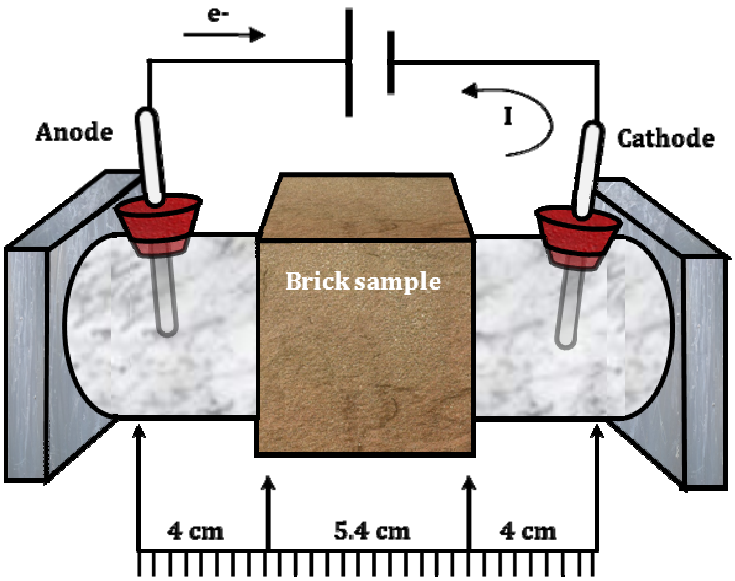

Figure 1: Schematic representation of the experimental setup for electrokinetic desalination of a brick using buffering clay.

Figure 1 shows a schematic representation of the experimental setup, based on the case studied in [7]. Half brick pieces of 5.4 cm length and 125 cm^2 cross sectional area are suggested to a constant current of 10 mA for a few days. The bricks are contaminated with NaCl and KCl to compare the dependence of removal rate of chloride on the counterion. In this case, only results from simulations for the KCl case are shown. The distance between the electrodes and the brick surface is 4 cm.

In the simulation, a treatment of 3 days is presented, showing profiles every 12 hours. A Faraday efficiency factor of $\eta = 0.2$ is included, what means that the conversion between the electric and the ionic current is assumed not ideal. The effective ionic current applied as boundary conditions is 2 mA. Loose of energy are expected due to polarization effects and also the conductivity of the solid matrix.

Table 1 shows the composition of the solid matrix assumed for the brick and the carbonated clay. The brick pieces used in [7] were yellow and new from brickwork by Webers, Denmark. The yellow colour is related to the higher proportion of CaCO3. The brick is considered mostly as an inert matrix with a certain amount of calcium carbonated. The clay is considered as a combination of inert clayey materials and an important proportion of calcite. The contaminant salt is included in the system as solid KCl, which dissolves completely in the pore solution. Table 2 shows the set of chosen chemical reactions considered in the process. The equilibrium constant is given in decimal logarithm scale for the given stoichiometric relation.

	Brick	Carbonated clay
Solid inert materials	2750 mol/m^3	1000 mol/m^3
$CaCO_3$ (Calcite)	50 mol/m^3	1000 mol/m^3
KCl (s) (Sylvite, prior dissolution)	50 mol/m^3	1 mol/m^3
KCl (aq)	0.1662 mol/L	0.0021 mol/L
Initial porosity	0.2990	0.4787

Table 1: Solid matrix characteristics for the electrokinetic desalination system.

Aqueous reactions:	$\log_{10}(K_{eq})$
$OH^- \rightleftarrows H_2O - H^+$	14.00
$CaCO_3(aq) \rightleftarrows Ca^{+2} + CO_2^{-2}$	-3.22
$HCO_3^- \rightleftarrows H^+ + CO_3^{-2}$	-10.33
$CO_2(aq) + H_2O \rightleftarrows H^+ + HCO_3^-$	-16.68
$CaHCO_3^+ \rightleftarrows Ca^{+2} + H^+ + CO_3^{-2}$	-11.43
$CaOH^+ \rightleftarrows Ca^{+2} + H_2O - H^+$	12.78
$CaCl^+ \rightleftarrows Ca^{+2} + Cl^-$	0.29
$KCl(aq) \rightleftarrows K^+ + Cl^-$	0.50
$KOH(aq) \rightleftarrows K^+ + H_2O - H^+$	14.46
Solids reactions:	$\log_{10}(K_{sp})$
$CaCO_3(s) \rightleftarrows Ca^{+2} + CO_2^{-2}$	-8.48
$Ca(OH)_2(s) \rightleftarrows Ca^{+2} + 2H_2O - 2H^+$	22.81
$KOH(s) \rightleftarrows K^+ + H_2O - H^+$	24.6
$KCl(s) \rightleftarrows K^+ + Cl^-$	0.87

Table 2: Set of chemical reactions for the electrokinetic desalination system used in simulation 1. Equilibrium constants obtained from the database Sit.txt distributed in [24], and developed for Amphos 21, BRGM and HydrAsa for ANDRA, French National Radioactive Waste Management Agency.

Figure 2.a shows the pH profile during the duration of the treatment. Despite an acid front advance from the anode end, the pH is much higher than the expected value if not buffer substance were used. Not amended treatments will produce an acid environment with pH values close to 2. Figure 2.b shows that the calculated ionic current in along the sample is kept constant, but small variations in the interfaces of the materials. This feature gives high consistency to the model. Figure 3.c shows the effect of the electroosmotic transport term, transporting the bulk water phase from the anode to the cathode. These aspects are consistent with the results reported in

[7], where the clay at the anode compartment was dried and the cathode compartment experienced some water leaking.

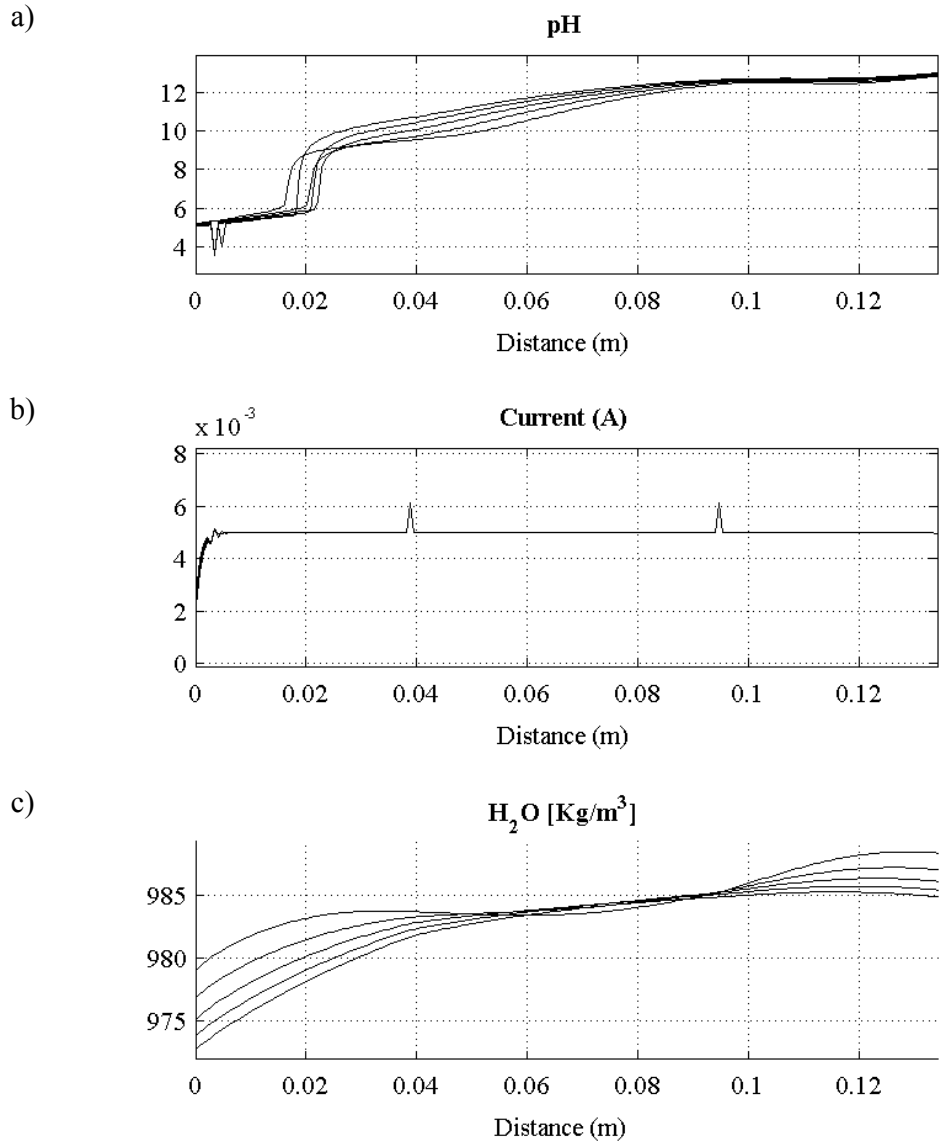

Figure 2: pH, ionic current and water profile along the sample in simulation 1

Figure 3 shows the composition of the solid matrix and changes in the porosity. Despite the advanced of the basic front, simulations do not predict the formation of $Ca(OH)_2$ at the cathode end. On the other hand, the calcium carbonate in the clay at the anode compartment experience severe alterations. It dissolves as consequence of the buffering process, increasing the porosity in this compartment. Changes in the porosity also affect the water profile shown in figure 2.c.

a)

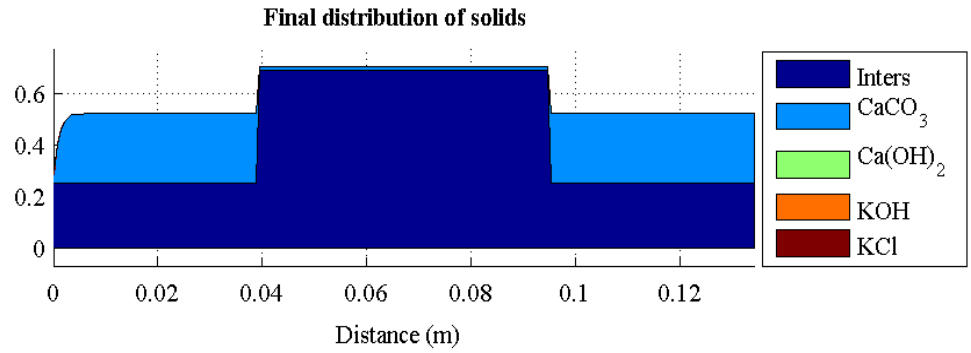

b)

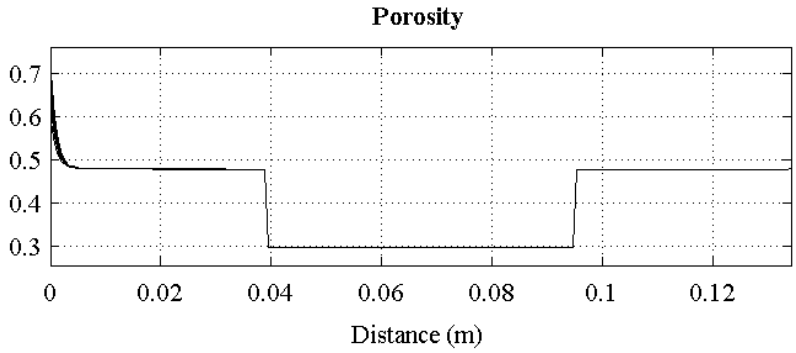

Figure 3: a) solid matrix composition, in total amount of moles and b) porosity along the sample.

Figure 4 shows the evolution of the chloride profile in the time and the distance. As expected, chloride accumulates in the anode compartment as result of the electromigration transport.

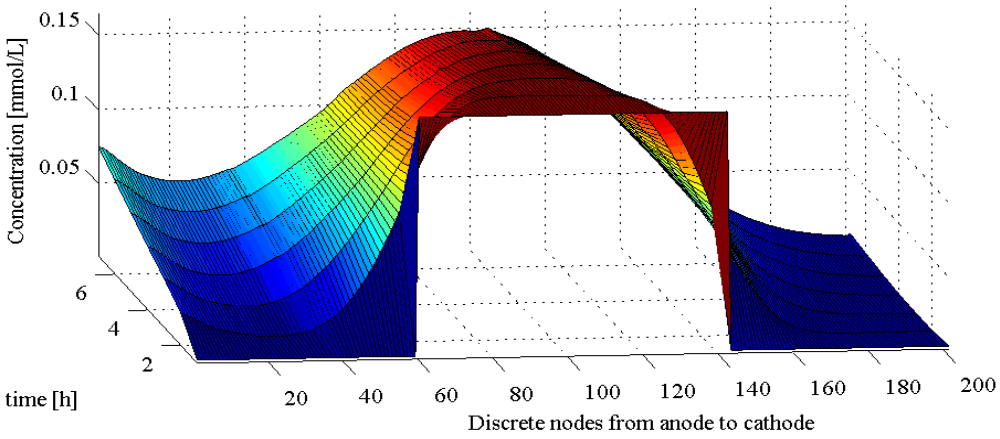

Figure 4: Chloride profile along the sample during the desalination treatment.

3.2 Simulation 2: Acid-enhanced EKR of a lead contaminated soil

Extended bibliography can be found about different electrokinetic remediation techniques for soil recuperation. In this case, simulations of an acid enhanced electrokinetic treatment of a soil contaminated with Pb are performed. Examples of this kind of application in lab and pilot scale can be found in [2,8,26,27]. A clayey calcareous soil, with a certain amount of $PbCO_3$ and PbO is assumed. An acid-enhanced procedure is used to force the dissolution of the solids containing lead, including lead hydroxides. Hindering the basic front will also avoid the formation of plumbites. The pH in the cathode compartment is forced to have a value lower than 5 by dropping HNO_3 when necessary. The acid-base reaction (16) is assumed instantaneous.

$$HNO_3 + OH^- \rightleftarrows NO_3^- + H_2O \qquad (16)$$

As result, the electrode reaction at the cathode would depend on the pH of the media. When the pH is lower than 5 the equation (2), water reduction, is assumed. When pH is higher than 5, nitric acid is injected in the system to control the alkaline front, and equation (16) will take place. In the anode electrode compartment, an electrolyte of $NaNO_3$ is used.

Figure 5 shows a representation of a standard lab-scale setup for soil remediation in horizontal column. A cylinder of 20 cm length and 100 cm^2 cross sectional area is filled with the soil. The sample is separated from the electrode compartments by paper filter slides.

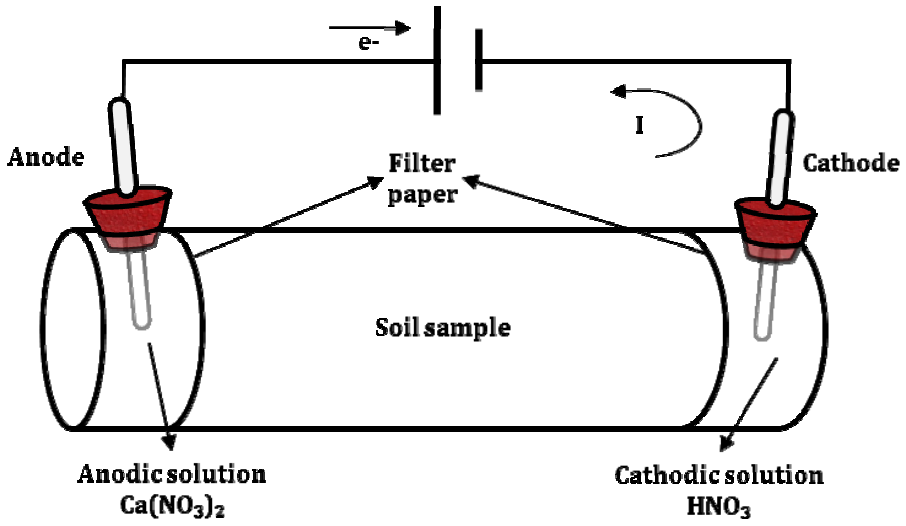

Figure 5: Schematic representation of the experimental setup for acid-enhanced electrokinetic remediation.

Aqueous reactions:	$\log_{10}(K_{eq})$
$OH^- \rightleftarrows H_2O - H^+$	14.00
$CaCO_3(aq) \rightleftarrows Ca^{+2} + CO_2^{-2}$	-3.22
$HCO_3^- \rightleftarrows H^+ + CO_3^{-2}$	-10.33
$CO_2(aq) + H_2O \rightleftarrows 2H^+ + CO_3^{-2}$	-16.68
$CaHCO_3^+ \rightleftarrows Ca^{+2} + H^+ + CO_3^{-2}$	-11.43
$CaOH^+ \rightleftarrows Ca^{+2} + H_2O - H^+$	12.78
$PbCO_3(aq) \rightleftarrows Pb^{+2} + CO_2^{-2}$	-7.00
$Pb(CO_3)_2^{-2} \rightleftarrows Pb^{+2} + 2\,CO_2^{-2}$	-10.13
$Pb(OH)_4^{-2} \rightleftarrows Pb^{+2} + 4H_2O - 4H^+$	38.90
$Pb(OH)_3^- \rightleftarrows Pb^{+2} + 3H_2O - 3H^+$	27.20
$Pb(OH)_2 \rightleftarrows Pb^{+2} + 2H_2O - 2H^+$	16.95
$Pb(OH)^- \rightleftarrows Pb^{+2} + H_2O - H^+$	7.51
$CaNO_3^+ \rightleftarrows Ca^{+2} + NO_2^-$	-0.60
$Ca(NO_3)_2 \rightleftarrows Ca^{+2} + 2NO_2^-$	-0.50
$PbNO_3^+ \rightleftarrows Pb^{+2} + NO_2^-$	-1.06
$Pb(NO_3)_2 \rightleftarrows Pb^{+2} + 2NO_2^-$	-1.48
Solids reactions:	$\log_{10}(K_{sp})$
$CaCO_3(s) \rightleftarrows Ca^{+2} + CO_2^{-2}$	-8.48
$Ca(OH)_2(s) \rightleftarrows Ca^{+2} + 2H_2O - 2H^+$	22.81
$PbO + \rightleftarrows Pb^+ + H_2O - 2H^+$	12.63
$Pb(OH)_2(s) \rightleftarrows Pb^{+2} + 2H_2O - 2H^+$	13.51
$PbCO_3(s) \rightleftarrows Pb^{+2} + CO_2^{-2}$	-13.29
$Ca(NO_3)_2(s) \rightleftarrows Ca^{+2} + 2NO_2^-$	5.98

Table 3: Set of chemical reactions used in the soil electrokinetic remediation system shown in simulation 2.

Characteristics of the soil	
Solid inert materials	1750 mol/m^3
$CaCO_3$	50 mol/m^3
$PbCO_3$	30 mol/m^3
PbO	20 mol/m^3
Initial porosity	0.4532

Table 4: Solid matrix characteristics for the soil electrokinetic remediation system shown in simulation 2. Composition of the solid matrix and initial porosity

Figures 6 and 7 show selected results from the simulations of the electrokinetic remediation treatment of the soil sample. The duration of the process is 60 hours at constant current of 1 mA. One profile each 12 hours is shown. The treatment proceeds very slowly due to the high reactivity of the solid matrix. This indicates that the efficiency and the rate of the process are limited by the chemical reaction. While the basic front is neutralized in the cathode compartment, an acid front develops from the anode. For this reason, the region close to the anode compartment shows important changes. The acid front produces the dissolution of the carbonates minerals as well as the PbO. As result, a change in the porosity is produced in the solid matrix, as appreciated in figure 6.b.

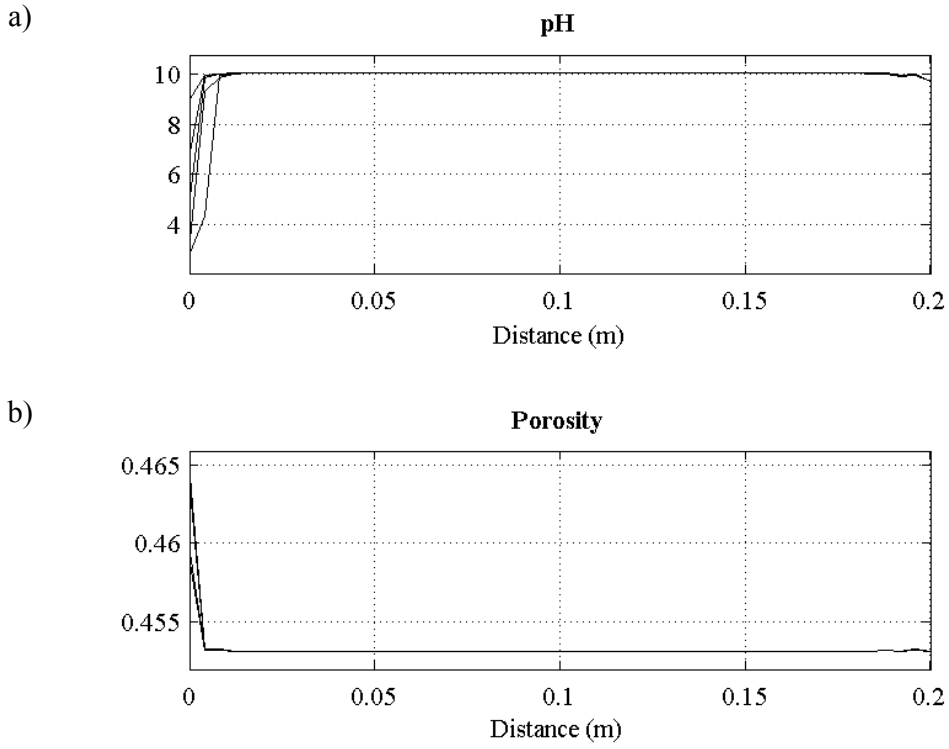

Figure 6: pH profile (a) and porosity (b) along the soil sample. Simulation of an EKR treatment of 60 hours at constant current of 1 mA.

Figure 7 shows that the target contaminant, lead, can be collected in both anode and cathode compartments. According to table 3, lead can react with the other species in the system forming positive, negative and not charged complexes.

a)

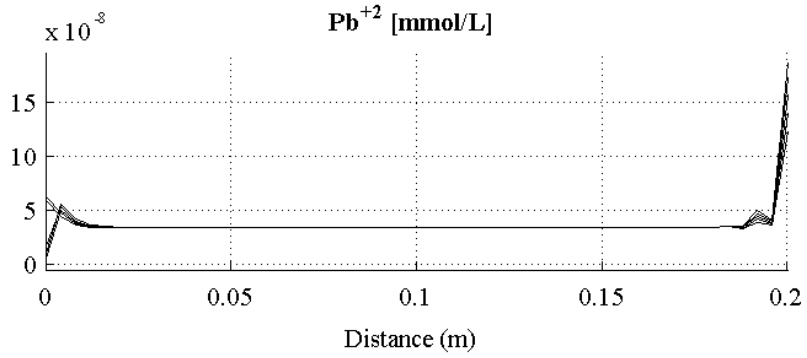

b)

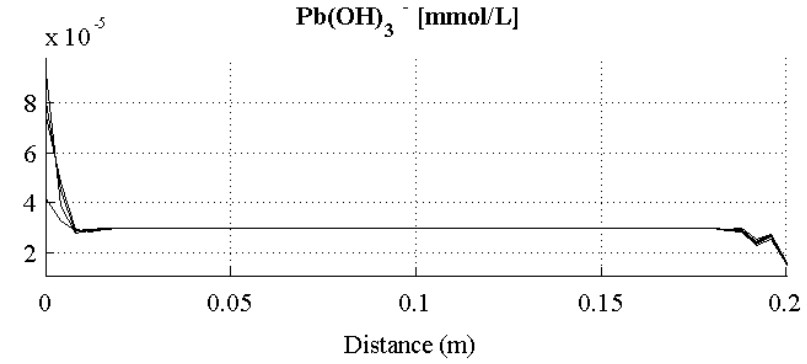

Figure 7: Pb^{+2} (a) and $Pb(OH)_3^-$ (b) profiles along the soil sample. Simulation of an EKR treatment of 60 hours at constant current of 1 mA. One profile each 12 hours is shown.

4 Conclusions

A mathematical model for the electrokinetic phenomena is described. The model is based on a finite element integration of the extended Poisson-Nernst-Planck system of equations coupled with a Newton-Raphson method for chemical equilibrium calculations. The model presented here gives good estimations of the results obtained from laboratory and pilot scale electrokinetic treatments. Apart from the prediction ability, the detailed definition of the transport process increases the understanding of the main physicochemical aspects affecting the process.

The model can be easily adapted for simulate different enhanced techniques and different chemical systems. Numerical simulations of different applications of electrokinetic techniques to the fields of Civil and Environmental Engineering are included, showing the versatility and consistency of the model. The strongly dependence of the chemical reactivity in the efficiency of the transport process has been outlined.

References

[1] Y.B. Acar, A.N. Alshawabkeh, "Principles of electrokinetic remediations", Environmental Sciences and Technology, 27, 2638-2647, 2993.

[2] A.N. Alshawabkeh, R.M. Bricka, D.B. Gent, "Pilot-scale electrokinetic cleanup of lead-contaminated soils", Journal of Geochemical and Geoenvironmental Engineering, 131 (3): 283-291, 2005.

[3] L.M. Ottosen, I.V. Christensen, I. Rörid-Dalgård, P.E. Jensen, H.K. Hansen, "Utilization of electromigration in civil and environmental engineering - Processes, transport rates and matrix changes", Journal of Environmental Sciences and Health, 43, 795-809, 2008.

[4] F. Garcia-Herruzo, J.M. Rodriguez-Maroto, R.A. Garcia-Delgado, C. Gomez-Lahoz, C. Vereda-Alonso, "Limpieza de suelos por electrodescontaminación 2: mejoras de la técnica en el movimiento de contaminantes", Ingeniería Química, 369, 215-220, 2000.

[5] A.B. Ribeiro, J.M. Rodríguez-Maroto, "Electrokinetic Modeling of Heavy Metals", in: M.N.V. Prasad, K.S. Sajwan, R. Naidu, "Electroremediation of Heavy Metal - Contaminated Soils - Processes and Applications in Trace Elements in The Environment", Taylor & Francis, 2005

[6] J.M. Rodríguez-Maroto, C. Vereda-Alonso, Electrokinetic Modeling of Heavy Metals, in: K. Reddy, C. Cameselle, Electrochemical Remediation Technologies For Polluted Soils, Sediments And Groundwater, John Wiley & Sons, United States, 2009

[7] L.M. Ottosen, I. Rörid-Dalgaard, "Desalination of a brick by application of an electric DC field", Materials and Structures, 42, 961-971, 2009.

[8] M.D. Garcia-Gutierrez, C. Gomez-Lahoz, J.M. Rodriguez-Maroto, C. Vereda-Alonso, F. Garcia-Herruzo, "Electrokinetic remediation of a soil contaminated by the pyritic sludge spill of Aznalcóllar (SW, Spain)" Electrochimica Acta, 52, 3372–3379, 2007.

[9] L.M. Ottosen, G.M. Nystrøm, P.E. Jensen, A. Villumsen, "Electrodialytic extraction of Cd and Cu from sediment from Sisimiut Harbour, Greenland", Journal of Hazardous Materials, 140, 271-279, 2007.

[10] J.D. Subirés-Muñoz, A. García-Rubio, C. Vereda-Alonso, C. Gómez-Lahoz, J.M. Rodríguez-Maroto, F. García-Herruzo, J.M Paz-García, "Feasibility Study of the use of different stractant agents in the remediation of a mercury contaminated soil from Almaden", Separation and Purification Technology (2011), doi:10.1016/j.seppur.2011.01.032.

[12] A.T. Yeung, J.K. Mitchell, "Coupled fluid, electrical, and chemical flows in soil", Geotechnique, 43(1), 121-134, 1993.

[11] A.N. Alshawabkeh, Y.B Acar, "Electrokinetic Remediation II, Theoretical Model", Journal of Geotechnical Engineering, 122(3), 186-196, 1996.

[13] S. Pamucku, "Electrochemical Transport and Transformations", in K.R. Reddy, C.Camesselle, "Electrochemical Remediation Technologies for Polluted Soils, Sediments and Groundwater", John Wiley and Sons, 2009.

[14] J.K. Mitchel, "Fundamental of Soil Behavior", 2nd ed. John Wiley and Sons, New York, 1993.

[15] B. Johannesson, “Comparison between the Gauss' law method and the zero current method to calculate multi-species ionic diffusion in saturated uncharged porous materials”, Computers and Geotechniques 37, 667-677, 2010
[16] J.M. Paz-García, B. Johannesson, L.M. Ottosen, A.B. Ribeiro, J.M. Rodríguez-Maroto, “Modeling of electrokinetics by finite element integration of the Nernst-Planck-Poisson system of equations”, Separation and Purification Technology (2011), doi:10.1016/j.seppur.2011.02.023
[17] B. Johannesson, Y. Hosokawa, K. Yamada, “Numerical calculations of the effect of moisture content and moisture flow on ionic multi-species diffusion in the pore solution of porous materials”, Compututers Structures 87, 39-46, 2009.
[18] O.C. Zienkiewicz, R.L. Taylor, “The Finite Element Method, Volume: 3, Fluid Dynamics”, 5 ed., Butterworth-Heinemann, Woburn, 2000.
[19] N.S. Ottosen, H. Petersson, Introduction to the Finite Element Method, Prentice Hall International (UK) Ltd, Hertfordshire, 1992.
[20] F.M.M. Morel, J.G. Hering, “Principles and Applications of Aquatic Chemistry”, Wiley Interscience, New York, 1993.
[21] R.A. Jacobs, R.F. Probstein, “Two-dimensional modeling of Electroremediation”, AIChE Journal 42(6), 1685-1696, 1996.
[22] IUPAC Compendium of Chemical Terminology, 2nd ed. 1997.
[23] W.H. Press, B.P. Flannery, S.A. Teukolsky, W.T. Vetterling, “Numerical Recipes in C: The Art of Scientific Computing, Chapter 9, Root Finding and Non-linear Sets of Equations”, Cambridge University Press, 1992.
[24] D.L. Parkhurst, C.A.J. Appelo, “User’s guide to PHREEQC (version 2) - A computer program for speciation, batch-reaction, one-dimensional transport, and inverse geochemical calculations”, U.S. Department of the Interior, Water-Resources Investigations Reports, 99-4259, 1999.
[25] L.O. Ottosen, I.Rörig-Dalgård, “Electrokinetic removal of Ca(NO3)2 from bricks to avoid salt-induced decay”, Electrochimia Acta, 52, 3454-3463, 2007.
[26] L.M. Ottosen, H.K. Hansen, A.B. Ribeiro, A. Villumsen, “Removal of Cu, Pb and Zn in an applied electric field in calcareous and non-calcareous soils”, Journal of Hazardous Materials, B85, 291–299, 2001
[27] Y.B. Acar, A.N. Alshawabkeh. "Electrokinetic remediation I: Pilot scale tests with lead spiked kaolinite”. Journal of Geotechnical and Geoenvironmental Engineering 122(3), 173-185, 1996.

A generalized physicochemical model is proposed for the description of electrochemically-induced transport processes taking place in electrokinetic treatments of inhomogeneous matrices.
The model includes the simultaneous transport of water and aqueous species throughout the porous medium, the monitoring of the degree of saturation, the pH value and the porosity, and a comprehensive set of homogeneous and heterogeneous chemical and electrochemical reactions involving solid, gaseous and aqueous species in both the electrolyte and the solid structure.

A numerical solution for the mathematical model is suggested, based on a finite elements integration of the Nernst-Planck-Poisson system taking into account competitive electrode reactions and coupled with a model for computing chemical equilibrium.

DTU Civil Engineering
Department of Civil Engineering
Technical University of Denmark

Brovej, Building 118
2800 Kgs. Lyngby
Telephone 45 25 17 00

www.byg.dtu.dk

ISBN: 9788778773609
ISSN: 1601-2917